



This work is licensed under Creative Commons Attribution 4.0 International. To view a copy of this license, visit <https://creativecommons.org/licenses/by/4.0/>

Future changes of Swiss river runoff and extreme vertically integrated moisture transport

Inauguraldissertation
der Philosophisch-naturwissenschaftlichen Fakultät
der Universität Bern

vorgelegt von

Regula Isabelle Mülchi

von Leuzigen, BE

Leiterin der Arbeit:

Prof. Dr. Olivia Romppainen-Martius
Geographisches Institut, Universität Bern

Co-Leiter der Arbeit:

Prof. em. Dr. Rolf Weingartner
Geographisches Institut, Universität Bern

Dr. Ole Rössler

Bundesanstalt für Gewässerkunde

Future changes of Swiss river runoff and extreme vertically integrated moisture transport

Inauguraldissertation
der Philosophisch-naturwissenschaftlichen Fakultät
der Universität Bern

vorgelegt von

Regula Isabelle Mülchi

von Leuzigen, BE

Leiterin der Arbeit:

Prof. Dr. Olivia Romppainen-Martius
Geographisches Institut, Universität Bern

Co-Leiter der Arbeit:

Prof. em. Dr. Rolf Weingartner
Geographisches Institut, Universität Bern

Dr. Ole Rössler

Bundesanstalt für Gewässerkunde

Von der Philosophisch-naturwissenschaftlichen Fakultät angenommen.

Bern, den 17. Februar 2021

Der Dekan:
Prof. Dr. Z. Balogh

Abstract

Climate change is likely to alter important hydrological variables due to increasing temperatures and changing precipitation patterns and extremes. Therefore, assessments of future changes in Swiss river runoff is crucial for adaptation and mitigation planning. In this thesis, changes in river runoff characteristics are analysed for runoff regimes and moderate low and high flows. In addition, changes in the atmospheric potential for floods are investigated.

In the first part of this thesis, new hydrological scenarios for Switzerland forced by the most up to date climate change scenarios (CH2018) are presented. The new dataset "Hydro-CH2018-Runoff" consists of daily runoff simulations for 93 meso-scale catchments in Switzerland for the period 1981-2099. The hydrological modelling system PREVAH (Precipitation-Runoff-Evapotranspiration HRU-related Model) was thoroughly calibrated and validated for each catchment. The calibrated parameters show satisfactory performance with a median Nash-Sutcliffe efficiency of 0.82 and a median Kling-Gupta efficiency of 0.89 in the calibration and validation period. The calibrated parameters were then used to simulate runoff under climate change for the period 1981-2099 on a daily basis. These simulations were driven by the high-resolution CH2018 scenarios consisting of 68 model chains of global and regional climate models covering 3 different Representative Concentration Pathways (RCP): RCP2.6, RCP4.5, and RCP8.5. The Hydro-CH2018-Runoff ensemble is freely available for download and can be used for further impact studies.

Climate change impacts on runoff regimes in Switzerland are assessed with the Hydro-CH2018-Runoff ensemble. By end of the 21st century, winter mean runoff is projected to increase while summer and autumn mean runoff are projected to decrease. In spring, runoff increases in high elevation catchments and decreases in lower lying catchments. The yearly mean runoff is projected to decrease in most catchments. The projected changes show a strong elevation dependence with high elevation catchments being more affected than low elevation catchments. Early significant changes emerge in winter and summer in catchments with mean altitudes above 1500 masl. Significant changes in catchments below 1500 masl emerge later in the century. However, not all catchments show a time of emergence in all seasons and in some catchments the detected significant changes are not persistent over time. The magnitude of change and the robustness in terms of climate model agreement on the sign of change (positive or negative) increase with increasing global mean temperatures or stronger emission scenarios. This amplification highlights the importance of climate change mitigation.

A strong elevation dependence is also found for projected changes in moderate low flows. In Alpine catchments (approx. >1500 masl), the magnitudes of moderate low flows are projected to increase and significant changes emerge early in the 21st century, while the frequency of low flows decreases. Seasonality of low flows shifts from winter and early spring to autumn except

in very high elevation catchments where seasonality does not change. In lower lying catchments (approx. <1500 masl), low flow situations are projected to occur more often and the runoff during low flows is projected to decrease. The seasonality of low flows in lower lying catchments hardly changes. The elevation dependence as well as the climate model agreement on the sign of change in moderate high flows is less clear and often not significant. Most catchments show slightly increasing magnitudes and frequencies in high flows except very high Alpine catchments which show decreasing magnitudes and frequencies. The seasonality of moderate high flows changes only in Alpine catchments with a shift towards early summer.

The Hydro-CH2018-Runoff ensemble is based on a single hydrological model. A comparison of the simulations with simulations from different Swiss research institutions for a subset of the catchments was performed. Despite fundamental methodological differences between the different hydrological simulations, a good agreement on the sign and the magnitude of change in seasonal runoff is found. Largest differences between the simulations are found in winter and spring for Alpine catchments (snow processes) and in summer and autumn in lower lying catchments (evapotranspiration processes).

The second part of this PhD thesis includes an analysis of future changes in the atmospheric potential for flood events in Switzerland. Extreme moisture transport (IVT) directed perpendicular to topography is strongly linked to major floods in Switzerland and serves as an important atmospheric flood precursor. In this thesis, future changes of IVT extremes directed towards orography are assessed for 9 climate models under a high emission scenario (RCP8.5). The results show that IVT extremes increase by 20-30% with climate change. The moisture component (TPW) of IVT is projected to increase by 25% while the wind component (SW) of IVT hardly changes. This suggests that the major driver of the increase in IVT is related to changes in the thermodynamics (Clausius-Clapeyron relationship) and not to changes in the dynamics. 100-year return levels of IVT are estimated using non-stationary Generalized Extreme Value (GEV) models with the covariates time, TPW and SW. Best performance is found for the covariates TPW and time. Since both covariates include a temporal trend, the estimated 100-year return levels increase by end of the century.

Contents

Abstract	i
Contents	iii
List of Figures	vii
List of Tables	xi
1 Introduction	1
1.1 Motivation	1
1.2 Aims and outline of this thesis	4
2 An ensemble of daily simulated runoff data (1981–2099) under climate change conditions for 93 catchments in Switzerland (Hydro-CH2018-Runoff ensemble)	7
2.1 Abstract	7
2.2 Introduction	8
2.3 Data Description and Development	9
2.3.1 Study Area	9
2.3.2 Input Data	10
2.3.3 Hydrological Model	11
2.3.4 Calibration and validation	13
2.3.5 Performance assessment	13
2.3.6 Simulation of runoff	14
2.4 Calibration and Validation Results	14
2.5 Data availability and remarks on the uncertainty	18
2.6 Conclusions and outlook	18
2.7 Acknowledgements	19
3 Future runoff regime changes and their time of emergence for 93 catchments in Switzerland	21
3.1 Abstract	21

3.2	Introduction	22
3.3	Data	23
3.4	Methods	25
3.4.1	Study area	25
3.4.2	Changes in runoff regimes	25
3.4.3	Changes with increasing global mean temperatures	26
3.4.4	Time of emergence of seasonal changes	27
3.5	Results	27
3.5.1	Seasonal and yearly mean changes	27
3.5.2	Changes in the runoff regime	31
3.5.3	Time of emergence	33
3.5.4	Changes in seasonal means with warming levels	35
3.6	Discussion	38
3.7	Conclusions	40
3.8	Data availability	41
3.9	Acknowledgements	41
4	Moderate runoff extremes in Swiss rivers and their seasonal occurrence in a changing climate	43
4.1	Abstract	43
4.2	Introduction	44
4.3	Data	46
4.4	Methods	47
4.5	Results	49
4.5.1	Future changes in moderate low flows	49
4.5.2	Future changes in moderate high flows	53
4.5.3	(Co-)occurrence of low and high flows	56
4.6	Discussion	61
4.6.1	Changes in moderate low flows	61
4.6.2	Changes in moderate high flows	62
4.6.3	Time of emergence of significant changes	63
4.6.4	Changes in the (co-)occurrence of low and high flow events	63
4.6.5	Uncertainties	64
4.7	Conclusions	64
4.8	Acknowledgements	65
5	Comparison of hydrological modelling results from four Swiss research institutions	67
5.1	Introduction	67
5.2	Data and Methods	67

5.3	Comparison between UBE-UZH-WSL	69
5.4	Comparison between UBE-UZH-WSL-ETHZ	71
5.5	Conclusions	72
6	Vertically integrated moisture transport extremes directed perpendicular to the Swiss topography intensify under climate change	75
6.1	Introduction	75
6.2	Data	78
6.3	Methods	80
6.4	Results	81
6.4.1	Large-scale moisture transport	81
6.4.2	IVT intensity changes	82
6.4.3	Seasonality of IVT extremes	84
6.4.4	GEV results	85
6.5	Summary and Discussion	90
6.5.1	Changes in moisture transport extremes	90
6.5.2	GEVs and associated return levels	94
6.6	Conclusions and Outlook	94
7	Summary, concluding remarks and outlook	97
7.1	Summary	97
7.2	Concluding remarks	99
7.3	Outlook	101
	Bibliography	103
A	Supporting information to chapter 2	117
B	Supporting information to chapter 3	131
C	Supporting information to chapter 6	141
D	Anthropogenic influence on runoff regime and runoff extremes	147
D.1	Abstract	147
D.2	Introduction	148
D.3	Data and Methods	149
D.3.1	Data	149
D.3.2	Catchment characteristics	150
D.3.3	Bias correction	150
D.3.4	Hydrological model GR4J-Cemaneige	151
D.3.5	Analysis of temperature, precipitation, and runoff	153
D.3.6	Analysis of extremes	154

D.4	Results	154
D.4.1	Comparison of climatological indices	154
D.4.2	Comparison of the runoff regime	156
D.4.3	Sensitivity of the indices to the catchment and the bias correction reference period	159
D.4.4	Extreme events	159
D.5	Discussion	161
D.6	Summary & Conclusions	165
D.7	Acknowledgements	166
D.8	References Appendix D	166
D.9	Appendix to Appendix D	172

List of Figures

1.1	Schematic overview of the different parts of this thesis.	4
2.1	Overview of the study catchments and the location of the gauging stations	9
2.2	Performance of PREVAH for 93 catchments	16
2.3	Runoff regimes of six representative catchments for observations, control simulations, and Hydro-CH2018 simulations	17
3.1	Overview of the study region and the location of the gauging stations	24
3.2	Multimodel median of seasonal and yearly mean changes under RCP8.5 by 2085 for winter, spring, summer, autumn, and yearly means	28
3.3	Multimodel median of seasonal and yearly mean changes under RCP2.6 by 2085 for winter, spring, summer, autumn, and yearly means	29
3.4	Elevation dependence of the multimodel median of seasonal and yearly mean changes by 2085 under RCP2.6 and RCP8.5	31
3.5	Runoff regimes for the six representative catchments Rosegbach, Kander, Plessur, Emme, Venoge, and Verzasca	32
3.6	Time of emergence for winter, spring, summer, autumn, year	34
3.7	Temporal evolution of time of emergence for the different seasons	36
3.8	Multimodel median of seasonal and yearly mean changes by +1.5°C, +2°C, and +3°C global warming for winter, spring, summer, autumn, and year	37
4.1	Overview of the study region and the location of the gauging stations	47
4.2	Median monthly occurrence of moderate low flows and high flows for the reference period and end of the century	50
4.3	Relative changes of magnitude by end of the century for moderate low flows and moderate high flows for the year, winter, and summer	51
4.4	Multi-model median of intensity and seasonal occurrence of low flows and seasonal lowest flows in Alpine catchments: Rosegbach, Kander, and Plessur	54
4.5	Multi-model median of intensity and seasonal occurrence of low flows and seasonal lowest flows in low lying catchments: Emme, Venoge, and Verzasca	55

4.6	Multi-model median of intensity and seasonal occurrence of high flows and seasonal highest flows in Alpine catchments: Rosegbach, Kander, and Plessur	57
4.7	Multi-model median of intensity and seasonal occurrence of high flows and seasonal highest flows in low lying catchments: Emme, Venoge, and Verzasca	58
4.8	Time of emergence of moderate low flows and moderate high flows	59
4.9	Relative changes in the frequency of occurrences of moderate low flow events, of moderate high flow events, and co-occurrence of low and high flow events	60
5.1	Runoff regimes of observed data, UBE, UZH and WSL in the reference period and for the future period 2070-2099 under RCP8.5	70
5.2	Comparison of relative changes of seasonal runoff by 2070-2099 under RCP2.6 and under RCP8.5 between UBE and WSL, and UBE and UZH	71
5.3	Runoff regimes of observed data, UBE, UZH, WSL and ETHZ for the reference period and for the periods 2030-2039, 2050-2059 and 2080-2089 under RCP8.5 . .	72
5.4	Relative changes of runoff regimes by UBE, UZH, WSL and ETHZ for the periods 2030-2039, 2050-2059 and 2080-2089 under RCP8.5	73
6.1	Overview of the IVT directions and synoptic flow regimes conducive to floods . .	76
6.2	Time composites of IVT intensity and direction during IVT block maxima in the CanESM2 model for the period 1979-2008 and 2071-2100	82
6.3	30-year running means of IVT intensity, TPW, and SW during IVT block maxima	83
6.4	Relative changes of IVT intensity, TPW, and SW during IVT block maxima . .	84
6.5	Seasonality and intensity of IVT during IVT block maxima	85
6.6	Changes in IVT seasonality and intensity during IVT block maxima	86
6.7	Coefficient β_0 of the location parameter for the three covariates and three regions	86
6.8	Coefficient β_1 (unitless) of the location parameter for the three covariates and three regions	87
6.9	Scale parameters for the three covariates and three regions	88
6.10	Shape parameters for the three covariates and three regions	88
6.11	BIC scores for the GEV models either using no covariate or using the covariates time, TPW, or SW	89
6.12	Effective 100-year return levels using the covariates time, TPW, and SW	91
6.13	30-year averages of estimated 100-year return levels of IVT intensity for the reference period (1979-2008) and the future period (2071-2100)	92
A.1	Regimes for observations, control simulations, and CH2018 simulations - part 1 .	122
A.2	Regimes for observations, control simulations, and CH2018 simulations - part 2 .	123
A.3	Regimes for observations, control simulations, and CH2018 simulations - part 3 .	124
A.4	Regimes for observations, control simulations, and CH2018 simulations - part 4 .	125
A.5	Regimes for observations, control simulations, and CH2018 simulations - part 5 .	126
A.6	Regimes for observations, control simulations, and CH2018 simulations - part 6 .	127

A.7	Regimes for observations, control simulations, and CH2018 simulations - part 7 .	128
A.8	Regimes for observations, control simulations, and CH2018 simulations - part 8 .	129
B.1	Multimodel median of seasonal and yearly mean changes under RCP4.5 by 2085	135
B.2	Multimodel median of seasonal and yearly mean changes under RCP2.6 by 2060	136
B.3	Multimodel median of seasonal and yearly mean changes under RCP4.5 by 2060	137
B.4	Multimodel median of seasonal and yearly mean changes under RCP8.5 by 2060	138
B.5	Runoff regimes for the six representative catchments	139
C.1	Example of a Goodness-of-fit plot for a non-stationary GEV model	141
C.2	Time composites of IVT intensity and direction during IVT block maxima in the bcc-csm1-1 model	142
C.3	Time composites of IVT intensity and direction during IVT block maxima in the CSIRO-Mk3-6-0 model	142
C.4	Time composites of IVT intensity and direction during IVT block maxima in the GFDL-CM3 model	143
C.5	Time composites of IVT intensity and direction during IVT block maxima in the GFDL-ESM2G model	143
C.6	Time composites of IVT intensity and direction during IVT block maxima in the GFDL-ESM2M model	144
C.7	Time composites of IVT intensity and direction during IVT block maxima in the IPSL-CM5A-LR model	144
C.8	Time composites of IVT intensity and direction during IVT block maxima in the IPSL-CM5B-LR model	145
C.9	Time composites of IVT intensity and direction during IVT block maxima in the NorESM1-M model	145
D.1	Five catchments distributed over Switzerland	152
D.2	Climate indices of the industrial scenario and the non-industrial scenario for the Thur	155
D.3	Hydrological indices of the industrial and the non-industrial scenario for the Thur	158
D.4	Signal direction of differences in the ensemble median of the industrial and the non-industrial scenario	160
D.5	Change in occurrence probability (PR) of daily runoff	162
D.6	Climatological and hydrological indices for the river Emme	173
D.7	Climatological and hydrological indices for the river Venoge	174
D.8	Climatological and hydrological indices for the river Verzasca	175
D.9	Climatological and hydrological indices for the river Vorderrhein	176
D.10	Ensemble median of mean precipitation, mean temperature, potential evapotran- spiration, and mean runoff for the river Thur	177

List of Tables

2.1	List of parameters to be calibrated in PREVAH	12
2.2	Selection of six representative catchments and their main characteristics and regime types.	15
3.1	List of used GCM-RCM chains, their initial resolution, and the available RCPs. .	26
4.1	Overview of the available climate model chains and their initial grid spacings of 12 km (EUR-11) and 50 km (EUR-44).	48
4.2	Relative changes (in %) by end of the century and the seasonal occurrence (OCC) of moderate low and high flows for the six representative catchments.	52
5.1	Differences between the simulations of the four institutions.	68
5.2	Climate model chains used for the comparisons.	69
6.1	List of CMIP5 models, associated institutions, and horizontal and vertical resolution of the models.	79
6.2	Regions and their respective critical advection angles.	79
6.3	Differences of BIC scores between the fitted models with covariates and the stationary model for each region	90
A.1	93 catchments and their main characteristics and calibration period	117
A.2	List of available GCM-RCM combinations and their initial resolutions.	121
B.1	Overview of the main characteristics of the 93 catchments	131
D.1	Observational periods considered in this study	150
D.2	Main characteristics of the five catchments	151
D.3	Performance results of the different catchments for the calibration period and the validation period	153
D.4	Differences between the ensemble median of the industrial scenario and the ensemble median of the non-industrial scenario for different climatological and hydrological indices	157

Chapter 1

Introduction

1.1 Motivation

Anthropogenic climate change is unequivocal and strongly influences all components of the hydrological cycle (IPCC, 2013, 2014a,b). This also includes water on the Earth's surface such as rivers or lakes. Changing precipitation patterns and increasing temperatures influence various hydrological processes such as evapotranspiration or snow and glacier melt. Since Switzerland is a highly mountainous country, significant impacts of climate change on snow and glacier related processes are expected (CH2014, 2014). Under a high emission scenario, the new Swiss climate change scenarios CH2018 project a strong temperature increase (3.3-5.4°C) by end of the 21st century (CH2018, 2018). Mean precipitation is projected to increase in winter and to decrease in summer while extreme precipitation events are likely to intensify and become more frequent under climate change. Increasing temperatures are accompanied by an increase in the snow line and thus a change in precipitation type in winter resulting in more rain than snow. Glaciers will retreat and largely disappear by end of the 21st century in the Alpine area (Zekollari et al., 2019). These climate induced changes of hydrologically relevant variables will strongly influence river runoff in Switzerland.

Several studies on climate change impacts on the hydrology in Switzerland have been conducted in recent years with varying foci such as runoff regimes (Horton et al., 2006; Köplin et al., 2012, 2014a; Addor et al., 2014; Milano et al., 2015), low flows (Jenicek et al., 2018; Brunner et al., 2019a,b), high flows (Keller et al., 2018; Brunner et al., 2019a), or with a particular focus on glaciated catchments (Huss et al., 2008; Farinotti et al., 2012; Huss et al., 2014; Fatichi et al., 2015; Etter et al., 2017). However, most of these studies are either case studies or are based on older climate model generations and simple downscaling methods such as the delta change method. This method only corrects for the mean bias in the climate models and does not capture changes in variability and the transient property of climate change. More sophisticated statistical downscaling approaches such as quantile mapping (Gudmundsson et al., 2012; Teutschbein and Seibert, 2012) emerged in the past years. The Federal Office for Meteorology

and Climatology MeteoSwiss used this method to downscale coarse climate model output for Switzerland and provides high resolution and transient climate change scenarios (CH2018). The new scenarios based on quantile mapping produce more frequent and more intense extremes (Rössler et al., 2019). The CH2018 high-resolution dataset allows for the generation of new hydrological scenarios for Switzerland which cover the whole period from 1981-2099 and improve the quantification of potential changes in river runoff.

Therefore, the Swiss Federal Office for the Environment launched a national project called Hydro-CH2018 based on a mandate by Swiss Federal Council. The aim of this project is to improve the understanding of the impacts of climate change on water resources in Switzerland. The project includes several research projects led by different Swiss research institutions. One of the main goals of this project is to update hydrological scenarios with the newest high-resolution CH2018 scenarios for Switzerland (CH2018, 2018) to provide detailed information on climate change impacts on runoff. The first part of this thesis consists of the generation of those hydrological scenarios. The new dataset is called Hydro-CH2018-Runoff ensemble and is freely available for download from the Zenodo archive (Muelchi et al., 2020). The subsequent analysis of the Hydro-CH2018-Runoff ensemble focuses on changes in the runoff regimes and moderate low and high flows.

Chapters 2-5 of this thesis contribute to the Hydro-CH2018 project. Beside those chapters, the work of this thesis contributed to several other products within the Hydro-CH2018 project which will be released on 16 March 2021 at the final symposium:

- *Synthesis report*: A report summarizing the most important results of the Hydro-CH2018 project. The results of this thesis provided the majority of the content of chapters 1 and 3 (in German, French, Italian, English)
- *Brochure*: An easy to read brochure for the general public including results and statements from this thesis (in German, French, Italian, English)
- *Final project report*: A detailed project report with the most important findings and figures for reuse by interested people written by the author of this thesis (in German)
- *Special report on floods*: A report summarizing the current state of the knowledge about floods in Switzerland “Past, current, and future changes in floods in Switzerland”. The outcomes of this thesis contributed to chapter 6 “Future changes in floods”
- *Interactive web platforms*: Part of the results of this thesis will become interactively accessible on web platforms of the National Center for Climate Services (www.nccs.ch) and the Swiss Hydrological Atlas (www.hydrologischeratlas.ch). The author processed the data for the platforms and wrote explanatory notes about the content and the use of the data

- *Short additional project:* The FOEN funded a short additional project to create figures for other projects within Hydro-CH2018 and to make a comparison between modelling efforts from different research institutions

In Switzerland, changes in river runoff regimes and thus changes in the water availability have a strong impact on many economical and ecological sectors such as agriculture, energy, industry, fishery, or tourism, (e.g., Bürki et al., 2007; Hänggi and Weingartner, 2012; CH2014, 2014; Brönnimann et al., 2014; Köllner et al., 2017; Ehrbar et al., 2018; Henne et al., 2018; Zarrineh et al., 2020). Projections of mean runoff and moderate extremes and the associated information about future water availability are important to decision makers and planners in terms of adaptation and mitigation planning. Furthermore, the decision makers have a strong interest in the future development of floods since floods are one of the costliest and most devastating natural hazard in Switzerland (Hilker et al., 2009). Understanding future changes of flood magnitudes and frequencies is very important for the planning of preventive measures. Assessments of future changes in floods were made by several studies (e.g., Allamano et al., 2009; Köplin et al., 2014b; Beniston and Stoffel, 2016; Ragettli et al., 2019). They found increasing but often not significant changes in annual runoff maxima under climate change. Allamano et al. (2009) found seasonally distinct changes with increasing winter floods and decreasing summer floods. Also, seasonality of floods is projected to change depending on the regime type of the catchments (Köplin et al., 2014b). However, modeling floods under climate change remains a challenging task since precipitation and temperature changes are not necessarily well translated to changes in floods (Brunner et al., in review 2020).

The procedure used in the first part of this thesis follows what is called a classical top down approach (Dessai and Hulme, 2004). Simulations run with global climate models are used to drive regional climate models. The regional model output is further downscaled and fed into a hydrological model. Such a top down model approach is subject to large uncertainties introduced at every level of the model chain. An alternative to this approach is to focus on the processes that lead to floods and explore changes in these processes with climate change (Shepherd et al., 2018). The second part of this thesis focuses on changes in the atmospheric potential for floods. The atmospheric potential is an important ingredient for the generation of floods. Previous studies analysed atmospheric conditions potentially leading to floods in Switzerland (e.g., Massacand et al., 1998; Martius et al., 2006; Hoinka and Davies, 2007; Stucki et al., 2012; Froidevaux and Martius, 2016; Giannakaki and Martius, 2016). Froidevaux and Martius (2016) found a strong relationship between extreme moisture transport directed perpendicular to orography and major flood events in Switzerland. Such extreme moisture transports are characterized by high vertically integrated water vapor transport (IVT, $\text{kg m}^{-1}\text{s}^{-1}$). In the last years, 70% of the past 14 major floods in Switzerland were associated with extreme IVT directed perpendicular to topography (Froidevaux and Martius, 2016). Other studies also emphasized the importance of IVT direction for flood generation in Norway (Schaller et al., 2020) and in Britain (Griffith et al.,

2020). Extreme IVT is often linked to atmospheric rivers (ARs), which are long and narrow filaments with strong horizontal water vapor transport (Ralph et al., 2018). Previous studies assessed future changes of ARs in Europe (Lavers et al., 2013; Gao et al., 2016; Ramos et al., 2016; Shields and Kiehl, 2016; Whan et al., 2020) and found generally increasing frequencies and intensities of ARs and IVT under climate change. The strong link between extreme IVT and major flood events in the past motivates the second part of this thesis analyzing how extreme IVT and thus potential flood precursors may evolve under climate change.

1.2 Aims and outline of this thesis

This thesis consists of two main parts (see Figure 1.1). The first part of this thesis is part of Hydro-CH2018 project and addresses the hydrological part of this PhD project focusing on future changes in river runoff. The first goal is to develop new hydrological scenarios for Switzerland using the most up to date climate change scenarios and thus providing a comprehensive and state of the art dataset for future research on changes in river runoff. The second goal is to analyse potential changes in runoff characteristics using the new hydrological scenarios. Characteristics of particular interest are runoff regimes and moderate low and high flows.

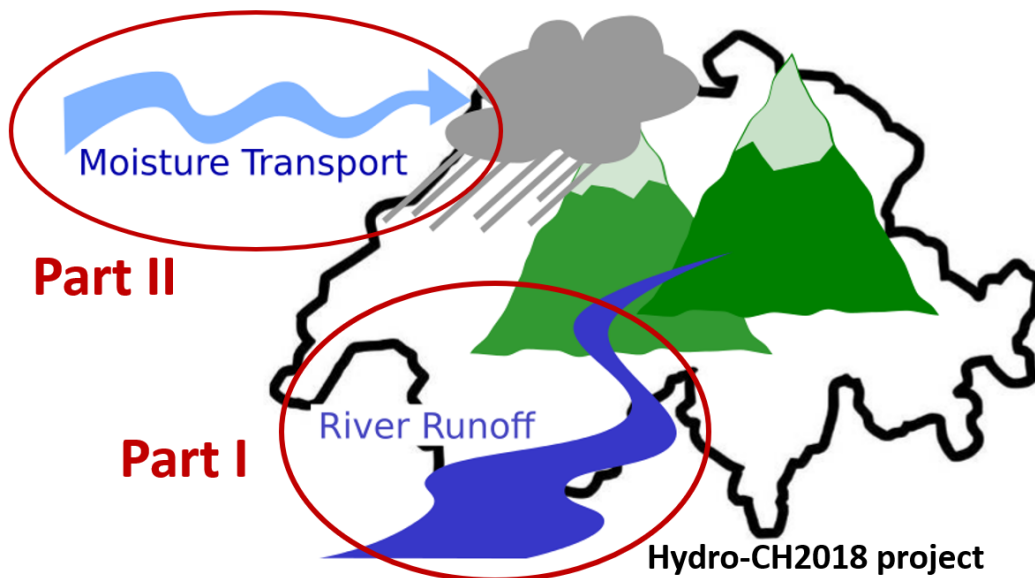


Figure 1.1: Schematic overview of the different parts of this thesis.

The second part of the thesis focuses on extreme IVT directed perpendicular to the Alps - an important atmospheric flood precursors for Switzerland. Investigating changes in the atmospheric potential for floods complements the hydrological projections and provides another

insight into the evolution of floods under climate change. The goal in the second part of this thesis is to analyse future changes in extreme IVT perpendicular to orography and to estimate future return periods.

This thesis is structured as follows: In chapter 2 the new hydrological scenarios, its modelling setup, and simulations are introduced. Analysis on future changes of river runoff regimes and their time of emergence are described in chapter 3. Chapter 4 includes an analysis of changes in the magnitude and seasonality of moderate low and high flows. The first part of the thesis ends with a comparison of the results of modelling efforts by different Swiss institutions for few study catchments in chapter 5. Chapter 6 discusses the results from the second part of this thesis about changes in extreme moisture transports directed towards Switzerland. The main findings of this thesis are summarized in chapter 7 together with a synthesis and an outlook on future research opportunities deepening and complementing the work of this thesis. Supporting information to Chapters 2, 3, and 6 are presented in Appendices A-C. Moreover, Appendix D contains the manuscript of a paper on the anthropogenic influence on runoff regimes and runoff extremes for five catchments in Switzerland. The first results of this study were produced in the authors' MSc thesis and further elaborated during this PhD thesis.

Chapter 2

An ensemble of daily simulated runoff data (1981–2099) under climate change conditions for 93 catchments in Switzerland (Hydro-CH2018-Runoff ensemble)

This chapter contains a manuscript that has been written together with Ole Rössler, Jan Schwanbeck, Rolf Weingartner, and Olivia Martius. The manuscript has been submitted under the title "An ensemble of daily simulated runoff data (1981–2099) under climate change conditions for 93 catchments in Switzerland (Hydro-CH2018-Runoff ensemble)" in *Geoscience Data Journal* (Muelchi et al., in review 2020a).

2.1 Abstract

We present a new ensemble of daily runoff simulations for meso-scale catchments in Switzerland for the period 1981–2099: The Hydro-CH2018-Runoff ensemble. The ensemble contains runoff simulations for 93 catchments in Switzerland covering a wide range of different catchment characteristics governed by pluvial, nival and glacial runoff regimes. The hydrological modelling system PREVAH was thoroughly calibrated and validated for each catchment. The simulations show satisfactory performance with a median Nash-Sutcliffe efficiency of 0.82 in the calibration and validation period. The calibrated parameters were then used to simulate runoff under climate change for each of the 93 catchments. These simulations were driven by the high-resolution new Swiss climate change scenarios (CH2018) consisting of 68 GCM-RCM combinations covering 3 different emission scenarios: RCP2.6, RCP4.5, and RCP8.5. The simulations show good agreement between simulated and observed runoff regimes in the reference

period. The Hydro-CH2018-Runoff ensemble is publicly available under <http://doi.org/10.5281/zenodo.3937485> (Muelchi et al., 2020) and can be used for further impact studies.

2.2 Introduction

Climate change influences all components of the hydrological cycle mainly due to changing precipitation patterns and increasing temperatures (IPCC, 2013). This also includes water on the Earth’s surface such as rivers. Potential climate change related changes in river runoff volume and regime may have substantial impacts on many sectors, among them water management, agriculture, tourism, energy production, fishery, and ecology. River runoff scenarios provide a basis for adaptation planning and show the impact and benefits of potential mitigation measures in support of governments and planning bodies as well as economy and agriculture in their decision making.

In Switzerland, climate change will have strong effects on runoff (CH2014, 2014) as many catchments in Switzerland are sensitive to changes in air temperatures and precipitation. Climate change induced changes in runoff have already been observed in the last decades (Weingartner, 2019). Due to the importance of snow and glaciers for runoff generation, seasonal shifts in runoff regimes are expected (Horton et al., 2006; Köplin et al., 2012, 2014a). The studies cited above are based on climate change scenarios using a delta change approach. This approach does not capture changes in variability and does not capture the transient nature of climate change. Updated climate change scenarios for Switzerland (CH2018) run with the newest generation of climate models (CH2018, 2018) allow us to address these limitations and to produce a new data set of hydrological scenarios – the Hydro-CH2018-Runoff data set.

The CH2018 climate change scenarios were developed using the statistical downscaling approach “quantile mapping” (Gudmundsson et al., 2012). A previous study found that quantile mapping produces higher and more frequent extremes (Rössler et al., 2019). The CH2018 climate change scenarios are available on high spatial (2x2 km) and temporal (daily) resolution and cover a period of 120 years. Using these climate change scenarios allows for a deeper understanding of changes in runoff and their transient evolution.

The Hydro-CH2018-Runoff data set is part of the Hydro-CH2018 project which is based on a mandate by the Swiss Federal Council and aims to provide information for adaptation to climate change. One of the main goals of this project is to compile new hydrological simulations for Switzerland. The Hydro-CH2018-Runoff ensemble contains a comprehensive set of hydrological simulations for Switzerland. We extensively calibrated and validated discharge for 93 rivers in Switzerland using the hydrological model PREVAH. The model was fed with the CH2018 climate change scenarios for Switzerland. The resulting ensemble of runoff simulations are transient in time and cover 120 years (1981 – 2099) , three different emission scenarios (RCP2.6, RCP4.5,

RCP8.5) defined by the IPCC (IPCC, 2013; Moss et al., 2010; Van Vuuren et al., 2011), and different GCM-RCM representations. Our simulations provide a basis for detailed analyses of climate induced changes of runoff regimes or for impact studies. The data set is part of the Swiss climate services coordinated by the National Centre for Climate Services (NCCS).

2.3 Data Description and Development

2.3.1 Study Area

A total of 93 catchments distributed across Switzerland and thereby covering different climatic, geological and hydrological properties are calibrated and simulated (Figure 2.1). The most important hydrological characteristics are summarized in Table A.1. The average area of the catchments is 314 km² and catchment areas range from 14 km² to 1700 km². The mean altitude of the catchments ranges between 476 masl and 2700 masl with an average mean elevation of 1344 masl across all catchments. 22 catchments are glaciated. The degree of glaciation varies between 0.2% and 22% (see Table A.1 for more details).

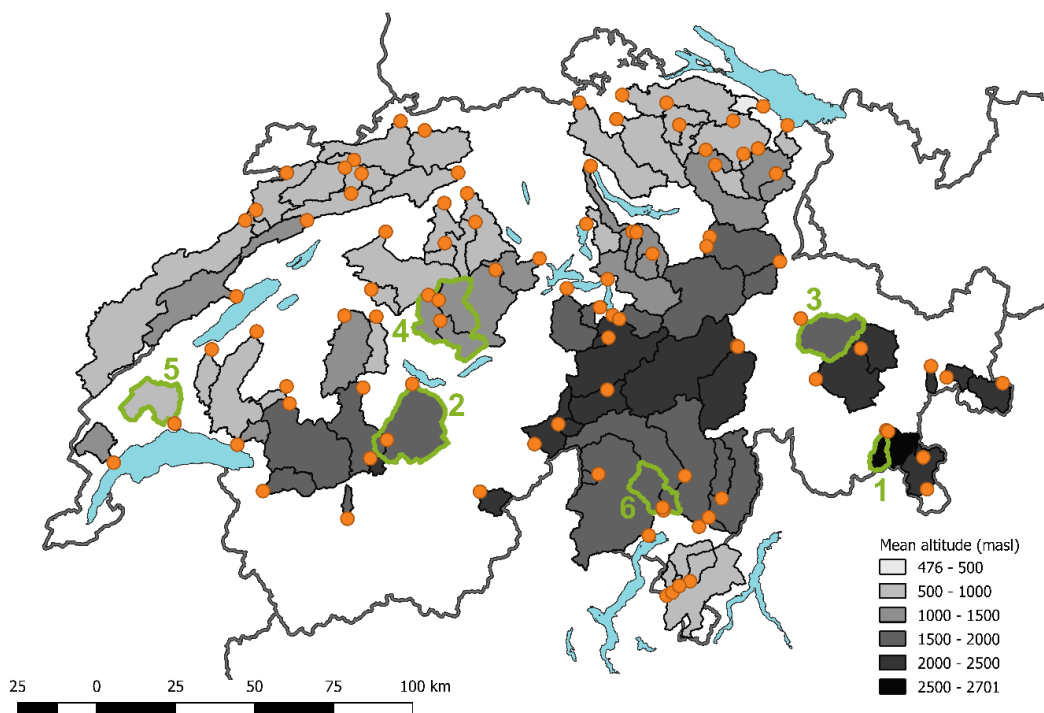


Figure 2.1: Overview of the study catchments and the location of the gauging stations (orange dots). Shadings indicate mean altitude of the respective catchments. Green contours indicate the six example catchments: Rosegbach - Pontresina (1), Kander - Hondrich (2), Plessur - Chur (3), Emme - Emmenmatt (4), Venoge - Ecublens (5), Verzasca - Lavertezzo (6).

The catchment selection covers the whole range of flow regimes in Switzerland (Weingartner and Aschwanden, 1992, Figure 2.1). The Alpine runoff regimes, in high mountain areas above a mean altitude of 1550 masl in northern Switzerland and in the highest catchments in southern Switzerland, are mainly glacier and snow driven regimes with low flows in winter and peak flows in summer. Pluvial catchments are predominant in the Swiss Plateau, which are driven mainly by precipitation, snow melt and evapotranspiration resulting in low flows towards the end of summer/autumn and higher flows in winter and early spring. However, the interannual variability in these catchments is very high due to the variability in precipitation. The lower lying catchments in the southern part of Switzerland follow a pluvial regime with multiple yearly peaks. These regimes are dominated by the precipitation patterns in these areas as well as by snowmelt in spring (Weingartner, 2019).

2.3.2 Input Data

2.3.2.1 Swiss Climate Change Scenarios CH2018

The Swiss Climate Change Scenarios CH2018 are provided by the Swiss Federal Office for Meteorology and Climatology MeteoSwiss and represent the latest generation of high-resolution climate data for Switzerland (CH2018, 2018). Scenarios for daily temperature and daily precipitation are available for different emission pathways on a 2 by 2 km grid covering the period 1981-2099. CH2018 is based on a top down approach, downscaling the outcomes of the EURO-CORDEX initiative (Jacob et al., 2014; Kotlarski et al., 2014). In EURO-CORDEX, regional climate models (RCMs) were run for a domain over Europe using the boundary conditions prescribed by Global Circulation Models (GCMs). The EURO-CORDEX simulations were run for two horizontal grid resolutions of approximately 12 km (EUR-11) and 50 km (EUR-44). The forcing is based on three Representative Concentration Pathways (RCP) used in the last IPCC Assessment Report (IPCC, 2013): RCP2.6 assuming compliant mitigation efforts, RCP4.5 assuming non-compliant mitigation efforts, and RCP8.5 assuming unabated emissions (Moss et al., 2010; Van Vuuren et al., 2011). In CH2018, EURO-CORDEX simulations for temperature and precipitation were statistically downscaled to a 2 by 2 km grid for Switzerland using quantile mapping. Quantile mapping implicitly corrects for potential biases in the RCM. Table A.2 gives an overview of the high resolution GCM-RCM combinations run for the different RCP pathways. Some of the GCM-RCM combinations are run for both spatial resolutions (EUR-11 and EUR-44), and only the higher resolved combinations are used for the ensemble statistics (black crosses in Table A.2). In total, this study uses 30 (20 for the ensemble statistics) climate simulations under RCP8.5, 25 (16 for the ensemble statistics) simulations under RCP4.5, and 12 (8 for the ensemble statistics) simulations under RCP2.6.

2.3.2.2 Glacier Scenarios

Future glacier extents are updated every 5 years to account for glacier retreat under climate change. We used the glacier projections for the Alpine region provided by Zekollari et al. (2019). These projections are based on the glacier evolution model GloGEMflow, which was validated over the European Alps. The projections show that glaciers in the European Alps largely disappear under RCP8.5 scenario while under RCP2.6 approximately one third of the ice volume remains in the Alps (Zekollari et al., 2019). The glacier model was driven by the same GCM-RCM combinations from EURO-CORDEX. However, these simulations were downscaled within GloGEMflow and not via CH2018 (Zekollari et al., 2019). For GCM-RCM combinations, which were run on both resolutions (EUR-11 and EUR-44), glacier data is available for the EUR-11 boundary conditions, only. In this study, glacier scenarios of the higher resolved models (EUR-11) were also used for the lower resolved model combinations (EUR-44).

2.3.2.3 Observational data

Daily discharge measurements at the outlet of the catchments are provided by the Swiss Federal Office for the Environment (FOEN, 2019) and are used for the calibration and validation of the hydrological model. The meteorological data for the calibration consists of observed spatially interpolated gridded daily temperature information TabsD (Frei, 2014; MeteoSwiss, 2019b) and gridded daily precipitation sums RhiresD (Frei and Schär, 1998; MeteoSwiss, 2019a) with a grid resolution of 2.2 km. This data was also used for the 10-year warm-up run of the model prior to the simulation.

2.3.2.4 Geospatial Information

Geospatial information was used to delineate hydrological response units (HRUs) for each catchment. Information about elevation, aspect, flow direction, and slope were derived from the digital elevation model over Europe (EU-DEM; Copernicus, 2016). EU-DEM is available on a 25 x 25 m grid with a vertical accuracy of ± 7 m RMSE across Europe. To determine the land use per HRU, the freely available CORINE Land Cover map (CLC2012; Copernicus, 2012) with 44 standard classes and a horizontal resolution of 100m was used. Both elevation and land use information were provided by the Copernicus programme of the European Environment Agency (EEA).

2.3.3 Hydrological Model

The semi-distributed hydrological modelling system PREVAH (Precipitation - Runoff - Evapotranspiration HRU-related Model; Viviroli et al., 2009) is a conceptual, process-oriented hydrological model. PREVAH was designed for catchments with complex topography to investigate many different aspects of hydrology such as water balance modelling, flood and drought estimation, and forecasting (Viviroli et al., 2009). PREVAH is based on the process-oriented structure

of the HBV-model (Hydrologiska Byråns Vattenbalansavdelning; Bergström, 1976; Lindström et al., 1997), but uses hydrological response units (HRUs) for spatial discretization. HRUs are areas with a similar hydrological response and are derived from physical catchment characteristics. All grid elements (500 x 500 m) of one HRU class are located in the same elevation band of 100 m and show similar aspects, land use and soil characteristics.

PREVAH includes various sub-models to account for hydrologically relevant processes such as snow melt, glacier melt, soil moisture, evapotranspiration, runoff and baseflow generation, and routing components. It also incorporates storage modules for snow, interception, soil moisture, saturated and unsaturated runoff storages, as well as optional storages in the glacier module for snow and ice in case of glaciated catchments. In this study, 13 free parameters for non-glaciated catchments and 2 additional parameters for glaciated catchments were calibrated (Table 2.1).

Table 2.1: List of parameters to be calibrated in PREVAH, the parameters needed for the glacier module are highlighted in italics.

Abbreviation	Description	Unit
RAINC	Precipitation adjustment	%
SNOWC	Snow adjustment	%
T0M	Threshold temperature for rain-snow	°C
TMFSNOW	Temperature melt factor for snowmelt	mm d ⁻¹ K ⁻¹
RMFSNOW	Radiation melt factor for snow	mm h ⁻¹ K ⁻¹ W ⁻¹ m ²
BETA	Non-linearity parameter for infiltration	-
SGR	Threshold for quick runoff formation	mm
K0H	Storage time for surface runoff	h
K1H	Storage time for interflow	h
K2H	Storage time for slow base flow	h
CG1H	Storage time for quick base flow	h
SLZ1MAX	Maximum content of quick base flow storage	mm
PERC	Percolation rate	mm h ⁻¹
<i>CICEMF</i>	Temperature melt factor for ice	mm d ⁻¹ K ⁻¹
<i>CAICE</i>	Radiation melt factor for ice	mm h ⁻¹ K ⁻¹ W ⁻¹ m ²

Gridded daily mean temperature and daily precipitation totals are available for this study and are used to drive the model. For each catchment, the gridded meteorological input is averaged across elevation zones of 100 m vertical extent. According to the availability and quality of the meteorological variables in the CH2018 scenarios, the estimation of the potential evapotranspiration was calculated using a simple approach based on the equation of Hamon (1961), which requires as inputs only daily temperature data and the maximum sunshine duration (day length).

2.3.4 Calibration and validation

Proper calibration of the model for each catchment is important for later simulations under climate change since good performance in the observed period increases the confidence for simulations under different climate conditions (Krysanova et al., 2018). The calibration of the 93 catchments was done using the automated parameter estimation procedure PEST (Doherty, 2005). PEST is an open source model-independent software to select model parameters resulting in the best fit to observations according to its objective function. The objective function is defined as the squared sum of weighted residuals and four observation groups are specified with equal weight:

- Observed runoff
- Inverted observed runoff to account for low flow conditions
- Observed monthly mean runoff to account for the regime
- Observed yearly volumes in the calibration period to account for volume

The calibration and validation time covers for most catchments the period from 1985 to 2014. Even years were used for calibration and uneven years for validation. In catchments with shorter observed time series, the period from the first fully observed year to 2014 is used for calibration and validation. Again, with even years for calibration and uneven years for validation. Table A.1 shows the exact period used for each catchment. The intention of using every second year within 30 years for calibration is to minimize the potential effect of random and non-random trends by using too short calibration periods. Climate change is already observed in the period 1985-2014. PREVAH is therefore trained to also simulate runoff under changing conditions. During the calibration process, PREVAH was run for the whole period while comparing the simulations with observations only for even years. We intentionally chose uneven years for the validation period since some of the years include periods of extreme weather such as very dry summer (e.g., 2003), severe floods (e.g., 2005, 2011) or winters with extreme snowfall and thus extreme snowmelt in spring (e.g., 1999). This leads to the assumption that if the model performs well in uneven years (validation), the calibrated parameters produce stable results also for more extreme or changing conditions.

2.3.5 Performance assessment

The results of the calibration were assessed by calculating the Nash-Sutcliffe Efficiency (NSE; Nash and Sutcliffe, 1970) and the Kling-Gupta Efficiency (KGE; Gupta et al., 2009) for the calibration and the validation period, separately. NSE is the mean squared error normalized by the variance of observations (Equation 2.1).

$$NSE = 1 - \frac{\sum_{t=1}^N (Q_{obs}(t) - Q_{sim}(t))^2}{\sum_{t=1}^N (Q_{obs}(t) - \overline{Q_{obs}})^2} \quad (2.1)$$

Where N is the length of the simulation period in days, $Q_{sim}(t)$ the simulated discharge at time t , $Q_{obs}(t)$ the observed discharge at time t , and $\overline{Q_{obs}}$ the mean observed discharge.

KGE decomposes the NSE to three components: correlation, variability bias and mean bias and combines these components into one performance measure according to Equation 2.2.

$$KGE = 1 - (r - 1)^2 + \left(\frac{\sigma_{sim}}{\sigma_{obs}} - 1 \right)^2 + \left(\frac{\mu_{sim}}{\mu_{obs}} - 1 \right)^2 \quad (2.2)$$

Where r is the linear correlation between the simulations and observations, σ is the standard deviation of observations and simulations respectively, and μ the mean of the simulations and observations.

Both performance measures range between $-\infty$ and 1, with 1 being a perfect match between modelled runoff and observed runoff. Values greater than 0 indicate better predictive power than the mean of the observations. NSE tends to emphasize simulations of flood events and therefore strongly penalize for missed peak flows. The NSE was therefore also calculated using square root transformed data. This procedure can then be used as a measure for the overall performance. To accompany the standard performance measures, we also assess the performance by visually comparing the runoff regimes of the simulated runoff with observed runoff. The runoff regimes were calculated by averaging monthly means over the whole period (1985-2014) used for calibration and validation. Based on these measures, we excluded catchments with an NSE < 0.7 in the validation period and/or do not reproduce the regime curve. The remaining 93 catchments fulfilled those requirements and were used for the Hydro-CH2018-Runoff ensemble.

2.3.6 Simulation of runoff

Each model simulation was preceded by a 10-year spin up from 1971-1980 fed by observations to fill up the model storages. Every catchment was separately simulated with each individual CH2018 climate simulation for 1981-2099 using daily input data. For the whole simulation period, the land use defined for each HRU was kept constant except for glaciated catchments where the glacier extents were updated every five years. When the glacier disappears in an HRU, the land use of the respective HRUs below 3000 masl was converted to bare soil while the land use of HRUs above 3000 masl was converted to rock.

2.4 Calibration and Validation Results

The performance measures for the calibration and validation period as well as for square root transformed values is shown in Figure 2.2. Median NSE values across all catchments for the calibration as well as for the validation period are 0.82. NSE values range from the lowest values of 0.7 to highest values of 0.91 (Figure 2.2a). The interquartile range in the validation

period is slightly higher than in the calibration period, which underlines the good performance of the model for unexperienced runoff observations in the calibration period. The median NSE of square root transformed data is slightly higher than the non-transformed NSE with a median of 0.83 in the calibration period and 0.84 in the validation period (Figure 2.2a). This is also true for the interquartile range of square root transformed NSE indicating a good overall performance.

The median KGE value across all catchments is 0.89 in both periods and ranges between 0.71 and 0.93 in the calibration period and 0.75 and 0.96 in the validation period. The interquartile ranges of KGE are smaller than for NSE (Figure 2.2a). The relation between NSE in the validation period and the catchment area and mean elevation is shown in Figure 2.2b and Figure 2.2c to explore potential dependencies between validation performance and catchment properties. No clear relationship between catchment properties and performance can be identified. However, some of the smaller catchments show smaller NSE values than the large catchments (Figure 2.2b). This may be due to the use of daily precipitation and temperature data.

Table 2.2: Selection of six representative catchments and their main characteristics and regime types.

Gauging station	Mean elevation (masl)	Area (km ²)	Glaciation (%)	Regime type ¹
Rosegbach – Pontresina	2701	67	21.7	a-glaciaire
Kander – Hondrich	1846	491	5.1	b-glacio-nival
Plessur – Chur	1865	264	0	Nival alpin
Emme – Emmenmatt	1072	443	0	Nivo-pluvial préalpin
Venoge - Ecublens	694	228	0	Nivo-pluvial jurassien
Verzasca – Lavertezzo	1663	185	0	Nivo-pluvial méridional

¹ after Weingartner and Aschwanden (1992)

The validation of the runoff regimes of a subset of six catchments is shown in Figure 2.3 (for other catchments see Appendix Figures A.1-A.8). The six catchments represent typical runoff regimes in different parts of Switzerland (see Table 2.2 and highlighted catchments in Figure 2.1): Rosegbach – highly glaciated, Kander – partially glaciated, Plessur – high-alpine snow influenced, Emme – pre-alpine snow influenced, Venoge – lowland rain dominated, and Verzasca – southern-alpine pluvial.

Figure 2.3 shows that the control run, fed by observations and modelled with the calibrated parameters (purple), results in similar runoff regimes as the observed regimes (red). The model is able to reproduce the seasonal cycle of the regimes and matches well with the observations. Green shadings show the runoff regime of the simulated runoff driven by the CH2018 scenarios for the reference period 1981-2010 for all models under RCP8.5. For the reference period, the

RCP8.5 input should not differ from the climatological forcing.

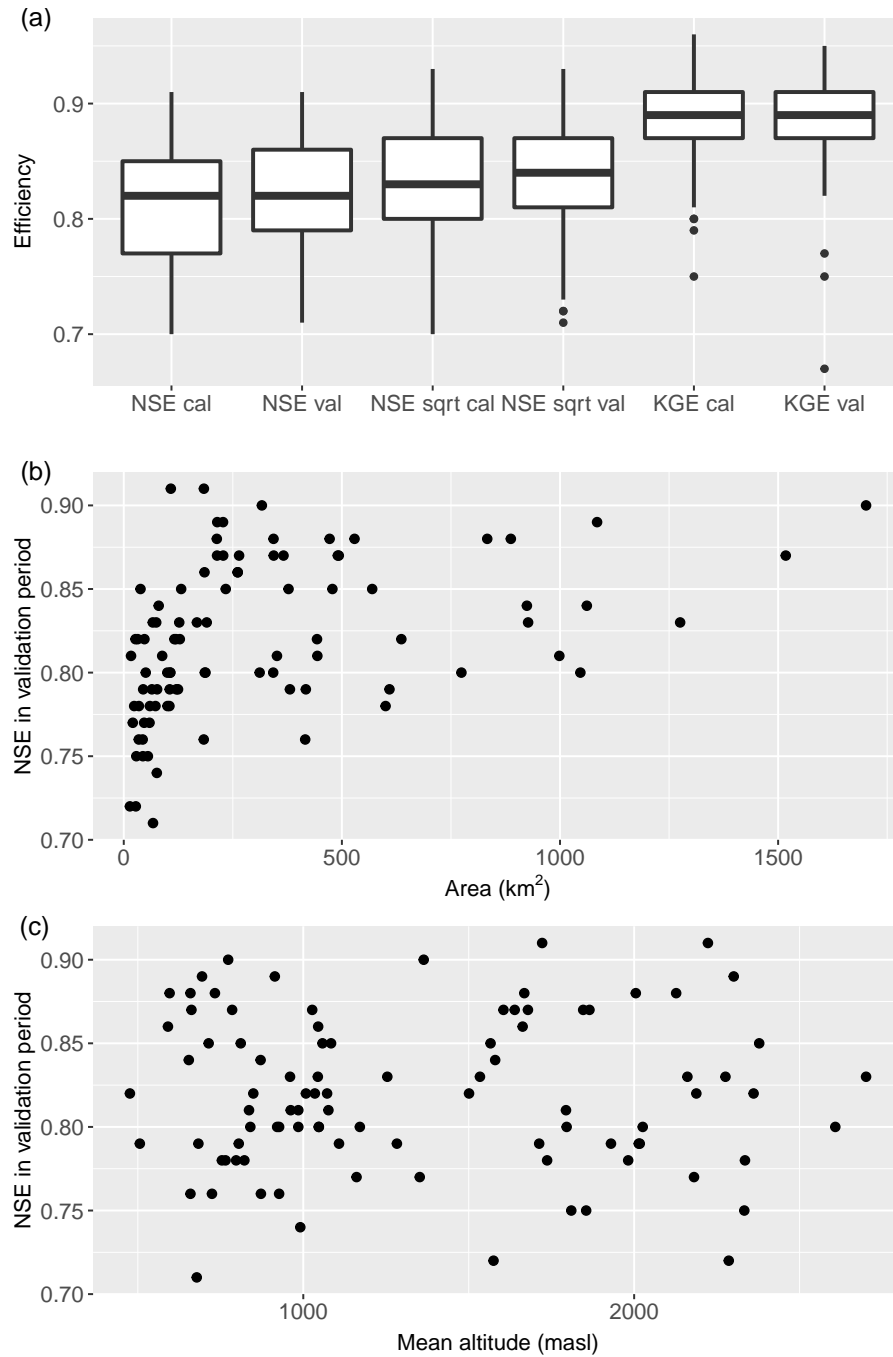


Figure 2.2: Performance of PREVAH for 93 catchments. Performance measures for calibration (cal) and validation (val) periods among all catchments (a), relation of the NSE in the validation period to catchment area (b), relation of NSE in the validation period to mean altitude of the catchment (c).

A visual comparison of the regimes yields the following results: The simulated regimes follow the seasonal cycle of the observed regimes in all catchments. However, patterns of seasonal over- and/or underestimations can be found. For the glaciated catchments Rosegbach and Kander, autumn runoff driven by the CH2018 scenarios is slightly overestimated compared to observations. Such an overestimation can also be found in other glaciated catchments (see Figures A.1-A.8). The Hydro-CH2018-Runoff ensemble slightly underestimates runoff in late spring in the snowmelt-driven river Plessur. The pluvial catchment Emme shows a slight overestimation in winter in the reference period of the Hydro-CH2018-Runoff ensemble. In the southern alpine river Verzasca, the Hydro-CH2018-Runoff simulations miss the peak in spring likely due to missing snowmelt intensity. Such a bias between the Hydro-CH2018-Runoff simulations and the observations in spring is found in 6 of the southern alpine catchments (Figures A.1-A.8).

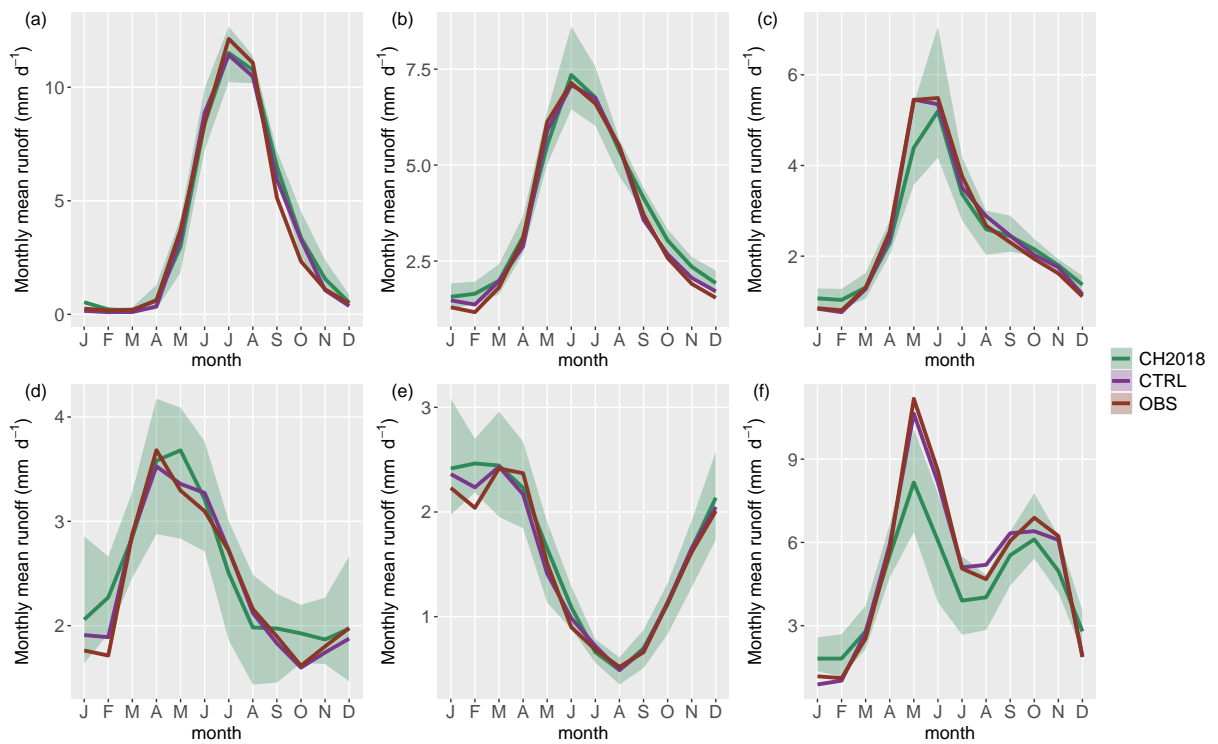


Figure 2.3: Runoff regimes of six representative catchments for observations (OBS, red) for 1985-2014, control simulations with calibrated parameters (CTRL, purple) for 1985-2014, and simulations driven by the CH2018 scenarios (CH2018, green) for the reference period 1981-2010 (RCP8.5) for Rosegbach - Pontresina (a), Kander - Hondrich (b), Plessur - Chur (c), Emme - Emmenmatt (d), Venoge - Ecublens (e), Verzasca - Lavertezzo (f).

2.5 Data availability and remarks on the uncertainty

This study provides daily runoff simulations for 93 Swiss catchments and a total of 68 GCM-RCM combinations covering three different emission scenarios: RCP2.6, RCP4.5, RCP8.5. The daily simulations as well as monthly, seasonal, and yearly means are available for each catchment and GCM-RCM combination under doi: <http://doi.org/10.5281/zenodo.3937485> (Muelchi et al., 2020). Since some of the GCM-RCM combinations are available for different resolutions (EUR-11 and EUR-44), the usage of the higher resolution (EUR-11) is recommended (see Table A.2) resulting in a reduced ensemble of 46 GCM-RCM combinations. This avoids giving double weight to single model combinations in the calculation of ensemble statistics.

The Hydro-CH2018-Runoff dataset consists of runoff simulations based on the CH2018 climate change scenarios for Switzerland and represent the most up to date simulations for meso-scale rivers in Switzerland. Nevertheless, different sources of uncertainty have to be considered. First, the post-processing and downscaling of the climate model output with quantile mapping assumes stationary model biases. Second, stationarity is assumed for calibration i.e., that the calibrated parameters still hold for conditions under climate change. Third, the Hydro-CH2018-Runoff ensemble was created using only one hydrological model. A comparison for some catchments with the results of two other hydrological models (PREVAH-WSL and HBV-light) showed a strong agreement on the climate change signal in the runoff among the hydrological models (not shown here). However, the magnitude of change can vary, particularly in summer and autumn in highly glaciated catchments. This is mainly due to the different handling of glacier retreat and glacier melt modelling. Similar differences between models in glaciated catchments were also found in a previous study by Addor et al. (2014).

2.6 Conclusions and outlook

A total of 93 catchments distributed across Switzerland covering many different catchment characteristics were successfully calibrated and show satisfactory performance both in terms of NSE and KGE and in terms of reproduction of the runoff regimes. Runoff simulations for these catchments were then fed with the CH2018 high-resolution climate change scenarios for Switzerland. For the first time, transient 119-year long daily runoff simulations are available for a large ensemble of climate models and the underlying RCP2.6, RCP4.5, and RCP8.5 emission scenarios.

The Hydro-CH2018-Runoff data set allows for a comprehensive assessment of climate change impacts on the runoff in Switzerland. The simulations can be analyzed for potential changes in runoff indicators and for their timing. The results of such an assessment can be further used as a basis for adaptation planning and negotiating mitigation action. The use of the Hydro-CH2018-Runoff data set is not restricted to hydrological assessments, but the data can also be used for impact studies in other sectors such as agriculture, energy production, ecology, etc.

2.7 Acknowledgements

Authors would like to acknowledge funding of the Swiss Federal Office for the Environment under the project Hydro-CH2018. We would also like to thank the developers of the calibration software PEST. We thank Harry Zekollari, MeteoSwiss and FOEN for providing the necessary data for this study. Calculations were performed on UBELIX (<http://www.id.unibe.ch/hpc>), the HPC cluster at the University of Bern.

Chapter 3

Future runoff regime changes and their time of emergence for 93 catchments in Switzerland

This chapter contains a manuscript that has been written together with Ole Rössler, Jan Schwabeck, Rolf Weingartner, and Olivia Martius. The manuscript has been submitted under the title "Future runoff regime changes and their time of emergence for 93 catchments in Switzerland" in Hydrology and Earth System Sciences (Muelchi et al., in review 2020c).

3.1 Abstract

Assessments of climate change impacts on runoff regimes are essential for adaptation and mitigation planning. Changing runoff regimes and thus changing seasonal patterns of water availability have strong influence on various sectors such as agriculture, energy production or fishery. In this study, we use the most up to date local climate projections for Switzerland (CH2018) that were downscaled with a post-processing method (quantile mapping). This enables detailed information on changes in runoff regimes and their time of emergence for 93 rivers in Switzerland under three emission pathways RCP2.6, RCP4.5, and RCP8.5.

Changes in seasonal patterns are projected with increasing winter runoff and decreasing summer and autumn runoff. Spring runoff is projected to increase in high elevation catchments and to decrease in lower lying catchments. Despite strong increases in winter and partly in spring, the yearly mean runoff is projected to decrease in most catchments. Results show a strong elevation dependence for the signal and magnitude of change. Compared to lower lying catchments, runoff changes in high elevation catchments (above 1500 masl) are larger in winter, spring, and summer due to the strong influence of reduced snow accumulation and earlier snow melt as well as glacier melt. Under RCP8.5 (RCP2.6) and for catchments with mean altitude below 1500 masl, average relative runoff change in winter is +27% (+5%), in spring -5% (-

6%), in summer -31% (-4%), in autumn -21% (-6%), and -8% (-4%) throughout the year. For catchments with mean elevation above 1500 masl, runoff changes on average by +77% (+24%) in winter, by +28% (+16%) in spring, by -41% (-9%) in summer, by -15% (-4%) in autumn, and by -9% (-0.6%) in the yearly mean. The changes and the climate model agreement on the signal of change increase with increasing global mean temperatures or stronger emission scenarios. This amplification highlights the importance of climate change mitigation. Under RCP8.5, early times of emergence in winter (before 2065; period 2036-2065) and summer (before 2065) were found for catchments with mean altitudes above 1500 masl. Significant changes in catchments below 1500 masl emerge later in the century. However, not all catchments show a time of emergence in all seasons and in some catchments the detected significant changes are not persistent over time.

3.2 Introduction

Anthropogenic climate change is unequivocal and will affect regional and local hydrology (IPCC, 2013, 2014a,b). Thanks to major research efforts, projections of regional and local temperature and precipitation changes became more precise and more reliable. The new Swiss Climate Change Scenarios (CH2018) are the result of a large modelling effort to downscale regional climate projections to local scales for Switzerland (CH2018, 2018). The projected warming in Switzerland will likely be stronger than the global mean warming: Without major mitigation efforts, mean temperatures are projected to increase by up to 6.8°C by end of the 21st century in Switzerland under a RCP8.5 scenario. This strong increase in temperatures is accompanied by changes in many other hydrologically relevant variables such as precipitation amounts, precipitation type (snow vs. rain), and glacier volumes. The projected combination of increasing temperatures, changing precipitation patterns, retreating glaciers, and changes in snowpack potentially has a strong impact on runoff regimes. Runoff regimes reflect the integral response in time and space of the hydrological conditions within a catchment and hence water supply. Understanding and assessing changes in runoff regimes is crucial for many different sectors such as agriculture, fishery, hydropower generation, and tourism. Assessments of climate change impacts on river runoff are therefore particularly important for decision makers in terms of adaptation planning but can also serve as a basis for mitigation policies.

Several studies on climate change impacts on the hydrology in Switzerland have been conducted in recent years focussing on changes in runoff regimes (Horton et al., 2006; Köplin et al., 2012, 2014a; Addor et al., 2014; Milano et al., 2015), on changes in low flows (Jenicek et al., 2018; Brunner et al., 2019a,b), on changes in high flows (Keller et al., 2018; Brunner et al., 2019a), or on glaciated catchments (Huss et al., 2008; Farinotti et al., 2012; Huss et al., 2014; Fatichi et al., 2015; Etter et al., 2017). Studies on climate change impacts on different aspects of the hydrology in the Alpine area have also been carried out in Austria (e.g., Hanzer et al., 2018; Wijngaard et al., 2016; Prasch et al., 2011; Weber et al., 2010; Tecklenburg et al., 2012), in Italy

(e.g., Groppelli et al., 2011), in Germany (e.g., Hattermann et al., 2015; Nilson et al., 2014), and in France (e.g., Ruiz-Villanueva et al., 2015; Vidal et al., 2016). Most of these studies are case studies or focus on selected aspects of the hydrology. Previous studies focusing on changes in runoff regimes and including many catchments with different properties in Switzerland (Horton et al., 2006; Köplin et al., 2012, 2014a; Addor et al., 2014) found a shift in seasonality with increasing winter runoff, decreasing summer runoff, unchanging yearly mean runoff for lower lying catchments and strongly increasing yearly mean runoff for high alpine catchments. However, these studies are either based on older climate model generations or on climate simulations downscaled with a delta change approach. This approach does not capture changes in variability and the transient properties of climate change. More sophisticated downscaling approaches such as quantile mapping (Teutschbein and Seibert, 2012; Gudmundsson et al., 2012) have been developed. They not only correct for the mean bias but for the full distribution and are applicable to long-term climate simulations and allow establishing transient scenarios. Using quantile mapping as downscaling approach can result in partly different runoff characteristics. This has been shown for one test catchment by Rössler et al. (2019). Therefore, the present study is based on the Hydro-CH2018-Runoff ensemble (Muelchi et al., 2020, in review 2020a) run with the most up to date local climate change scenarios for Switzerland (CH2018), which used the quantile mapping approach to downscale the coarse climate model output. The Hydro-CH2018-Runoff ensemble includes transient daily simulations (1981-2099) for 93 catchments in Switzerland and three different greenhouse gas (GHG) concentration pathways: RCP2.6, RCP4.5, and RCP8.5. The new ensemble allows for a detailed quantification of changes in runoff regimes. In this study, we investigate changes in runoff regimes and their seasonality under different RCP scenarios. The transient property of the simulations enables the estimation of the time of emergence of those changes. The time of emergence reflects the time when the climate signal emerges significantly from natural variability and is of particular importance to the question of how much time is left for adaptation planning. In this study, we not only analyse the time of emergence but also its evolution over time. Also, the ensemble allows for the quantification of changes by different global warming levels as these warming levels are policy relevant. The framing of the results as a function of global mean temperature change rather than time allows for a direct link to the Paris agreement target providing information on expected changes associated with a +2°C world and the consequences of missing this target. In this study, we assess changes for global warming levels of +1.5°C, +2°C, and +3°C.

3.3 Data

For this study, we use the Hydro-CH2018-Runoff ensemble of daily discharge simulations for 93 medium-sized catchments in Switzerland (Muelchi et al., 2020, in review 2020a). The catchments cover a wide variety of catchment characteristics with different governing hydrological processes distributed all over Switzerland (Figure 3.1). The hydrological modelling system PREVAH (Viviroli et al., 2009) is used for simulating the hydrological response to the climate change sce-

narios. PREVAH is a semi-distributed model based on hydrological response units and includes different submodels to account for important hydrological processes related to snow, glacier, and soil moisture dynamics, as well as evapotranspiration. PREVAH was calibrated and validated for each catchment (for more details see Muelchi et al. (in review 2020a)). The calibrated parameters were kept constant for the simulation of runoff under climate change and the land use was held unchanged for non-glaciated catchments. The minor impact of land use changes on changes in the runoff regime for Switzerland was assessed by Köplin et al. (2014a). For glaciated catchments, glacier extents were updated every 5 years according to the glacier projections by Zekollari et al. (2019) that are based on the same climatic data set. The land use of areas where glaciers disappear was replaced by rock for areas above 3000 masl and by bare soil for areas below 3000 masl.

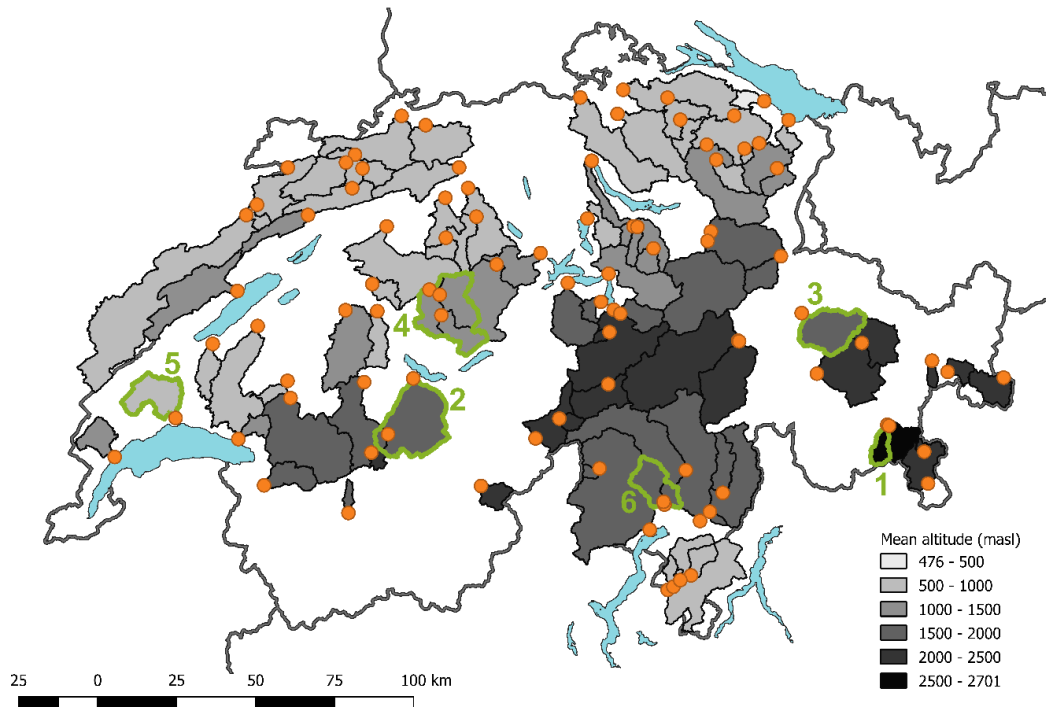


Figure 3.1: Overview of the study region and the location of the gauging stations (orange dots). Shadings indicate mean altitude of the respective catchment. Green contours indicate the six example catchments: Rosegbach – Pontresina (1), Kander – Hondrich (2), Plessur – Chur (3), Emme – Emmenmatt (4), Venoge – Ecublens (5), Verzasca – Lavertezzo (6).

The meteorological input used for the simulations consists of the new Swiss climate change scenarios CH2018 (CH2018, 2018). The CH2018 scenarios used EURO-CORDEX simulations (Jacob et al., 2014; Kotlarski et al., 2014) and applied a statistical downscaling (quantile mapping; Teutschbein and Seibert, 2012; Gudmundsson et al., 2012) on the available chains of Global

Circulation Models and Regional Climate Models (GCM-RCM chains). The results consist of gridded high-resolution (2x2 km) daily temperature and precipitation data for Switzerland for the period 1981-2099. This dataset was then used to drive the hydrological model resulting in the Hydro-CH2018-Runoff ensemble consisting of daily runoff time series for 1981-2099 for each of the GCM-RCM chain. The Hydro-CH2018-Runoff ensemble consists of simulations for three different GHG concentration pathways: 8 simulations under RCP2.6, 16 simulations under RCP4.5, and 20 simulations under RCP8.5. The GCM-RCM chains and their underlying emission scenarios used for this study are listed in Table 3.1. For the analysis of changes in runoff constrained by different warming levels, the global mean temperatures of the driving GCMs (CMIP5, Taylor et al., 2012) were used.

3.4 Methods

3.4.1 Study area

The study area consists of 93 catchments distributed over Switzerland (Figure 3.1) and covering a wide range of catchment characteristics with an average catchment size of 314 km² (range 14-1700 km²) and a mean altitude of 1344 masl (range 476-2700 masl). 22 out of 93 catchments are glaciated with a varying degree of glaciation between 0.2-22%. The present runoff regimes range from glacier fed catchments in high alpine areas, mainly snow driven catchments (mean altitude above 1550 masl) in the Alps and Prealps to rain fed catchments predominant in the Swiss Plateau and at lower elevations in the southern part of Switzerland. Six catchments (highlighted in Figure 3.1) are used as example catchments representing typical runoff regimes: Rosegbach – highly glaciated (22%), Kander – partially glaciated (5%), Plessur – high-alpine snow influenced, Emme – pre-alpine rain and snow influenced, Venoge – lowland rain dominated, and Verzasca – southern-alpine rain and snow dominated. An overview of the catchment characteristics can be found in the Supplement (Table B.1).

3.4.2 Changes in runoff regimes

The simulations are analyzed using yearly and seasonal mean changes under the three RCPs (2.6, 4.5, 8.5). All changes are specified for 30-year periods to remove the inter-annual variability. The reference period covers the years 1981-2010 and is compared with the far future period 2085 (2070-2099). The median among all simulations within an RCP pathway is considered as the best estimate. To get an indication of the robustness of the estimation, the changes are highlighted when at least 90% of the simulations show the same direction of change (positive or negative). For the analysis of changes in runoff regime, monthly means for 30-year periods were calculated with the median representing the best estimate and the uncertainty band showing the full range among all models within an RCP. To simplify the interpretation of the results, this study only focuses on changes by 2085 under RCP8.5 and RCP2.6. These two emission scenarios

reproduce the potential range of changes in the full Hydro-CH2018-Runoff ensemble. Results for the near future period of 2060 (2045-2074) and for RCP4.5 can be found in the Supplement.

3.4.3 Changes with increasing global mean temperatures

For the analysis of changes as a function of global mean temperature change, temperature targets of +1.5°C, +2°C, and +3°C with respect to pre-industrial state were defined. Since the temperature targets are defined with respect to the pre-industrial state, the observed warming between the pre-industrial state (1864-1900) and the reference period (1981-2010) has to be

Table 3.1: List of used GCM-RCM chains, their initial resolution, and the available RCPs.

GCM	RCM	RCP8.5		RCP4.5		RCP2.6	
		EUR-11	EUR-44	EUR-11	EUR-44	EUR-11	EUR-44
ICHEC-EC-EARTH	KNMI-RACMO22E		X		X		
	DMI-HIRMAM5	X		X		X	
	CLMcom-CCLM4-8-17	X		X			
	CLMcom-CCLM5-0-6		X				
	SMHI-RCA4	X		X		X	
MOHC-HadGEM2-ES	CLMcom-CCLM4-8-17	X		X			
	CLMcom-CCLM5-0-6		X				
	KNMI-RACMO22E		X		X		X
	SMHI-RCA4	X		X			X
MPI-M-MPI-ESM-LR	CLMcom-CCLM4-8-17	X		X			
	CLMcom-CCLM5-0-6		X				
	SMHI-RCA4	X		X			X
	MPI-CSC-REMO2009-2	X		X		X	
MIROC-MIROC5	CLMcom-CCLM5-0-6		X				
	SMHI-RCA4		X		X		X
CCCma-CanESM2	SMHI-RCA4		X		X		
CSIRO-QCCCE-CSIRO-Mk3-6-0	SMHI-RCA4		X		X		
IPSL-IPSL-CM5A-MR	SMHI-RCA4	X		X			
NCC-NorESM1-M	SMHI-RCA4		X		X		X
NOAA-GFDL-GFDL-ESM2M	SMHI-RCA4		X		X		

subtracted from the temperature targets. The observed warming is estimated to be 0.6°C and thus the remaining global warming for the 1.5°C , 2°C , and 3°C temperature target is 0.9°C , 1.4°C , and 2.4°C , respectively (Morice et al., 2012; CH2018, 2018, for technical details). For each of the driving GCMs used in the Hydro-CH2018-Runoff ensemble for RCP8.5, we computed differences in moving 30-year averages of global mean temperatures compared to the reference period. The time periods (30-year windows) when global mean temperature change exceed $+0.9^{\circ}\text{C}$, $+1.4^{\circ}\text{C}$, and $+2.4^{\circ}\text{C}$ were selected for each GCM. Subsequently, the seasonal and yearly changes in runoff were extracted for each of the time periods and the driving GCM in the GCM-RCM combination. Again, catchments with robust signals are highlighted, where at least 90% of simulations agree on the signal direction.

3.4.4 Time of emergence of seasonal changes

The time of emergence indicates the time of significant changes in the distribution of the seasonal and yearly means. The Kolmogorov-Smirnov test was used to test whether two 30-year samples of seasonal or yearly means are drawn from the same distribution. This test was conducted on the distributions of moving 30-year windows and the distribution of the reference period. This was done for each simulation under RCP8.5 and each catchment separately. Constraining the analysis to the RCP8.5 ensemble was motivated by the sufficiently large number of simulations (20 simulations) within the ensemble. The time of emergence is then defined as the last year of 30-year moving window where the Kolmogorov-Smirnov test was rejected for the first time at 95% significance. Significance of changes in the seasonal and yearly mean are discussed when at least 66% of the models detect a significant change in the same 30-year window. Since the time of emergence may not be constant in time, we also analyze the temporal evolution of rejections of the null hypothesis (p-values smaller than 0.05).

3.5 Results

3.5.1 Seasonal and yearly mean changes

Changes in the multimodel median of seasonal and yearly mean runoff by end of the century (2085) are shown in Figure 3.2 for RCP8.5 and in Figure 3.3 for RCP2.6 (see Figure B.1 for RCP4.5 and Figures B.2-B.4 for the period 2060). Highlighted catchments show changes where at least 90% of the models agree on the signal of change.

In winter, all catchments show positive mean runoff changes compared to the reference period under RCP8.5 by end of the century (Figure 3.2a). The mean runoff changes range from +2% to +221%, where strongest changes are found in higher elevation catchments. The mean change among all catchments is +48%. 84 out of 93 catchments show strong agreement ($\geq 90\%$) on the signal direction. Under RCP2.6, 87 out of 93 catchments show positive changes with mean runoff changes across all catchments of +13% (Figure 3.3a). However, only 41 catch-

ments show robust model agreement on the signal direction. The range among the catchments is between -3% and +58%, again with stronger changes in the mountainous areas.

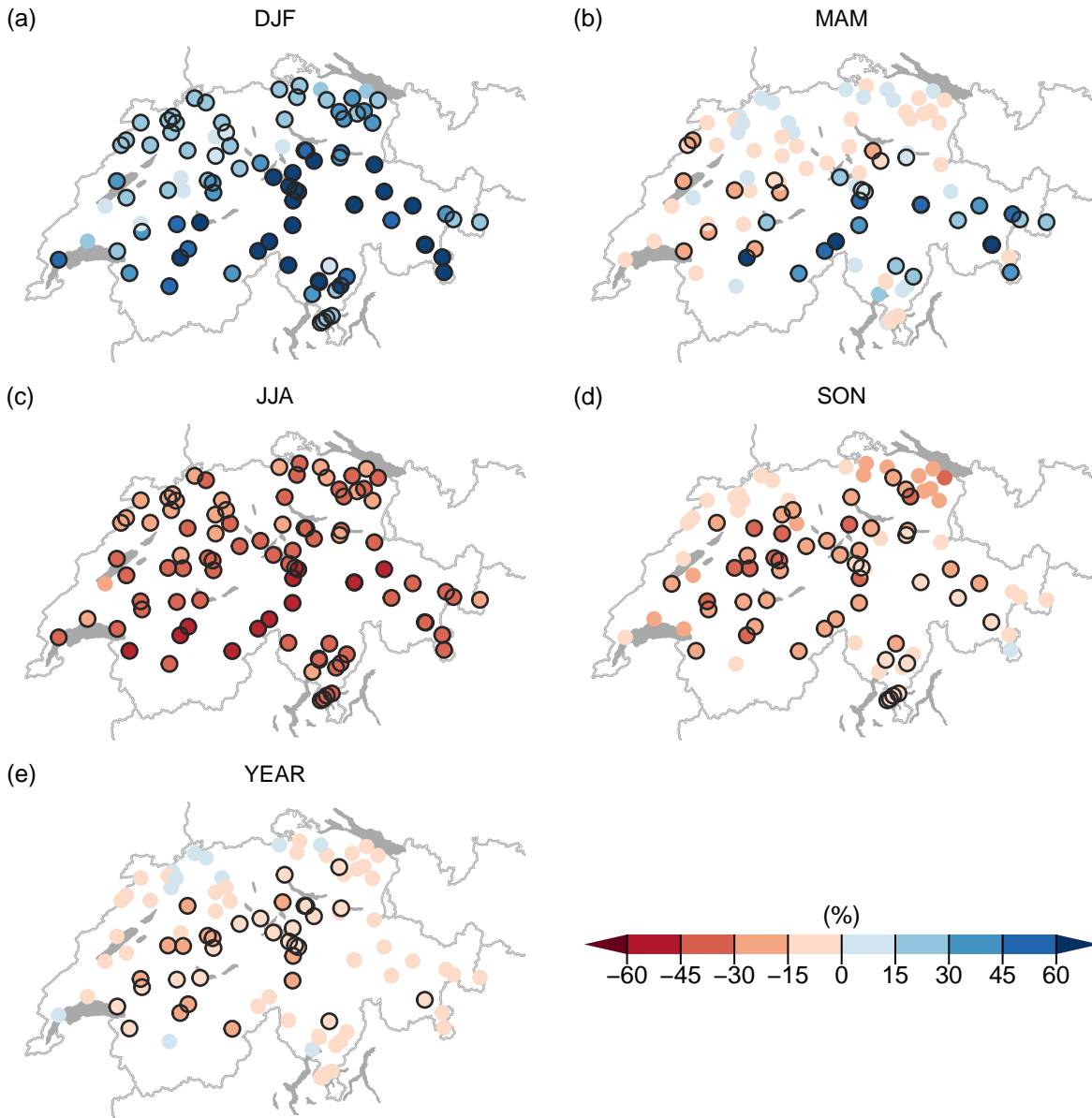


Figure 3.2: Multimodel median of seasonal and yearly mean changes under RCP8.5 by 2085 for winter (a), spring (b), summer (c), autumn (d), and yearly means (e). Black circles indicate changes with at least 90% of the models agreeing on the direction of change

In spring, both positive and negative changes in mean runoff are found (Figures 3.2b and 3.3b). The mean change across all catchments is +9% under RCP8.5 (Figure 3.2b). While most of the lower catchments show a decrease in runoff (up to -21%), the higher elevation catchments exhibit an increase (up to +166%) under RCP8.5. The strong increase in spring runoff is mainly

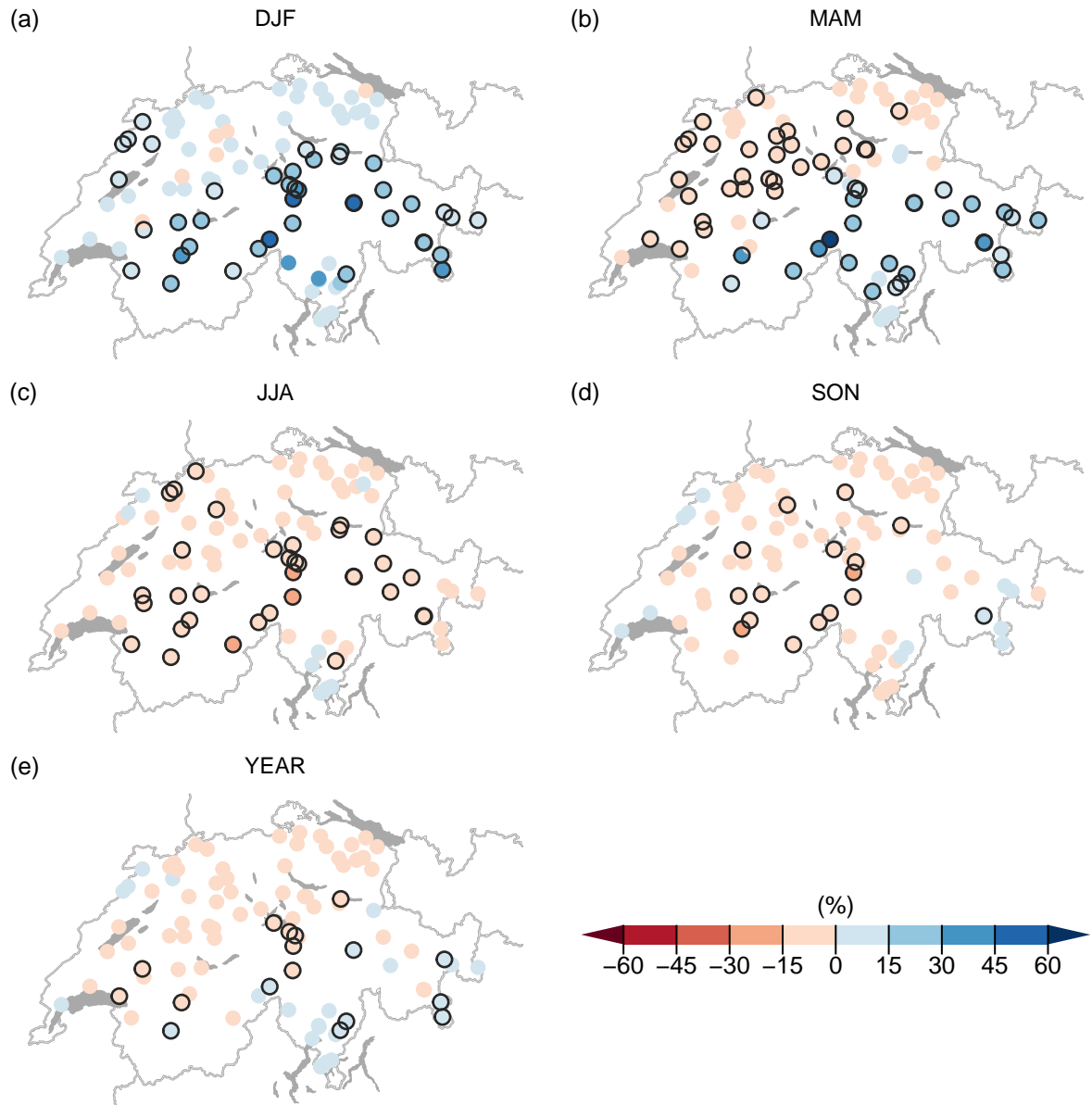


Figure 3.3: Same as Figure 3.2 but for RCP2.6.

found in the highest elevation catchments (Figure 3.2b), where snowmelt is enhanced due to higher temperatures by shifting the snowmelt season from early summer to spring (not shown). However, only 34 out of 93 catchments exhibit robust changes across the climate models. Compared to the high emission scenario, the changes in the low emission scenario (RCP2.6) tend to be more moderate and some catchments change the signal of change from positive changes in RCP8.5 to negative changes in RCP2.6 (Figure 3.3b). Thus under RCP2.6, the changes range from -15% to +70% with a slightly positive mean (+3%) across all catchments. 58 catchments show robust changes in spring mean runoff under RCP2.6.

In summer and under RCP8.5, all catchments show a decrease in mean runoff ranging from -16% to -59% with mean change of -35% across all catchments (Figure 3.2c). Again, stronger changes are found in higher elevation catchments, where summer runoff is projected to decrease by up to half of the runoff of the reference period. Except for one catchment, the agreement on the signal direction among the climate models is robust. Under RCP2.6, the signals and changes are less clear (Figure 3.3c). The average change across all catchments is negative (-6%) but mean runoff change ranges from -26% to +4%. 9 out of 93 catchments show positive but non robust mean runoff changes in summer while 34 catchments yield robust negative signals.

In autumn, all but one catchment show decreasing runoff under RCP8.5 (Figure 3.2d). Changes range from -36% to +4% with an average change of -19% across all catchments. More than 50% of the catchments (50 catchments) reveal robust changes. In contrast to the changes in summer, the autumn runoff tends to decrease stronger in the lower lying catchments than in the higher elevation catchments. Under RCP2.6, the changes are much smaller compared to RCP8.5 with an average change of -5% (ranging from -20% to +10%) (Figure 3.3d). The changes are also less robust with only 17 catchments showing good agreement on the signal of change.

Despite the strong increases in winter and partly in spring, the yearly runoff is projected to decrease by -8% (range: -23% to +4%) under RCP8.5 (Figure 3.2e) and -2% (range: -13% to +11%) under RCP2.6 (Figure 3.3e) on average. While 82 (out of 93) catchments show negative changes under RCP8.5, only 65 catchments yield negative changes under RCP2.6. However, the robustness on the year mean runoff change signal is weaker than for the seasonal mean changes.

Considering the results above, the changes in seasonal and yearly mean runoff are strongly dependent on the mean elevation of the catchment. This dependence is highlighted in Figure 3.4 where changes in runoff are plotted against mean altitude of the catchments. The higher elevation catchments generally show stronger changes in winter, spring, and summer compared to the lower elevation catchments. For autumn and yearly runoff, no distinct pattern can be seen. Under RCP8.5 and for catchments with mean altitude below 1500 masl, average relative change is +27% in winter, -5% in spring, -31% in summer, -21% in autumn, and -8% in the

yearly mean (Figure 3.4a). For catchments with mean elevation above 1500 masl, runoff changes on average by +77% in winter, by +28% in spring, by -41% in summer, by -15% in autumn, and by -9% in the yearly mean. However, the changes in the higher elevation catchments are less pronounced under RCP2.6 with an average change in catchments below 1500 masl of +5% in winter, -6% in spring, -4% in summer, -6% in autumn, and -4% in yearly mean runoff (Figure 3.4b). In higher elevated catchments (>1500 masl), the mean changes under RCP2.6 amount to +24% in winter, +16% in spring, -9% in summer, -4% in autumns, and -0.6% in the year.

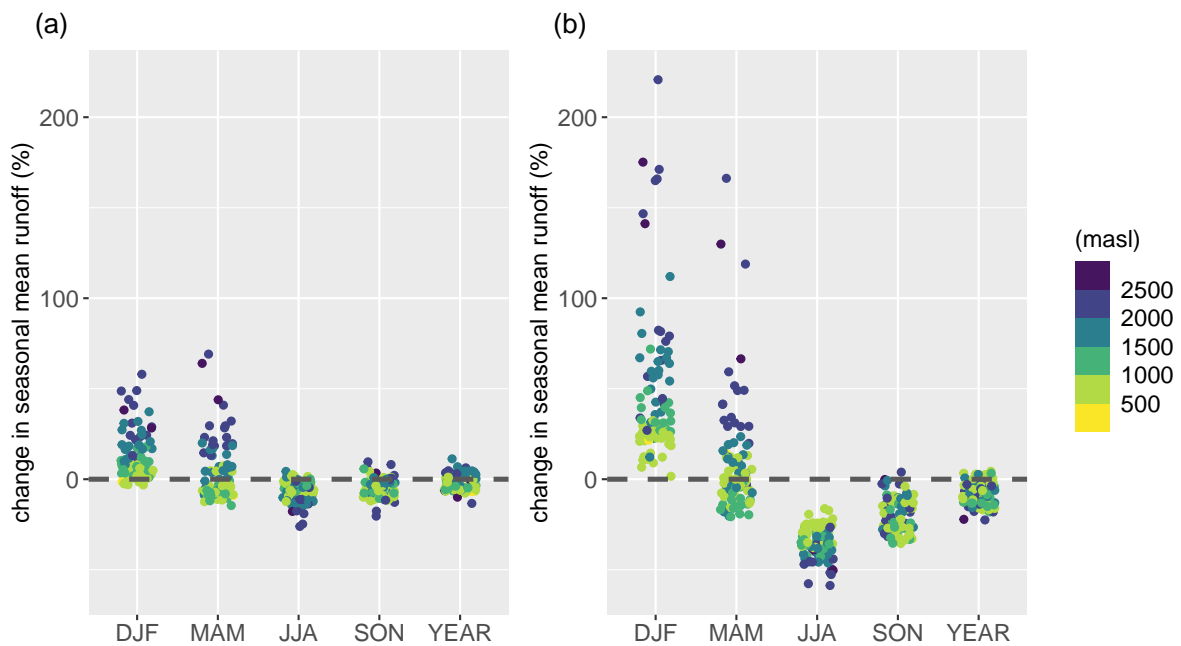


Figure 3.4: Elevation dependence of the multimodel median (dots) of seasonal and yearly mean changes by 2085 under RCP2.6 (a) and RCP8.5 (b). Colours indicate the mean altitude of the 93 catchments.

3.5.2 Changes in the runoff regime

Changes in runoff regime for six example catchments representing typical runoff regime types in Switzerland: Rosegbach – Pontresina, Kander – Hondrich, Plessur – Chur, Emme – Emmenmatt, Venoge – Ecublens, and Verzasca – Lavertezzo (highlighted catchments in Figure 3.1) are depicted in Figure 3.5. Again, results for RCP4.5 can be found in the Supplement (Figure B.5). The runoff regimes with absolute monthly mean runoff presented in this chapter help to interpret the relative changes of seasonal and yearly runoff means discussed in section 4.1.

The glaciated catchment Rosegbach-Pontresina exhibits strong changes in all months under RCP8.5 (Figure 3.5a). The typical glacier runoff regime with low flows in winter and peak flows

in summer in the reference period changes to a more nival type regime with a peak runoff in late spring and early summer under RCP8.5 (Figure 3.5a). While there are strong relative (percent) increases in the winter months, the contribution of winter runoff to the total runoff remains small. The mean runoff between June and September drops dramatically due to missing snow and glacier melt contributions. However, runoff in late spring and summer remains the major contributor to the yearly volume. Under RCP2.6, the changes for winter, spring, and autumn runoff are small. In summer and early autumn, the runoff decreases significantly, and the summer peak shifts from July/August to June/July. The change in summer runoff under RCP2.6 is approximately halved compared to the changes under RCP8.5.

A similar behavior with a shift of the peak in the runoff regime from summer to late spring/early

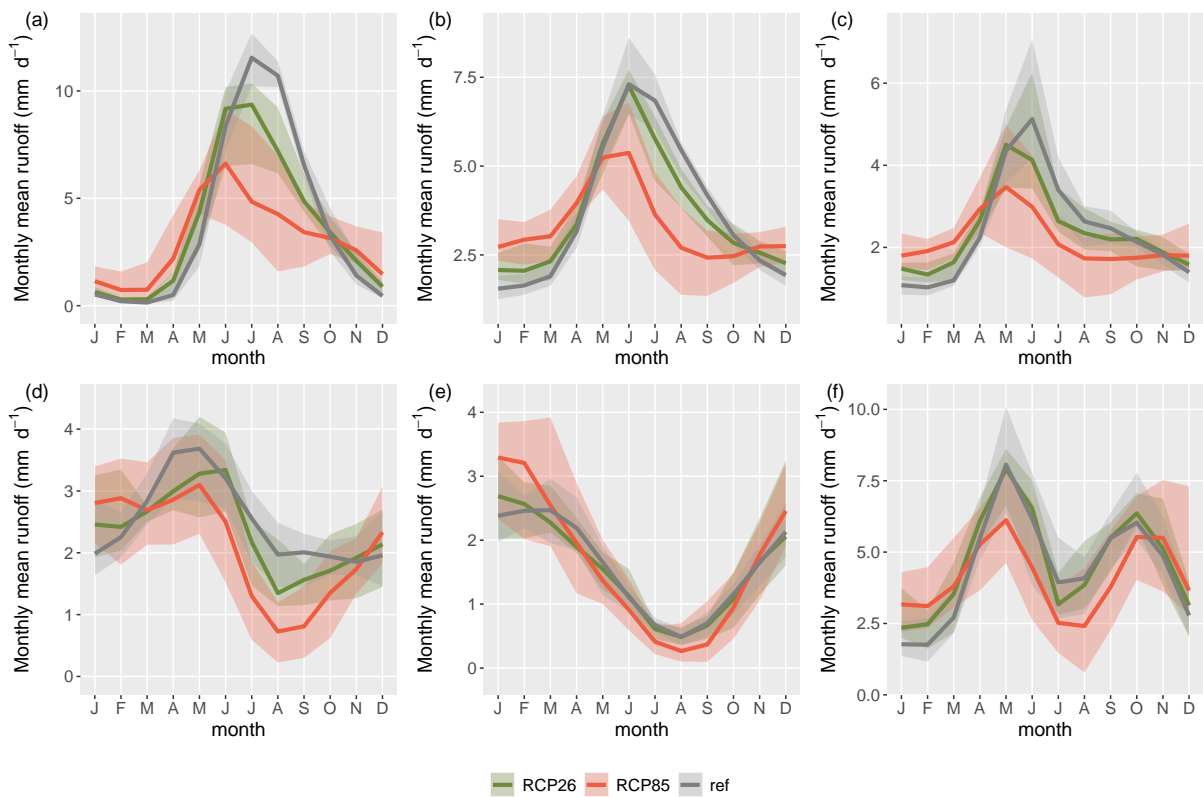


Figure 3.5: Runoff regimes for the six representative catchments Rosegbach (a), Kander (b), Plessur (c), Emme (d), Venoge (e), and Verzasca (f). Thick lines represent the multi-model median for the reference period (grey), for 2085 under RCP2.6 (green), and for 2085 under RCP8.5 (red). Shadings show the full model range for each RCP.

summer is also found for the runoff regime in the partially glaciated catchment Kander – Hondrich under RCP8.5 (Figure 3.5b). The regime is characterized by a strong peak in early summer runoff in the reference period. Under RCP8.5, the summer runoff decreases significantly while winter runoff increases. This leads to a flattening of the runoff regime curve resulting in similar importance of winter and summer runoff with respect to the yearly volume. Under RCP2.6,

there is also a decrease in July, August, and September, but less pronounced compared to the decrease under RCP8.5.

The nival regime of the river Plessur-Chur also experiences a shift in peak flow from June to May under both emission scenarios (Figure 3.5c). Due to the increase in winter and decrease in summer runoff, the regime curve flattens under RCP8.5. The results also show increasing winter runoff and decreasing summer runoff under RCP2.6 but far less pronounced than under RCP8.5.

In the reference period, the runoff regime in the pluvial catchment Emme – Emmenmatt shows a peak in spring and early summer due to snowmelt and stable mean runoff from August to February (Figure 3.5d). By end of the century under RCP8.5, the peak runoff in spring almost disappears. The runoff decreases strongly in the summer months and less strongly in the autumn months.

The shape of the runoff regime curve of the river Venoge – Ecublens remains the same for the reference period and the two emission scenarios with higher runoff in winter and lower runoff in summer (Figure 3.5e). While the regime changes only marginally under RCP2.6, the amplitudes under RCP8.5 becomes more distinct with higher winter runoff and lower summer runoff than in the reference period. However in comparison to other catchments this change is smaller.

The southern alpine catchment Verzasca – Lavertezzo shows a two peaked runoff regime with a first runoff peak in late spring and a second runoff peak autumn in the reference period (Figure 3.5f). This pattern is still present by end of the century under both scenarios. However, the amplitude of the peaks is less pronounced under RCP8.5 because of increasing winter runoff and decreasing spring and summer runoff.

Summarizing the differences under RCP8.5 and RCP2.6 shows that the signal of change under RCP2.6 is in almost all months and catchments equal to the signal under RCP8.5. Comparisons with RCP4.5 (see Figure B.5 in the Supplement) show that the magnitude of changes increases the stronger the emission scenario and the more distant in time. Also, the model agreement on the direction of change among the climate models is weaker under the low emission scenario RCP2.6 than under RCP8.5.

3.5.3 Time of emergence

The time of emergence when at least 66% of the models (under RCP8.5) agree on significant changes in the distribution of seasonal and yearly means is depicted in Figure 3.6. In winter, 45 out of 93 catchments show a time of emergence in the 21st century i.e., a significant change in mean flow (Figure 3.6a). An elevation dependence can be identified with an earlier time of

emergence in higher elevated catchments and a later time of emergence in lower lying catchments. Particularly the high alpine catchments show an early time of emergence with 2046 (period 2017-2046) as the earliest time of emergence. The mean altitude of catchments with a time of emergence earlier than 2065 is greater than 1500 masl (with one exception). Among the 48 catchments that do not show a time of emergence, 46 catchments have a mean altitude lower than 1200 masl.

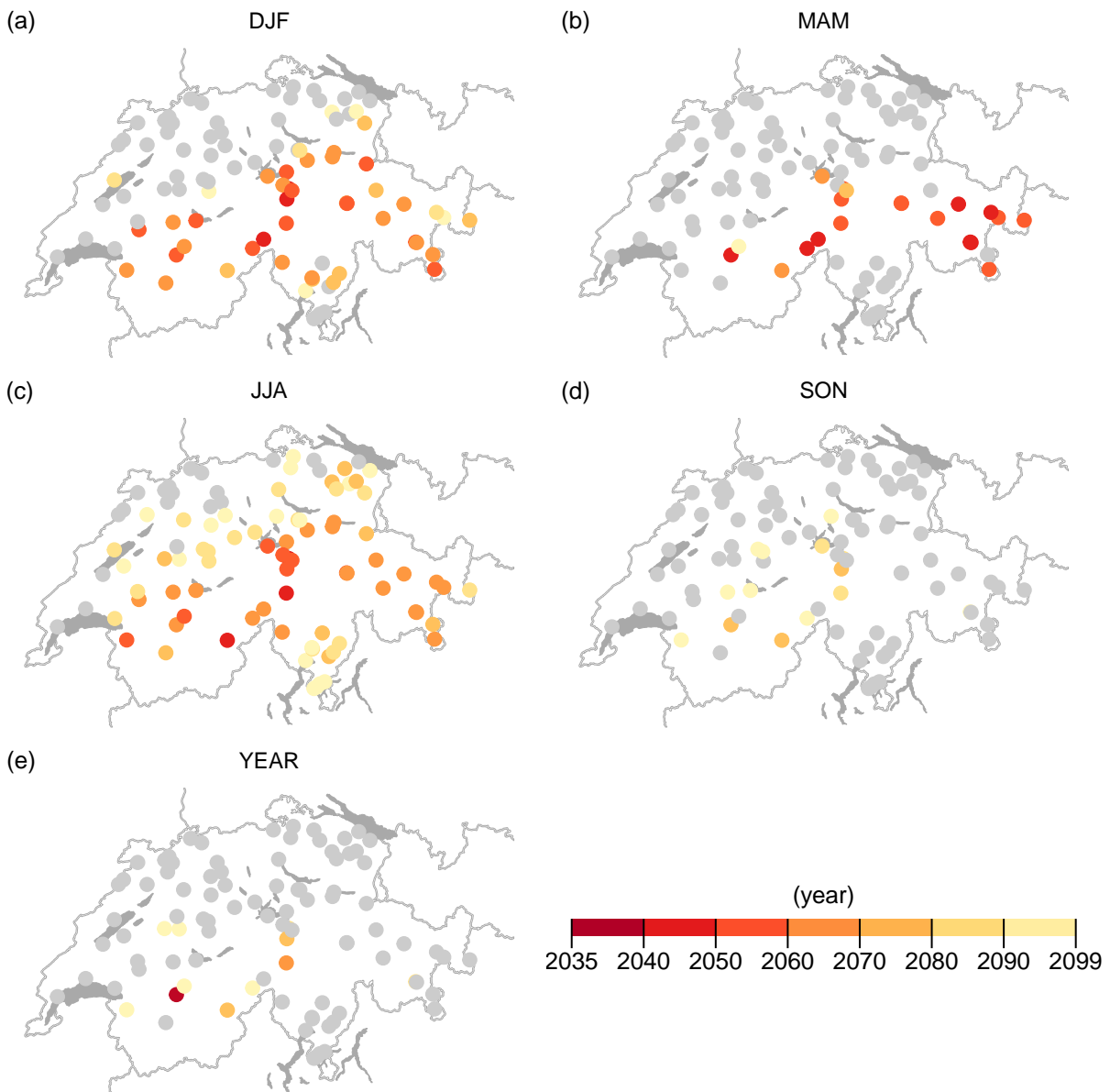


Figure 3.6: Time of emergence for winter (a), spring (b), summer (c), autumn (d), year (e) when at least 66% of the models agree on significant changes in the distribution of seasonal and yearly means.

In summer, 73 catchments exhibit a time of emergence and again generally an earlier time of emergence for higher elevation catchments (Figure 3.6c). Catchments showing a time of emergence earlier than 2065 are all located in mountainous area with mean altitudes higher than 1500 masl (again with one exception). The earliest time of emergence in summer is found for the year 2043 (period 2014-2043). Catchments without time of emergence show a mean elevation lower than 1000 masl (with one exception).

In spring, only 20 catchments exhibit a time of emergence (Figure 3.6b). Again, significant changes in the distribution is mainly found in the higher alpine catchments (above 1500 masl). 14 catchments (out of 93) exhibit a time of emergence in autumn (Figure 3.6d). In contrast to the other seasons, there is no clear elevation pattern distinguishable in autumn. For the yearly means, 11 catchments reveal a time of emergence in the 21st century (Figure 3.6e). Time of emergence in the yearly mean is not restricted to high alpine catchments but only two catchments below 1500 masl show significant changes (after 2095).

In all seasons, some of the catchments do not show a time of emergence, meaning that there is no statistically significant change in the distribution of the seasonal means. Clear patterns of significant changes in the distribution of seasonal means is mainly found in winter and summer. Due to the definition of time of emergence as the last year of a moving window where the Kolmogorov-Smirnov test is rejected for the first time, the time of emergence is not necessarily persistent over time. Figure 3.7 shows the temporal evolution of the time of emergence for the different seasons under RCP8.5. Most of the catchments show persistent significant changes after the first detection of a time of emergence. However, there are some catchments revealing a time of emergence in a certain period, but not showing a time of emergence afterwards. The problem of non-constant rejections affects 17 catchments in winter, 3 catchments in spring, 25 catchments in summer, and 6 catchments in autumn. Most of these catchments show a persistent time of emergence for the rest of the century few years after the first detection. However, this may lead to too early detections of time of emergence but not persistent in time.

3.5.4 Changes in seasonal means with warming levels

Changes in the multi-model median of seasonal and yearly mean runoff for different global warming levels is shown in Figure 3.8 for warming targets +1.5°C, +2°C, and +3°C. Generally, the pattern of change with global warming levels are similar than the patterns for the two emission scenarios. The range of change between the catchments as well as the climate model agreement increases with stronger global warming levels.

In winter, the mean runoff change across all catchments is +17% for a global warming of +1.5°C, +23% for +2°C, and +35% for +3°C (Figure 3.8a-c). With stronger global warming not only the mean increases but also the range of change across the catchments. While at +1.5°C global warming the range across all catchments is between -1% and +53%, the range for the +3°C

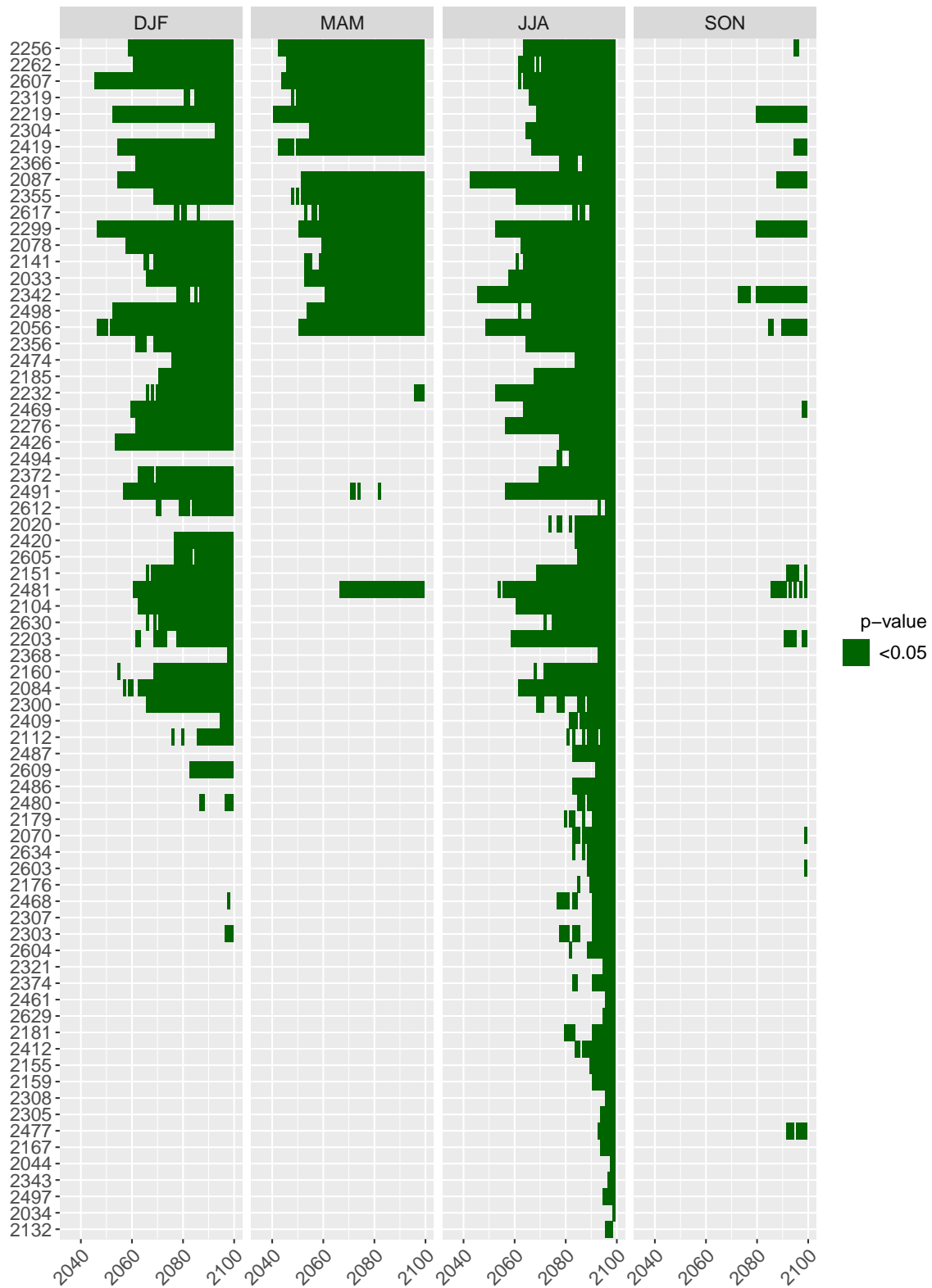


Figure 3.7: Temporal evolution of time of emergence for the different seasons. Periods where p -value of the Kolmogorov-Smirnov test is lower than 0.05 are highlighted. Only catchments with at least one detection of time of emergence in one of the seasons are shown. Catchments are ordered by mean altitude of the catchment with highest altitudes at the top.

global warming is +5% to +127%. While there are two catchments showing slightly negative changes at +1.5°C warming, all catchments show positive changes for stronger warming levels. Also, the agreement across the climate models per catchment increases with increasing warming.

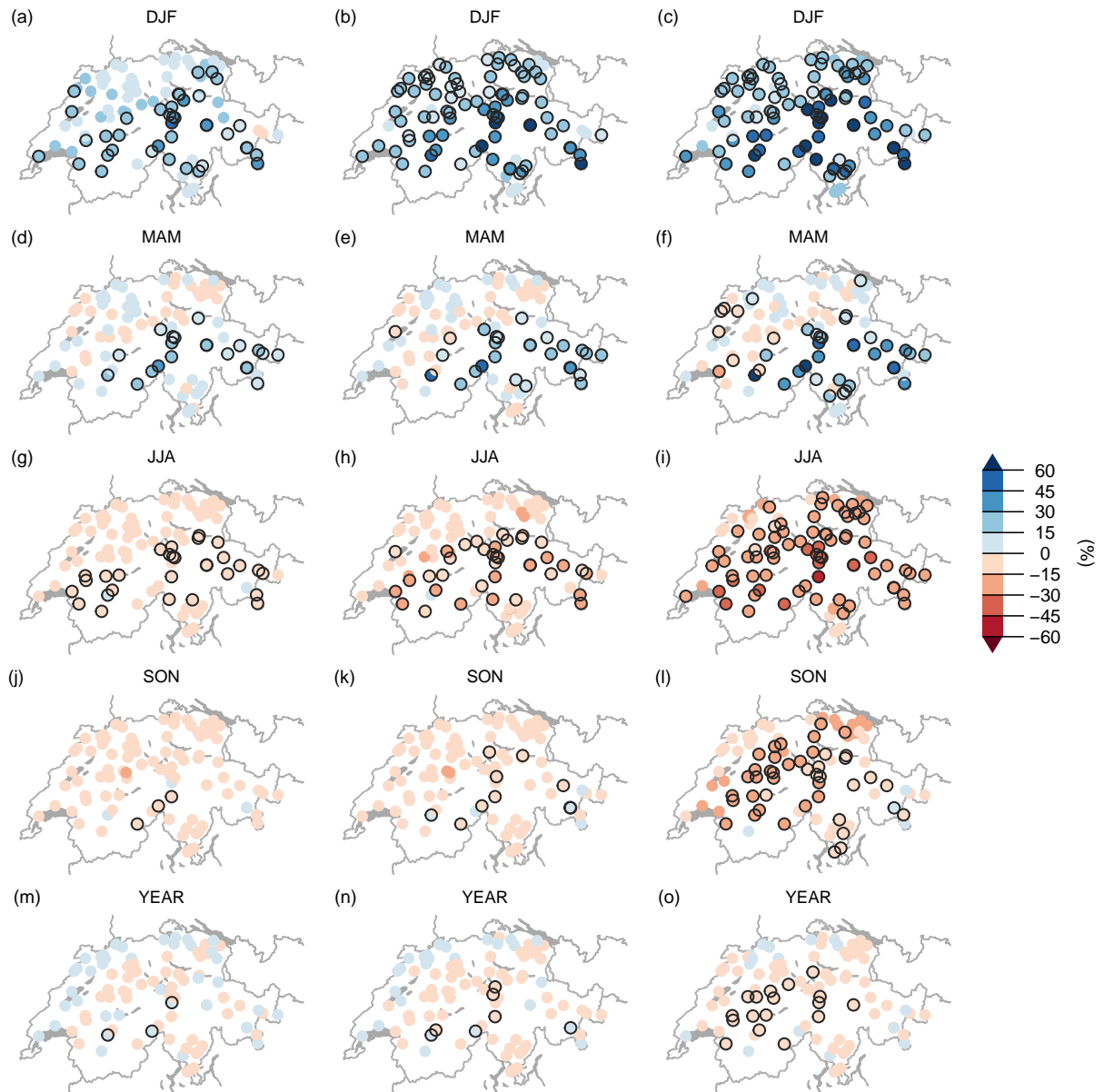


Figure 3.8: Multimodel median of seasonal and yearly mean changes by +1.5°C (left panels), +2°C (middle panels), and +3°C global warming for winter (a-c), spring (d-f), summer (g-i), autumn (j-l), and year (m-o). Black frames indicate changes with at least 90% model agreement for the direction of change.

The mean change in spring runoff among all catchments is +4% for +1.5°C, +6% for 2°C, and +10% for 3°C global warming (Figure 3.8d-f). The changes in spring vary dependent on

the elevation (see results in section 3.5.1) with positive changes mainly for the higher elevated catchments and negative changes for lower lying catchments. Even though the average across all catchments does only change little between warming levels, the range of change across the catchments and the model agreement per catchment increases with strong warming levels and thus the regional (elevation dependent) patterns get more pronounced.

In summer, the average among all catchments is -7% for 1.5°C global warming, -13% for 2°C warming, and -23% for 3°C global warming (Figure 3.8g-j). Again, the ranges across catchments and the model agreement increase with stronger warming levels. Compared to summer, the decrease in autumn runoff is smaller with an average across all catchments of -9% for 1.5°C, -7% for 2°C, and -13% for 3°C global warming. Most catchments (89 out of 93) show a negative multimodel median for both, 1.5°C and 3°C warming levels. While only three catchments show a model agreement of more than 90% for a 1.5°C global warming, there are 43 catchments showing robust model agreement on the direction of change for a 3°C global warming.

For yearly mean runoff, the mean among all catchments is +0.2% for 1.5°C, -0.9% for 2°C, and -3.7% for 3°C. Despite the slightly positive signal for 1.5°C warming, 53 catchments out of 93 show negative changes. This number increases to 66 catchments for 2°C and 77 catchments for 3°C. Also, the model agreement increases from 3 catchments with robust model agreement for 1.5°C to 17 catchments for 3°C.

3.6 Discussion

Winter runoff generally increases in Switzerland due to enhanced winter precipitation and increasing temperatures with climate change (CH2018, 2018). The higher temperatures lead to more liquid precipitation (rain) and less solid precipitation (snow) in winter. This leads to less snow accumulation and thus to more direct runoff in winter. The relative changes in winter in glaciated catchments are very high, but in terms of contribution to the yearly volume still neglectable. In nival and pluvial catchments changes in winter runoff become more important in terms of water availability.

In spring, the glaciated and snow driven catchments show increasing runoff due to enhanced snowmelt (not shown), particularly in early spring. The combination of reduced snow accumulation in winter and earlier snowmelt shifts the peak in runoff regime to a month earlier. Lower lying catchments show decreasing runoff in spring due to reduced snow accumulation in winter and thus reduced available snow for snowmelt.

The summer runoff in Switzerland generally decreases with climate change. This decrease is governed by different processes according to the location and elevation of the catchments. In general, reduced summer precipitation and enhanced evapotranspiration lead to decreasing

runoff in Switzerland (not shown). In high alpine regions, where summer snowmelt and glacier melt dominate the runoff generation in the reference period, the lack of available snowpack and the glacier retreat amplify the decrease in summer runoff. The large model spread in summer in glaciated catchments stems from the sensitivity of the runoff response to the glaciation of the catchment. In catchments, where not all climate projections result in a complete disappearance of glaciers, the model spread increases strongly and future glacier retreat is hence a major source of uncertainty.

Autumn runoff is also projected to decrease due to reduced precipitation and enhanced evapotranspiration (not shown, CH2018, 2018). Again, in catchments where glacier melt is important in early autumn today, this decrease is amplified. However, looking at the regime changes, the decrease in autumn runoff is most noticeable in early autumn, while in late autumn (end of October and November) the changes are less significant and can even change direction to positive values (not shown). This pattern is mainly found in very high alpine catchments, where late autumn precipitation can fall more often as liquid precipitation instead of solid precipitation and thus cannot be stored as snowpack. For the yearly mean, a decrease in runoff emerges in most catchments, however with less robust signals among the climate models. This leads to the conclusion that throughout the year there will be less water available in Swiss rivers. The shift in seasonality and thus a shift in the seasonal availability of water will impact many different sectors.

In most catchments and seasons, the signal of change is the same for the high emission scenario (RCP8.5) and the low emission scenario (RCP2.6). Changes in seasonality or in the runoff regime get amplified by higher emissions and thus by increasing global mean temperatures. This amplification due to enhanced emissions and with intensified global warming shows the large benefits of mitigation. By mitigating climate change and following the RCP2.6 pathway, the magnitude of change can be reduced or even avoided (depending on the season and the runoff regime). However, some of the seasonal changes cannot be avoided by mitigation actions, particularly in high alpine catchments, where glacier retreat is also present (on a smaller magnitude) in the low emission scenario. Responsible planners and policy maker need to adapt to this shift in seasonality.

Previous studies on climate change impacts on the runoff regime in Switzerland (e.g., Köplin et al., 2012, 2014a; Horton et al., 2006) were driven by other emission scenarios, other and fewer climate model chains, different postprocessing methods of the climate model output, and/or different hydrological models and calibration. Despite these differences the signal of change in those studies agrees in most seasons with the signals in this study. A strong elevation dependence of changes was also found by Köplin et al. (2012). The largest difference concerns the yearly mean runoff. Köplin et al. (2012) found an increase (up to +50%) in yearly runoff for high altitude catchments and no change for lower lying catchments in the yearly volume. In contrast, our

study projects a decrease in the yearly mean runoff for high elevation catchments but also for most of the lower lying catchments. However, not all catchments show a robust decrease. This difference between our results and previous studies may arise from the transient property of the simulations, the different handling of glacier melt and the new projections of glacier extents. The Hydro-CH2018-Runoff ensemble uses transient glacier projections which are updated every 5 years in the hydrological model. Köplin et al. (2012) used static glacier projections for 30 years. Strongest uncertainties in glaciated catchments was also found by Addor et al. (2014). Also, the difference in the input data (transient projections versus delta change projections with same baseline time series for the reference period) may add to the different signals.

Even though not all catchments show a time of emergence in the 21st century, early significant changes in the distribution of seasonal means emerge particularly in high elevation catchments. This is due to the importance of snow and glacier melt for alpine runoff regimes. With climate change, the influence of snow and glacier decreases or lacks completely due to higher temperatures and its subsequent glacier retreat. Lower lying catchments show generally a later time of emergence. Köplin et al. (2014a) also assessed a time of emergence for Swiss catchments but only based on significant changes for two scenario periods and 10 climate models. Since their climate models were post-processed with a delta change approach, only the natural variability of the reference period is reflected in their simulations. Despite these differences in methodology and data, they also found earlier time of emergence in winter and summer for high elevation catchments. While the applied definition of time of emergence is commonly used in other climate change studies (e.g., Mahlstein et al., 2011), this definition also has disadvantages. For example, if the rejection of the null hypothesis (two samples are drawn from the same distribution) is unstable in its temporal evolution, the time of emergence may be determined too early. This has been shown for some of the catchments in the present study. However, in most catchments a persistent detection of significant changes in the distribution of the seasonal means has been found shortly after the first detection of significant changes.

Different sources of uncertainty affect our results. Uncertainties arise from all steps of the modelling chain: the scenarios of GHG concentrations, the climate model chains and their boundary and initial conditions, the post-processing method, the hydrological model and its calibration, and the underlying glacier projections.

3.7 Conclusions

Changes in runoff regimes and their time of emergence were assessed with the new hydrological scenarios for 93 catchments in Switzerland. This study is based on the newest generation of climate change scenarios post-processed with more sophisticated methods. Compared to previous studies on runoff regime changes, the results show similar change signals for most seasons. Strongest differences were found for the high elevation catchments which is likely due to the

transient property of the simulations and the implementation of more sophisticated glacier projections.

In general, winter runoff is projected to increase and summer runoff to decrease in Switzerland. The sign of change is robust across catchments, but the magnitude of change is more pronounced for high elevation catchments. Particularly in summer, when snow and glacier melt play an important role in runoff generation, glaciated catchments will face a strong decrease in runoff due the retreating glaciers. In rainfall dominated catchments, the changes are also often robust but on a smaller magnitude. While the higher elevated catchments show increasing spring runoff due to earlier snowmelt, the pluvial catchments in the lowlands will face decreasing spring runoff. A decrease in runoff is also found for autumn and yearly mean runoff in most catchments. These seasonal patterns amplify with global warming and with higher emission scenarios. Also, the model agreement among the climate models is more robust for the stronger the emission scenario and the farther future. Significant changes in the seasonal mean runoff was mainly found in summer and winter and only for few catchments in spring and autumn. Early time of emergence in winter (before 2060) and summer (before 2065) was found for higher elevation catchments above 1500 masl. Significant changes in catchments below 1500 masl emerge later in the century. However, not all catchments show a time of emergence in all seasons.

The amplification of changes by stronger global warming highlights the importance of climate change mitigation. By mitigating climate change and following the RCP2.6 pathway (global warming below 2°C), the magnitude of change can be reduced substantially. The strong decrease in summer runoff in glaciated catchments can be strongly damped but not avoided because glacier retreat is also projected for the low emission scenario. The present study can help to support adaptation planning in various sectors by presenting detailed information on changes in mean runoff.

3.8 Data availability

The data used in this study is available under <https://doi.org/10.5281/zenodo.3937485> (Muelchi et al., 2020).

3.9 Acknowledgements

Authors would like to thank Harry Zekollari, MeteoSwiss, and FOEN for providing the necessary data for this study. We also acknowledge the funding of the Swiss Federal Office for the Environment under the project Hydro-CH2018.

Chapter 4

Moderate runoff extremes in Swiss rivers and their seasonal occurrence in a changing climate

This chapter contains a manuscript that has been written together with Ole Rössler, Jan Schwabeck, Rolf Weingartner, and Olivia Martius. The manuscript has been submitted under the title "Moderate runoff extremes in Swiss rivers and their seasonal occurrence in a changing climate" in *Hydrology and Earth System Sciences* (Muelchi et al., in review 2020b).

4.1 Abstract

Future changes in runoff impact many sectors such as agriculture, energy production, or ecosystems. Therefore, assessments of runoff characteristics under climate change are crucial for decision-makers and water management planners. We study changes in moderate runoff extremes, i.e., low and high flows that occur once every year or season in today's climate. Daily runoff is simulated for 93 Swiss catchments for the period 1981-2099 under the Representative Concentration Pathway RCP8.5 using 20 downscaled regional climate models from the newest transient Swiss climate change scenarios.

The magnitude of moderate annual low flows is projected to decrease in lower lying catchments and to increase in Alpine catchments. Seasonal low flows in summer are projected to decrease and seasonal low flows in winter to increase. Moderate annual high flows are projected to slightly increase in most catchments but to decrease in high Alpine catchments. However, the climate model agreement on the sign of change in moderate high flows is not robust. The projected decrease in Alpine catchments contradicts results for extreme high flows from previous studies. This difference may be due to different indicators used (moderate extremes vs. extremes). The time of emergence indicates the timing of significant changes in the flow magnitudes. For low flows the time of emergence is early in 21st century in high Alpine catchments due

to early changes in winter low flows. In lower lying catchments, significant changes in low flows emerge later in the century. For moderate high flows, only few catchments indicate a significant change.

Shifts in the seasonality of moderate low flows due to climate change are found in many catchments. By end of the 21st century, low flows are projected to occur in late summer and early autumn in most catchments indicating that the lack of precipitation in summer and autumn exceeds the contributions from other processes such as snow and glacier melt contributions. For moderate high flows, changes in seasonality are found in Alpine catchments with a shift towards earlier occurrence in summer due to a reduced contribution of snow and glacier melt in summer. In the projections, low flows occur more frequently in lower lying catchments and less frequently in Alpine catchments. For high flows the frequency increases slightly in most catchments, but models often disagree on the sign of change. Changes in the annual co-occurrence of moderate low and high flows are mainly due to changes in the frequency of low flows that increases in lower lying catchments and decreases in Alpine catchments.

4.2 Introduction

Assessments of climate change impacts on hydrology are crucial for future water management and adaptation planning. This is especially true for extreme events, which potentially have severe ecological and societal impacts. In this study, we focus on moderate runoff extremes in both tails of the runoff distribution: moderate annual and seasonal low and high flows. Focusing on moderate extremes is motivated for several reasons. First, moderate extremes are important for water management planning. Second, very extreme floods and very extreme streamflow droughts are difficult to simulate because many processes are not fully understood or not yet resolved in hydrological models. Third, hydrological models are calibrated on observed flow conditions and may miss plausible but unexperienced extreme events. Fourth, climate change projections incorporate large uncertainties regarding small scale extreme events, particularly for extremes in precipitation, which are potential flood triggers. Therefore, we focus on moderate extremes, i.e., events that occur on average once every year or season in today's climate. The larger sample size (number of events) increases the robustness of the estimated changes.

Low flows have a strong impact on water quality, freshwater ecosystems, and human water use such as power production, drinking water production, irrigation for agriculture, fisheries, and recreation (IPCC, 2014a). Today, long-term water management planning for Switzerland must rely on low flow assessments from past observations. Since climate change is projected to alter low flow characteristics, low flow projections for the 21st century need to be integrated into water management planning. Changes in low flow indicators in the past decades have been already identified in Europe (Stahl et al., 2010) and in Switzerland (Weingartner and Schwanbeck, 2020). For Switzerland, increasing winter low flows and decreasing summer low flows have been

observed in nival (snow-driven) and pluvial (rain-driven) catchments. Low flows in glaciated catchments have increased in all seasons (Weingartner and Schwanbeck, 2020). Previous studies assessed climate change impacts on low flows mainly for macro-scale catchments or regions. van Vliet et al. (2013) investigated low flow changes on a global scale while other studies focused on European scales (e.g., Feyen and Dankers, 2009; Forzieri et al., 2014; Alderlieste et al., 2014; Papadimitriou et al., 2016; Vidal et al., 2016; Marx et al., 2018). For Switzerland, previous climate impact studies on low flows exist for lower lying catchments in the Swiss Plateau (Meyer et al., 2011), for large-scale catchments (Bernhard and Zappa, 2012), and for very extreme (100-year return periods) low flow regimes in aggregated regions (Brunner et al., 2019a). The studies found decreasing low flows in Central Europe but increasing low flows in Alpine areas, where runoff generation is mainly dominated by snow and glacier melt.

High flows may also cause severe damages and significant costs. Hence, potential changes in high flows have to be integrated in water management and infrastructure planning, as well. Assessing future changes in flood magnitude, flood frequency, and flood timing is thus crucial for decision makers. Past events can help to put potential future changes into perspective. Previous studies investigated past trends in floods in Europe (e.g., Stahl et al., 2012; Hall et al., 2014; Mangini et al., 2018; Blöschl et al., 2019; Bertola et al., 2020) and in Switzerland (e.g., Birsan et al., 2005; Allamano et al., 2009; Schmocker-Fackel and Naef, 2010a,b; Castellarin and Pistocchi, 2012). No clear and significant trend in flood magnitude was found in these studies since the studies sometimes disagree on the direction of trends. Various factors make it difficult to compare trends in flood magnitude between catchments and between different studies. The assessments depend heavily on the quality and homogeneity of the observations, the underlying methods such as the selection of indicators or statistical tests, and the investigated time periods. Flood frequencies increased in northern Switzerland and decreased in southern Switzerland in the recent past (Schmocker-Fackel and Naef, 2010a; Blöschl et al., 2019). Periods with many floods were found in the end of the 19th century and after 1968 in northern Switzerland (Schmocker-Fackel and Naef, 2010a). Several assessments of future changes in floods in Switzerland have also been made (Allamano et al., 2009; Köplin et al., 2014b; Beniston and Stoffel, 2016; Ragetti et al., 2019). Even though those studies differ substantially in methodological aspects and catchment selection, they found in general increasing but not necessarily significant changes in annual runoff maxima under climate change. Seasonal patterns of change were detected with increasing winter floods and decreasing summer floods (Allamano et al., 2009). Also, future shifts in the seasonality of floods depend on the regime type of the catchments (Köplin et al., 2014b).

Here we complement these assessments with a focus on moderate low and moderate high flows, i.e., annual or seasonal 7-day runoff minima and daily runoff maxima. The new Hydro-CH2018-Runoff dataset (Muelchi et al., 2020, in review 2020a) is used. It consists of 119-years (1981-2099) long daily runoff simulations driven by the most up to date climate change

scenarios for Switzerland CH2018 (CH2018, 2018). For the RCP8.5 emission pathway (Moss et al., 2010; Van Vuuren et al., 2011), we analyze (1) changes of moderate low and high flows under climate change, (2) the point in time when significant changes emerge, (3) changes in the seasonality of moderate extremes, and (4) changes in the frequency of their (co-) occurrence. In a companion paper, Muelchi et al. (in review 2020c) assessed changes in runoff regimes and their time of emergence. Here, we extend this analysis with assessments of moderate low and high flows. Since both studies are based on the same simulations (Hydro-CH2018-Runoff ensemble), they complement each other and give a comprehensive overview on hydrological changes in Switzerland. They also complement the above mentioned existing studies on future changes in extreme hydrological events.

4.3 Data

We analyse daily runoff simulations for 93 medium-sized (14-1700 km²) catchments distributed in Switzerland and covering a wide range of different runoff regime types including glaciated catchments (22 catchments, glaciation between 0.2-22%), mainly snow driven catchments in the Alpine area, and lower lying catchments mainly driven by precipitation and evapotranspiration. The locations of the catchments are depicted in Fig. 4.1 with six representative catchments highlighted in green. These representative catchments cover the most important regime types in Switzerland (Weingartner and Aschwanden, 1992): Rosegbach – highly glaciated (22%), Kander – partially glaciated (5%), Plessur – Alpine snow influenced, Emme – pre-Alpine rain and snow influenced, Venoge – lowland rain dominated, and Verzasca – southern-Alpine rain and snow dominated.

The data used for the analysis is the Hydro-CH2018-Runoff ensemble consisting of daily mean runoff simulations for each of these 93 catchments (Muelchi et al., 2020, in review 2020a). These simulations were run with the semi-distributed hydrological modelling system “PREcipitation-Runoff-EVApotranspiration HRU Model” (PREVAH Viviroli et al., 2009). PREVAH accounts for important hydrological processes such as evapotranspiration, soil moisture dynamics, snow accumulation, and snow melt. A glacier module was incorporated to account for glacier melt in glaciated catchments. PREVAH was calibrated (even years between 1985-2014) and validated (uneven years between 1985-2014) for each of the 93 catchments individually. Using observed discharge for calibration may put too much emphasis on high flow conditions and potentially overestimates low flow conditions. Therefore, the calibration was simultaneously performed on four observational groups: observed daily discharge measurements, inverted daily discharge, monthly mean runoff, and the annual volume. This ensures good performance for the general catchment response to meteorological forcing as well as for the discharge volume. Also low flows are represented in a satisfactory performance. The hydrological model is driven with daily temperature and precipitation data from the new high resolution (2 by 2 km) climate change scenarios for Switzerland CH2018 (CH2018, 2018) for each catchment separately. In non-glaciated

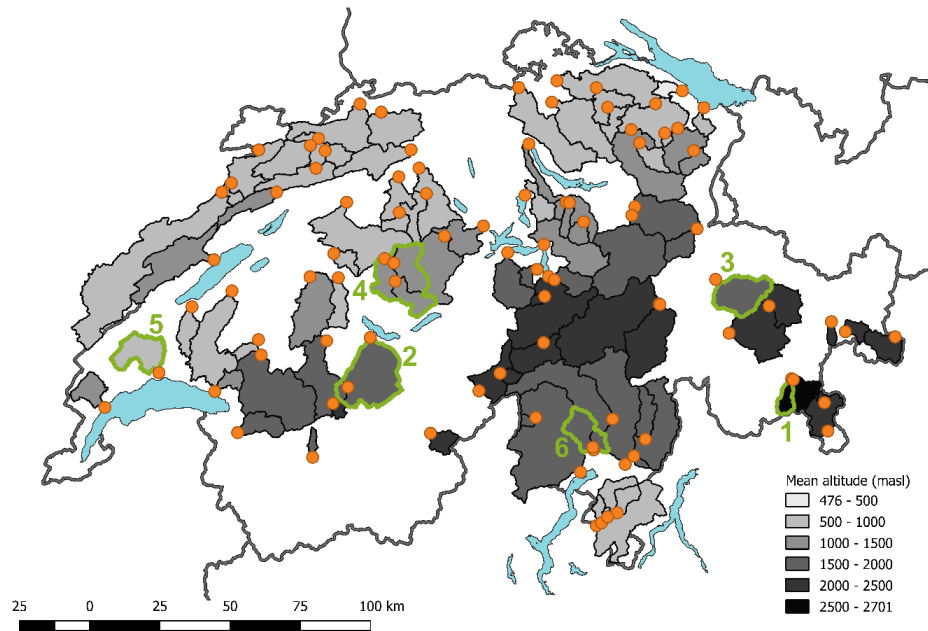


Figure 4.1: Overview of the study region and the location of the gauging stations (orange dots). Shadings indicate mean altitude of the respective catchment. Green contours indicate the six example catchments: Rosegbach – Pontresina (1), Kander – Hondrich (2), Plessur – Chur (3), Emme – Emmenmatt (4), Venoge – Ecublens (5), Verzasca – Lavertezzo (6). (adapted from Muelchi et al., in review 2020c)

catchments the land use was assumed to be constant over the simulation period. In glaciated catchments, the glaciated area was updated every 5 years in line with glacier projections by Zekollari et al. (2019) that were driven by the same climate model chains. Land use in areas where glaciers disappear during the simulation period were replaced by bare soil for areas below 3000 masl and by rock for areas above 3000 masl. The Hydro-CH2018-Runoff ensemble includes simulations for three different emission pathways: RCP2.6, RCP4.5, and RCP8.5. Because the number of available simulations per emission scenario differs, we constrained our analysis to the RCP8.5 pathway (Moss et al., 2010; Van Vuuren et al., 2011) where the largest number of simulations is available. In total, 20 daily simulations under the RCP8.5 emission pathway for the period 1981-2099 are available for each of the 93 catchments. Table 4.1 shows the climate model combinations used in this study.

4.4 Methods

The analysis focuses on moderate low flows and moderate high flows. Several indicators for low flow analysis exist focusing on different properties of low flows (Tallaksen and Van Lanen, 2004). For low flow we use the minimum 7-day moving average runoff (MAM7) within an extended

Table 4.1: Overview of the available climate model chains and their initial grid spacings of 12 km (EUR-11) and 50 km (EUR-44).

Global Climate Model	Regional Climate Model	EUR-11	EUR-44
ICHEC-EC-EARTH	KNMI-RACMO22E		X
	DMI-HIRMAM5	X	
	CLMcom-CCLM4-8-17	X	
	CLMcom-CCLM5-0-6		X
	SMHI-RCA4	X	
MOHC-HadGEM2-ES	CLMcom-CCLM4-8-17	X	
	CLMcom-CCLM5-0-6		X
	KNMI-RACMO22E		X
	SMHI-RCA4	X	
MPI-M-MPI-ESM-LR	CLMcom-CCLM4-8-17	X	
	CLMcom-CCLM5-0-6		X
	SMHI-RCA4	X	
	MPI-CSC-REMO2009-2	X	
MIROC-MIROC5	CLMcom-CCLM5-0-6		X
	SMHI-RCA4		X
CCCma-CanESM2	SMHI-RCA4		X
CSIRO-QCCCE-CSIRO-Mk3-6-0	SMHI-RCA4		X
IPSL-IPSL-CM5A-MR	SMHI-RCA4	X	
NCC-NorESM1-M	SMHI-RCA4		X
NOAA-GFDL-GFDL-ESM2M	SMHI-RCA4		X

season or a year. This indicator is proposed by the Swiss Federal Office for the Environment (FOEN) for low flow statistics. The 30-year average of MAM7 is then considered as moderate low flow and used to assess changes in moderate low flows under climate change. For moderate high flows, we use the 30-year average of the annual maxima per extended season or year as moderate high flow indicator. The seasons are defined as extended summer (May to October) and extended winter (November to April) season. The seasonal distinction is motivated by the fact that winter and summer low flows are governed by different processes and that they have different impacts. The indicators for the annual time window will be referred to as moderate low and moderate high flows while the indicators for the extended winter season and extended summer season will be referred to as the lowest and highest seasonal flows, respectively.

Percent changes are calculated as the relative difference between the 30-year mean of the future period (2070-2099) and the 30-year mean in the reference period (1981-2010) for each simulation. The multi-model median of the relative changes by end of the century is regarded as

the best estimate. To get an indication of the robustness of the projected changes, catchments are highlighted in the Figures when at least 90% of the simulations show the same direction of change (positive or negative).

To evaluate potential changes in the seasonality the day of the year for each event (low flow and high flow) is extracted. Since moderate low flows are calculated from 7-day averages, the last day of the 7-day period is considered as day of low flow event. Median seasonality is then derived by transforming the day of the year into angular values and by applying circular statistics. Finally, the angular values are transformed back to the day of the year.

To assess when significant changes in the distribution of moderate low and high flows occur, the time of emergence is used (Mahlstein et al., 2011). For each simulation, moderate low and high flow magnitude distributions of moving 30-year windows are tested against the 30-year reference period using the Kolmogorov-Smirnov test. The time of emergence is then defined as the last year of the first 30-year moving window where the Kolmogorov-Smirnov test is rejected with a p-value lower than 0.05 (95% significance). We highlight the time of emergence when at least 66% of the models detect a significant change in the same 30-year window for the first time. Note that the time of emergence may not necessarily be stable over time.

Changes in the frequency of moderate low and high flows are quantified by counting years when a pre-defined runoff threshold is exceeded or undercut. We use the median magnitude of moderate low and high flows in the reference period as threshold. For moderate high flows we count years with high flows exceeding this threshold. For low flows we consider years with low flows below the threshold. This was done for each seasonal and annual time window and each simulation separately. Finally, the percentual change in occurrence is calculated. We also investigate the co-occurrence of moderate low and high flows. Co-occurrence is considered when high flows exceeding the reference threshold and low flow undercutting the reference threshold occur in the same time window (year, extended winter, extended summer).

4.5 Results

4.5.1 Future changes in moderate low flows

Median seasonal occurrence of moderate annual low flows is shown in Fig. 4.2 for the reference period (Fig. 4.2a) and by end of the century (Fig. 4.2c). In Alpine catchments, annual low flows occur in late winter or early spring in the reference period. By end of the century, low flows occur in autumn. However, low flows in very high Alpine catchments do not change their seasonality. Median seasonal occurrence of low flows in pre-Alpine catchments shifts from late autumn to early autumn. In southern Alpine catchments, low flows change their median seasonal occurrence from winter and spring to early autumn. No clear change in seasonality is found for

lower lying catchments with low flows occurring in late summer and early autumn. Despite in very high Alpine catchments low flows occur between August and October by end of the century.

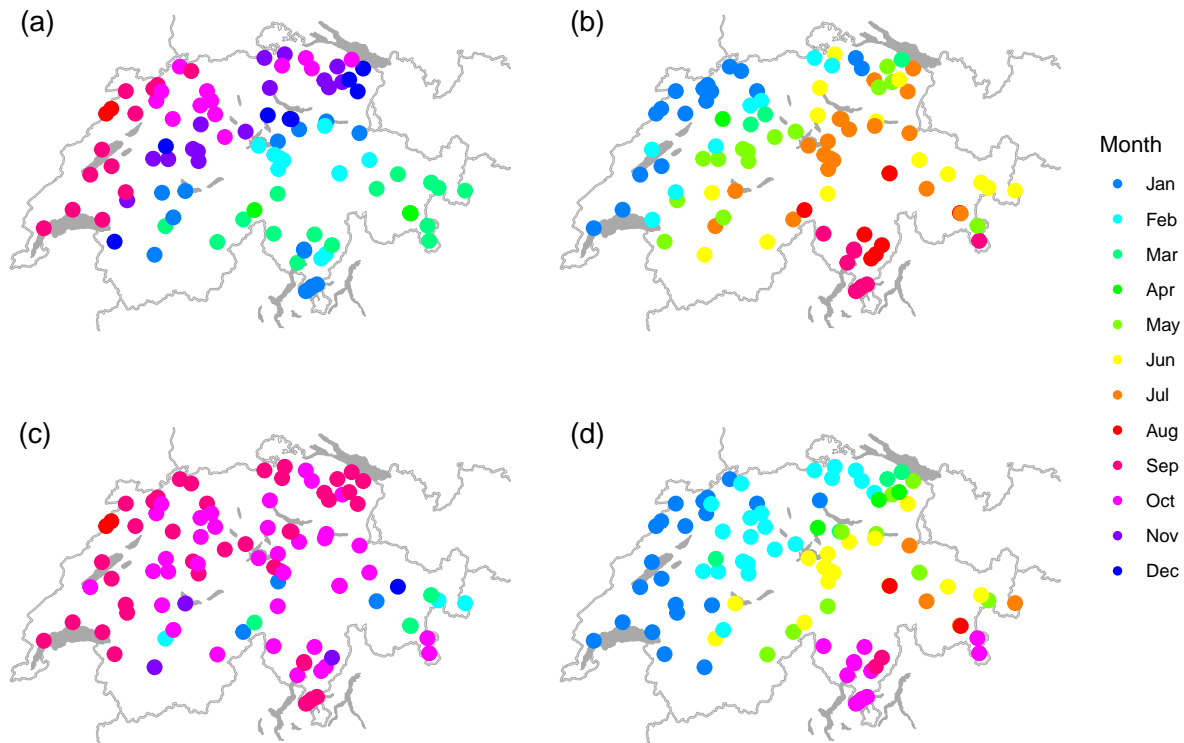


Figure 4.2: Median monthly occurrence of moderate low flows (left panels) and high flows (right panels) for the reference period (1981-2010, a, b) and end of the century (2070-2099, c, d).

The moderate annual low flows show distinctly different patterns of change in magnitude for Alpine and non-Alpine catchments (Fig. 4.3 left panels). Please note that the scale bar is limited to -60% and +60% for readability. While the annual low flows (Fig. 4.3a) decrease by up to -66% in most of the lower lying catchments (68 out of 93 catchments in total), the Alpine catchments (25 catchments with mean altitude above 1500 masl) show strong increases (up to +200%). Lowest winter flows in Alpine catchments coincide with the typical low flow season in the reference period while lowest summer flows in coincide with the typical low flow season in lower lying catchments. Lowest winter flows increase on average by +22%. An increase is found in two thirds of the catchments, again with stronger increases in very high Alpine catchments (Fig. 4.3c). In summer, the lowest flows decrease on average by -40% (maximum decrease -74%) (Fig. 4.3e). However, three high Alpine catchments still show an increase in lowest summer flows due to an increase in lowest flows in late spring (May). The model agreement (>90%) is stronger in summer (87 catchments) than in the annual (63) and winter (30) low flows.

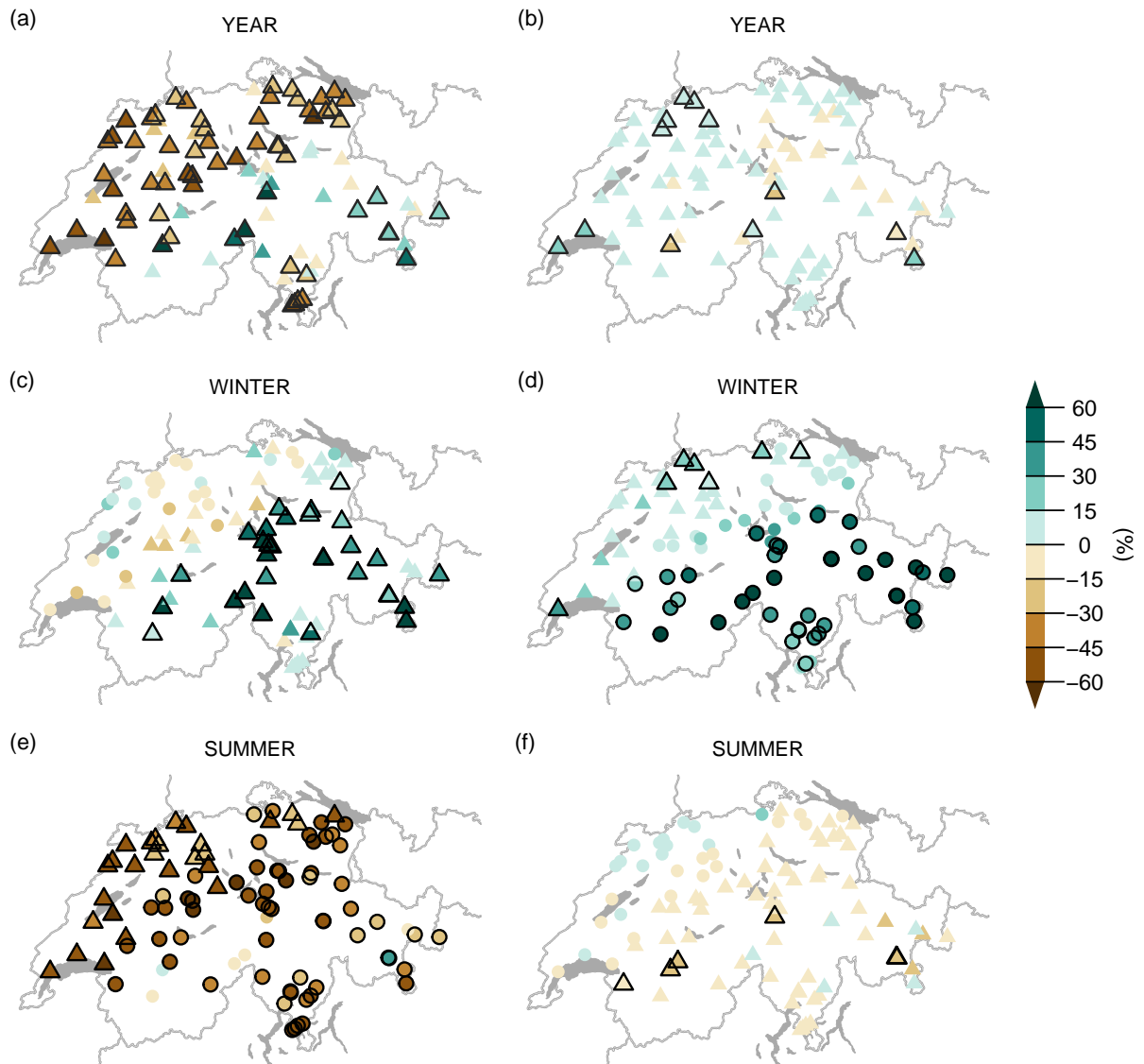


Figure 4.3: Relative changes of magnitude by end of the century for moderate low flows (left panels) and moderate high flows (right panels) for the year (a,b), winter (c,d), and summer (e,f). Triangles indicate catchments with annual moderate low and high flows occurring in the respective time window in the reference period. Circles indicate seasonal lowest and highest flows outside the typical low and high flow season. Black contours indicate changes with at least 90% of the models agreeing on the direction of change.

Table 4.2: Relative changes (in %) by end of the century and the seasonal occurrence (OCC) of moderate low and high flows for the six representative catchments. The seasonal occurrence indicates the season where the moderate flow extremes occur most frequently. Abbreviations: Seasonal occurrence in winter in the reference period and predominantly in summer in the future period (WS), seasonal occurrence in the winter in both periods (WW), seasonal occurrence in summer in the reference period and in winter in the future period (SW), and seasonal occurrence in summer in both periods (SS).

Catchment	Moderate low flows				Moderate high flows			
	Year	Winter	Summer	OCC	Year	Winter	Summer	OCC
Rosegbach	191%	199%	89%	WW	-20%	97%	-25%	SS
Kander	20%	41%	-37%	WW	8%	50%	-5%	SS
Plessur	-1%	32%	-43%	WS	-10%	43%	-14%	SS
Emme	-53%	-17%	-66%	WS	2%	13%	-7%	SW
Venoge	-45%	-16%	-47%	SS	22%	25%	4%	WW
Verzasca	-22%	42%	-53%	WS	6%	24%	-3%	SS

Transient changes of moderate low flow intensity and seasonality throughout the 21st century for three representative Alpine catchments and three representative lower lying catchments are shown in Figs. 4.4 and 4.5, respectively. The relative changes for each of the catchments and each of the time windows are summarized in table 4.2. The high Alpine catchment Rosegbach is highly glaciated in the reference period with a glacier coverage of 22% but loses most of the glacier coverage by end of the century (glacier coverage: 1%; not shown). The catchment shows strong increases in annual low flows and lowest seasonal flows (Fig. 4.4 top row). While the seasonality of the annual low flows and lowest winter flows does not change, the occurrence of lowest summer flows shifts from early summer to autumn. This indicates a change in the underlying processes leading to lowest summer flows: In the reference period, the retention of water in snow in ice still takes place in May. Under climate change, enhanced snowmelt increases runoff in early summer. Towards the end of the century, the contribution of snow and glacier melt in summer decreases. At the same time, precipitation in summer will decrease. This leads to a strong decrease in summer runoff. The combination of increasing runoff in early summer and decreasing runoff in late summer and early autumn results in a shift of lowest summer flows from early summer to early autumn. In the catchment Kander with only little glacier influence (Fig. 4.4 middle row), the annual low flows and lowest winter flows increase mainly due to enhanced winter precipitation falling as rain instead of snow. Lowest summer flows decrease by end of the century. The annual low flows and lowest seasonal flows occur earlier by end of the century. The nival catchment Plessur shows a strong shift in seasonality in the annual low flows from winter to autumn but no change in the magnitude of low flows (Fig. 4.4 bottom row). Lowest

winter flows increase and occur earlier in the season while the lowest summer flows decrease but do not change seasonality. The annual low flows and lowest seasonal flows decrease by end of the century in the pre-Alpine snow and rain influenced catchment Emme. The annual low flows show a clear shift in seasonality from late autumn/early winter to early autumn (Fig. 4.5 top row). A shift towards earlier occurrence is also found for lowest winter flows but not for the lowest summer flows. In the mainly rain and evaporation driven catchment Venoge, the annual low flows and lowest summer flows do not change their seasonality, but lowest winter flows tend to occur earlier in the season (Fig. 4.5 middle row). The magnitude of annual low flows and lowest seasonal flows decrease. The southern Alpine catchment Verzasca shows a decrease in the magnitude and a strong shift in occurrence from late winter to early autumn for annual low flows (Fig. 4.5 bottom row). Lowest winter flows increase while lowest summer flows decrease, both without change in the seasonality.

Figure 4.8 (left panels) shows the time of emergence for moderate low flows and lowest seasonal flows when at least 66% of the models show significant changes in the distribution. 43 catchments show a time of emergence for annual low flows with particularly early significant changes in glaciated and/or high Alpine catchments (earliest 2018-2047). The 20 catchments showing a time of emergence in lowest winter flows have a mean altitude higher than 1600 masl. In summer, 80 catchments show significant changes in lowest flows with an early time of emergence again found in high Alpine catchments, but also lower lying catchments show a time of emergence later in the century.

4.5.2 Future changes in moderate high flows

The median seasonal occurrence of annual high flows is shown in Fig. 4.2 for the reference period (Fig. 4.2b) and by end of the century (Fig. 4.2d). In Alpine catchments, the median seasonal occurrence shifts from summer to late spring and early summer. However, highly glaciated catchments do not change their high flow seasonality. Moderate high flows in pre-Alpine catchments occur in spring in the reference period and in winter in future. A change in seasonality is also found in southern Alpine catchments where high flows shift from late summer and early autumn to late autumn in future. In lower lying catchments, no change in high flow seasonality is found.

Relative changes of magnitude for moderate high flows by end of the century are depicted in Fig. 4.3 (right panels). The 30-year means of annual high flows (Fig. 4.3b) increase in 71 catchments (up to +28%) and decrease in 22 catchments (up to -22%). Compared to the changes in moderate low flows, the magnitude of change in high flows is smaller. There are no clear spatial patterns or elevation dependences and good model agreement (>90%) is only found in 12 catchments. Highest winter flows in lower lying catchments coincide with the typical high flow season in the reference period, while highest flows in higher elevation catchments are mainly

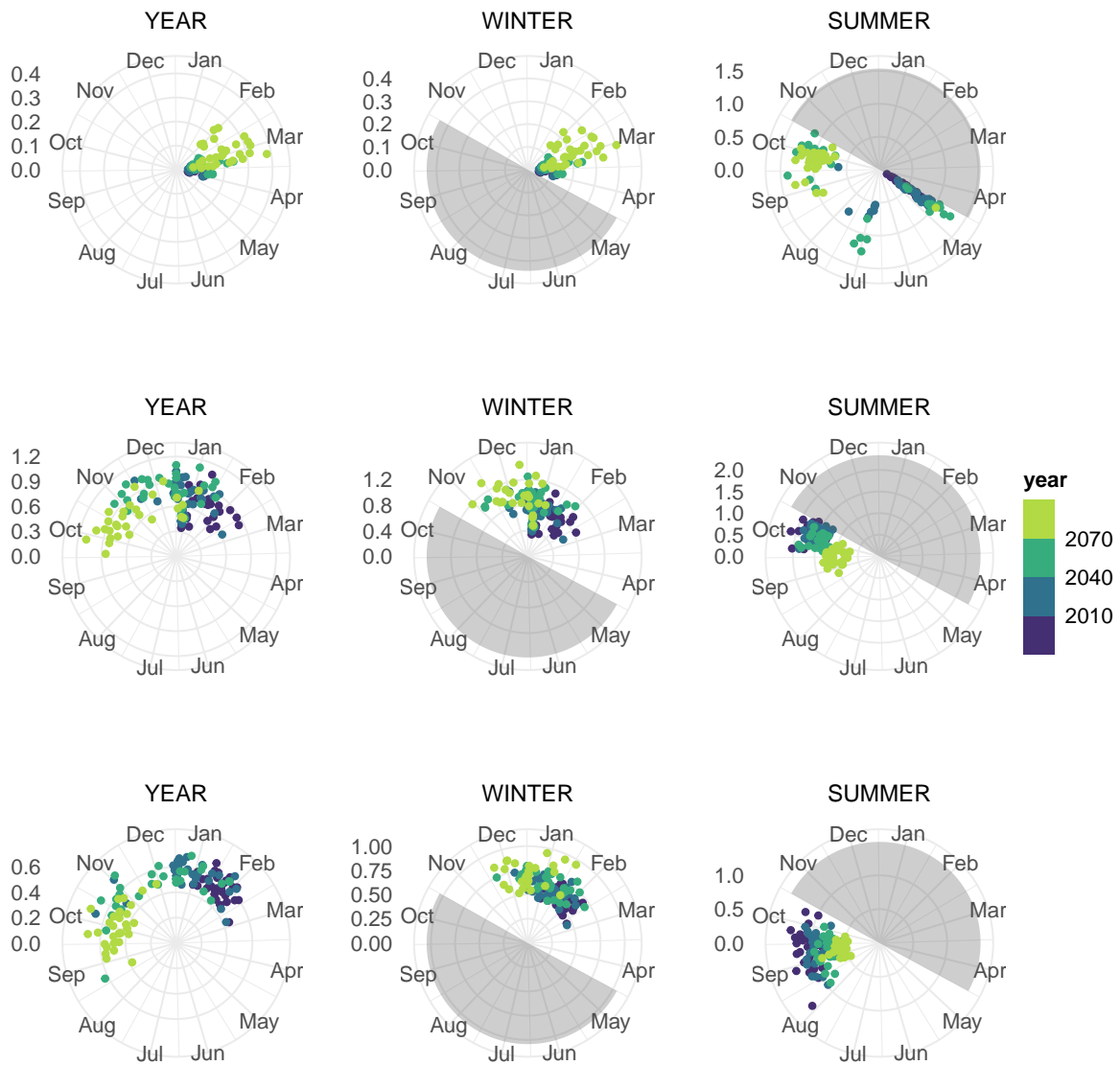


Figure 4.4: Multi-model median of intensity and seasonal occurrence of low flows and seasonal lowest flows in Alpine catchments: Rosegbach (top row), Kander (middle row), and Plessur (bottom row).

found in the summer half year. Highest winter flows increase in all catchments and model agreement is higher with 45 (out of 93) catchments showing a good agreement (Fig. 4.3d). Strongest increase in magnitude and good model agreement are found in high Alpine catchments. However, highest winter flows in high Alpine catchments are still small in magnitude. Highest winter flows in the lower lying catchments increase only moderately and model agreement is generally weak. Highest summer flows (Fig. 4.3f) decrease in 74 catchments (up to -26%) and increase in 19 catchments (up to +15%). Strongest reductions in highest summer flows are found in

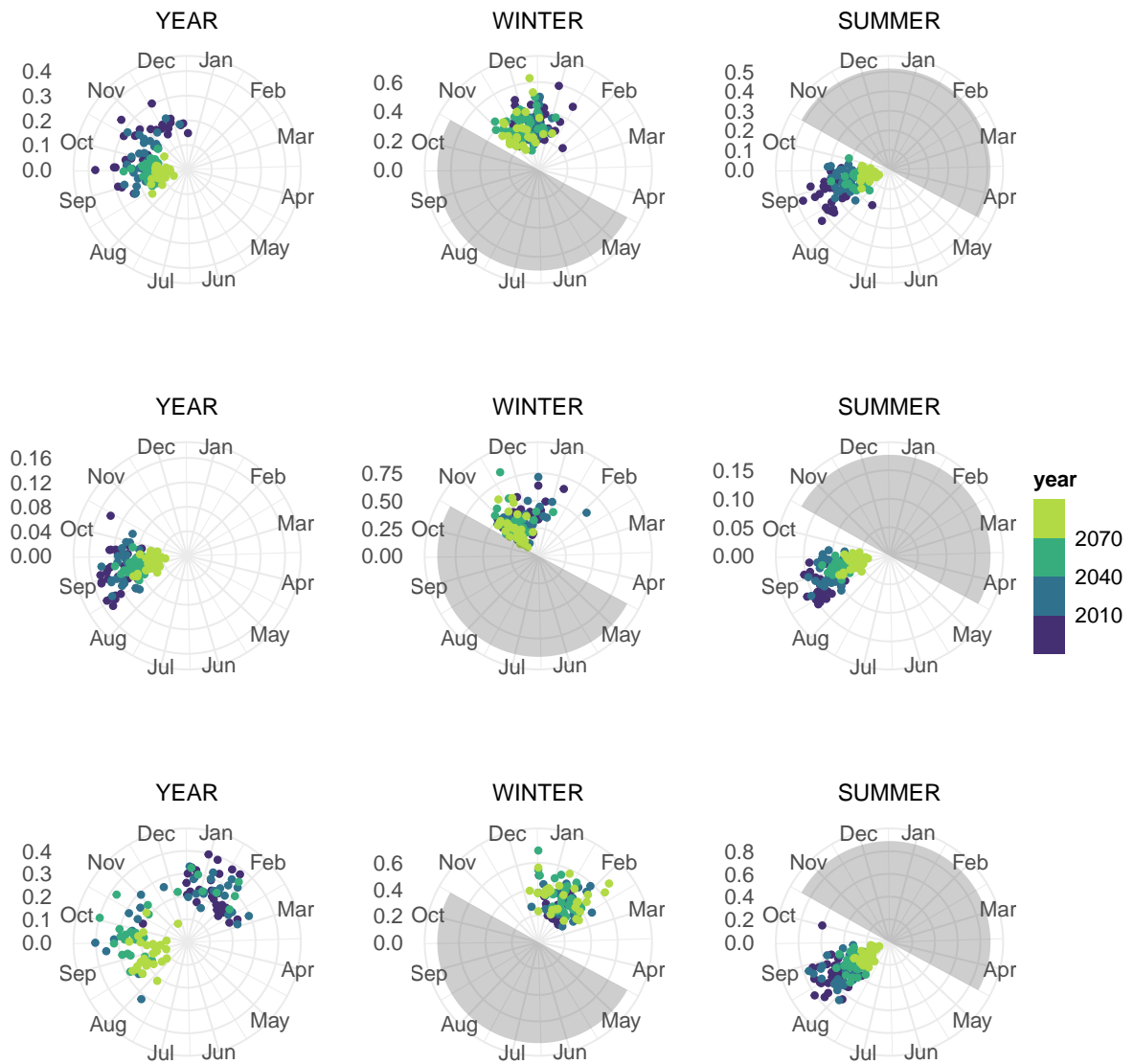


Figure 4.5: Multi-model median of intensity and seasonal occurrence of low flows and seasonal lowest flows in low lying catchments: Emme (top row), Venoge (middle row), and Verzasca (bottom row).

high Alpine catchments including the only six catchments showing good model agreement. A spatial cluster of increasing highest summer flows is found in the Jura mountains (north-west Switzerland).

Annual high flows and highest summer flows in the Rosegbach catchment decrease towards the end of the century and tend to occur earlier in summer while highest winter flows increase and occur more often later in the season (Fig. 4.6 top row). A similar pattern is also found for

the Plessur (Fig. 4.6 bottom row). In the Kander, the annual high flows increase slightly and shift to earlier in the year and can also occur in winter by end of the century (Fig. 4.6 middle row). Also, highest winter flows in the Kander increase, and highest summer flows show a small decrease without a significant shift in the occurrence. The high flows in the Emme and the Verzasca do not change their seasonality but highest winter flows increase and highest summer flows decrease (Fig. 4.7 top and bottom rows). The pluvial catchment Venoge shows increasing moderate annual high flows and seasonal highest flows with no change in the seasonality (Fig. 4.7 middle rows).

The time of emergence of moderate high flows is depicted in Fig. 4.8 (right panels). Compared to moderate low flows, there are fewer catchments exhibiting significant changes and these catchments are mostly high Alpine catchments. For annual high flows, three high Alpine (>2000 masl) catchments show a time of emergence with earliest time of emergence of 2078 (2049-2078). The 27 catchments showing significant changes in highest winter flows (earliest 2044, 2013-2044) are also located in the Alpine ridge (>1500 masl mean altitude). In summer, only six catchments (>1800 masl) show a time of emergence and the earliest time of emergence is 2071 (2042-2071).

4.5.3 (Co-)occurrence of low and high flows

So far we have assessed changes in the magnitude and seasonality of low and high flows, in this section we address changes in frequency and the co-occurrence of high and flow events. For this we need to set a threshold to identify events. The threshold discharge value is defined as a value occurring every second year in the reference period (i.e., median in the reference period).

Figure 4.9 illustrates relative changes in the occurrence of low flows (Fig. 4.9 a-c) and high flows (Fig. 4.9 d-f) by end of the century (2070-2099) that fall below resp. exceed median values. For annual low flows, the occurrence of low flow events increases in 70 catchments. These catchments are mainly found in rain dominated areas and to a lesser extent also in snow dominated areas. Catchments showing fewer occurrences are only found in high Alpine areas. Good model agreement is found in 56 catchments. Lowest flows occur also more often in summer (sometimes occurring every year) in almost all regions except few very high elevation catchments. Most of the catchments (82) show a good model agreement on the increase of lowest summer flow occurrence. Lowest winter flows tend to occur less often in mountainous areas while lower lying catchments still show an increase in occurrence. However, only mountainous catchments show good model agreement.

Changes in the occurrence of high flows are less clear than for low flows. For annual high flows, 58 catchments show increasing occurrences, and 30 catchments show decreasing occurrences. However, the changes are often small. Also, no clear spatial or elevation pattern emerges and model agreement is weak. For the highest winter flows, all catchments will face more years

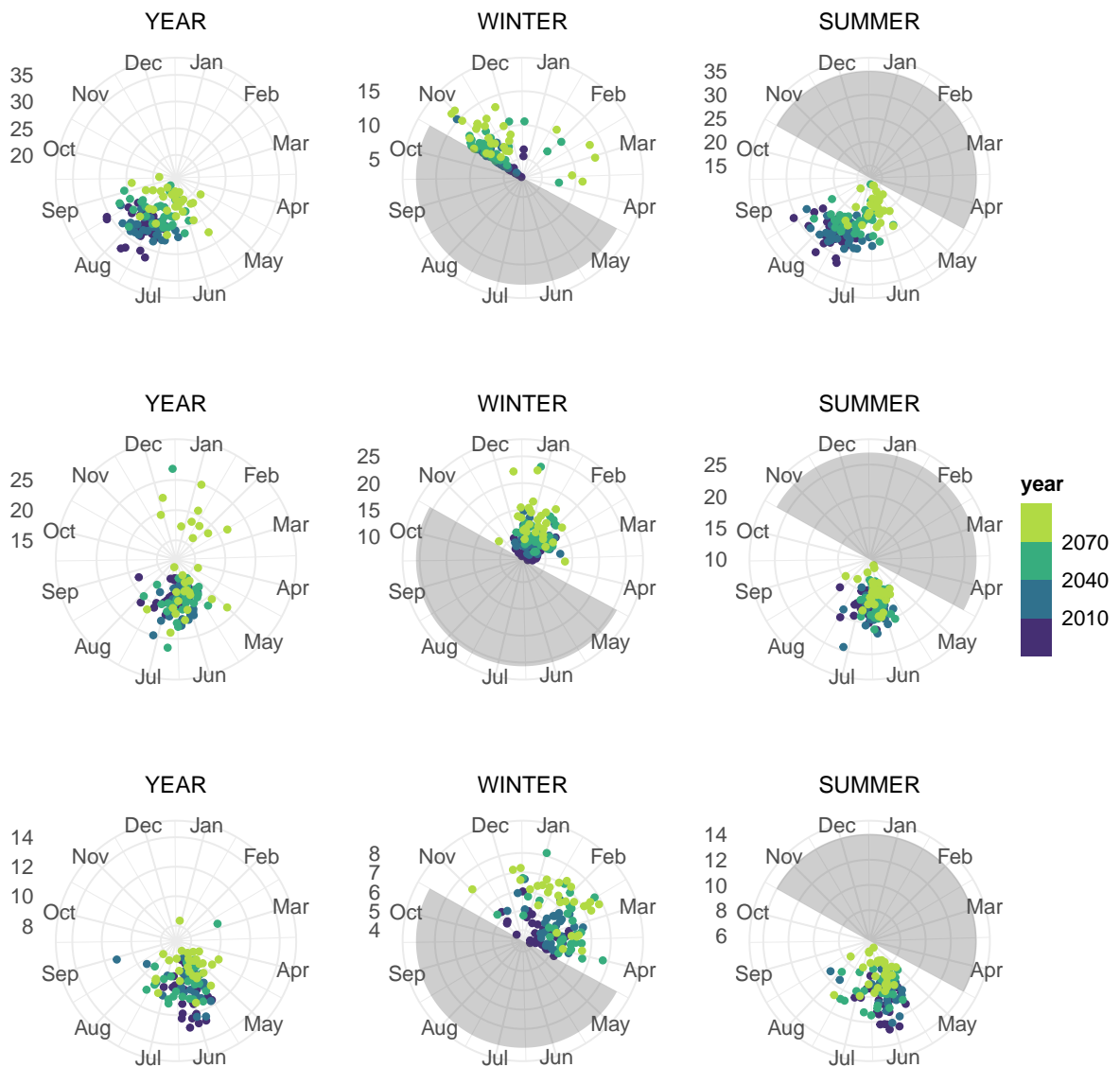


Figure 4.6: Multi-model median of intensity and seasonal occurrence of high flows and seasonal highest flows in Alpine catchments: Rosegbach (top row), Kander (middle row), and Plessur (bottom row).

with more frequent high flow events than today, particularly in the high Alpine regions. In contrast, the occurrence of highest summer flow events will decrease by end of the century in most catchments. Model agreement is weaker in summer than in winter.

Figure 4.9 (g-i) shows changes in the co-occurrence of moderate high and low flows defined as the occurrence of a high flow event and a low flow event in the same time window. Annual co-occurrence increases in most catchments, particularly in the lower lying catchments. In high

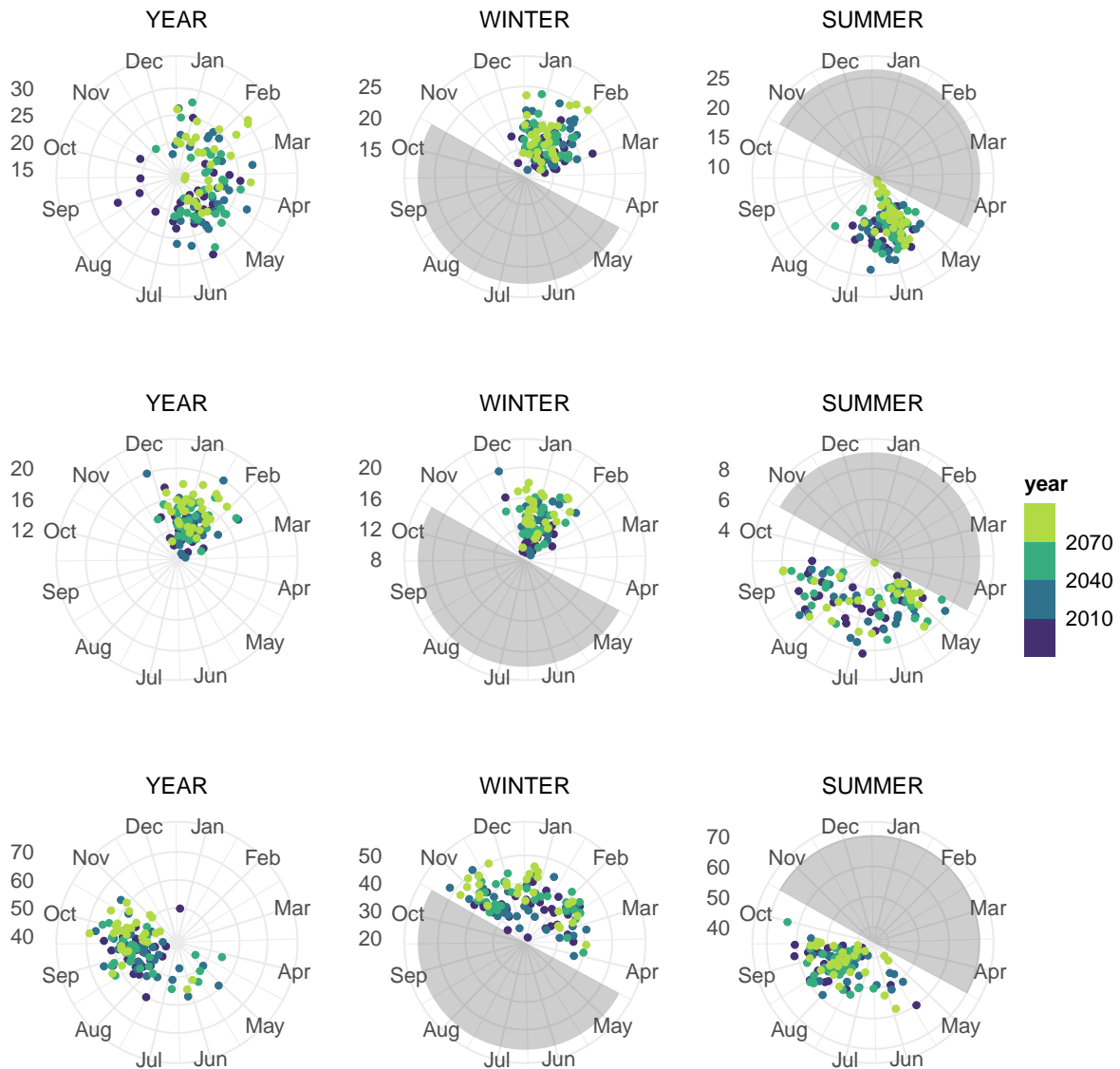


Figure 4.7: Multi-model median of intensity and seasonal occurrence of high flows and seasonal highest flows in low lying catchments: Emme (top row), Venoge (middle row), and Verzasca (bottom row).

Alpine catchments, this co-occurrence decreases mainly due to the strong increase in winter runoff. Winter co-occurrence decreases mainly in high altitude catchments but also in few of the lower lying catchments. In summer, most catchments (85 catchments) show increasing co-occurrence by end of the century. Only 8 high Alpine catchments show decreasing co-occurrence. In contrast to high flow occurrence, the model agreement is stronger in summer (48) than in winter (14) co-occurrence.

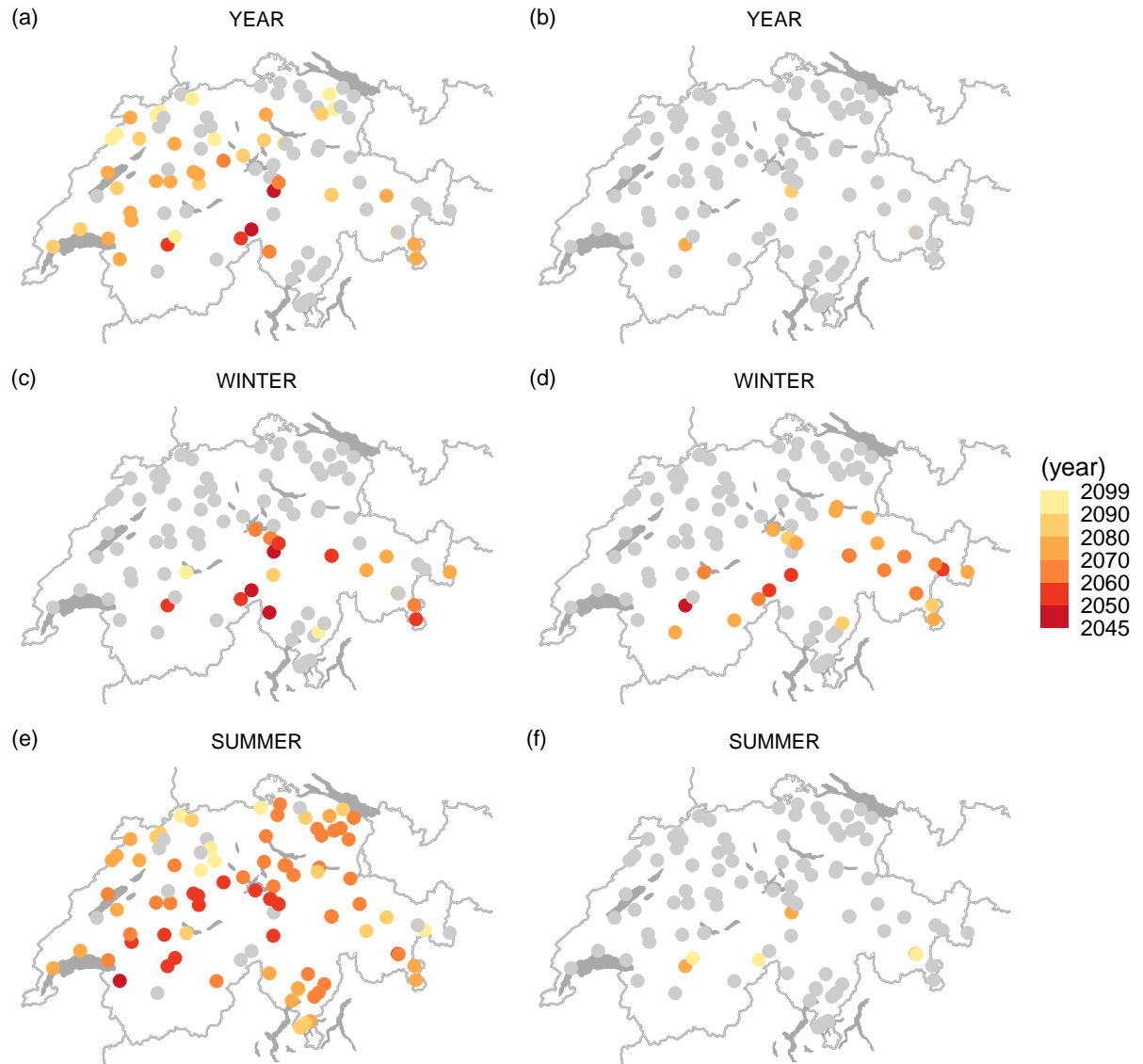


Figure 4.8: Time of emergence of moderate low flows (left panels) and moderate high flows (right panels) when at least 66% of the models agree on significant changes in the distribution of moderate low and high flows, respectively.

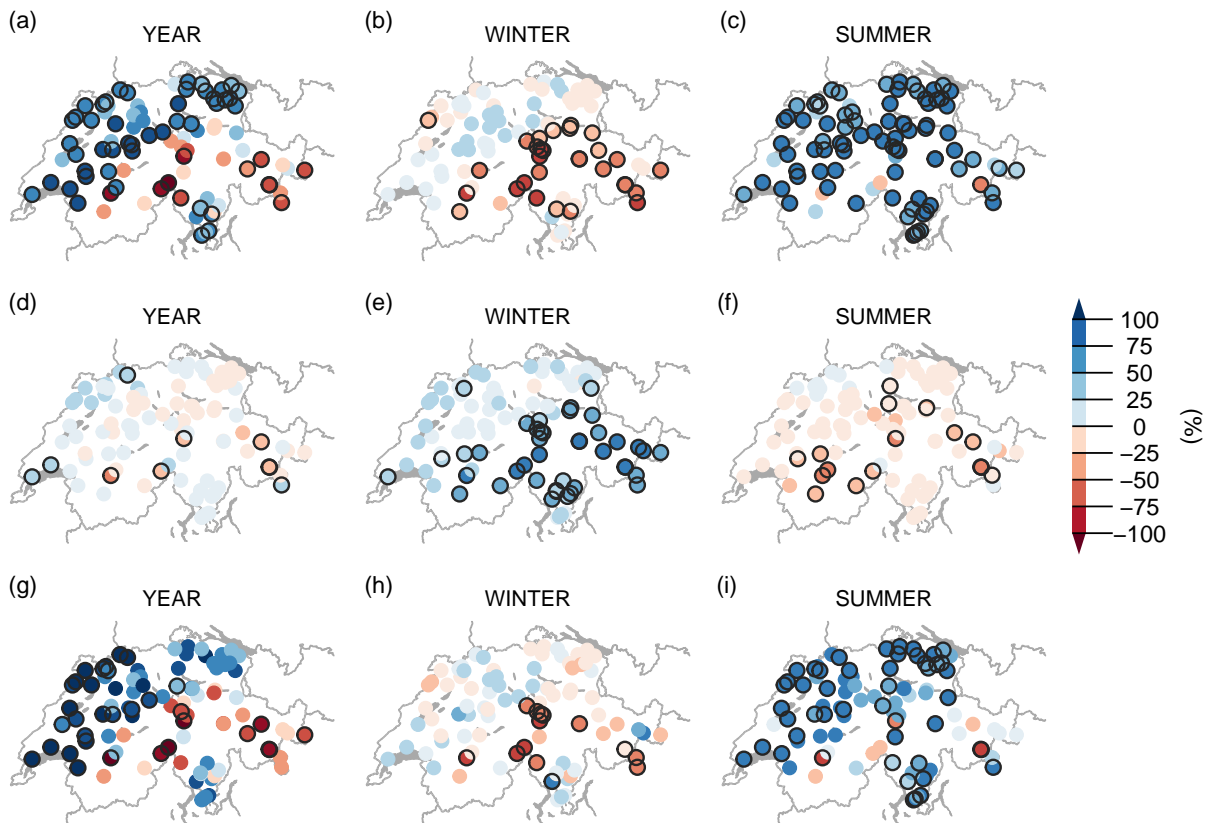


Figure 4.9: Relative changes in the frequency of occurrences of moderate low flow events (lower than the median of the reference period, top panels), of moderate high flow events (higher than the median of the reference period, middle panels), and co-occurrence of low and high flow events (bottom panels) by end of the century. Black circles indicate changes with at least 90% of the models agreeing on the direction of change.

4.6 Discussion

4.6.1 Changes in moderate low flows

Low flows in Alpine regions typically occur in winter and early spring when precipitation falls as snow and accumulates. The storage as snow limits the direct runoff and only little runoff (baseflow) occurs in winter. Since higher temperatures result in both a change of the precipitation type (more precipitation falls as rain instead of snow) and an enhancement of earlier snow melt, the lowest winter flows are projected to increase in the future. Also, the seasonal occurrence shifts from late winter to late autumn. This shift indicates that snow storage no longer dominates low flows, but summer drought in combination with lack of snow and glacier melt becomes the main driver of low flows. However, this is not the case in highly glaciated catchments with very high mean altitudes, where the seasonality of low flows does not change. Considering the summer half year, the lowest summer flows in Alpine catchments decrease due to the combination of decreasing summer precipitation, enhanced evapotranspiration and the reduced contribution of snow and glacier melt to the runoff. An exception are catchments in very high altitudes, which show increasing lowest summer flows by end of the century. Increasing lowest winter flows in Alpine areas have been identified in observations (Weingartner and Schwanbeck, 2020) and our results show that this trend continues with climate change. The findings are also in agreement with results for projections of very extreme low flow regimes (100-year return period Brunner et al., 2019a).

In the present climate, low flows occur mostly in late summer and autumn in lower lying catchments. In these catchments runoff volumes during low flow conditions are projected to decrease in all time periods, with the reduction in the summer half year being much stronger than in the winter half year. The reasons for the reduction in summer are the decreasing summer precipitation and the higher temperatures enhancing evapotranspiration. The projected lowest summer flow reduction is in line with observed trends (Weingartner and Schwanbeck, 2020) but the changes get amplified under climate change. Even though the climate change scenarios project increasing winter precipitation, the lowest winter flows decrease mainly due to a shift in the occurrence from winter to late autumn. The seasonality of annual low flows does not change in mainly rainfed catchments. In pre-Alpine regions, the seasonality of annual low flows shifts from late autumn to early autumn.

In the snow- and rain-driven southern Alpine regions, there are typically two periods of low flows: one in late summer and one in winter, with the winter minimum often being lower in the reference period. Under climate change, the seasonal occurrence of low flows shifts from winter to late summer and early autumn. At the same time, runoff in low flow situations decreases by end of the century.

Increasing lowest winter flows in Alpine regions may be beneficial for energy production, but the decreasing lowest summer flows may have severe impacts in agricultural regions where water is needed for irrigation. Also, the decreasing water availability during low flows may have implications on the cooling of infrastructures and in combination with increasing water temperatures may foster water stress for ecosystems.

4.6.2 Changes in moderate high flows

In Alpine areas moderate annual high flow and highest summer flows will decrease in the projections. This can be explained by the decreasing contribution of melt water together with decreasing summer precipitation and enhanced evapotranspiration. In future, Alpine areas will face about half of the present mean runoff in summer (Muelchi et al., in review 2020c). This decrease is also reflected in moderate high flows. This is in contrast to the highest winter flows which are projected to increase with climate change. However, highest winter flows are still smaller in magnitude than highest summer flows. Decreases in the runoff volume during highest summer flows and increases in highest winter flows were also found by Allamano et al. (2009) for mountainous regions. However, the decreasing annual high flows in Alpine areas contradict the results of Köplin et al. (2014b), who found increasing high flows in the Alpine area. The reason for the different results is not conclusively clear, but in Köplin et al. (2014b) very extreme floods are considered, while this study considers moderate high flows.

Annual high flows in the Alpine region usually occur in summer, when the snow line is high, melting processes are in progress, and precipitation intensities are largest. In glaciated catchments, high flows occur at the end of summer when glacier melt reaches its peak in the reference period. In snow influenced catchments today, the high flows tend to occur in early summer during the snowmelt. In both regime types, seasonal occurrence is shifted to earlier months such that the high flows occur earlier in summer in future. An exception are highly glaciated catchments with high mean elevation, which will also have snow and glacier influence in summer in the future. In these catchments, the seasonal occurrence hardly changes. Köplin et al. (2014b) also found shifts in the occurrence of extreme floods in Alpine areas. Their results show a shift in nival catchments from summer to autumn, whereas our results show a shift to earlier spring and early summer.

In lower-lying areas annual high flow and highest winter flows tend to increase, although the increase is often not robust across models. In summer, the highest flows tend to decrease again with no robust signals across models. Moderate high flows occur in winter in pluvial catchments and this will not change in future. In catchments partly influenced by snow, where high flows occur in spring, the seasonal occurrence is shifted from spring to late winter. This behavior is in agreement with the results of Köplin et al. (2014b). In the southern Alpine areas, the annual high flows also tend to increase and will shift from late summer and early autumn to

late autumn, which was also found by Köplin et al. (2014b) for extreme floods.

The increased water availability in winter in Alpine regions may be beneficial for energy production. But increasing high flows in mainly lower lying catchments may increase the potential of flood damages. However, this increase is not robust among the climate models and moderate high flows only partially reflect severe floods.

4.6.3 Time of emergence of significant changes

Significant and robust changes in the magnitude of moderate low flows emerge mainly for annual low flows and lowest summer flows. The majority of the catchments show a significant change in magnitude for summer low flows. High Alpine catchments show earlier significant changes in lowest summer flows than lower lying catchments. Early times of emergence in high Alpine catchments were also found for summer mean flow in Muelchi et al. (in review 2020c). In winter, only Alpine catchments show a significant change in lowest winter flows. The main reason for this are snowpack related processes like the change in precipitation type (snow vs. rain) together with smaller snow accumulations and associated enhanced direct runoff.

The magnitude of high flows significantly changes only for few catchments. This is due to the large variability across the climate models. To detect a time of emergence, we require that at least 66% of the models agree on significant changes in the distribution of high flows.

4.6.4 Changes in the (co-)occurrence of low and high flow events

The frequency of annual moderate low flow events increase in lower lying catchments, while fewer low flows events are detected in Alpine catchments. However, the frequency of the lowest summer flows will increase in almost all catchments. In some catchments, the frequency almost doubles. This may have implications in agricultural areas where irrigation plays an important role. High flow events in winter will occur more often, while summer high flow events will occur less often. A clear pattern in occurrence of annual high flow events is not detectable because model agreement is weak. However, most catchments show a tendency towards more occurrences. Co-occurrence of low and high flow events in the same year increases in most lower lying catchments. In contrast, high elevation catchments show a decreasing co-occurrence mainly due to the increase in low flows. The changes in co-occurrence are dominated by changes in low flow occurrence. Since low flows in lower lying (high Alpine) catchments tend to occur much less (more) often, co-occurrence also decreases (increases). Co-occurrence of high and low flow events in the same extended season are important for ecosystems since the recovery time may be shortened. Information about the co-occurrence is also important for insurance companies for their risk assessments.

4.6.5 Uncertainties

Uncertainties in our results are larger for moderate high flows than for moderate low flows. The larger uncertainties in high flows are due to several reasons. First, high flows are difficult to model since many different processes interact with each other. In particular, small-scale precipitation patterns have a strong influence on high flows and the input data from the climate models does not reflect small-scale precipitation processes well (Ban et al., 2015). Second, the uncertainty arising from internal variability of extreme precipitation is large and is thus also reflected in our results. Third, our results represent 30-year averages as well as averages across models. Therefore, a lot of information is averaged out. Other sources of uncertainty also affect our results such as the climate models and their boundary and initial conditions, the post-processing method, the hydrological model and its calibration, and the underlying glacier projections.

4.7 Conclusions

We assessed changes in moderate low and high flows (annual and seasonal flow maxima and minima) for 93 catchments in Switzerland under climate change. Runoff simulations were driven by the newest transient climate change scenarios (CH2018) for Switzerland for 1981-2099 based on the RCP8.5 scenario. This study analyzes not only changes in the magnitude of moderate low and high flows but also on changes in their seasonal occurrence and their frequency. Thanks to the transient property of the simulations, also the timing of significant changes (time of emergence) could be assessed.

The projections indicate the following results. For low flows, a strong elevation dependence of the changes over time was found. While low flow magnitudes decrease in lower lying catchments, they increase in Alpine catchments extending observed trends in the past (Weingartner and Schwanbeck, 2020). Low flows decrease by -40% in summer, and increase by +22% in winter. The results for low flow magnitudes are in line with projections of previous studies (e.g., Meyer et al., 2011; Bernhard and Zappa, 2012; Brunner et al., 2019a). A shift in seasonality was found for most of the catchments. By end of the century, low flows will occur predominantly in late summer and autumn in most of the catchments. This indicates that the lack of precipitation in summer exceeds the contribution of other processes such as snow and glacier melt contributions. The pronounced projected decrease in summer low flows in most of the catchments (except some high Alpine catchments) may become one of the most important challenges in terms of water management. In contrast, increasing winter low flows in Alpine catchments may be beneficial for hydropower production.

For moderate high flows, relative changes are smaller than for low flows. Most of the catchments show an increase in moderate high flows but the model agreement on the changes is not

robust with the exception of a few catchments in northern Switzerland and the Jura mountains. High Alpine catchments show a decrease in the highest summer flows, mainly due to reduced melt water in future, and an increase in the highest winter flows. The magnitude of winter high flows in Alpine catchments is much smaller than for summer high flows. Thus, the increasing winter high flows are not that important from a hydrological point of view but may become relevant for ecosystems. Projected changes in magnitude and shifts in seasonality of moderate high flows in lower lying catchments are in line with previous studies (e.g., Köplin et al., 2014b; Brunner et al., 2019a). For Alpine catchments, our results do not agree with other projections in terms of magnitude and in some cases in terms of seasonality. This contradiction may arise due to the different indicators considered. While our study focuses on moderate high flows, the other studies focused on extreme high flows, which can be governed by different processes than moderate high flows.

Significant changes in the magnitude of low flows emerge early in the 21st century for high Alpine catchments because of an increase in winter flows. For many lower lying catchments a significant decrease in summer low flow magnitude is detected but later in the 21st century. Changes in the magnitude of high flows are mostly not robust across climate models and thus not significant.

Low flow events will occur more often in lower lying catchments and less often in high Alpine catchments. Like the weak signal in the magnitude of high flows, also changes in the occurrence of high flow events are small. However, most of the catchments will experience an increasing frequency in the occurrence of high flow events. An elevational pattern was found for the co-occurrence of moderate low and high flow events, with increasing co-occurrence in lower lying catchments and decreasing co-occurrence in high Alpine catchments. This pattern is dominated by changes in the frequency and magnitude of moderate low flows.

4.8 Acknowledgements

Authors would like to thank Harry Zekollari, MeteoSwiss, and FOEN for providing the necessary data for this study. We also acknowledge the funding of the Swiss Federal Office for the Environment under the project Hydro-CH2018.

Chapter 5

Comparison of hydrological modelling results from four Swiss research institutions

5.1 Introduction

In the context of the Hydro-CH2018 project several projects at different Swiss research institutions were realized. Each of the projects focused on a particular aspect of the Swiss hydrology. This project at the University of Bern (UBE; part of this thesis) concentrated on producing high quality and comprehensive hydrological scenarios for Switzerland with a focus on river runoff and their regimes. The University of Zurich (UZH) focused on quantifying the contributions of snow and glacier melt to discharge. The Swiss Federal Institute for Forest, Snow and Landscape Research (WSL) assessed changes in the general water balance in Switzerland. And the Swiss Federal Institute of Technology Zurich (ETHZ) produced very high resolution stochastic climate data using a weather generator for two study catchments. These four projects included hydrological modelling for different purposes and different selection of catchments. Since some of the catchments were modelled by more than one institution, a comparison of the results becomes possible. Such a comparison between the simulations allows for estimating the robustness of the modelled results and thus an estimation of the uncertainty that arises from the hydrological models.

5.2 Data and Methods

The main differences between the modelling setups are summarized in table 5.1. UBE and WSL both used the structure and core of the hydrological model "Precipitation - Runoff - Evapotranspiration HRU Model" (PREVAH) but with different set ups and extensions. UZH used a modified "Hydrologiska Byråns Vattenbalansavdelning" (HBV) model called HBV-light and ETHZ used the Topographic Kinematic Approximation and Integration model (TOKAPI).

Table 5.1: Most important differences between the simulations of the four institutions.

Provider	Model	Resolution	CH2018	Glacier Data
UBE	PREVAH	daily	gridded	Zekollari et al. 2019
UZH	HBV light	daily	gridded	internal routine
WSL	PREVAH	hourly	station data	Zekollari et al. 2019
ETHZ	TOKAPI-ETH	hourly	weather generator	–

These four models differ substantially in their model structure, the way hydrological processes are represented and the required input data (variable, resolution, geographic information, etc.). While the models of UBE and ETHZ were calibrated and validated with measurements, the models of UZH and WSL were regionalized. All four institutions used the new Swiss Climate Change Scenarios CH2018 (CH2018, 2018) as original meteorological input. UBE and UZH used the gridded versions of temperature and precipitation and WSL interpolated station data with their own interpolation method. ETHZ used a stochastic weather generator to increase the horizontal and temporal resolution of CH2018 for two example catchments.

A total of 26 catchments were simulated by WSL and UBE and 12 catchments by UZH and UBE. The UBE project calibrated the hydrological model for each catchment individually (see chapter 2). Thus a good regime coverage can be guaranteed. In contrast to this method, the UZH and WSL have regionalized their hydrological model for the catchment areas. A regionalization allows for the estimation of runoff in ungauged catchments. However, the simulated and observed regimes may differ. Therefore, only three example catchments were selected for the comparison of absolute changes in runoff regimes. These catchments provide a good regime coverage in the reference period in the simulations of all three institutions. For the other catchments only relative changes are analysed. Since the three institutions worked with a different selection of climate models, the climate models simulated by all three institutions are used. A list of the corresponding climate model chains under RCP8.5 can be found in Table 5.2. Due to this different climate model selection, the results in this chapter may slightly differ from the results of the previous chapters (chapters 2-3).

Two example catchments were simulated by all four institutions: The Kleine Emme at Emmen and the Thur at Andelfingen. While the simulations of the UBE, UZH and WSL were fed directly with the results of CH2018, ETH produced its own meteorological input data using a weather generator. The weather generator was driven with the forcing of the CH2018 models (list of models in table 5.2) for three periods: 1976-2005 as reference and 2030-2039, 2050-2059 and 2080-2089 for future conditions. The weather generator generates many time series for a single year, which were driven with the same conditions. A total of 450 one-year simulations are available for the reference period and 100 one-year simulations for each climate

model chain and future period. The monthly mean per period is compared with the monthly means of the simulations of the UBE, UZH and WSL for the same period. Since the institutions selected different sets of climate models, the comparison is only done for climate models under RCP8.5 which were used by all four institutions (see Table 5.2). Due to the differences in the meteorological input data, the hydrological models and the type of simulations differences in the results are expected.

Table 5.2: Climate model chains used for the comparisons.

Global Climate Model	Regional Climate Model	UBE-UZH- WSL	UBE-UZH- WSL-ETHZ
ICHEC-EC-EARTH	KNMI-RACMO22E	X	
	DMI-HIRMAM5	X	X
	CLMcom-CCLM4-8-17	X	X
	CLMcom-CCLM5-0-6	X	
	SMHI-RCA4	X	X
MOHC-HadGEM2-ES	CLMcom-CCLM4-8-17	X	X
	CLMcom-CCLM5-0-6	X	
	KNMI-RACMO22E	X	
	SMHI-RCA4	X	X
MPI-M-MPI-ESM-LR	CLMcom-CCLM4-8-17	X	X
	CLMcom-CCLM5-0-6	X	
	SMHI-RCA4	X	X
	MPI-CSC-REMO2009-2	X	X
MIROC-MIROC5	CLMcom-CCLM5-0-6	X	
	SMHI-RCA4	X	
CCCma-CanESM2	SMHI-RCA4	X	
IPSL-IPSL-CM5A-MR	SMHI-RCA4	X	X
NCC-NorESM1-M	SMHI-RCA4	X	

5.3 Comparison between UBE-UZH-WSL

Figure 5.1 shows the results of three selected catchments: Kleine Emme at Emmen, Thur at Andelfingen and Simme at Oberried. The uncertainty bands represent the climate model variability. The spread of the climate models varies between the catchments with generally smaller spread in the reference period than in the future period. The results show a good agreement of the regime curves in the reference period compared to the measurements. Also the runoff regimes for the year 2085 (period 2070-2099) under RCP8.5 show similar patterns in the simulations of the different institutions. This illustrates the robustness of the new hydrological

scenarios. Figure 5.2 shows the relative changes of seasonal runoff for the year 2085 under RCP2.6 and RCP8.5 of the simulations by UBE compared to the WSL and UZH simulations. The differences in the relative changes are generally smaller for RCP2.6 than for RCP8.5 because the magnitude of change under the low emission scenario is also smaller compared to the high emission scenario. Differences between the simulations are larger in winter and spring in the Alpine catchments than in the lower lying catchments. This can be explained by the different representation of snow and glacier accumulation and melt processes. Another reason are the very large relative changes in winter which in fact are only marginal absolute changes (see Figure 5.1 for Simme-Oberried). In summer and autumn, the differences between the results tend to be larger in the lower-lying catchments. In general, the sign of change (increase or decrease) is the same in the different simulations but the magnitude of change may differ between the simulations.

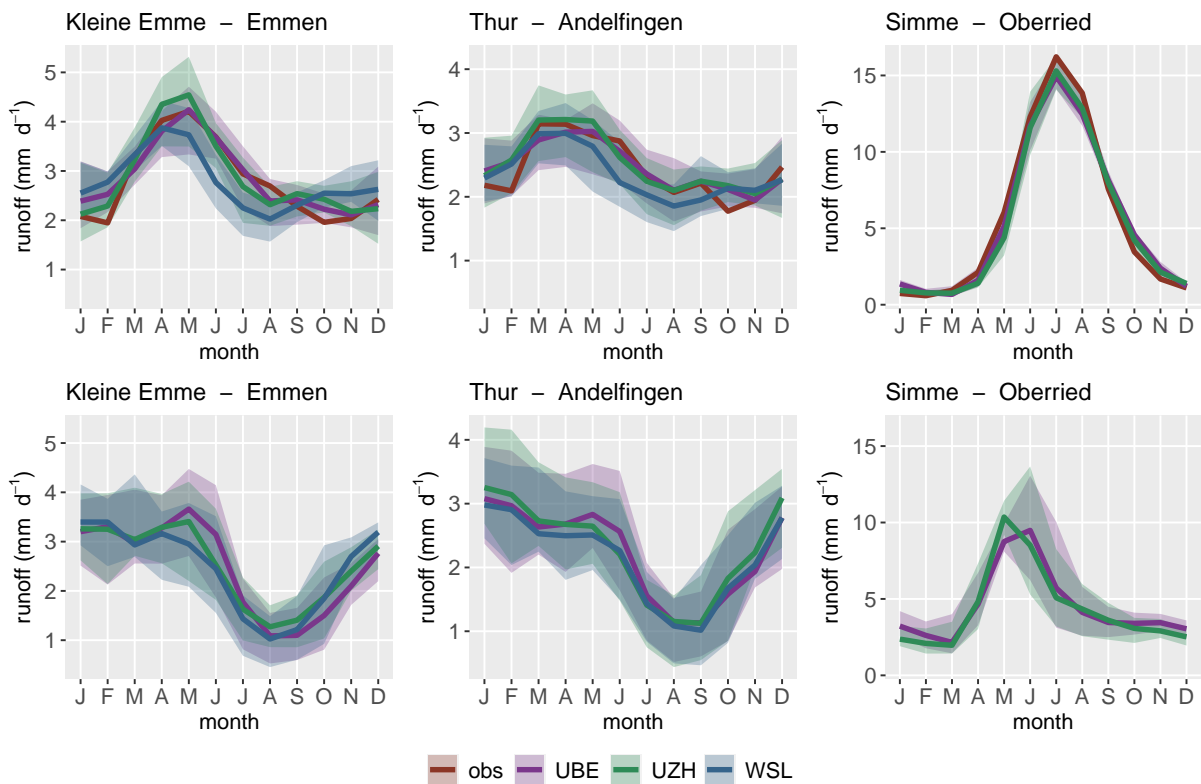


Figure 5.1: Runoff regimes of observed data (obs, red), UBE (violet), UZH (green) and WSL (blue) in the reference period (top) and for the future period 2070-2099 under RCP8.5 (bottom) for the Kleine Emme at Emmen, the Thur at Andelfingen and the Simme at Oberried. The uncertainty bands indicate the climate model spread (minimum and maximum).

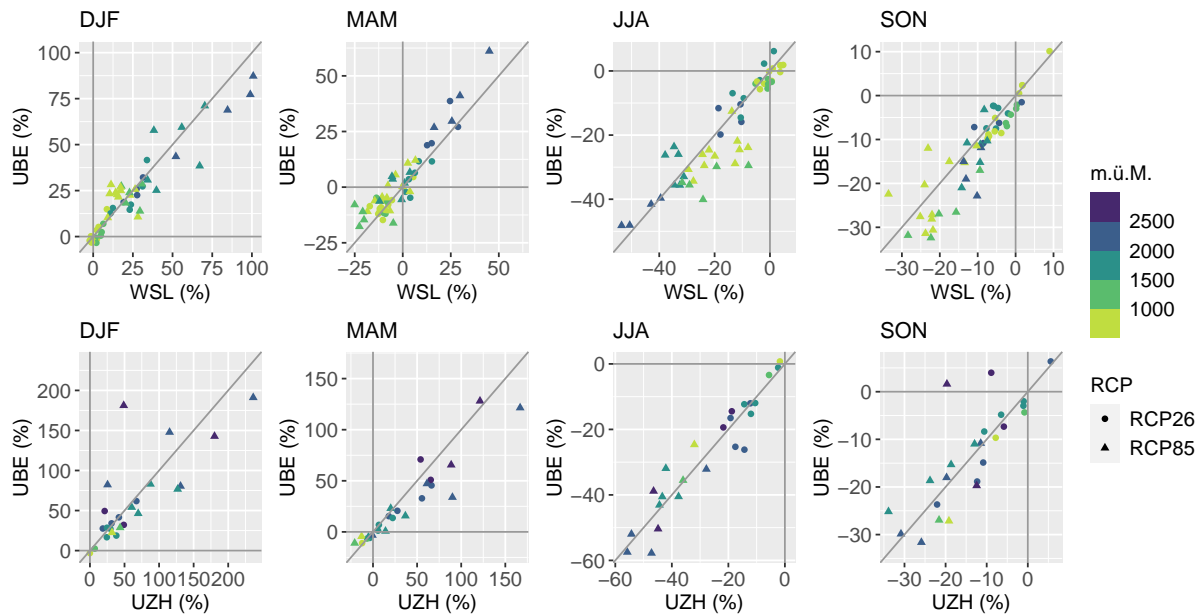


Figure 5.2: Comparison of relative changes of seasonal runoff by 2070-2099 under RCP2.6 (points) and under RCP8.5 (triangles) between UBE and WSL (top), and UBE and UZH (bottom). The color scale represents the mean height of the catchments.

5.4 Comparison between UBE-UZH-WSL-ETHZ

Figure 5.3 shows the regime curves simulated by the four institutes for the Kleine Emme and the Thur for different 10-year periods under RCP8.5. The runoff regimes of the UBE, UZH and WSL are similar in all periods. However, there are differences to the monthly averages simulated by the ETHZ. Compared to the results of the UBE, UZH and WSL the results of the ETHZ show significantly higher runoff in late summer (August) for the Kleine Emme in all periods and significantly lower runoff in late spring and summer for the Thur. These differences for the Thur become smaller towards the end of the century. Figure 5.4 shows the relative changes of the regime curves for different periods. In most months, the sign of change (positive or negative) are the same for all simulations. However, there are a few exceptions. While the UBE, UZH and WSL show an increase or only a small decrease in early summer (June) until the middle of the century, the data of the ETHZ show strong decreases in early summer already in the near future. The relative changes in late summer (August and September) by end of the century are significantly smaller for the simulations by the ETHZ compared to the simulations by the other institutes.

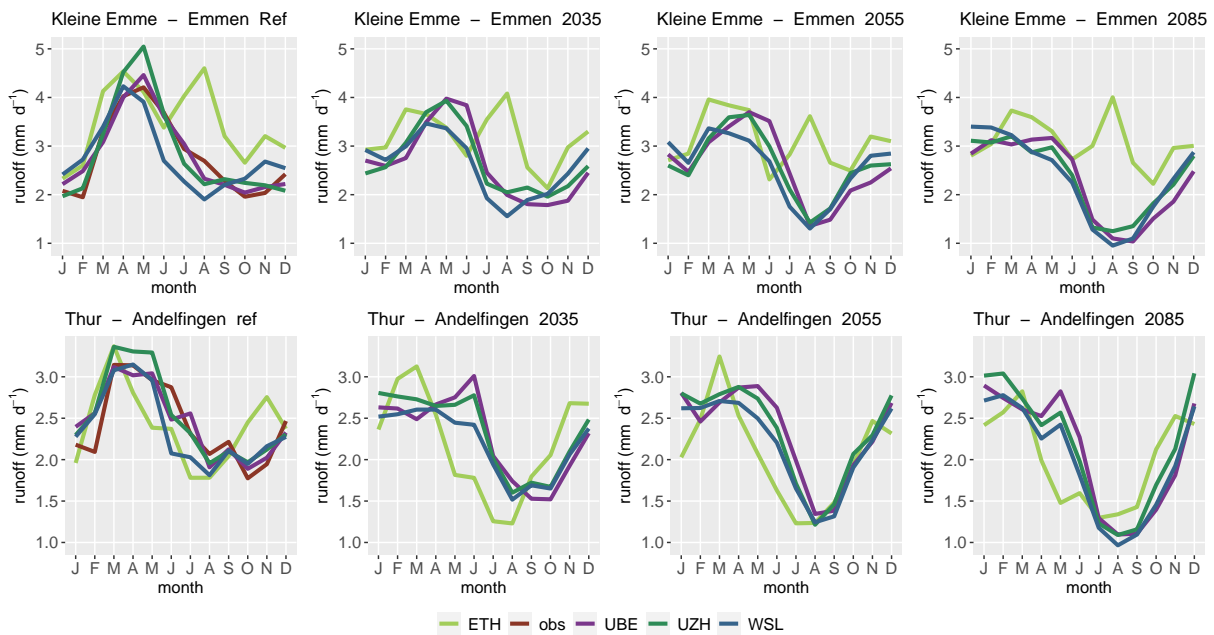


Figure 5.3: Runoff regimes of observed data (obs, red), UBE (violet), UZH (dark green), WSL (blue) and ETHZ (light green) for the reference period (left) and for the periods 2030-2039 (center left), 2050-2059 (center right) and 2080-2089 (right) under RCP8.5 for the Kleine Emme at Emmen (top) and the Thur at Andelfingen (bottom)

5.5 Conclusions

Within the national Hydro-CH2018 project, several projects at different Swiss research institutions included hydrological modelling with different foci. Some catchments were modelled by more than one institution and thus a comparison of the modelling results became possible. A first comparison was made for the results of UBE, UZH, and WSL. Although the climate input data, the hydrological models, and their model parameters differ, an overall good agreement on the sign and the magnitude of change in seasonal runoff is found. Differences between the magnitudes of change are largest in winter and spring for Alpine catchments (snow processes) and in summer and autumn for lower lying catchments (evaporation processes). In a second comparison, the results were compared to simulations driven with data from a weather generator (ETHZ) with largest differences found in late spring/early summer and late summer.

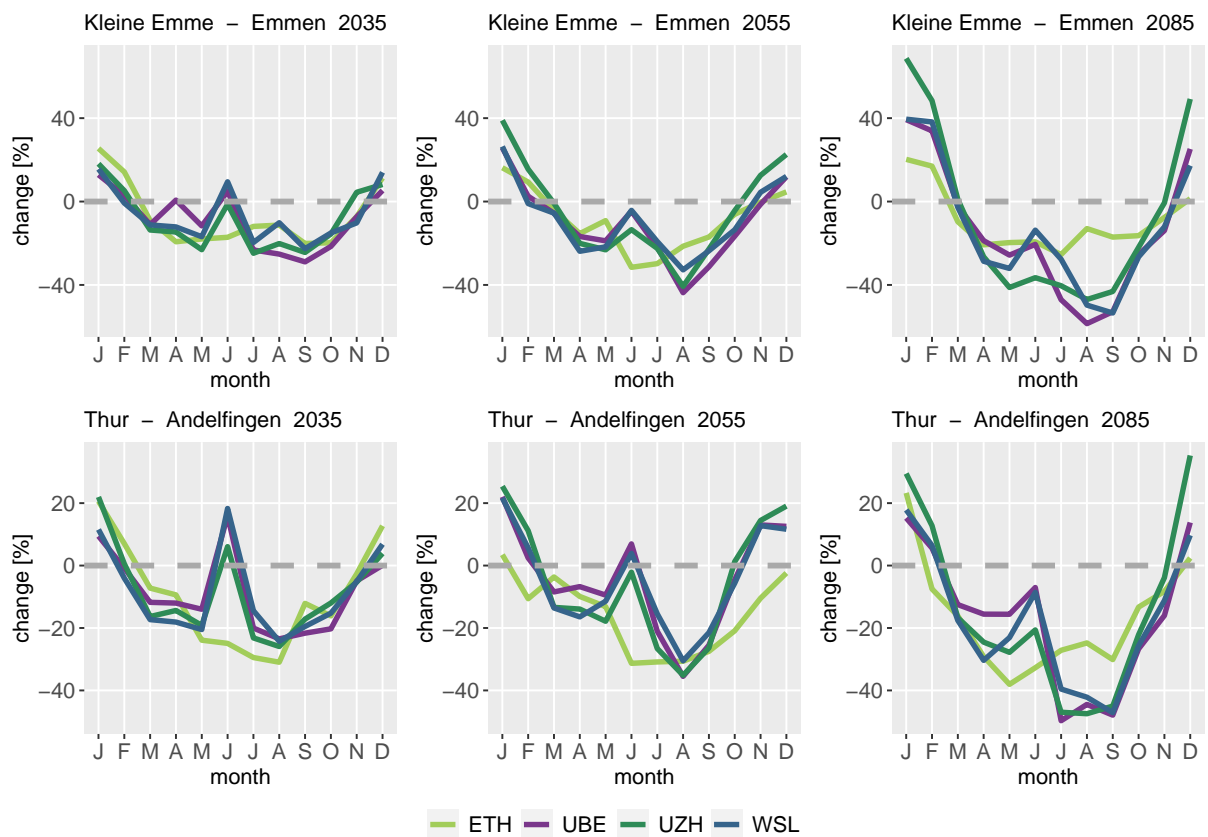


Figure 5.4: Relative changes of runoff regimes by UBE (violet), UZH (dark green), WSL (blue) and ETHZ (light green) for the periods 2030-2039 (left), 2050-2059 (center) and 2080-2089 (right) under RCP8.5 for the Kleine Emme at Emmen (top) and the Thur at Andelfingen (bottom)

Chapter 6

Vertically integrated moisture transport extremes directed perpendicular to the Swiss topography intensify under climate change

This chapter discusses the analysis of the atmospheric potential for floods in Switzerland and how this evolves under climate change. The chapter was written together with Olivia Martius.

6.1 Introduction

Floods are a devastating and costly natural hazard in Switzerland (Hilker et al., 2009). Extreme precipitation, soil moisture excess, and snowmelt are key flood drivers (e.g., Berghuijs et al., 2019). Understanding the triggering mechanisms of floods is very important for flood preparedness. Several studies have investigated the atmospheric conditions leading to extreme precipitation and flood events in Switzerland on the Alpine north side (e.g., Stucki et al., 2012; Froidevaux and Martius, 2016; Giannakaki and Martius, 2016) and on the Alpine south side (e.g., Massacand et al., 1998; Martius et al., 2006; Hoinka and Davies, 2007). These studies suggest that the key ingredient for extreme precipitation potentially leading to floods is the forced ascent of a deep, saturated, moist neutral air mass over topography. Such air masses are characterized by high vertically integrated water vapor transport (IVT, $\text{kg m}^{-1}\text{s}^{-1}$). The studies show that not only the magnitude of the moisture flux is important, but also the direction of the flux relative to the topography (Gheusi and Davies, 2004; Martius et al., 2006; Froidevaux and Martius, 2016). Froidevaux and Martius (2016) found a strong relationship between extreme IVT and major flood events in Switzerland. 10 out of 14 major flood events in the past forty

years were related to extreme IVT directed perpendicular to orography. They identified three regions (northwestern, northeastern and southern Switzerland) where high IVT with a flow direction perpendicular to the Alps is associated with flooding in Switzerland. Figure 6.1 shows a schematic of these flow situations and associated flow directions. Synoptic situations with extreme IVT represent an important atmospheric flood potential predictor and are used for an automated flood awareness system in Switzerland (Mahlstein et al., 2019).

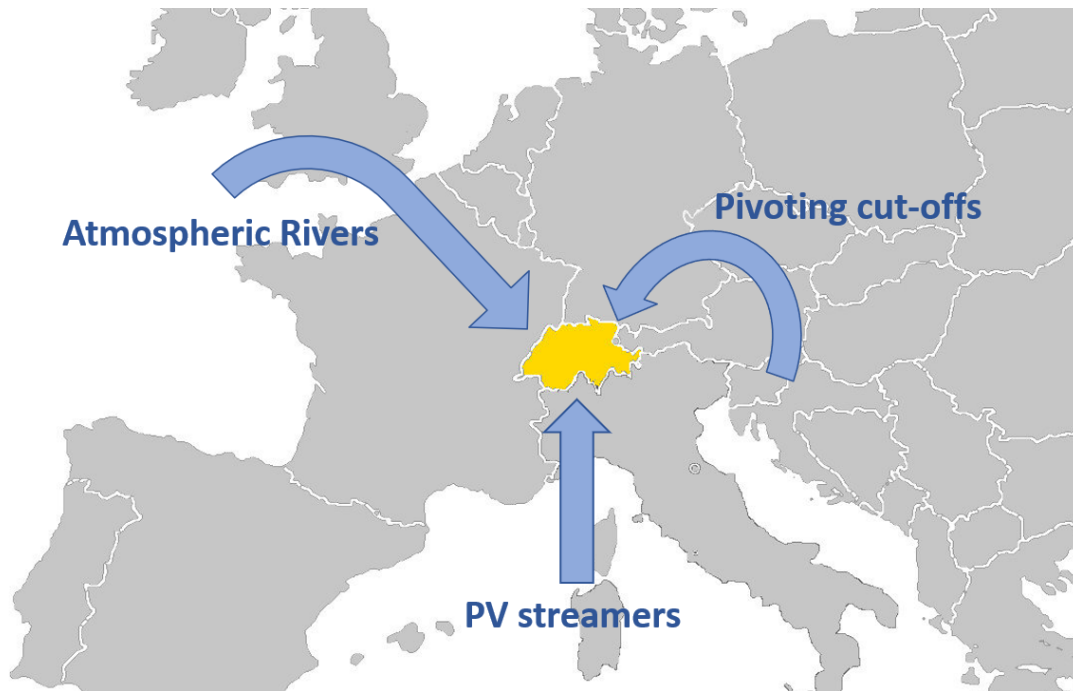


Figure 6.1: Schematic overview of the IVT directions and synoptic flow regimes conducive to floods identified by Froidevaux and Martius (2016).

The importance of IVT direction for flood generation was also highlighted by Griffith et al. (2020) for Britain and by Schaller et al. (2020) for Norway. Froidevaux and Martius (2016) identified synoptic flow situations with extreme IVT that can potentially lead to floods. In northwestern Switzerland (W), extreme IVT from the northwest was associated with major floods. These extreme IVT situations are often linked to so-called atmospheric rivers (ARs) transporting the moisture from the North Atlantic towards Switzerland. Atmospheric rivers are long and narrow atmospheric structures with strong horizontal water vapor transport (Glossary of Meteorology; Ralph et al., 2018). In southern Switzerland (S), major floods are associated with potential vorticity (PV) streamers which are related to an upper-level trough located over western Europe. These PV streamers transport moisture from the Atlantic and the Mediterranean Sea towards the southern side of the Alps (Winschall et al., 2012). In northeastern Switzerland (E), upper-level PV cut-offs pivoting around the Alps are associated with major floods transporting high amounts of moisture from the northeast towards Switzerland.

Due to the strong link between extreme IVT directed towards the Alps and major flood events in the past, the question arises how extreme IVT may evolve under climate change. Future changes in moisture transport in ARs were assessed in several studies globally (Espinoza et al., 2018; Massoud et al., 2019), for the US west coast (Dettinger, 2011; Pierce et al., 2013; Warner et al., 2015; Payne and Magnusdottir, 2015; Gao et al., 2015; Hagos et al., 2016; Shields and Kiehl, 2016; Gershunov et al., 2019) and in Europe (Lavers et al., 2013; Gao et al., 2016; Ramos et al., 2016; Shields and Kiehl, 2016; Whan et al., 2020). The studies found generally increasing frequencies and intensities of ARs with climate change. Most of this increase could be related to thermodynamic changes (i.e., increasing atmospheric moisture due to increasing temperatures) but Gao et al. (2016) also found significant dynamical contributions related to shifts in the mid-latitude jet stream.

Some of the extreme IVT flow situations conducive to floods in Switzerland do not fulfill the length and width criteria of ARs (Fazan, 2014). Therefore, we focus on extreme IVT in Switzerland that is not necessarily classified as atmospheric river but the moisture transport is directed perpendicular to the Swiss mountains. Studies about changes of extreme IVT that are not classified as ARs are scarce. Lavers et al. (2015) assessed changes in IVT globally and found that average IVT in the mid-latitudes increases by 30-40% under RCP8.5. However, to the knowledge of the authors no studies on future changes of non-AR extreme IVT exist for Europe. In this study, we analyze future changes of direction dependent IVT extremes potentially leading to floods in Switzerland using global climate models forced by the RCP8.5 pathway (Moss et al., 2010; Van Vuuren et al., 2011) for the period 1979-2100.

IVT is decomposed into a moisture related and a wind related component. The analysis of the relative importance of the two components hints to the relative contribution of thermodynamic and dynamical changes to the total change in extreme IVT. The partitioning of potential changes in extremes into thermodynamically and dynamically driven contributions is motivated by the reduced uncertainties of the thermodynamic contribution (e.g., Shepherd, 2014; Pfahl et al., 2017; Shepherd et al., 2018).

To estimate the values of a variable (here IVT) for return periods that are beyond the observational/modeled time-scale (e.g., 100 years), generalized extreme value (GEV) models can be fitted to the observed/modeled distributions (Coles, 2001). Since climate change is likely to increase IVT (Lavers et al., 2015), the non-stationarity needs to be considered in the fitting of the GEV (Katz, 2010). This is done by including covariates (see e.g., Coles, 2001; Zwiers et al., 2011; Ragno et al., 2019; Wehner et al., 2020). The use of covariates serves two purposes: i) they capture the non-stationarity and ii) they allow to identify drivers of change (e.g., Zwiers et al., 2011). The fitted non-stationary GEV models enable the estimation of 100-year return levels of moisture transport for present-day conditions and future conditions.

6.2 Data

For this study, 9 global climate models from the Coupled Model Intercomparison Project phase 5 CMIP5 (Taylor et al., 2012) were used (see Table 6.1 for details on the horizontal and the vertical resolution). The choice of models was constrained by the availability of 6-hourly pressure (p , Pa), specific humidity (q , kg kg^{-1}), zonal (u , m s^{-1}) and meridional (v , m s^{-1}) wind components as well as a sufficient number of vertical levels (at least 17 levels) for the vertical integration. For all models, historical simulations (1979-2005) and RCP8.5 simulations (2006-2100, ensemble member r1i1p1) were extracted. For each grid point IVT was calculated according to Lavers et al. (2012):

$$IVT = \frac{1}{g} \sqrt{\left(\int_{psurf}^{ptop} q(p)u(p)dp \right)^2 + \left(\int_{psurf}^{ptop} q(p)v(p)dp \right)^2} \quad [\text{kg m}^{-1} \text{ s}^{-1}] \quad (6.1)$$

Where g is the acceleration due to gravity, $psurf$ is the lowest pressure level and $ptop$ the highest pressure level in each model.

We then decompose IVT in two components: a humidity related component and a wind related component. The first component is the total precipitable water (TPW):

$$TPW = \frac{1}{g} \sqrt{\left(\int_{psurf}^{ptop} q(p) + q_{ice}(p) + q_{liquid}(p) \right)^2} \quad [\text{kg m}^{-2} \text{ or mm}] \quad (6.2)$$

Where q_{ice} represents the cloud ice and q_{liquid} the cloud water. The TPW integrates all moisture within an air column and thus also incorporates water components stored in clouds. This is slightly different from the calculation of IVT only using specific humidity.

Dividing IVT by TPW results in the remaining part of IVT, hereafter referred to as steering wind (SW) and is considered as the wind component of IVT:

$$SW = \frac{IVT}{TPW} \quad [\text{m s}^{-1}] \quad (6.3)$$

Next representative grid points located upstream west (W), south (S) and east (E) of the Alps need to be identified in the CMIP5 model fields to analyse the time evolution of the direction dependent IVT in these regions. The CMIP5 models have different horizontal resolution and varying representation of the Alpine orography. Therefore, we developed a grid point selection procedure that is applicable to all models. First, three to four grid points north and south of the Alps were selected depending on the initial model resolution and the location of the grid points relative to orography. Then an area average IVT was calculated incorporating both magnitude and direction. This is done with vector geometry and results in a final IVT vector for each region (W, S, E), time step and model. To make sure that we consider IVT potentially reaching the Alps, we extracted for each region (W, E, S) IVT advected from the directional sectors defined

by Froidevaux and Martius (2016) but extended to 90° angles (Table 6.2).

Table 6.1: List of CMIP5 models, associated institutions, and horizontal and vertical resolution of the models.

Model	Modelling Center	Institution	Latitude	Longitude	Vertical levels
bcc-csm1-1	BCC	Beijing Climate Center, China Meteorological Administration	2.7906	2.8125	17
CanESM2	CCCma	Canadian Centre for Climate Modelling and Analysis	2.7906	2.8125	35
CSIRO-Mk3-6-0	CSIRO-QCCCE	Commonwealth Scientific and Industrial Research Organisation in collaboration with the Queensland Climate Change Centre of Excellence	1.8653	1.875	18
GFDL-CM3	NOAA GFDL	Geophysical Fluid Dynamics Laboratory	2	2.5	23
GFDL-ESM2G	NOAA GFDL	Geophysical Fluid Dynamics Laboratory	2.0225	2	24
GFDL-ESM2M	NOAA GFDL	Geophysical Fluid Dynamics Laboratory	2.0225	2.5	24
IPSL-CM5A-LR	IPSL	Institut Pierre-Simon Laplace	1.8947	3.75	17
IPSL-CM5B-LR	IPSL	Institut Pierre-Simon Laplace	1.8947	3.75	17
NorESM1-M	NCC	Norwegian Climate Center	1.8947	2.5	17

Table 6.2: Regions and their respective critical advection angles.

Region	Advection angle
West (W)	270° - 360°
East (E)	330° - 60°
South (S)	135° - 225°

6.3 Methods

Yearly IVT maxima for each model and each region were extracted to analyze changes in extreme IVT. These yearly maxima correspond to the block maxima later used in the Generalized Extreme Value (GEV) analysis. In a first step, IVT block maxima as well as TPW and SW on IVT block maxima time steps were analyzed in terms of intensity changes. The ratio between TPW and SW was used to assess the importance of each variable to the total IVT. In a second step, the seasonality of IVT extremes was assessed by using 30-year means (1979-2008 and 2071-2100) of the time of their occurrence within each year. For this, the day of the year when IVT maxima occur was converted into angular values and the circular mean of those angular value was calculated. In a third step, GEV models (see Coles, 2001) were fitted to IVT block maxima. The GEV distribution function is described as

$$G(x) = \exp \left[- \left(1 + \xi \left(\frac{x - \mu}{\sigma} \right) \right)^{-1/\xi} \right] \quad (6.4)$$

With the three parameters location (β), scale (σ), and shape (ξ) characterizing the GEV distribution. The shape parameter describes the limit distribution as Fréchet distribution for $\xi > 0$, as Gumbel distribution for $\xi = 0$, and as Weibull distribution for $\xi < 0$. We fitted non-stationary GEV models such that the location parameter is linearly dependent on a covariate:

$$\mu(t) = \beta_0 + \beta_1 COV(t) \quad (6.5)$$

Where $COV(t)$ denotes the value of the particular covariate in year t (Coles, 2001). In a non-stationary case, the GEV distribution function has to be slightly modified by replacing μ with $\mu(t)$ such that

$$G(x) = \exp \left[- \left(1 + \xi \left(\frac{x - \mu(t)}{\sigma} \right) \right)^{-1/\xi} \right] \quad (6.6)$$

Three covariates were tested for their suitability: time, TPW at IVT block maxima time steps, and SW at IVT block maxima time steps. The covariates were normalized before the fitting process to ensure comparability. Normalization was performed by subtracting the mean and dividing by the standard deviation. This results in a normalized covariate with a mean of 0 and a standard deviation of 1. In total, we fitted 81 non-stationary GEV models for IVT block maxima using 9 climate models, 3 regions, and 3 covariates. GEV parameters were estimated with the maximum likelihood estimation (MLE). Compared to other methods, performance of MLE may be erratic when using small sample sizes ($n < 25$) potentially resulting in unrealistic shape parameter estimates (Martins and Stedinger, 2000). Since our sample size is large ($n = 122$) for each model fitting attempt, we consider MLE as a suitable method. After the fitting procedure, QQ-Plots were visually inspected to ensure the goodness-of-fit of each fitted GEV model (see example in Figure C.1).

Fitting non-stationary GEV models also has implications on the estimation of return levels (RL). In contrast to a stationary GEV model, RLs vary over time. RLs for 100-year events were retrieved for each fitted model. This corresponds to the effective return levels proposed by Katz et al. (2002). Due to the high variability in the covariates TPW and SW, effective RLs can become noisy and hard to interpret. Another way to look at the RLs is to average the RLs over 30 years in the reference period (1979 – 2008) and compare them to RLs of 30 years by end of the 21st century. Averaging the RL smoothes out the high variability in the covariates TPW and SW.

To compare performance of the non-stationary GEV models, the Bayesian Information Criterion (BIC) is used. The BIC is defined as

$$BIC = \ln(n)k - 2\ln(\hat{L}) \quad (6.7)$$

Where n is the number of observations in the model, k is the number of parameters used in the model and \hat{L} represents the likelihood estimation (Schwarz, 1978). The lower the BIC score, the better the model fit to the block maxima. The BIC penalizes for each added parameter. BIC scores of the non-stationary GEV models are compared to a stationary GEV model to assess whether the inclusion of covariates improves the model. Also, BIC scores of the non-stationary models are compared to select the best performing model.

6.4 Results

6.4.1 Large-scale moisture transport

Composites of direction dependent IVT on block maxima days for each region (W, E, S) are shown in Figure 6.2 for the period 1979-2008 (top row) and for the period 2071-2100 (middle row) using data from the CanESM2 model. Absolute IVT differences between the two periods are shown in the bottom row. Composites of other models can be found in the Appendix (Figures C.2-C.9). All models show similar spatial patterns of IVT block maxima. However, the magnitudes of IVT block maxima differ between the models. The results illustrate that the direction dependent selection is working. The IVT patterns identified by Froidevaux and Martius (2016) are represented in the composites. During IVT block maxima in the western region (W), a high IVT area extends from the North Atlantic in a long and narrow, atmospheric river-like structure to the Alps, with very high IVTs reaching the Alps from a northwestern direction. In the southern region (S) a high IVT area extends from the Mediterranean Sea to the Alps and reaches the Alps from a southward direction. In the eastern region (E) high IVT is present north of Switzerland. The extreme IVT reaches Switzerland from the northeast but IVT values are smaller than in the other two regions. The vectors of IVT show an anticyclonic flow for the western region and cyclonic flow in the southern and eastern region.

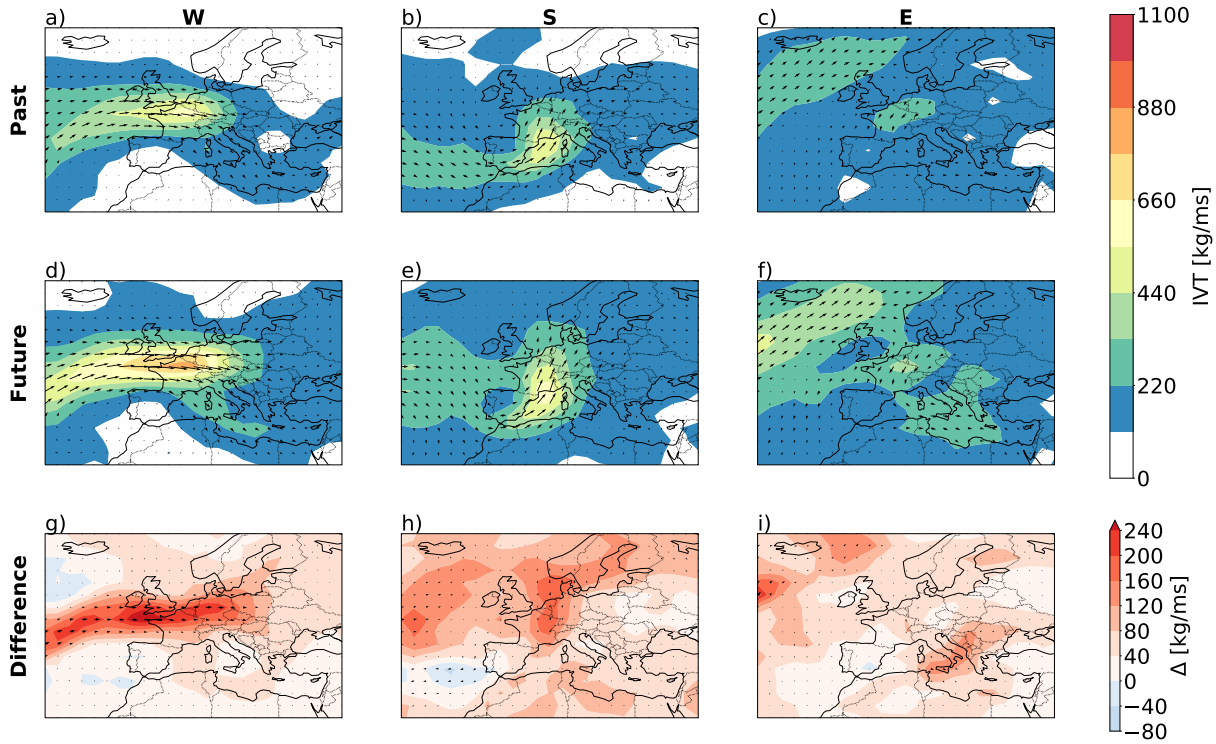


Figure 6.2: Time composites of IVT intensity and direction during IVT block maxima in the CanESM2 model for the period 1979-2008 (a-c) and 2071-2100 (d-f) for the western region (left), the southern region (middle), and the eastern region (right). Absolute differences between the two periods for the different regions are shown in the lower panels (g-i).

6.4.2 IVT intensity changes

The temporal evolution of IVT intensity and its two components TPW and SW is depicted in Figure 6.3. Relative changes by end of the century (2071-2100) compared to the reference period (1979-2008) are shown in Figure 6.4. The multi-model median of IVT intensities in the reference period is largest for the western region ($569 \text{ kg m}^{-1}\text{s}^{-1}$), followed by the southern region ($483 \text{ kg m}^{-1}\text{s}^{-1}$) and smallest in the eastern region ($228 \text{ kg m}^{-1}\text{s}^{-1}$). In all three regions, IVT intensities during block maxima are increasing over time. By end of the 21st century, 30-year average IVT intensities amount to $693 \text{ kg m}^{-1}\text{s}^{-1}$ in the western region, $630 \text{ kg m}^{-1}\text{s}^{-1}$ in the southern region and $284 \text{ kg m}^{-1}\text{s}^{-1}$ in the eastern region. This corresponds to a relative change by approximately +30% in the western and southern region and by +20% in the eastern region. Even though the models agree on the positive sign of changes, the range between the different model projections is large.

TPW values during IVT block maxima also increase over time. TPW values are highest in the southern region with 26 mm in the reference period and increase to 32 mm by end of the century followed by the western region with 24 mm in the reference period and 30 mm in the

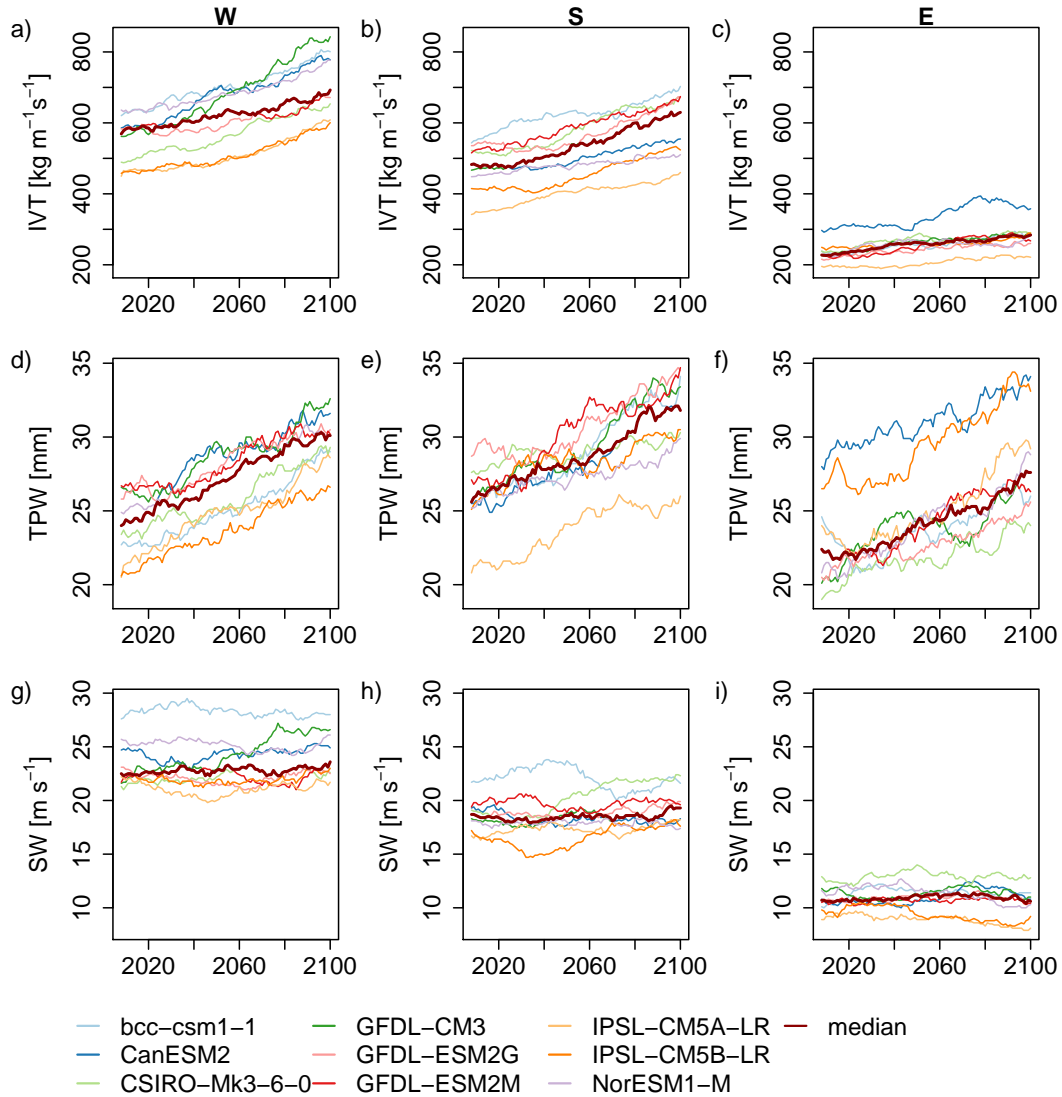


Figure 6.3: 30-year running means of IVT intensity (a-c), TPW (d-f), and SW (g-i) during IVT block maxima for the western region (left panels), southern region (middle panels), and eastern region (right panels).

future period. The eastern region exhibits smaller TPW values than the two other regions with 22 mm in the reference period increasing to 28 mm by end of the century. The multi-model median of TPW increases by +25% in all three regions. Even though the median change is constant between regions, the individual models show different change magnitudes for each region.

Average SW intensities during IVT block maxima are 23 m s^{-1} in the western region, 19 m s^{-1} in the southern region, and 11 m s^{-1} in the eastern region. Only small changes are found by the end of the 21st century. In the western and the southern region, the changes in SW are slightly positive with +1.6% in the western region and +2.3% in the southern region. However,

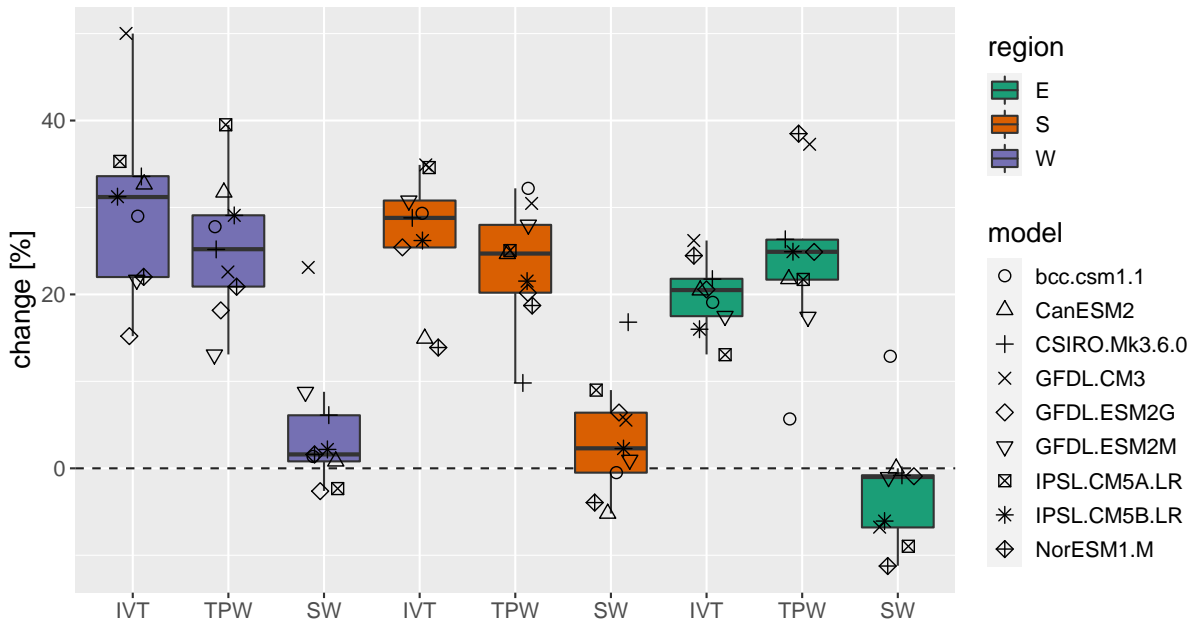


Figure 6.4: Relative changes of IVT intensity, TPW, and SW during IVT block maxima by end of the century (2071-2100) compared to the reference period (1979-2008).

in both regions also slightly negative changes are found in some of the models. In the eastern region, the median change in SW is slightly negative with -2.5%.

In the reference period, the ratio between TPW and SW is approximately 1 in the western region, thus the two components are equally important for IVT. This ratio is 1.4 in the southern region and 2 in the eastern region. In these two regions, TPW contributes more to IVT than SW. The ratio increases by end of the century in all regions indicating that relative contributions of TPW increase by end of the century while contributions of SW decrease.

6.4.3 Seasonality of IVT extremes

The mean seasonality and intensity of IVT block maxima for the reference period (1979-2008) and by end of the century (2071-2100) for each climate model and region are shown in Figure 6.5. Figure 6.6 highlights the differences in seasonality and intensity by end of the century. IVT maxima occur typically in late autumn in the western region, in early autumn in the southern region, and in summer in the eastern region. In the western region, four models show a shift to later in the year and five models a shift to earlier in the year. The three models showing the strongest shifts towards later in the year also show largest positive changes in SW by end of the century. The models indicating earlier occurrence experience negative or only small changes in SW. In the southern and eastern region, six models show a later IVT block maxima occurrence and three models an earlier occurrence. In the southern region, the largest shifts towards later in

the year coincide again with largest positive changes in SW and vice versa. No relation between changes in seasonality and changes in SW are found in the eastern region.

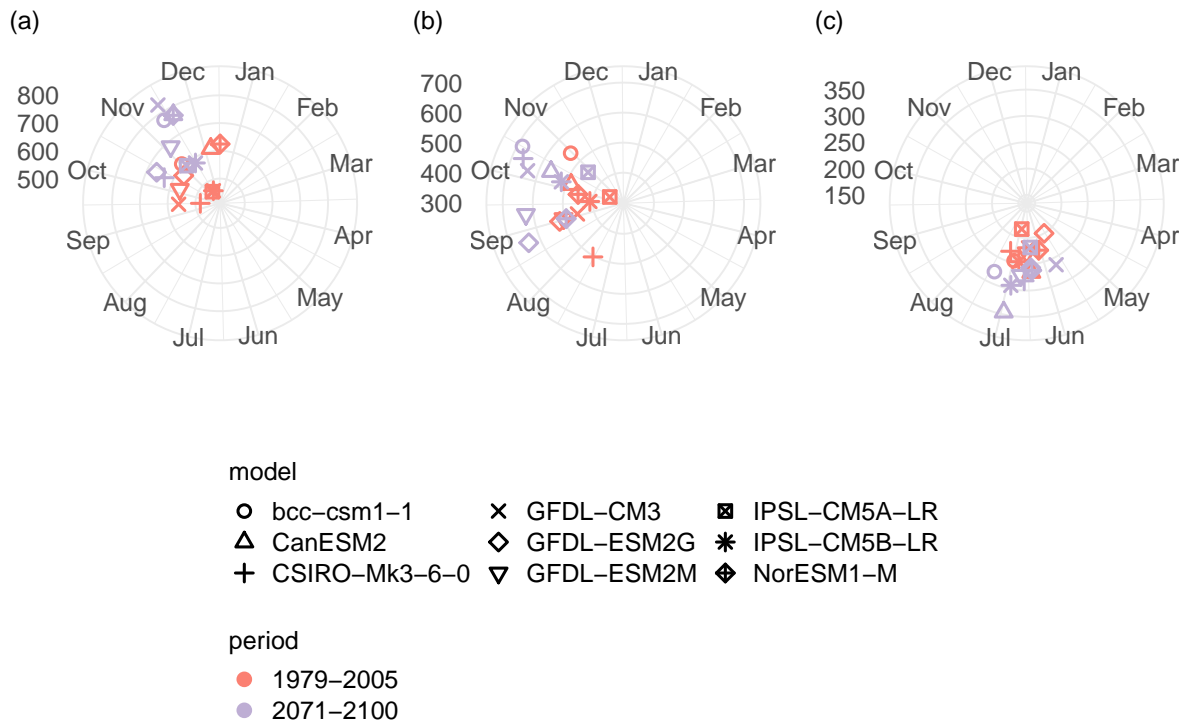


Figure 6.5: Seasonality and intensity (radius, scale on the left side of each panel) of IVT during IVT block maxima for the western region (a), the southern region (b), and the eastern region (c) in the reference period (red) and the future period (purple).

6.4.4 GEV results

The results for the fitted GEV models are depicted in Figures 6.7-6.13. The location parameters of the GEV models are fitted using the normalized covariates time, TPW, and SW. The fitted coefficients of the location parameter β_0 and β_1 for the three regions and the three covariates are shown in Figures 6.7 and 6.8, respectively. The coefficient β_0 shows only small differences between the three covariates and the different climate models within each region. The multi-model median of β_0 is $580 \text{ kg m}^{-1}\text{s}^{-1}$ in the western region, $500 \text{ kg m}^{-1}\text{s}^{-1}$ in the southern region, and $230 \text{ kg m}^{-1}\text{s}^{-1}$ in the eastern region. The multi-model median of β_1 (unitless due to the normalization of the covariates) in the western region ranges between 36 and 53 with time showing highest β_1 and SW showing generally smallest values but the largest model range. In the southern region, multi-model median values are again larger for time (47) and TPW (44) than for SW (33). The climate model range is smaller for time and SW than for TPW. However, both time and SW show several strong outliers within the models. In the eastern region, the

median for β_1 is largest for TPW (25) followed by SW (16) and time (13). In contrast to the other regions, the inter-model ranges are smaller in the eastern region.

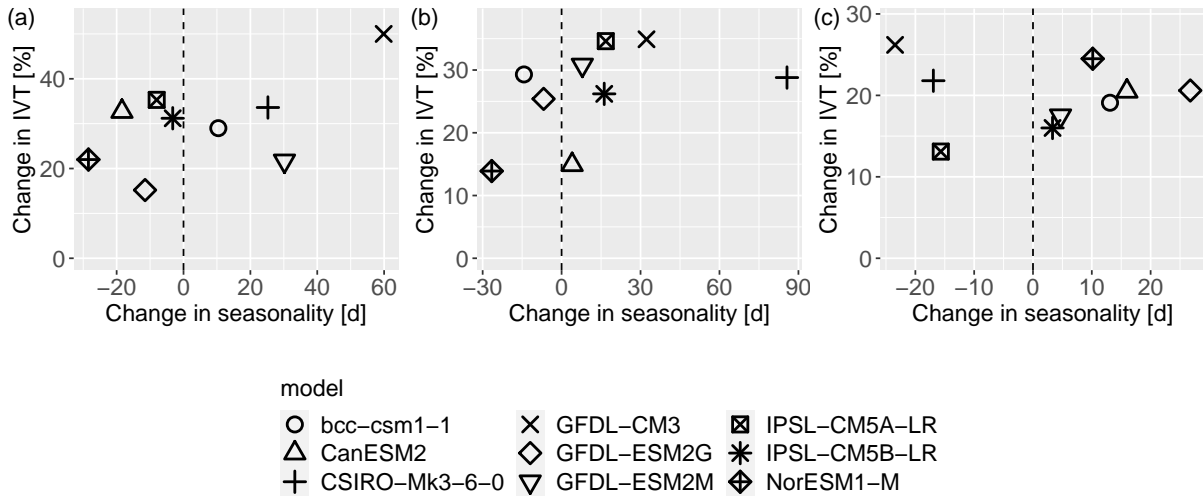


Figure 6.6: Changes in IVT seasonality and intensity during IVT block maxima by end of the 21st century (2071-2100) for the western region (a), the southern region (b), and the eastern region (c).

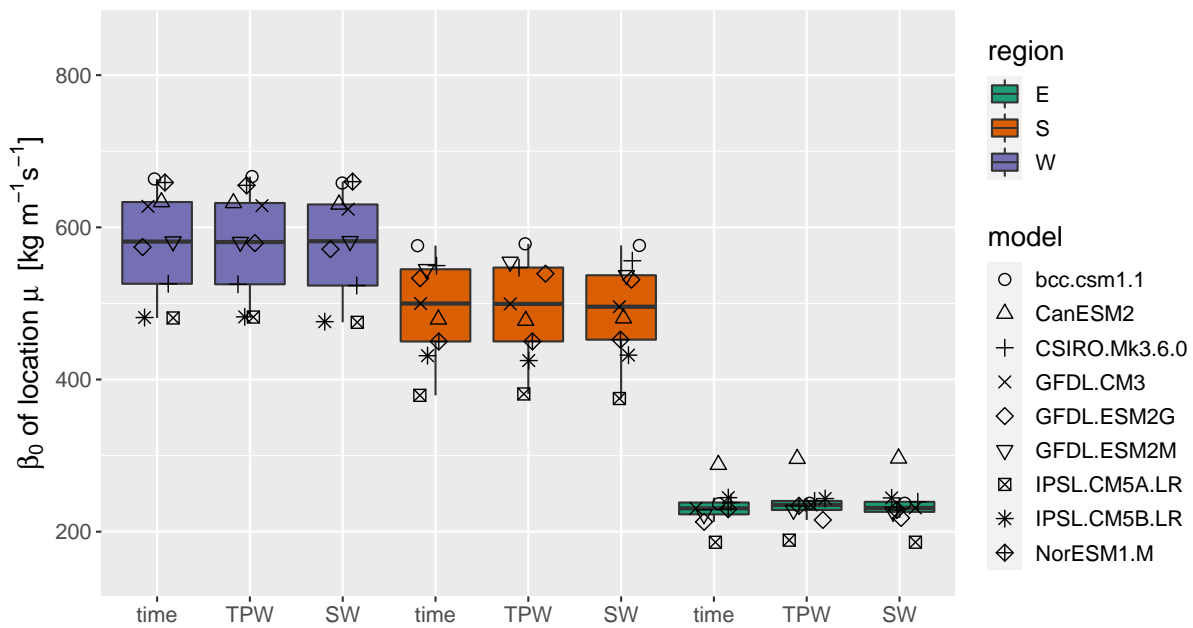


Figure 6.7: Coefficient β_0 of the location parameter for the three covariates and three regions.

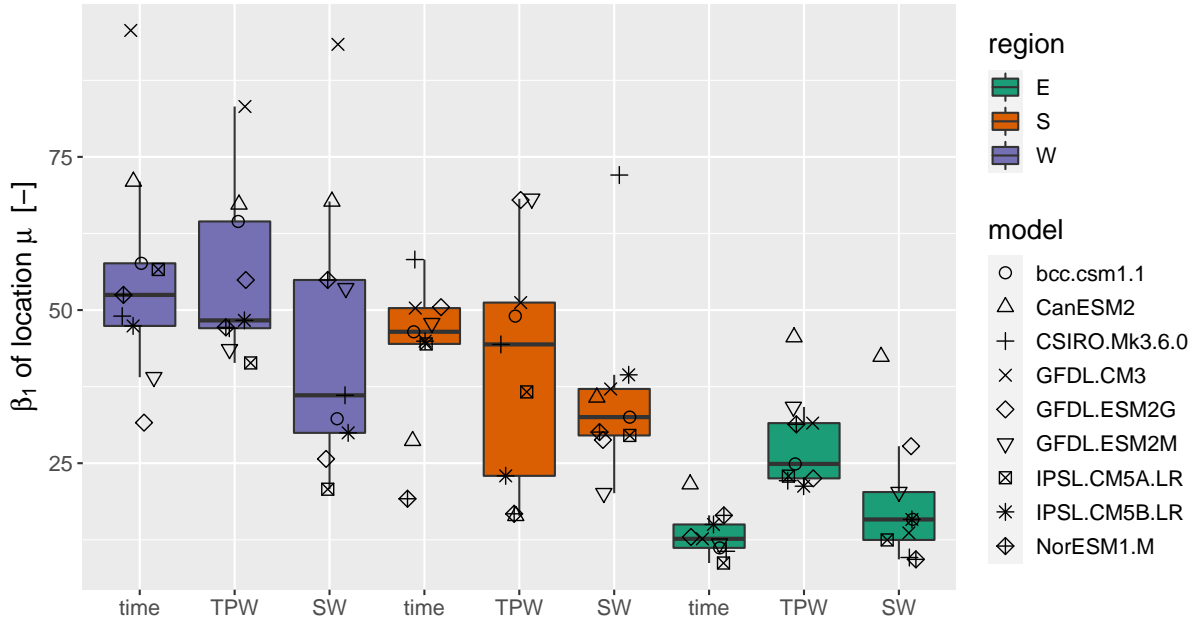


Figure 6.8: Coefficient β_1 (unitless) of the location parameter for the three covariates and three regions.

The results for the scale parameter (σ) are summarized in Figure 6.9. The largest scale parameters are found in the western region ($85\text{--}90 \text{ kg m}^{-1}\text{s}^{-1}$), followed by the southern region ($74\text{--}76 \text{ kg m}^{-1}\text{s}^{-1}$) and the eastern region ($49\text{--}55 \text{ kg m}^{-1}\text{s}^{-1}$). In all regions, the models with SW as covariate have the largest scale parameters on average and the models with TPW as covariate have the smallest scale parameters. Figure 6.10 shows the results for the shape parameter (ξ). The shape parameter is negative or equal to 0 for most models, regions, and covariates indicating an upper bound for extreme IVT. Positive shape parameters are only found in three cases. While in the western and southern region, the model with the covariate TPW has the most negative shapes on average, the model with the covariate SW has the most negative shape parameters in the eastern region.

Figure 6.11 depicts BIC scores of the fitted GEV distributions for the different climate models and the three regions. The lower the BIC scores, the better the GEV model fit. The BIC scores of the GEV models without using covariates (“no cov” in Figure 6.11) are used as a benchmark. Table 6.3 summarizes the differences of BIC scores between the non-stationary and stationary GEV models. In the western and the southern region, improvements are found for all covariates in all climate models. Using TPW as a covariate performs best in five climate models in the western region followed by time (in three climate models) and SW (two models). SW performs very well in climate models that show the strongest positive changes in the SW values on block maxima time steps. In the other models, SW performs worse than

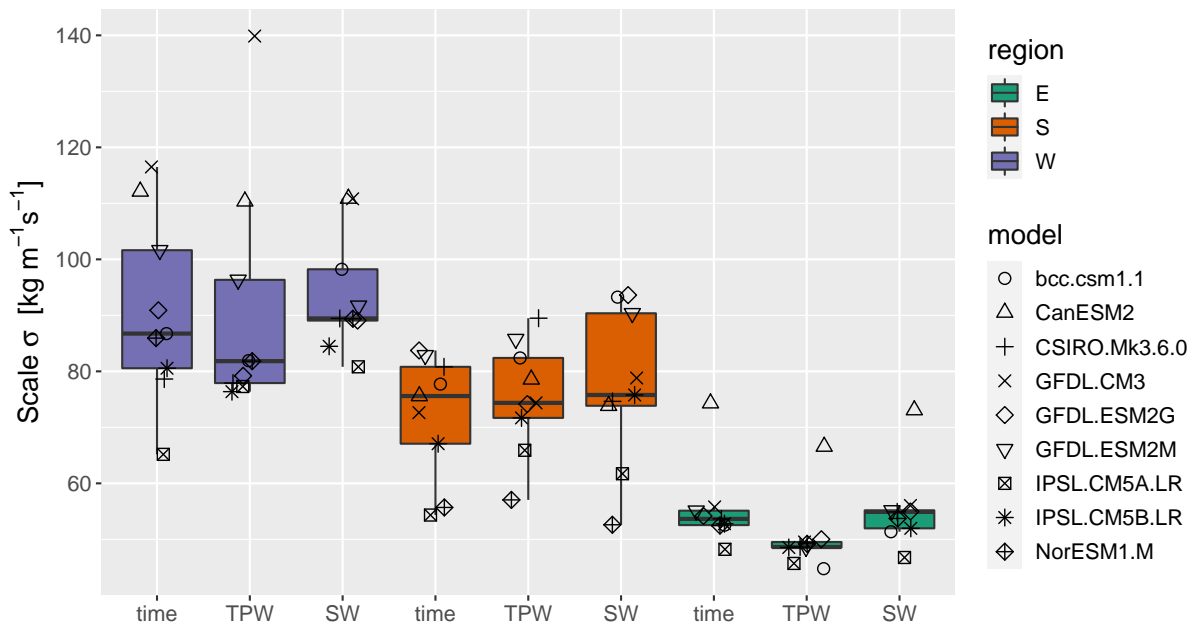


Figure 6.9: Scale parameters for the three covariates and three regions.

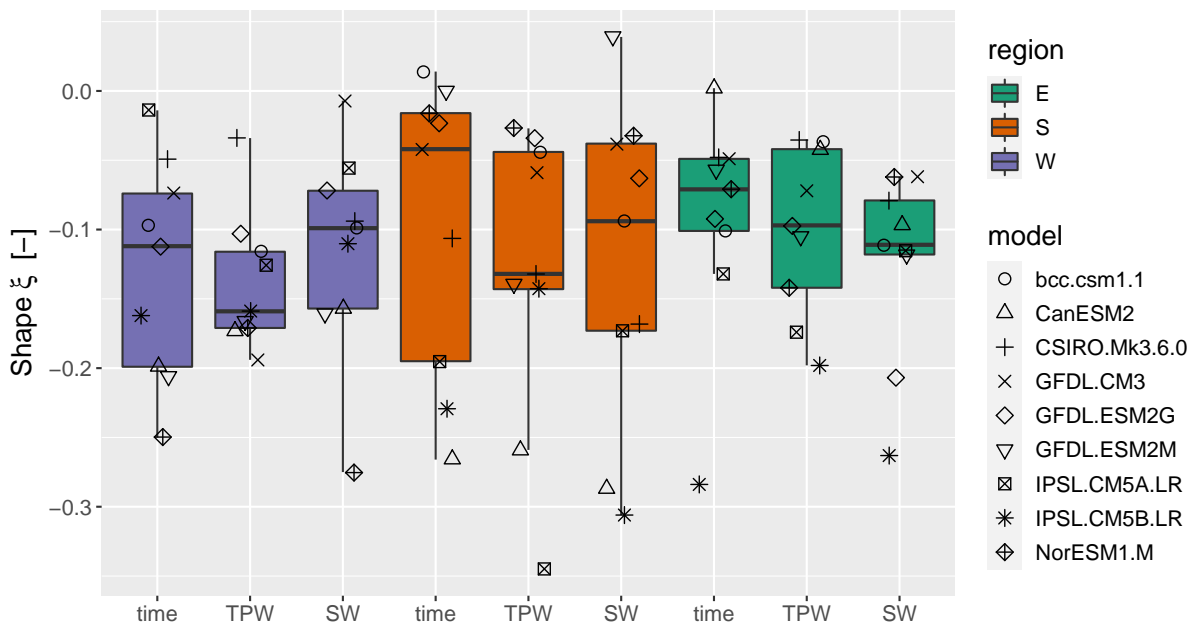


Figure 6.10: Shape parameters for the three covariates and three regions.

the other covariates. In the southern region, largest improvements in are found in four climate models for the covariate time, in two models for TPW, and in three models for SW. In the eastern region, TPW as covariate performs best in all climate models compared to the other covariates. The GEV models using covariates time and SW perform similar as the GEV model which does not use any covariates. Performance of the GEV fit even decreases in two climate models when including SW as a covariate and in one climate model when using time as covariate.

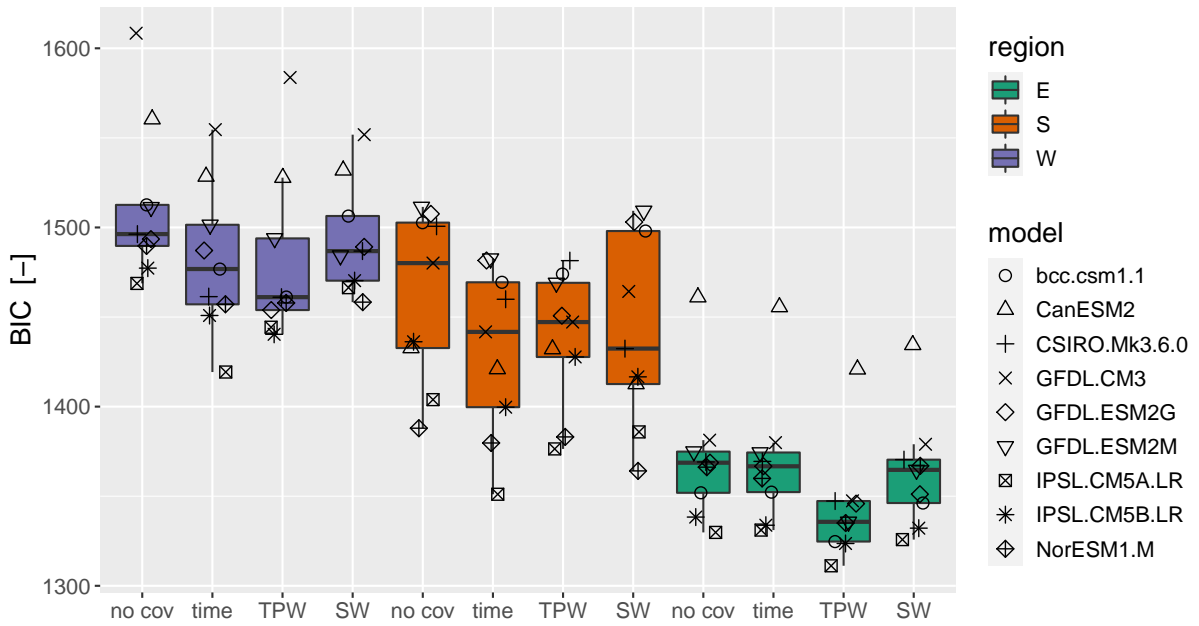


Figure 6.11: BIC scores for the GEV models either using no covariate (no cov) or using the covariates time, TPW, or SW.

Figure 6.12 shows the effective return levels for 100-year events for each year in the period 1979-2100. This figure highlights the effect of fitting non-stationary models with different covariates. In all fitted GEV models, the 100-year return levels are not constant over time. Using time as a covariate (Figure 6.12a-c) results in a linear increase of the 100-year return level. The slopes of the effective return levels differ across the climate models. The effective return levels when using TPW (Figure 6.12d-f) or SW (Figure 6.12g-i) as a covariate show high variability over time. Despite the high variability, TPW shows an increase over time in the effective 100-year return levels. Such an increase is not found for SW. This behavior is also present in Figure 6.13 showing 30-year means of return levels for 100-year events in the reference period (1979-2008) and in the future period (2071-2100) for the three regions and the different covariates. In the western region, the average 100-year return levels in the reference period range from 833-896 $\text{kg m}^{-1}\text{s}^{-1}$ and increase to 903-942 $\text{kg m}^{-1}\text{s}^{-1}$ by end of the 21st century (Figure 6.13a). Using time as covariate results in a very strong increase, while TPW shows smaller increases. For SW,

Table 6.3: Differences of BIC scores between the fitted models with covariates and the stationary model for each region. Covariates showing the largest improvement are highlighted in bold and covariates showing worse performance than the stationary model are highlighted in italics.

model	W			S			E		
	time	TPW	SW	time	TPW	SW	time	TPW	SW
bcc.csm1.1	36	51	6	33	29	5	0	27	6
CanESM2	32	33	29	12	1	20	6	40	27
CSIRO.Mk3.6.0	35	35	10	41	19	68	0	22	<i>-1</i>
GFDL.CM3	54	25	57	38	33	16	1	34	2
GFDL.ESM2G	6	40	4	26	57	5	2	23	18
GFDL.ESM2M	10	17	27	29	42	2	1	39	10
IPSL.CM5A.LR	50	25	2	53	28	18	<i>-1</i>	19	4
IPSL.CM5B.LR	26	37	7	37	9	20	5	15	6
NorESM1.M	33	32	31	8	5	24	6	31	<i>-1</i>

hardly any change in average return levels are found. The average 100-year return levels increase from 738-768 kg m⁻¹s⁻¹ in the reference period to 833-869 kg m⁻¹s⁻¹ in the future period for the southern region (Figure 6.13b). The increase in return levels is again strongest when using time as covariate followed by TPW. For the covariate SW hardly any change in the return levels is found and only the model projecting strongest increase in SW shows an increase in the 100-year return level. In contrast to the western region, the covariate SW also shows similar increase like TPW. In the eastern region, the average 100-year return levels increase from 396-421 kg m⁻¹s⁻¹ to 419-466 kg m⁻¹s⁻¹ by end of the century again showing strongest increase when using time as covariate and almost no change when using SW as covariate. Selecting the best covariates for each region results on average in an increase of the 100-year return level of 59 kg m⁻¹s⁻¹ in the western region, 121 kg m⁻¹s⁻¹ in the southern region, and 20 kg m⁻¹s⁻¹ in the eastern region.

6.5 Summary and Discussion

6.5.1 Changes in moisture transport extremes

Western Region

In the western region, extreme moisture transports directed towards Swiss orography in the western region originate in the North Atlantic and are often associated with atmospheric rivers (Froidevaux and Martius, 2016). Thus, extreme moisture transports are strongly linked to the dynamics over the North Atlantic, i.e., the location and strength of troughs and ridges governing the position and speed of the jet stream. Atmospheric river like patterns were also found in the climate model composites with high IVT over the Atlantic, France and northwestern

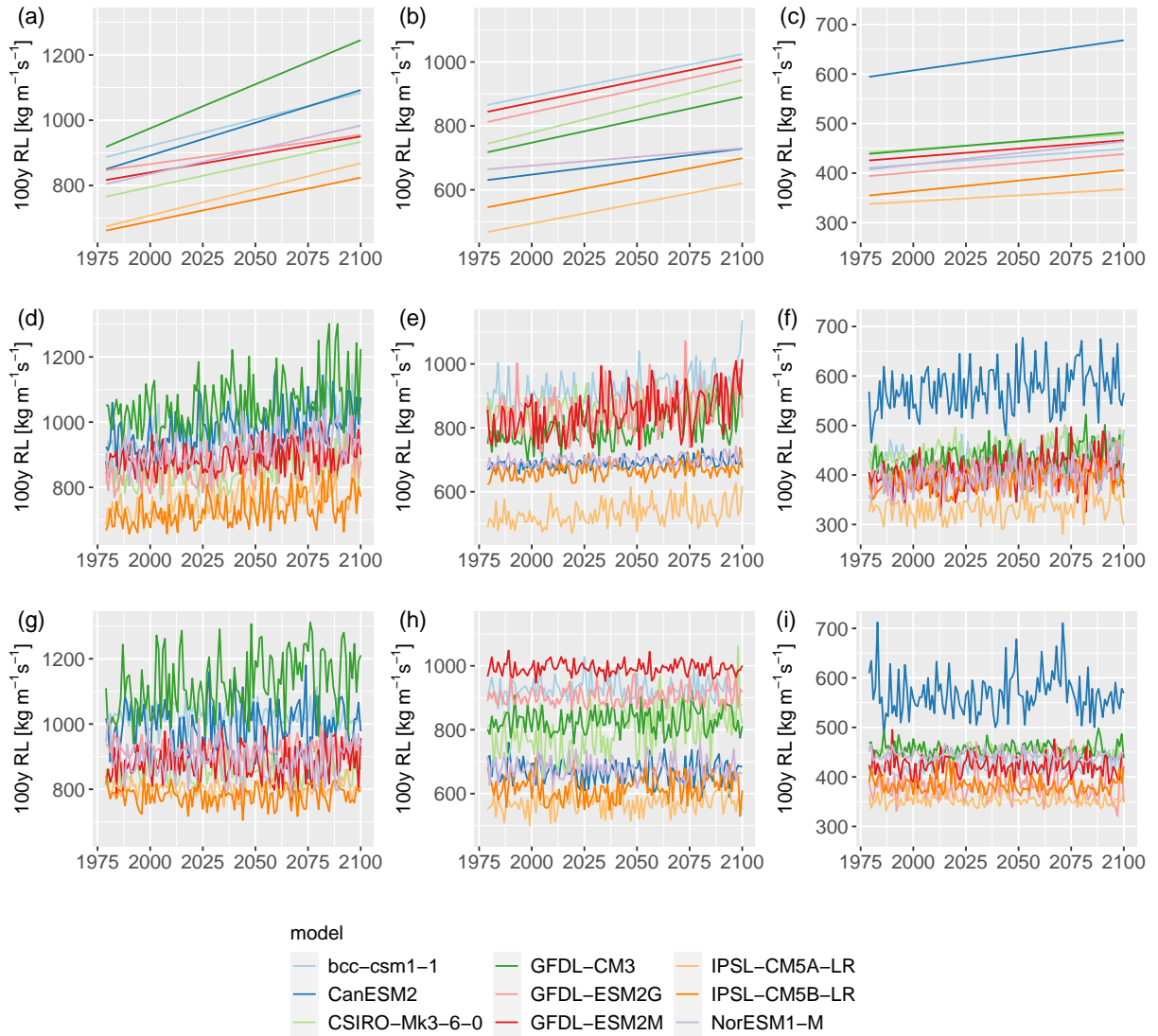


Figure 6.12: Effective 100-year return levels (RL) using the covariates time (a-c), TPW (d-f), and SW (g-i) for the western region (left panels), the southern region (middle panels), and the eastern region (right panels).

Switzerland. However, IVT during block maxima reach about $570 \text{ kg m}^{-1}\text{s}^{-1}$ on average in the reference period in the western region. Decomposing IVT into its components yields similar values for the moisture related component TPW and the wind related component SW indicating the importance of both the thermodynamic and the dynamic components. Towards the end of the 21st century, IVT extremes are projected to increase by 30% on average. While TPW increases by 25% by end of the century, the SW component increases only marginally by 1.6% on average. Some models even suggest a decrease in SW by end of the century. Thus, the increase in IVT extremes with climate change can be predominantly related to thermodynamic changes. The Clausius-Clapeyron relationship describes an increase in the water holding capac-

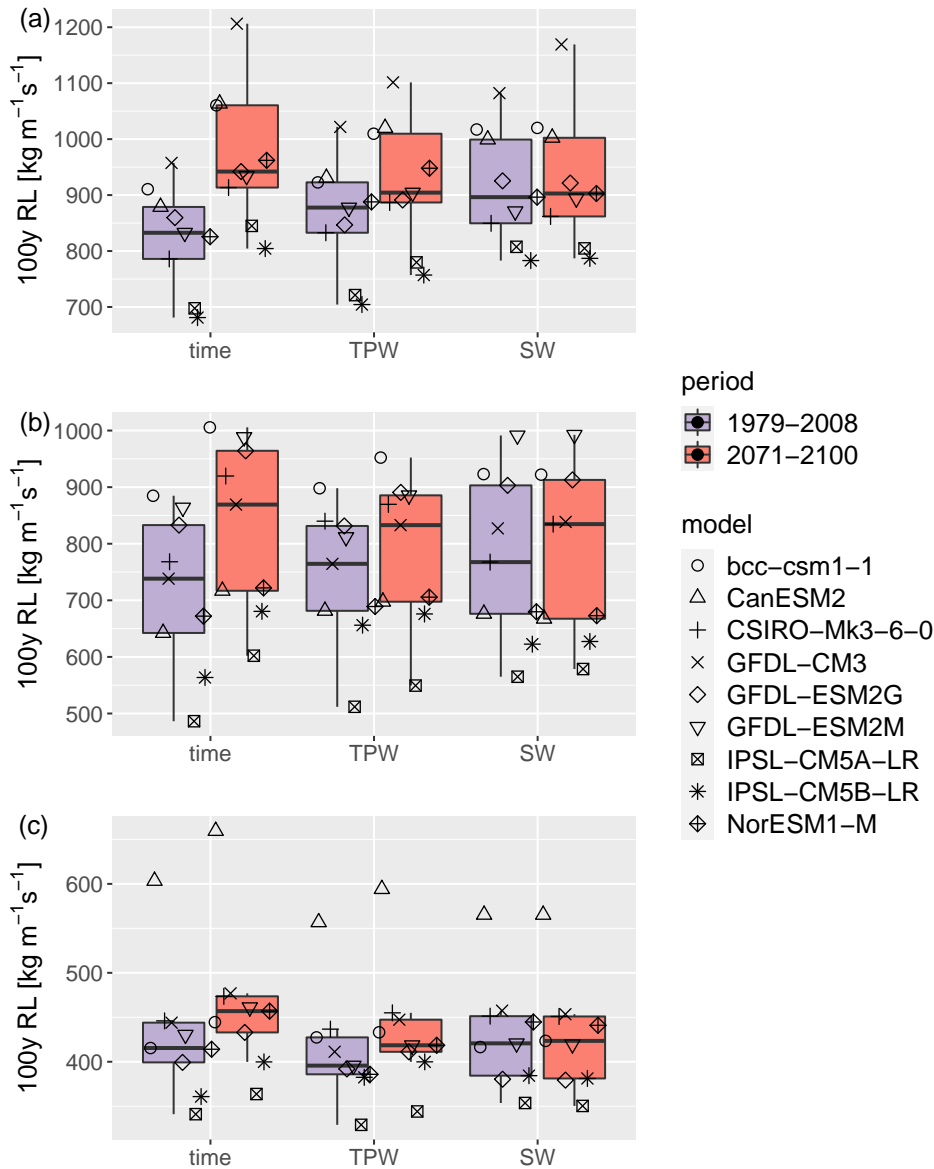


Figure 6.13: 30-year averages of estimated 100-year return levels (RL) of IVT intensity for the reference period (1979-2008) and the future period (2071-2100) for the western region (a), southern region (b) and eastern region (c).

ity of air of approximately $7\% \text{ K}^{-1}$. The average global temperatures increase in the models used in this study is 3.5 K by end of the 21st century compared to the reference period. Following the Clausius-Clapeyron relationship, this would correspond to an increase of approx. 25% in TPW. Even though the IVT block maxima are defined as yearly maxima and may not occur at the same time of the year every year, the average magnitude change in TPW during block maxima yields is approximately what can be expected from the Clausius-Clapeyron relationship. IVT block maxima typically occur in late autumn in the western region. Five models project

earlier occurrence and four models project later occurrence. Models showing strong shifts in seasonality towards later in the year also project smaller positive changes in TPW due to lower temperatures and strongest positive changes in SW. However, the other models do not confirm these patterns.

Southern Region

In the southern region, upper-level troughs and associated low-level cyclonic flow over western Europe transport moist air from the Mediterranean Sea towards the Alps (Froidevaux and Martius, 2016). A band of high IVT air extending from the Mediterranean Sea towards the Alps along the eastern flank of an upper-level trough is also present in the composites of the climate models confirming that the climate models are able to represent similar structures as found by Froidevaux and Martius (2016). IVT intensities during block maxima are approximately $480 \text{ kg m}^{-1}\text{s}^{-1}$ in the reference period and are thus a bit smaller than in the western region. The contribution of TPW to IVT is larger than the contribution of SW with a TPW to SW ratio of approximately 1.4. IVT maxima are projected to increase by 30% and TPW is projected to increase by 25% (again following the CC relationship). A slight positive change in the multi-model median was found for SW but two models project a negative change. With the positive changes in TPW and hardly any change in SW the relative contribution of TPW increases in future and decreases for SW. This points towards a strong thermodynamic driver of the changes in IVT extremes. In the southern region, IVT block maxima typically occur in early autumn (September and October). Two thirds of the climate models suggest a slight shift towards late autumn. Like in the western region, models projecting stronger shifts in seasonality also project stronger increases in SW.

Eastern Region

For the eastern region, Froidevaux and Martius (2016) found extreme IVT directed towards orography can be associated with upper-level cut offs and high IVT reaches Switzerland from a northeastern direction. In the climate models a cyclonic structure of high IVT is found. IVT values during block maxima are smaller than in the other two regions. In the reference period, IVT intensities reach approximately $230 \text{ kg m}^{-1}\text{s}^{-1}$. This is in agreement with the results based on ERA-Interim by Froidevaux and Martius (2016). Compared to the other regions, TPW in the eastern region is much smaller. Less moisture is expected due to the lack of a large potential moisture source (such as an ocean) in the vicinity. Also, SW intensities are much smaller than in the other regions. The contribution of TPW to IVT is twice as large than the contribution of SW to IVT. While IVT maxima increase about 20% by end of the century, TPW shows stronger increase of about 25%. This strong increase is compensated by a small decrease in SW. IVT block maxima in the eastern region occur typically in summer. Two thirds of the models project a slight shift of the seasonality towards late summer.

6.5.2 GEVs and associated return levels

Since IVT block maxima are increasing over time GEV models were fitted with a dynamic location parameter to account for this non-stationarity. The location parameter was modelled with a linear model using three covariates: time, TPW, and SW. The intercept of the location parameter β_0 is very similar for all covariates. Highest β_0 was found for the western region, followed by the southern and the eastern region. This reflects the different levels of IVT maxima per region. The coefficient β_1 is always positive. For time and TPW as covariates positive β_1 result in a positive shift of the location parameter. For SW, positive β_1 may not necessarily result in an increase of the location parameter since no clear trend was found in this covariate. In the western and the southern region, using time or TPW as covariate results in higher β_1 than using SW. In the eastern region, β_1 is largest for TPW. The scale parameter showed highest values when using SW as a covariate. This indicates large variability in this parameter. The shape parameter is negative in almost all model fits. This suggests that the tail of the GEV distribution follows a Weibull distribution implying the existence of an upper bound in the distribution of IVT maxima. IVT maxima can thus not reach infinitely large values which has important implications in the retrieval of very extreme return levels.

Comparing the performance of the fitted non-stationary models with the performance of a stationary model showed that using covariates improves the models in almost all cases. Exceptions were only found in the eastern region where the covariate SW resulted in lower performance for two models and time resulted in lower performance in one model. Good performance was mainly found for TPW and time. Using SW as covariate showed good performance in models with large SW trends. Over all models, best performance was found for TPW as covariate in the western and the eastern region and for time in the southern region. The best covariates for each region also showed large β_1 coefficients. Fitting non-stationary GEV models has implications for the estimation of return levels. The effective 100-year return levels vary over time and increase by end of the century when using time or TPW as a covariate because of the existing trend in the covariates. This suggests that the atmospheric potential for floods increases with climate change. However, the atmospheric potential represents only one but important ingredient for floods. The generation of floods involves a complex process chain and is highly dependent on the location and the predominant catchment-specific characteristics as well as the antecedent conditions within a catchment.

6.6 Conclusions and Outlook

Moisture transport (IVT) extremes directed towards orography in Switzerland are important atmospheric flood precursors. This study investigated future changes of direction dependent IVT extremes under climate change (RCP8.5 pathway) for three regions in Switzerland: West, South, and East. IVT was further decomposed into a moisture related component (TPW) and

a wind related component (SW). Generalized extreme value models were fitted for IVT block maxima with a dynamic location parameter. This allowed the estimation of 100-year return levels accounting for non-stationarities in IVT.

The results of this study show that extreme moisture transports potentially leading to floods will increase with climate change. Thus, the atmospheric potential for floods increases. By the end of the 21st century, IVT block maxima increase by 30% in the western and southern region and by 20% in the eastern region. The contribution of TPW to IVT is largest for the eastern region, followed by the southern and the western region. TPW is also projected to increase by 25% and hardly any changes in SW are found. Therefore, the contribution of TPW to IVT will increase with climate change. This suggests that the major driver of the increase in IVT is related to changes in the thermodynamics (Clausius-Clapeyron relationship) and not to changes in the dynamics.

Fitting non-stationary GEV models using covariates time, TPW and SW improves the performance of the fitting compared to a stationary GEV model. TPW as covariate results in best performance for the western and the eastern region, and time as covariate results in best performance for the southern region. Since both covariates include a temporal trend, the estimated 100-year return levels increase by end of the century.

This study provided a first glimpse on how extreme IVT potentially leading to floods in Switzerland will change under climate change. Many further questions and analyzes could be addressed to get a complete picture of future changes in IVT, among them:

- Beside visually inspecting QQ-Plots to assess the goodness of fit of the fitting, a Kolmogorov-Smirnov test could be used (Koch et al., 2019)
- Conduct similar analysis but as a function of global warming levels
- Use analogues to attribute changes in IVT to changes in thermodynamics vs changes in dynamics
- Identify moisture sources and potential changes in sources with a tracking method
- Analyze changes in the frequency and duration of extreme IVT events using a pre-defined threshold

Chapter 7

Summary, concluding remarks and outlook

7.1 Summary

The first part of this PhD thesis focuses on future changes in river runoff under climate change in Switzerland. Such climate change impact assessments are critically important for decision-makers and planners in terms of adaptation and mitigation planning. This part consists of three major steps: i) the generation of new hydrological scenarios, ii) the analysis of future changes in runoff regimes, and iii) the analysis of future changes in moderate low and high flows.

In chapter 2, the new hydrological scenarios "Hydro-CH2018-Runoff" are presented. The Hydro-CH2018-Runoff ensemble consists of daily runoff simulations for 93 meso-scale catchments in Switzerland. The selected catchments cover a wide range of different catchment characteristics and runoff regimes governed by pluvial, nival, and glacial processes. The hydrological modelling system PREVAH (Viviroli et al., 2009) was used to simulate runoff under climate change. PREVAH is a semi-distributed model based on hydrological response units and includes different submodels to account for important hydrological processes related to snow, glacier, and soil moisture dynamics, as well as evapotranspiration. PREVAH was calibrated (even years) and validated (uneven years) for each catchment separately using observations between 1985-2014. The results show satisfactory performance with a median Nash-Sutcliffe efficiency of 0.82 and a median Kling-Gupta efficiency of 0.89 in the calibration and the validation period. The calibrated parameters were then used to simulate runoff under climate change for the period 1981-2099. The simulations were driven by daily precipitation and temperature data from the high-resolution new CH2018 scenarios (CH2018, 2018). In total, 68 GCM-RCM combinations for the period 1981-2099 covering 3 different emission scenarios (RCP2.6, RCP4.5, RCP8.5) were used for the simulations. To account for glacier retreat, glacier extents were updated every 5 years according to the glacier projections by Zekollari et al. (2019) that are based on the same GCM-RCM combinations. The simulations show good agreement between simulated and

observed runoff regimes in the reference period and can thus be used for further climate impact studies. The Hydro-CH2018-Runoff ensemble is downloadable from the Zenodo archive under <http://doi.org/10.5281/zenodo.3937485>.

In chapter 3, climate change impacts on runoff regimes in Switzerland are assessed. The previously described Hydro-CH2018-Runoff ensemble was used to determine future changes in runoff regimes and their time of emergence for the 93 catchments in Switzerland. Projected changes in seasonal patterns show increasing winter runoff and decreasing summer and autumn runoff. In spring, runoff is projected to increase in high elevation catchments and to decrease in lower lying catchments. The yearly mean runoff is projected to decrease in most catchments. A strong elevation dependence of the sign and magnitude of change is found with high elevation catchments (above 1500 masl) facing larger changes in winter, spring, and summer due to the strong influence of snow and glacier related processes (accumulation and melt). Not all catchments show a time of emergence in all seasons and in some catchments the detected significant changes are not persistent over time. However, early times of emergence are found in winter and summer (before 2065; period 2036-2065) for catchments with mean altitudes above 1500 masl under RCP8.5. Significant changes emerge later in the 21st century in catchments with mean altitudes below 1500 masl. The magnitude of the changes and the climate model agreement on the sign of change (positive or negative) increase with increasing global mean temperatures or stronger emission scenarios. This amplification highlights the importance of climate change mitigation.

In chapter 4, the results of chapter 3 are complemented with an analysis of changes of moderate low and high flows. The results show a strong elevation dependence. In Alpine catchments (approx. >1500 masl), the magnitude of moderate low flows increases while their frequency decreases with early significant changes in the 21st century. In low altitude catchments (approx. <1500 masl), the magnitude of moderate low flows decreases and the frequency increases by end of the 21st century with significant changes emerging later in the century. Moderate low flows predominantly occur in late summer and early autumn by end of the century. The elevation dependence as well as the climate model agreement on the sign of change in moderate high flows is less clear and often not significant. Most catchments show slightly increasing magnitudes and frequencies in high flows while very high Alpine catchments show decreasing magnitudes and frequencies. The seasonality of moderate high flows changes only in Alpine catchments with a shift from late summer to early summer.

In chapter 5, a comparison between the modelling results from different Swiss research institutions is presented. A first comparison was made between the results of this thesis, the University of Zurich, and the Swiss Federal Institute for Forest, Snow and Landscape Research. Although the climate input data, the hydrological models, and their model parameters differ, an overall good agreement on the sign and the magnitude of change in seasonal runoff is found.

Differences between the magnitudes of change are largest in winter and spring for Alpine catchments (snow processes) and in summer and autumn for lower lying catchments (evaporation processes). In a second comparison, the results were compared to simulations driven with data from a weather generator by the ETH Zurich. The differences between the simulations are larger than in the first comparison with strongest differences found in late spring/early summer and late summer.

The second part of this PhD thesis (chapter 6) focuses on future changes in moisture transport (IVT) extremes directed towards orography in Switzerland. These IVT extremes are important atmospheric flood precursors. IVT extremes for three regions in Switzerland were analysed in 9 climate models (from CMIP5) under a high emission scenario (RCP8.5). The results show that IVT extremes increase by 30% in the western and the southern region and by 20% in the eastern region of Switzerland. The moisture component (TPW) of IVT is projected to increase by 25% while the wind component (SW) of IVT hardly changes with climate change. This suggests that the major driver of the increase in IVT is related to changes in the thermodynamics (Clausius-Clapeyron relationship) and not to changes in the dynamics. To estimate 100-year return levels, non-stationary Generalized Extreme Value (GEV) models were fitted using the covariates time, TPW and SW. The non-stationary models improve the fitting compared to a stationary GEV model. TPW as covariate results in best performance for the western and the eastern region, and time as covariate results in best performance for the southern region. Since both covariates include a temporal trend, the estimated 100-year return levels increase by end of the century.

7.2 Concluding remarks

The results of the first part of this thesis provide a detailed analysis of future changes in river runoff in Switzerland. Observed trends in the past with increasing winter runoff and decreasing summer runoff are projected to continue and to intensify with climate change. Yearly mean runoff is also projected to decrease by end of the 21st century. Projected changes are amplified by higher emissions and thus stronger global temperature increase. In winter, enhanced precipitation together with more liquid than solid precipitation lead to more direct runoff. In summer, the combination of earlier snow melt and retreating glaciers lead to smaller contributions of snow and glacier to runoff. In addition, decreasing summer precipitation and enhanced evapotranspiration also result in less summer runoff. The seasonal changes are more pronounced in Alpine catchments due to the importance of snow and glacier related processes and less pronounced in lower lying catchments which are mainly driven by precipitation and evapotranspiration processes. However, lower lying catchments are strongly affected by climate change in terms of low flows. Low flows are projected to decrease in summer when water demand is highest for irrigation in agricultural regions. Also, the decreasing water availability in summer may have implications for the cooling of infrastructures and in combination with increasing water temperatures may

foster water stress for ecosystems. In winter, low flows are projected to increase particularly in Alpine catchments which may be beneficial for electricity production. These changes in the seasonal availability of water may trigger potential conflicts among water users. Therefore, the presented results may serve as a basis for future discussions in the decision-making process in terms of adaptation planning but also in terms of mitigation actions. For example, the results could be used for the planning of reservoirs which are able to absorb potential water limitations during low flow conditions in summer. The author also provided results for a low flow indicator called Q347 (not shown in this thesis, but similar results as for the low flow analysis in chapter 4) upon which the minimal residual water is defined in the water protection law of Switzerland. The way this minimal residual water is defined in the law may need to be changed due to changes in the Q347.

Understanding future changes of flood magnitudes and frequencies is crucial due to the devastating and costly nature of floods. In this thesis, a two-fold attempt was made to assess potential changes in floods. First, the Hydro-CH2018-Runoff simulations were analysed in terms of moderate high flows. Secondly, changes in extreme IVT serving as important atmospheric flood precursor were analysed in global climate models. The results for moderate high flows show a small but in most cases not robust increase in high flow magnitude and frequency in most of the catchments. In this analysis, annual maxima were averaged over 30 years and do not represent major floods. In a short analysis, we also compared the largest three flood events in the present period and the future period (not shown in this thesis). The results show a stronger increase in high flow magnitude when only considering the three highest annual maxima per period than for moderate high flows. However, the results of this short analysis are not robust nor significant due to the small sample size ($n=3$). Even though the results are not robust across all climate models, they show a tendency towards increasing flood magnitudes and frequencies with climate change. On the other hand, extreme IVT directed towards the Alps intensify significantly (+20-30%) with climate change. Thus, the atmospheric potential for floods increases. The atmospheric potential represents only one but an important ingredient for floods. The generation of floods involves a complex process chain and is highly dependent on the location and the predominant catchment-specific characteristics as well as the antecedent conditions within a catchment. However, the increase in the atmospheric potential for floods together with the slightly increasing trends in moderate high flows points towards a increase in flood magnitudes with climate change.

Although the new Hydro-CH2018-Runoff simulations represent the most up to date and state of the art data set for meso-scale rivers in Switzerland, some limitations to the data set have to be mentioned. Uncertainties arise from all steps of the modelling chain: the scenarios of greenhouse gas concentrations, the climate model chains and their boundary and initial conditions, the post-processing and downscaling method, the hydrological model and its calibration, and the underlying glacier projections. The most important uncertainties regarding hydrological

modelling are mentioned hereafter. First, it is assumed that the calibrated parameters are also valid in a changing climate. This is a strong assumption and is under debate in the scientific community. In this thesis, the calibration was done on even years between the period 1985-2014. Using every second year within 30 years for calibration minimizes the potential effect of random and non-random trends by using too short calibration periods. Since increasing temperature and changing precipitation patterns are already observed in the calibration period, the hydrological model is trained to simulate runoff under changing conditions. The model shows good performance also in the validation period (uneven years). In this period, several floods (e.g., 1999, 2005, 2007, 2011) and droughts (e.g., 2003, 2011, 2015) occurred and the hydrological model is able to capture these events. Second, the land use (except glacier extents) was hold constant during the 119 years of simulation. It is likely that land use will change in future. However, land use changes are highly influenced by political decisions in Switzerland and not that much by natural changes. Last, the Hydro-CH2018-Runoff ensemble is based on only one hydrological model. A comparison for some catchments with the results of two other hydrological models (PREVAH-WSL and HBV-light) show a good agreement on the climate change signal in the runoff among the hydrological models. The good agreement between our results and the results from other modelling efforts by different research institutions gives confidence that our simulations can be further used for other research studies within the field of hydrology or further impact studies (e.g., agricultural or ecological studies).

7.3 Outlook

The work presented in this thesis provides plenty of follow-up research questions and the most important ones are listed below. For the hydrological part of this thesis, the most important research questions are:

- *Compound drought events*: Chapter 4 focused on future changes in the magnitude and frequency of low flows or hydrological droughts. While a hydrological drought may have severe impact on the river itself and the ecosystems in and surrounding the river, an impact on agriculture is not necessarily given. The compound occurrence of a hydrological drought (runoff deficit), a meteorological drought (precipitation deficit) and an agricultural drought (soil moisture deficit) reinforces the impacts and may lead to severe water stress in many sectors. Further investigations on future changes in the compound occurrence of different droughts types, the spatial extent of compound droughts, and their temporal co-occurrence with other extremes (such as heat) would provide important information.
- *Meteorological drivers of droughts*: Many previous studies found key meteorological drivers for floods in Switzerland. Meteorological situations leading to hydrological droughts are less known. Identifying the key meteorological drivers (precipitation, radiation, wind) and the associated large-scale weather situations as well as the hydrological preconditions (e.g.,

winter snow accumulation) that reinforce hydrological droughts would provide a deeper understanding of future changes of hydrological droughts.

- *Better flood projections in the next round of climate change scenarios?*: The results of this thesis are based on daily simulations of runoff. A daily resolution may be good enough to reproduce the hydrological regime but may not be high enough to depict all important flood generation processes. Operational flood forecasts today are mostly driven by hourly meteorological input to also reflect the daily cycle of temperature and precipitation. A new generation of climate change scenarios for Switzerland may be released in the next years. Higher spatially and also temporally resolved climate change scenarios may allow for better projections of floods and more robust conclusions.

A short outlook of potential research questions on the topic of moisture transport extremes was already given in chapter 6 and is extended here:

- *Global warming as driver*: The results of chapter 6 could be transformed into a slightly different perspective by conducting similar analysis but as a function of global warming levels. This would reduce some of the uncertainty in the climate models and would provide information on critical warming levels.
- *Frequency and duration of high IVT events*: Not only the intensity of IVT extremes is important for flood generation but also the duration of high IVT events. Also, the frequency of high IVT events is of interest for future planning and risk analysis. The frequency and duration of high IVT events could be investigated by setting a threshold of IVT (e.g., 30-year mean of IVT block maxima in the reference period or a particular quantile of IVT).
- *Thermodynamics vs dynamics*: The attribution of IVT changes to changes in thermodynamics and dynamics could be addressed in a different way. One possibility would be to work with analogues. By only considering analogous situations, the dynamic contribution to IVT would be kept constant and the resulting changes could be attributed to changes in thermodynamics.
- *Large-scale situation*: A detailed analysis of the large-scale situation leading to the most extreme IVT events in the present and in future would also give insight into potential changes in the dynamics.
- *Moisture tracking*: Using backward trajectories of moisture would allow the identification of moisture sources leading to extreme IVT in the climate models. Also, potential changes of moisture sources could be analyzed.

Bibliography

- Addor, N., Rössler, O., Köplin, N., Huss, M., Weingartner, R., and Seibert, J.: Robust changes and sources of uncertainty in the projected hydrological regimes of Swiss catchments, *Water Resources Research*, 50, 7541–7562, <https://doi.org/10.1002/2014WR015549>, 2014.
- Alderlieste, M. A., Van Lanen, H. A., and Wanders, N.: Future low flows and hydrological drought: how certain are these for Europe?, in: *Hydrology in a Changing World*, vol. 363, pp. 60–65, 2014.
- Allamano, P., Claps, P., and Laio, F.: Global warming increases flood risk in mountainous areas, *Geophysical Research Letters*, 36, <https://doi.org/10.1029/2009GL041395>, 2009.
- Ban, N., Schmidli, J., and Schär, C.: Heavy precipitation in a changing climate: Does short-term summer precipitation increase faster?, *Geophysical Research Letters*, 42, 1165–1172, <https://doi.org/10.1002/2014GL062588>, 2015.
- Beniston, M. and Stoffel, M.: Rain-on-snow events, floods and climate change in the Alps: Events may increase with warming up to 4 C and decrease thereafter, *Science of the Total Environment*, 571, 228–236, <https://doi.org/10.1016/j.scitotenv.2016.07.146>, 2016.
- Berghuijs, W. R., Harrigan, S., Molnar, P., Slater, L. J., and Kirchner, J. W.: The relative importance of different flood-generating mechanisms across Europe, *Water Resources Research*, 55, 4582–4593, <https://doi.org/10.1029/2019WR024841>, 2019.
- Bergström, S.: Development and application of a conceptual runoff model for Scandinavian catchments, Tech. Rep. RHO 7, SMHI Report, Norrköping, Sweden, 1976.
- Bernhard, L. and Zappa, M.: Natürlicher Wasserhaushalt der Schweiz und ihrer bedeutendsten Grosseinzugsgebiete, Comissioned by the Swiss Federal Office for the Environment, 2012.
- Bertola, M., Viglione, A., Lun, D., Hall, J., and Blöschl, G.: Flood trends in Europe: are changes in small and big floods different?, *Hydrology and Earth System Sciences*, 24, 1805–1822, <https://doi.org/10.5194/hess-24-1805-2020>, 2020.
- Birsan, M.-V., Molnar, P., Burlando, P., and Pfaundler, M.: Streamflow trends in Switzerland, *Journal of Hydrology*, 314, 312–329, <https://doi.org/10.1016/j.jhydrol.2005.06.008>, 2005.

- Blöschl, G., Hall, J., Viglione, A., Perdigão, R. A., Parajka, J., Merz, B., Lun, D., Arheimer, B., Aronica, G. T., Bilibashi, A., et al.: Changing climate both increases and decreases European river floods, *Nature*, 573, 108–111, <https://doi.org/10.1038/s41586-019-1495-6>, 2019.
- Brönnimann, S., Appenzeller, C., Croci-Maspoli, M., Fuhrer, J., Grosjean, M., Hohmann, R., Ingold, K., Knutti, R., Liniger, M. A., Raible, C. C., et al.: Climate change in Switzerland: a review of physical, institutional, and political aspects, *Wiley Interdisciplinary Reviews: Climate Change*, 5, 461–481, 2014.
- Brunner, M. I., Farinotti, D., Zekollari, H., Huss, M., and Zappa, M.: Future shifts in extreme flow regimes in Alpine regions, *Hydrology and Earth System Sciences*, 23, 4471–4489, <https://doi.org/10.5194/hess-23-4471-2019>, 2019a.
- Brunner, M. I., Gurung Björnsen, A., Zappa, M., Zekollari, H., Farinotti, D., and Stähli, M.: Present and future water scarcity in Switzerland: Potential for alleviation through reservoirs and lakes, *Science of the Total Environment*, 666, 1033–1047, <https://doi.org/10.1016/j.scitotenv.2019.02.169>, 2019b.
- Brunner, M. I., Melsen, L. A., Wood, A. W., Rakovec, O., Mizukami, N., Knoben, W. J. M., and Clark, M. P.: Flood hazard and change impact assessments may profit from rethinking model calibration strategies, *Hydrological and Earth System Science Discussions*, <https://doi.org/10.5194/hess-2020-192>, in review 2020.
- Bürki, R., Abegg, B., Elsasser, H., Amelung, B., et al.: Climate change and tourism: assessment and coping strategies, chap. Climate change and tourism in the alpine regions of Switzerland, pp. 165–172, Maastricht, Germany, 2007.
- Castellarin, A. and Pistocchi, A.: An analysis of change in alpine annual maximum discharges: implications for the selection of design discharges, *Hydrological Processes*, 26, 1517–1526, <https://doi.org/10.1002/hyp.8249>, 2012.
- CH2014: CH2014-Impacts. Toward Quantitative Scenarios of Climate Change Impacts in Switzerland, OCCR, FOEN, MeteoSwiss, C2SM, Agroscope, and ProClim, Bern, Switzerland, 136 pp., 2014.
- CH2018: CH2018 – Climate Scenarios for Switzerland, Tech. rep., National Centre for Climate Services, Zurich, Switzerland, 271 pp., ISBN: 978-3-9525031-4-0, 2018.
- Coles, S.: *An Introduction to Statistical Modeling of Extreme Values*, Springer, London, UK, 2001.
- Copernicus: Corine Land Cover (CLC), Version 2020 20u1, available at: <https://land.copernicus.eu/pan-european/corine-land-cover> (last access: 19 April 2020), 2012.

- Copernicus: European Digital Elevation Model (EU-DEM), version 1.1, available at: <https://land.copernicus.eu/imagery-in-situ/eu-dem/eu-dem-v1.1?tab=metadata> (last access: 19 April 2020), 2016.
- Dessai, S. and Hulme, M.: Does climate adaptation policy need probabilities?, *Climate policy*, 4, 107–128, 2004.
- Dettinger, M.: Climate change, atmospheric rivers, and floods in California—a multimodel analysis of storm frequency and magnitude changes 1, *Journal of the American Water Resources Association*, 47, 514–523, <https://doi.org/10.1111/j.1752-1688.2011.00546.x>, 2011.
- Doherty, J.: PEST Model-Independent Parameter Estimation User Manual, Watermark Numerical Computing, Tech. rep., Brisbane, Australia, 2005.
- Ehrbar, D., Schmocker, L., Vetsch, D. F., and Boes, R. M.: Hydropower potential in the periglacial environment of Switzerland under climate change, *Sustainability*, 10, 2794, <https://doi.org/10.3390/su10082794>, 2018.
- Espinoza, V., Waliser, D. E., Guan, B., Lavers, D. A., and Ralph, F. M.: Global analysis of climate change projection effects on atmospheric rivers, *Geophysical Research Letters*, 45, 4299–4308, <https://doi.org/10.1029/2017GL076968>, 2018.
- Etter, S., Addor, N., Huss, M., and Finger, D.: Climate change impacts on future snow, ice and rain runoff in a Swiss mountain catchment using multi-dataset calibration, *Journal of Hydrology: Regional Studies*, 13, 222–239, <https://doi.org/10.1016/j.ejrh.2017.08.005>, 2017.
- Farinotti, D., Usselman, S., Huss, M., Bauder, A., and Funk, M.: Runoff evolution in the Swiss Alps: Projections for selected high-alpine catchments based on ENSEMBLES scenarios, *Hydrological Processes*, 26, 1909–1924, <https://doi.org/10.1002/hyp.8276>, 2012.
- Faticchi, S., Rimkus, S., Burlando, P., Bordoy, R., and Molnar, P.: High-resolution distributed analysis of climate and anthropogenic changes on the hydrology of an Alpine catchment, *Journal of Hydrology*, 525, 362–382, <https://doi.org/10.1016/j.jhydrol.2015.03.036>, 2015.
- Fazan, V.: North Atlantic atmospheric rivers in the ERA-Interim dataset: Detection, climatology and link to Swiss floods, Master’s thesis, University of Bern, Faculty of Science, 2014.
- Feyen, L. and Dankers, R.: Impact of global warming on streamflow drought in Europe, *Journal of Geophysical Research: Atmospheres*, 114, <https://doi.org/10.1029/2008JD011438>, 2009.
- FOEN: Hydrological Data Service for watercourses and lakes, available at: <https://www.bafu.admin.ch/bafu/en/home/topics/water/state/data/obtaining-monitoring-data-on-the-topic-of-water/hydrological-data-service-for-watercourses-and-lakes.html> (last access: 15 August 2019), 2019.

- Forzieri, G., Feyen, L., Rojas, R., Flörke, M., Wimmer, F., and Bianchi, A.: Ensemble projections of future streamflow droughts in Europe, *Hydrology and Earth System Sciences*, 18, 85–108, <https://doi.org/10.5194/hess-18-85-2014>, 2014.
- Frei, C.: Interpolation of temperature in a mountainous region using nonlinear profiles and non-Euclidean distances, *International Journal of Climatology*, 34, 1585–1605, <https://doi.org/10.1002/joc.3786>, 2014.
- Frei, C. and Schär, C.: A precipitation climatology of the Alps from high-resolution rain-gauge observations, *International Journal of Climatology*, 18, 873–900, [https://doi.org/10.1002/\(SICI\)1097-0088\(19980630\)18:8%3C873::AID-JOC255%3E3.0.CO;2-9](https://doi.org/10.1002/(SICI)1097-0088(19980630)18:8%3C873::AID-JOC255%3E3.0.CO;2-9), 1998.
- Froidevaux, P. and Martius, O.: Exceptional integrated vapour transport toward orography: an important precursor to severe floods in Switzerland, *Quarterly Journal of the Royal Meteorological Society*, 142, 1997–2012, <https://doi.org/10.1002/qj.2793>, 2016.
- Gao, Y., Lu, J., Leung, L. R., Yang, Q., Hagos, S., and Qian, Y.: Dynamical and thermodynamical modulations on future changes of landfalling atmospheric rivers over western North America, *Geophysical Research Letters*, 42, 7179–7186, <https://doi.org/10.1002/2015GL065435>, 2015.
- Gao, Y., Lu, J., and Leung, L. R.: Uncertainties in projecting future changes in atmospheric rivers and their impacts on heavy precipitation over Europe, *Journal of Climate*, 29, 6711–6726, <https://doi.org/10.1175/JCLI-D-16-0088.1>, 2016.
- Gershunov, A., Shulgina, T., Clemesha, R. E., Guirguis, K., Pierce, D. W., Dettinger, M. D., Lavers, D. A., Cayan, D. R., Polade, S. D., Kalansky, J., et al.: Precipitation regime change in Western North America: the role of atmospheric rivers, *Scientific reports*, 9, 1–11, <https://doi.org/10.1038/s41598-019-46169-w>, 2019.
- Gheusi, F. and Davies, H. C.: Autumnal precipitation distribution on the southern flank of the Alps: A numerical-model study of the mechanisms, *Quarterly Journal of the Royal Meteorological Society: A journal of the atmospheric sciences, applied meteorology and physical oceanography*, 130, 2125–2152, <https://doi.org/10.1256/qj.03.06>, 2004.
- Giannakaki, P. and Martius, O.: Synoptic-scale flow structures associated with extreme precipitation events in northern Switzerland, *International journal of climatology*, 36, 2497–2515, <https://doi.org/10.1002/joc.4508>, 2016.
- Griffith, H. V., Wade, A. J., Lavers, D. A., and Watts, G.: Atmospheric river orientation determines flood occurrence, *Hydrological Processes*, 34, 4547–4555, <https://doi.org/10.1002/hyp.13905>, 2020.

- Groppelli, B., Soncini, A., Bocchiola, D., and Rosso, R.: Evaluation of future hydrological cycle under climate change scenarios in a mesoscale Alpine watershed of Italy, *Natural Hazards and Earth System Sciences*, 11, 1769, <https://doi.org/10.5194/nhess-11-1769-2011>, 2011.
- Gudmundsson, L., Bremnes, J. B., Haugen, J. E., and Engen-Skaugen, T.: Downscaling RCM precipitation to the station scale using statistical transformations—a comparison of methods, *Hydrology and Earth System Sciences*, 16, 3383–3390, <https://doi.org/10.5194/hess-16-3383-2012>, 2012.
- Gupta, H. V., Kling, H., Yilmaz, K. K., and Martinez, G. F.: Decomposition of the mean squared error and NSE performance criteria: Implications for improving hydrological modelling, *Journal of Hydrology*, 377, 80–91, <https://doi.org/10.1016/j.jhydrol.2009.08.003>, 2009.
- Hagos, S. M., Leung, L. R., Yoon, J.-H., Lu, J., and Gao, Y.: A projection of changes in landfalling atmospheric river frequency and extreme precipitation over western North America from the Large Ensemble CESM simulations, *Geophysical Research Letters*, 43, 1357–1363, <https://doi.org/10.1002/2015GL067392>, 2016.
- Hall, J., Arheimer, B., Borga, M., Brázdil, R., Claps, P., Kiss, A., Kjeldsen, T., Kriauciuniene, J., Kundzewicz, Z., Lang, M., et al.: Understanding flood regime changes in Europe: A state of the art assessment, *Hydrology and Earth System Sciences*, 18, 2735–2772, <https://doi.org/10.5194/hess-18-2735-2014>, 2014.
- Hamon, W. R.: Estimating potential evapotranspiration, *Journal of Hydraulic Engineering Div.-ASCE*, 87, 107–120, 1961.
- Hänggi, P. and Weingartner, R.: Variations in discharge volumes for hydropower generation in Switzerland, *Water resources management*, 26, 1231–1252, <https://doi.org/10.1007/s11269-011-9956-1>, 2012.
- Hanzer, F., Förster, K., Nemeč, J., and Strasser, U.: Projected cryospheric and hydrological impacts of 21st century climate change in the Ötztal Alps (Austria) simulated using a physically based approach, *Hydrology and Earth System Sciences*, 22, 1593–1614, <https://doi.org/10.5194/hess-22-1593-2018>, 2018.
- Hattermann, F. F., Huang, S., and Koch, H.: Climate change impacts on hydrology and water resources, *Meteorologische Zeitschrift*, 24, 201–211, <https://doi.org/10.1127/metz/2014/0575>, 2015.
- Henne, P. D., Bigalke, M., Büntgen, U., Colombaroli, D., Conedera, M., Feller, U., Frank, D., Fuhrer, J., Grosjean, M., Heiri, O., et al.: An empirical perspective for understanding climate change impacts in Switzerland, *Regional environmental change*, 18, 205–221, <https://doi.org/10.1007/s10113-017-1182-9>, 2018.

- Hilker, N., Badoux, A., and Hegg, C.: The Swiss flood and landslide damage database 1972-2007, *Natural Hazards and Earth System Sciences*, 9, 913–925, 2009.
- Hoinka, K. P. and Davies, H. C.: Upper-tropospheric flow features and the Alps: An overview, *Quarterly Journal of the Royal Meteorological Society: A journal of the atmospheric sciences, applied meteorology and physical oceanography*, 133, 847–865, <https://doi.org/10.1002/qj.69>, 2007.
- Horton, P., Schaefli, B., Mezghani, A., Hingray, B., and Musy, A.: Assessment of climate-change impacts on alpine discharge regimes with climate model uncertainty, *Hydrological Processes*, 20, 2091–2109, <https://doi.org/10.1002/hyp.6197>, 2006.
- Huss, M., Farinotti, D., Bauder, A., and Funk, M.: Modelling runoff from highly glacierized alpine drainage basins in a changing climate, *Hydrological Processes*, 22, 3888–3902, <https://doi.org/10.1002/hyp.7055>, 2008.
- Huss, M., Zemp, M., Joerg, P. C., and Salzmann, N.: High uncertainty in 21st century runoff projections from glacierized basins, *Journal of Hydrology*, 510, 35–48, <https://doi.org/10.1016/j.jhydrol.2013.12.017>, 2014.
- IPCC: Climate change 2013: the physical science basis: Working Group I contribution to the Fifth assessment report of the Intergovernmental Panel on Climate Change, Cambridge University Press, Cambridge, United Kingdom and New York, NY, USA, 2013.
- IPCC: Climate Change 2014: Impacts, Adaptation, and Vulnerability. Part A: Global and Sectoral Aspects. Contribution of Working Group II to the Fifth Assessment Report of the Intergovernmental Panel on Climate Change, 1132 pp., Cambridge University Press, Cambridge, United Kingdom and New York, NY, USA, 2014a.
- IPCC: Climate Change 2014: Impacts, Adaptation, and Vulnerability. Part B: Regional Aspects. Contribution of Working Group II to the Fifth Assessment Report of the Intergovernmental Panel on Climate Change, 688 pp., Cambridge University Press, Cambridge, United Kingdom and New York, NY, USA, 2014b.
- Jacob, D., Petersen, J., Eggert, B., Alias, A., Christensen, O. B., Bouwer, L. M., Braun, A., Colette, A., Déqué, M., Georgievski, G., et al.: EURO-CORDEX: new high-resolution climate change projections for European impact research, *Regional environmental change*, 14, 563–578, <https://doi.org/10.1007/s10113-013-0499-2>, 2014.
- Jenicek, M., Seibert, J., and Staudinger, M.: Modeling of future changes in seasonal snowpack and impacts on summer low flows in alpine catchments, *Water Resources Research*, 54, 538–556, <https://doi.org/10.1002/2017WR021648>, 2018.
- Katz, R. W.: Statistics of extremes in climate change, *Climatic change*, 100, 71–76, <https://doi.org/10.1007/s10584-010-9834-5>, 2010.

- Katz, R. W., Parlange, M. B., and Naveau, P.: Statistics of extremes in hydrology, *Advances in Water Resources*, 25, 1287–1304, 2002.
- Keller, L., Rössler, O., Martius, O., and Weingartner, R.: Delineation of flood generating processes and their hydrological response, *Hydrological Processes*, 32, 228–240, <https://doi.org/10.1002/hyp.11407>, 2018.
- Koch, E., Koh, J., Davison, A. C., Lepore, C., and Tippet, M. K.: Trends in the extremes of environments associated with severe US thunderstorms, *Journal of Climate*, pp. 1–38, <https://doi.org/10.1175/JCLI-D-19-0826.1>, 2019.
- Köllner, P., Gross, C., Schächli, B., Füssler, J., Lerch, J., and Nauser, Markus, B. U.-W. N. S.: Klimabedingte Risiken und Chancen. Eine schweizweite Synthese, Tech. Rep. Umwelt-Wissen Nr.1706: 148S., Bundesamt für Umwelt, Bern, Umwelt-Wissen Nr.1706: 148S., 2017.
- Köplin, N., Schädler, B., Viviroli, D., and Weingartner, R.: Relating climate change signals and physiographic catchment properties to clustered hydrological response types, *Hydrology and Earth System Sciences*, 16, 2267–2283, <https://doi.org/10.5194/hess-16-2267-2012>, 2012.
- Köplin, N., Rössler, O., Schädler, B., and Weingartner, R.: Robust estimates of climate-induced hydrological change in a temperate mountainous region, *Climatic Change*, 122, 171–184, <https://doi.org/10.1007/s10584-013-1015-x>, 2014a.
- Köplin, N., Schädler, B., Viviroli, D., and Weingartner, R.: Seasonality and magnitude of floods in Switzerland under future climate change, *Hydrological Processes*, 28, 2567–2578, <https://doi.org/10.1002/hyp.9757>, 2014b.
- Kotlarski, S., Keuler, K., Christensen, O. B., Colette, A., Déqué, M., Gobiet, A., Goergen, K., Jacob, D., Lüthi, D., Van Meijgaard, E., et al.: Regional climate modeling on European scales: a joint standard evaluation of the EURO-CORDEX RCM ensemble, *Geoscientific Model Development*, 7, 1297–1333, <https://doi.org/10.5194/gmd-7-1297-2014>, 2014.
- Krysanova, V., Donnelly, C., Gelfan, A., Gerten, D., Arheimer, B., Hattermann, F., and Kundzewicz, Z. W.: How the performance of hydrological models relates to credibility of projections under climate change, *Hydrological Sciences Journal*, 63, 696–720, <https://doi.org/10.1080/02626667.2018.1446214>, 2018.
- Lavers, D. A., Villarini, G., Allan, R. P., Wood, E. F., and Wade, A. J.: The detection of atmospheric rivers in atmospheric reanalyses and their links to British winter floods and the large-scale climatic circulation, *Journal of Geophysical Research: Atmospheres*, 117, <https://doi.org/10.1029/2012JD018027>, 2012.
- Lavers, D. A., Allan, R. P., Villarini, G., Lloyd-Hughes, B., Brayshaw, D. J., and Wade, A. J.: Future changes in atmospheric rivers and their implications for winter flooding in Britain,

- Environmental Research Letters, 8, 034 010, <https://doi.org/10.1088/1748-9326/8/3/034010>, 2013.
- Lavers, D. A., Ralph, F. M., Waliser, D. E., Gershunov, A., and Dettinger, M. D.: Climate change intensification of horizontal water vapor transport in CMIP5, *Geophysical Research Letters*, 42, 5617–5625, <https://doi.org/10.1002/2015GL064672>, 2015.
- Lindström, G., Johansson, B., Persson, M., Gardelin, M., and Bergström, S.: Development and test of the distributed HBV-96 hydrological model, *Journal of Hydrology*, 201, 272–288, 1997.
- Mahlstein, I., Knutti, R., Solomon, S., and Portmann, R. W.: Early onset of significant local warming in low latitude countries, *Environmental Research Letters*, 6, 034 009, <https://doi.org/10.1088/1748-9326/6/3/034009>, 2011.
- Mahlstein, I., Bhend, J., Spirig, C., and Martius, O.: Developing an Automated Medium-Range Flood Awareness System for Switzerland Based on Probabilistic Forecasts of Integrated Water Vapor Fluxes, *Weather and Forecasting*, 34, 1759–1776, <https://doi.org/10.1175/WAF-D-18-0189.1>, 2019.
- Mangini, W., Viglione, A., Hall, J., Hundecha, Y., Ceola, S., Montanari, A., Rogger, M., Salinas, J. L., Borzì, I., and Parajka, J.: Detection of trends in magnitude and frequency of flood peaks across Europe, *Hydrological Sciences Journal*, 63, 493–512, <https://doi.org/10.1080/02626667.2018.1444766>, 2018.
- Martins, E. S. and Stedinger, J. R.: Generalized maximum-likelihood generalized extreme-value quantile estimators for hydrologic data, *Water Resources Research*, 36, 737–744, 2000.
- Martius, O., Zenklusen, E., Schwierz, C., and Davies, H. C.: Episodes of Alpine heavy precipitation with an overlying elongated stratospheric intrusion: A climatology, *International Journal of Climatology: A Journal of the Royal Meteorological Society*, 26, 1149–1164, <https://doi.org/10.1002/joc.1295>, 2006.
- Marx, A., Kumar, R., Thober, S., Rakovec, O., Wanders, N., Zink, M., Wood, E. F., Pan, M., Sheffield, J., and Samaniego, L.: Climate change alters low flows in Europe under global warming of 1.5, 2, and 3 C, *Hydrology and Earth System Sciences*, 22, 1017–1032, <https://doi.org/10.5194/hess-22-1017-2018>, 2018.
- Massacand, A. C., Wernli, H., and Davies, H. C.: Heavy precipitation on the Alpine southside: An upper-level precursor, *Geophysical Research Letters*, 25, 1435–1438, 1998.
- Massoud, E., Espinoza, V., Guan, B., and Waliser, D.: Global climate model ensemble approaches for future projections of atmospheric rivers, *Earth's Future*, 7, 1136–1151, <https://doi.org/10.1029/2019EF001249>, 2019.

- MeteoSwiss: RhiresD - Daily precipitation (final analysis, 1961 – last month), available at: <https://www.meteoswiss.admin.ch/home/climate/swiss-climate-in-detail/raeumliche-klimaanalysen.html> (last access: 15 August 2019), 2019a.
- MeteoSwiss: TabsD - Daily mean temperature (1961 – present), available at: <https://www.meteoswiss.admin.ch/home/climate/swiss-climate-in-detail/raeumlicheklimaanalysen.html> (last access: 15 August 2019), 2019b.
- Meyer, R., Schädler, B., Viviroli, D., and Weingartner, R.: Klimaänderung und Niedrigwasser - Auswirkungen der Klimaänderung auf die Niedrigwasserverhältnisse im Schweizer Mittelland für 2021-2050 und 2070-2099, Comissioned by the Swiss Federal Office for the Environment, 2011.
- Milano, M., Reynard, E., Köplin, N., and Weingartner, R.: Climatic and anthropogenic changes in Western Switzerland: Impacts on water stress, *Science of The Total Environment*, 536, 12–24, <https://doi.org/10.1016/j.scitotenv.2015.07.049>, 2015.
- Morice, C. P., Kennedy, J. J., Rayner, N. A., and Jones, P. D.: Quantifying uncertainties in global and regional temperature change using an ensemble of observational estimates: The HadCRUT4 data set, *Journal of Geophysical Research: Atmospheres*, 117, <https://doi.org/10.1029/2011JD017187>, 2012.
- Moss, R. H., Edmonds, J. A., Hibbard, K. A., Manning, M. R., Rose, S. K., Van Vuuren, D. P., Carter, T. R., Emori, S., Kainuma, M., Kram, T., et al.: The next generation of scenarios for climate change research and assessment, *Nature*, 463, 747–756, <https://doi.org/10.1038/nature08823>, 2010.
- Muelchi, R., Rössler, O., Schwanbeck, J., Weingartner, R., and Martius, O.: Hydro-CH2018-Runoff ensemble (version v1), Zenodo, <https://doi.org/http://doi.org/10.5281/zenodo.3937485>, 2020.
- Muelchi, R., Rössler, O., Schwanbeck, J., Weingartner, R., and Martius, O.: An ensemble of daily simulated runoff data (1981–2099) under climate change conditions for 93 catchments in Switzerland (Hydro-CH2018-Runoff ensemble), *Geoscience Data Journal*, in review 2020a.
- Muelchi, R., Rössler, O., Schwanbeck, J., Weingartner, R., and Martius, O.: Moderate runoff extremes in Swiss rivers and their seasonal occurrence in a changing climate, *Hydrology and Earth System Sciences*, in review 2020b.
- Muelchi, R., Rössler, O., Schwanbeck, J., Weingartner, R., and Martius, O.: Future runoff regime changes and their time of emergence for 93 catchments in Switzerland, *Hydrology and Earth System Sciences Discussions*, pp. 1–25, <https://doi.org/10.5194/hess-2020-516>, in review 2020c.

- Nash, J. and Sutcliffe, J.: River flow forecasting through conceptual models part I: A discussion of principles, *Journal of Hydrology*, 10, 282–290, [https://doi.org/10.1016/0022-1694\(70\)90255-6](https://doi.org/10.1016/0022-1694(70)90255-6), 1970.
- Nilson, E., Krahe, P., Klein, B., Lingemann, I., Horsten, T., Carambia, M., Larina, M., and Maurer, T.: Auswirkungen des Klimawandels auf das Abflussgeschehen und die Binnenschifffahrt in Deutschland. Schlussbericht KLIWAS-Projekt 4.01., BfG, Koblenz, https://doi.org/10.5675/Kliwas_43/2014_4.01, 2014.
- Papadimitriou, L. V., Koutroulis, A. G., Grillakis, M. G., and Tsanis, I. K.: High-end climate change impact on European runoff and low flows—exploring the effects of forcing biases, *Hydrology and Earth System Sciences*, 20, 1785–1808, <https://doi.org/10.5194/hess-20-1785-2016>, 2016.
- Payne, A. E. and Magnusdottir, G.: An evaluation of atmospheric rivers over the North Pacific in CMIP5 and their response to warming under RCP 8.5, *Journal of Geophysical Research: Atmospheres*, 120, 11–173, <https://doi.org/10.1002/2015JD023586>, 2015.
- Pfahl, S., O’Gorman, P. A., and Fischer, E. M.: Understanding the regional pattern of projected future changes in extreme precipitation, *Nature Climate Change*, 7, 423–427, <https://doi.org/10.1038/Nclimate3287>, 2017.
- Pierce, D. W., Cayan, D. R., Das, T., Maurer, E. P., Miller, N. L., Bao, Y., Kanamitsu, M., Yoshimura, K., Snyder, M. A., Sloan, L. C., et al.: The key role of heavy precipitation events in climate model disagreements of future annual precipitation changes in California, *Journal of Climate*, 26, 5879–5896, <https://doi.org/10.1175/JCLI-D-12-00766.1>, 2013.
- Prasch, M., Marke, T., Strasser, U., and Mauser, W.: Large scale integrated hydrological modelling of the impact of climate change on the water balance with DANUBIA, *Advances in Science and Research*, 7, 61, <https://doi.org/10.5194/asr-7-61-2011>, 2011.
- Ragettli, S., Tong, X., Zhang, G., Wang, H., Zhang, P., and Stähli, M.: Climate change impacts on summer flood frequencies in two mountainous catchments in China and Switzerland, *Hydrology Research*, nh2019118, <https://doi.org/10.2166/nh.2019.118>, 2019.
- Ragno, E., AghaKouchak, A., Cheng, L., and Sadegh, M.: A generalized framework for process-informed nonstationary extreme value analysis, *Advances in Water Resources*, 130, 270–282, <https://doi.org/10.1016/j.advwatres.2019.06.007>, 2019.
- Ralph, F. M., Dettinger, M. D., Cairns, M. M., Galarneau, T. J., and Eylander, J.: Defining “atmospheric river”: How the Glossary of Meteorology helped resolve a debate, *Bulletin of the American Meteorological Society*, 99, 837–839, 2018.

- Ramos, A. M., Tomé, R., Trigo, R. M., Liberato, M. L., and Pinto, J. G.: Projected changes in atmospheric rivers affecting Europe in CMIP5 models, *Geophysical Research Letters*, 43, 9315–9323, <https://doi.org/10.1002/2016GL070634>, 2016.
- Rössler, O., Kotlarski, S., Fischer, A. M., Keller, D., Liniger, M., and Weingartner, R.: Evaluating the added value of the new Swiss climate scenarios for hydrology: An example from the Thur catchment, *Climate Services*, 13, 1–13, <https://doi.org/10.1016/j.cliser.2019.01.001>, 2019.
- Ruiz-Villanueva, V., Stoffel, M., Bussi, G., Francés, F., and Bréthaut, C.: Climate change impacts on discharges of the Rhone River in Lyon by the end of the twenty-first century: model results and implications, *Regional Environmental Change*, 15, 505–515, <https://doi.org/10.1007/s10113-014-0707-8>, 2015.
- Schaller, N., Sillmann, J., Müller, M., Haarsma, R., Hazeleger, W., Hegdahl, T. J., Kelder, T., van den Oord, G., Weerts, A., and Whan, K.: The role of spatial and temporal model resolution in a flood event storyline approach in Western Norway, *Weather and Climate Extremes*, 29, 100259, <https://doi.org/10.1016/j.wace.2020.100259>, 2020.
- Schmocker-Fackel, P. and Naef, F.: More frequent flooding? Changes in flood frequency in Switzerland since 1850, *Journal of Hydrology*, 381, 1–8, <https://doi.org/10.1016/j.jhydrol.2009.09.022>, 2010a.
- Schmocker-Fackel, P. and Naef, F.: Changes in flood frequencies in Switzerland since 1500, *Hydrology and Earth System Sciences*, 14, 1581–1594, <https://doi.org/10.5194/hess-14-1581-2010>, 2010b.
- Schwarz, G.: Estimating the dimension of a model, *The Annals of Statistics*, 6, 461–464, 1978.
- Shepherd, T. G.: Atmospheric circulation as a source of uncertainty in climate change projections, *Nature Geoscience*, 7, 703–708, <https://doi.org/10.1038/Ngeo2253>, 2014.
- Shepherd, T. G., Boyd, E., Calel, R. A., Chapman, S. C., Dessai, S., Dima-West, I. M., Fowler, H. J., James, R., Maraun, D., Martius, O., Senior, C. A., Sobel, A. H., Stainforth, D. A., Tett, S. F. B., Trenberth, K. E., van den Hurk, B. J. J. M., Watkins, N. W., Wilby, R. L., and Zenghelis, D. A.: Storylines: an alternative approach to representing uncertainty in physical aspects of climate change, *Climatic Change*, 151, 555–571, <https://doi.org/10.1007/s10584-018-2317-9>, 2018.
- Shields, C. A. and Kiehl, J. T.: Atmospheric river landfall-latitude changes in future climate simulations, *Geophysical Research Letters*, 43, 8775–8782, <https://doi.org/10.1002/2016GL070470>, 2016.

- Stahl, K., Hisdal, H., Hannaford, J., Tallaksen, L., Van Lanen, H., Sauquet, E., Demuth, S., Fendekova, M., and Jordar, J.: Streamflow trends in Europe: evidence from a dataset of near-natural catchments, *Hydrology and Earth System Sciences*, 14, 2367–2382, <https://doi.org/10.5194/hess-14-2367-2010>, 2010.
- Stahl, K., Tallaksen, L. M., Hannaford, J., and Van Lanen, H.: Filling the white space on maps of European runoff trends: estimates from a multi-model ensemble, *Hydrology and Earth System Sciences*, 16, 2035–2047, <https://doi.org/10.5194/hess-16-2035-2012>, 2012.
- Stucki, P., Rickli, R., Brönnimann, S., Martius, O., Wanner, H., Grebner, D., and Luterbacher, J.: Weather patterns and hydro-climatological precursors of extreme floods in Switzerland since 1868, *Meteorologische Zeitschrift*, 21, 531–550, 2012.
- Tallaksen, L. M. and Van Lanen, H. A.: *Hydrological drought: processes and estimation methods for streamflow and groundwater*, vol. 48, Elsevier, 2004.
- Taylor, K. E., Stouffer, R. J., and Meehl, G. A.: An overview of CMIP5 and the experiment design, *Bulletin of the American Meteorological Society*, 93, 485–498, <https://doi.org/10.1175/BAMS-D-11-00094.1>, 2012.
- Tecklenburg, C., Francke, T., Kormann, C., and Bronstert, A.: Modeling of water balance response to an extreme future scenario in the Ötztal catchment, Austria, *Advances in Geosciences*, 32, 63–68, <https://doi.org/10.5194/adgeo-32-63-2012>, 2012.
- Teutschbein, C. and Seibert, J.: Bias correction of regional climate model simulations for hydrological climate-change impact studies: Review and evaluation of different methods, *Journal of Hydrology*, 456, 12–29, <https://doi.org/10.1016/j.jhydrol.2012.05.052>, 2012.
- van Vliet, M. T., Franssen, W. H., Yearsley, J. R., Ludwig, F., Haddeland, I., Lettenmaier, D. P., and Kabat, P.: Global river discharge and water temperature under climate change, *Global Environmental Change*, 23, 450–464, <https://doi.org/10.1016/j.gloenvcha.2012.11.002>, 2013.
- Van Vuuren, D. P., Edmonds, J., Kainuma, M., Riahi, K., Thomson, A., Hibbard, K., Hurtt, G. C., Kram, T., Krey, V., Lamarque, J.-F., et al.: The representative concentration pathways: an overview, *Climatic Change*, 109, 5, <https://doi.org/10.1007/s10584-011-0148-z>, 2011.
- Vidal, J.-P., Hingray, B., Magand, C., Sauquet, E., and Ducharne, A.: Hierarchy of climate and hydrological uncertainties in transient low-flow projections, *Hydrology and Earth System Sciences*, 20, 3651–3672, <https://doi.org/10.5194/hess-20-3651-2016>, 2016.
- Viviroli, D., Zappa, M., Gurtz, J., and Weingartner, R.: An introduction to the hydrological modelling system PREVAH and its pre-and post-processing-tools, *Environmental Modelling & Software*, 24, 1209–1222, <https://doi.org/10.1016/j.envsoft.2009.04.001>, 2009.

- Warner, M. D., Mass, C. F., and Salathé Jr, E. P.: Changes in winter atmospheric rivers along the North American west coast in CMIP5 climate models, *Journal of Hydrometeorology*, 16, 118–128, <https://doi.org/10.1175/JHM-D-14-0080.1>, 2015.
- Weber, M., Braun, L., Mauser, W., and Prasch, M.: Contribution of rain, snow-and icemelt in the Upper Danube discharge today and in the future, *Geogr. Fis. Dinam. Quat*, 33, 221–230, 2010.
- Wehner, M., Gleckler, P., and Lee, J.: Characterization of long period return values of extreme daily temperature and precipitation in the CMIP6 models: Part 1, model evaluation, *Weather and Climate Extremes*, 30, 100 283, <https://doi.org/10.1016/j.wace.2020.100283>, 2020.
- Weingartner, R.: Veränderungen der Abflussregimes der Schweiz in den letzten 150 Jahren. Synthesebericht zum Projekt Hydro-CH2018, Tech. rep., Bundesamt für Umwelt, Bern, Switzerland, 2019.
- Weingartner, R. and Aschwanden, H.: Discharge regime—the basis for the estimation of average flows, Tech. Rep. Plate 5.2, Hydrological Atlas of Switzerland, Bern, Switzerland, 1992.
- Weingartner, R. and Schwanbeck, J.: Veränderung der Niedrigwasserabflüsse und der kleinsten saisonalen Abflüsse in der Schweiz im Zeitraum 1961-2018, Comissioned by the Swiss Federal Office for the Environment, p. 41pp., 2020.
- Whan, K., Sillmann, J., Schaller, N., and Haarsma, R.: Future changes in atmospheric rivers and extreme precipitation in Norway, *Climate Dynamics*, 54, 2071–2084, <https://doi.org/10.1007/s00382-019-05099-z>, 2020.
- Wijngaard, R. R., Helfricht, K., Schneeberger, K., Huttenlau, M., Schneider, K., and Bierkens, M. F.: Hydrological response of the Ötztal glacierized catchments to climate change, *Hydrology Research*, 47, 979–995, <https://doi.org/10.2166/nh.2015.093>, 2016.
- Winschall, A., Pfahl, S., Sodemann, H., and Wernli, H.: Impact of North Atlantic evaporation hot spots on southern Alpine heavy precipitation events, *Quarterly Journal of the Royal Meteorological Society*, 138, 1245–1258, <https://doi.org/10.1002/qj.987>, 2012.
- Zarrineh, N., Abbaspour, K. C., and Holzkämper, A.: Integrated assessment of climate change impacts on multiple ecosystem services in Western Switzerland, *Science of The Total Environment*, 708, 135 212, <https://doi.org/10.1016/j.scitotenv.2019.135212>, 2020.
- Zekollari, H., Huss, M., and Farinotti, D.: Modelling the future evolution of glaciers in the European Alps under the EURO-CORDEX RCM ensemble, *The Cryosphere*, 13, 1125–1146, <https://doi.org/10.5194/tc-13-1125-2019>, 2019.
- Zwiers, F. W., Zhang, X., and Feng, Y.: Anthropogenic influence on long return period daily temperature extremes at regional scales, *Journal of Climate*, 24, 881–892, <https://doi.org/10.1175/2010JCLI3908.1>, 2011.

Appendix A

Supporting information to chapter 2

Table A.1: 93 catchments and their main characteristics and calibration period.

ID	station	river	area (km ²)	mean altitude (masl)	glaciation (%)	calibration period
2020	Bellinzona	Ticino	1517.5	1679	0	1984-2014
2033	Ilanz	Vorderrhein	774	2026	1.8	1984-2014
2034	Payerne	Broye	415.9	724	0	1984-2014
2044	Andelfingen	Thur	1701.6	773	0	1984-2014
2056	Seedorf	Reuss	833.2	2005	6.4	1984-2014
2070	Emmenmatt	Emme	443	1072	0	1984-2014
2078	Le Prese	Poschiavino	167.7	2161	3.9	1984-2014
2084	Ingenbohl	Muota	316.6	1364	0	1984-2014
2087	Andermatt	Reuss	190.2	2276	2.9	1984-2014
2104	Weesen	Linth	1061.5	1580	1.6	1984-2014
2106	Muenchenstein	Birs	887.3	733	0	1984-2014
2112	Appenzell	Sitter	74.4	1254	0	1984-2014
2122	Moutier	Birse	185.8	927	0	1984-2014
2126	Waengi	Murg	80.1	654	0	1984-2014
2132	Neftenbach	Toess	343.3	659	0	1984-2014
2141	Tiefencastel	Albula	529	2127	0.5	1984-2014
2151	Oberwil	Simme	343.7	1639	2.4	1984-2014
2155	Wiler	Emme	924.1	871	0	1984-2014
2159	Belp	Guerbe	116.1	849	0	1984-2014

Continuation of Table A.1						
ID	station	river	area (km ²)	mean altitude (masl)	glaciation (%)	calibration period
2160	Broc	Sarine	636.3	1501	0	1984-2014
2167	Ponte Tresa	Tresa	609.1	805	0	1984-2014
2176	Zuerich	Sihl	342.6	1047	0	1984-2014
2179	Thoerishaus	Sense	351.2	1076	0	1984-2014
2181	Halden	Thur	1085	914	0	1984-2014
2185	Chur	Plessur	264.4	1865	0	1984-2014
2202	Liestal	Ergolz	261.2	591	0	1984-2014
2203	Aigle	Grande Eau	131.6	1566	0.8	1984-2014
2210	Ocourt	Doubs	1275.4	960	0	1984-2014
2219	Oberried	Simme	34.7	2335	22.6	1984-2014
2232	Adelboden	Allenbach	28.8	1855	0	1984-2014
2256	Pontresina	Rosegbach	66.5	2701	21.7	1984-2014
2262	Pontresina	Berninabach	106.9	2608	14.4	1984-2014
2270	Combe des Sarrasins	Doubs	998.5	985	0	1984-2014
2276	Isenthal	Grosstalbach	43.9	1810	6.7	1984-2014
2299	Erstfeld	Alpbach	20.7	2181	19.7	1984-2014
2300	Euthal	Minster	59.1	1352	0	1984-2014
2303	Jonschwil	Thur	492.9	1027	0	1984-2014
2304	Zernez	Ova dal Fuorn	55.3	2333	0	1984-2014
2305	Herisau	Glatt	16.7	836	0	1984-2014
2307	Sonceboz	Suze	127.2	1044	0	1984-2014
2308	Goldach	Goldach	50.4	840	0	1984-2014
2312	Salmsach	Aach	47.4	476	0	1984-2014
2319	Zernez	Ova da Cluozza	26.9	2361	0	1984-2014
2321	Pregassona	Cassarate	75.8	991	0	1984-2014
2342	Brig	Saltina	76.5	2017	2.5	1984-2014
2343	Huttwil	Langeten	59.9	765	0	1984-2014
2355	Davos	Landwasser	183.7	2223	0	1984-2014
2356	Cavergno	Riale di Calneggia	23.9	1982	0	1984-2014
2366	La Roesa	Poschiavino	14.1	2286	0	1984-2014
2368	Locarno	Maggia	926.9	1534	0	1985-2014

Continuation of Table A.1						
ID	station	river	area (km ²)	mean altitude (masl)	glaciation (%)	calibration period
2369	Yvonand	Mentue	105.3	683	0	1984-2014
2370	Le Noirmont	Doubs	1046.7	985	0	1984-2014
2372	Mollis	Linth	600.2	1737	2.9	1984-2014
2374	Mogelsberg	Necker	88.1	962	0	1984-2014
2386	Frauenfeld	Murg	213.3	596	0	1984-2014
2409	Eggiwil	Emme	124.4	1283	0	1984-2014
2412	Vuippens	Sionge	43.4	872	0	1984-2014
2415	Rheinsfelden	Glatt	417.4	506	0	1984-2014
2419	Reckingen	Rhone	214.3	2301	11.8	1984-2014
2420	Lumino	Moesa	471.9	1668	0	1984-2014
2426	Mels	Seez	106.1	1796	0	1984-2014
2432	Ecublens	Venoge	227.6	694	0	1984-2014
2434	Olten	Duennern	233.8	714	0	1984-2014
2450	Zofingen	Wigger	366.2	662	0	1984-2014
2461	Magliaso	Magliasina	34.4	927	0	1984-2014
2468	St. Gallen	Sitter	261.1	1045	0	1984-2014
2469	Hondrich	Kander	490.7	1846	5.1	1984-2014
2471	Murgenthal	Murg	183.4	659	0	1984-2014
2474	Buseno	Calancasca	120.5	1930	0.2	1984-2014
2477	Zug	Lorze	100.2	822	0	1984-2014
2478	Soyhieres	Birse	569.5	811	0	1984-2014
2479	Delemont	Sorne	213.9	785	0	1984-2014
2480	Boudry	Areuse	377.7	1084	0	1984-2014
2481	Buochs	Engelberger Aa	228	1605	2.5	1984-2014
2486	Vevey	Veveyse	64.5	1108	0	1984-2014
2487	Werthenstein	Kleine Emme	311.5	1171	0	1984-2014
2491	Buerglen	Schaechen	107.9	1722	1.5	1986-2014
2493	Gland	Promenthouse	119.8	1035	0	1986-2014
2494	Pollegio	Ticino	443.8	1794	0	1987-2014
2497	Nebikon	Luthern	104.7	754	0	1988-2014
2498	Castrisch	Glenner	380.9	2014	1.1	1989-2014
2500	Ittigen	Worble	67.1	678	0	1989-2014

Continuation of Table A.1						
ID	station	river	area (km ²)	mean altitude (masl)	glaciation (%)	calibration period
2603	Langnau	Ilfis	187.4	1047	0	1990-2014
2604	Biberbrugg	Biber	31.9	1008	0	1990-2014
2605	Lavertezzo	Verzasca	185.1	1663	0	1990-2014
2607	Oberwald	Goneri	38.4	2378	4	1991-2014
2609	Einsiedeln	Alp	46.7	1161	0	1992-2014
2610	Vicques	Schulte	72.7	797	0	1992-2014
2612	Lavertezzo	Riale di Pincascia	44.5	1713	0	1993-2014
2617	Muestair	Rom	128.5	2188	0	1995-2014
2629	Agno	Vedeggio	99.9	921	0	2004-2014
2630	Sion	Sionne	27.6	1575	0	2007-2014
2634	Emmen	Kleine Emme	478.3	1058	0	1984-2014

Table A.2: List of available GCM-RCM combinations and their initial resolutions. Models with black crosses (X) should be used for ensemble statistics. Models with red crosses (X) are available but should not be used for ensemble statistics to avoid double weighting of model combinations.

GCM	RCM	RCP8.5		RCP4.5		RCP2.6	
		EUR-11	EUR-44	EUR-11	EUR-44	EUR-11	EUR-44
ICHEC-EC-EARTH	KNMI-RACMO22E		X		X		
	DMI-HIRMAM5	X	(X)	X	(X)	X	
	CLMcom-CCLM4-8-17	X		X			
	CLMcom-CCLM5-0-6		X				
	SMHI-RCA4	X	(X)	X	(X)	X	(X)
MOHC-HadGEM2-ES	CLMcom-CCLM4-8-17	X	(X)	X			
	CLMcom-CCLM5-0-6		X				
	ICTP-RegCM4-3						
	KNMI-RACMO22E		X		X		X
	SMHI-RCA4	X	(X)	X	(X)		X
MPI-M-MPI-ESM-LR	CLMcom-CCLM4-8-17	X	(X)	X	(X)		
	CLMcom-CCLM5-0-6		X				
	MPI-CSC-REMO2009-1	(X)	(X)	(X)	(X)	(X)	(X)
	SMHI-RCA4	X	(X)	X	(X)		X
	MPI-CSC-REMO2009-2	X	(X)	X	(X)	X	(X)
MIROC-MIROC5	CLMcom-CCLM5-0-6		X				
	SMHI-RCA4		X		X		X
CCCma-CanESM2	SMHI-RCA4		X		X		
CSIRO-QCCCE-CSIRO-Mk3-6-0	SMHI-RCA4		X		X		
IPSL-IPSL-CM5A-MR	SMHI-RCA4	X	(X)	X	(X)		
NCC-NorESM1-M	SMHI-RCA4		X		X		X
NOAA-GFDL-GFDL-ESM2M	SMHI-RCA4		X		X		

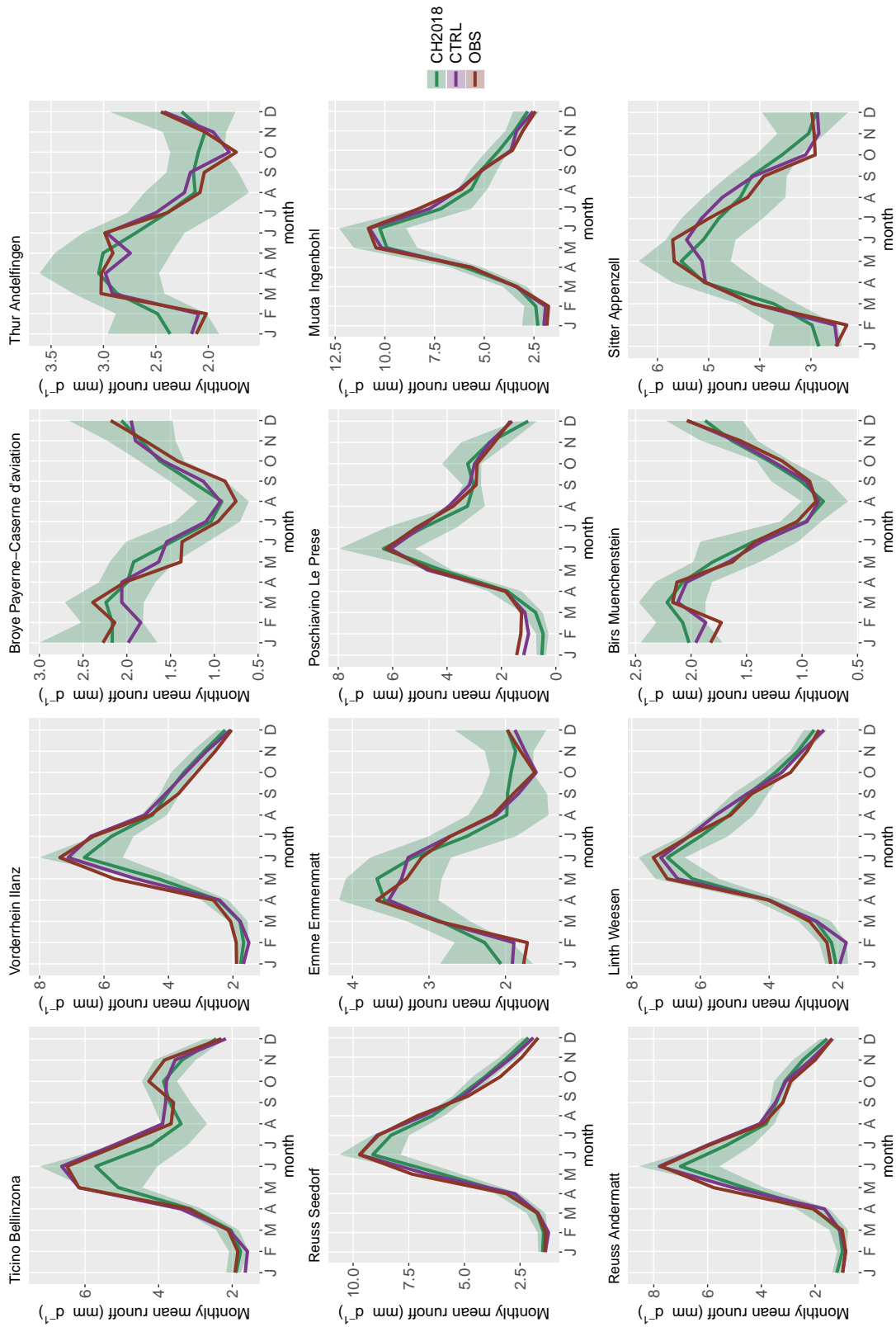


Figure A.1: Runoff regimes for observations (OBS, red) for 1985-2014, control simulations with calibrated parameters (CTRL, purple) for 1985-2014, and simulations driven by the CH2018 scenarios (CH2018, green) for the reference period 1981-2010.

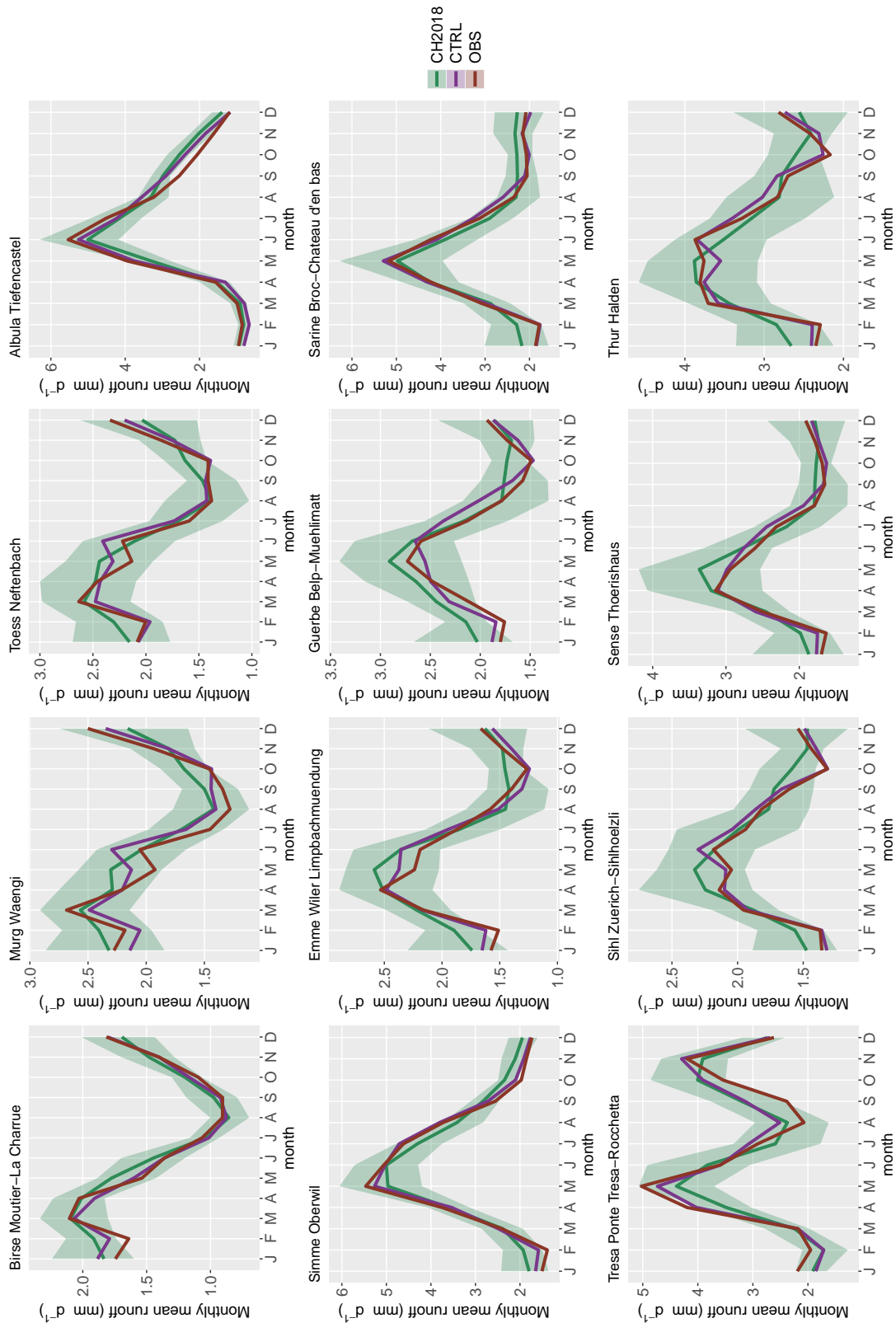


Figure A.2: Runoff regimes for observations (OBS, red) for 1985-2014, control simulations with calibrated parameters (CTRL, purple) for 1985-2014, and simulations driven by the CH2018 scenarios (CH2018, green) for the reference period 1981-2010.

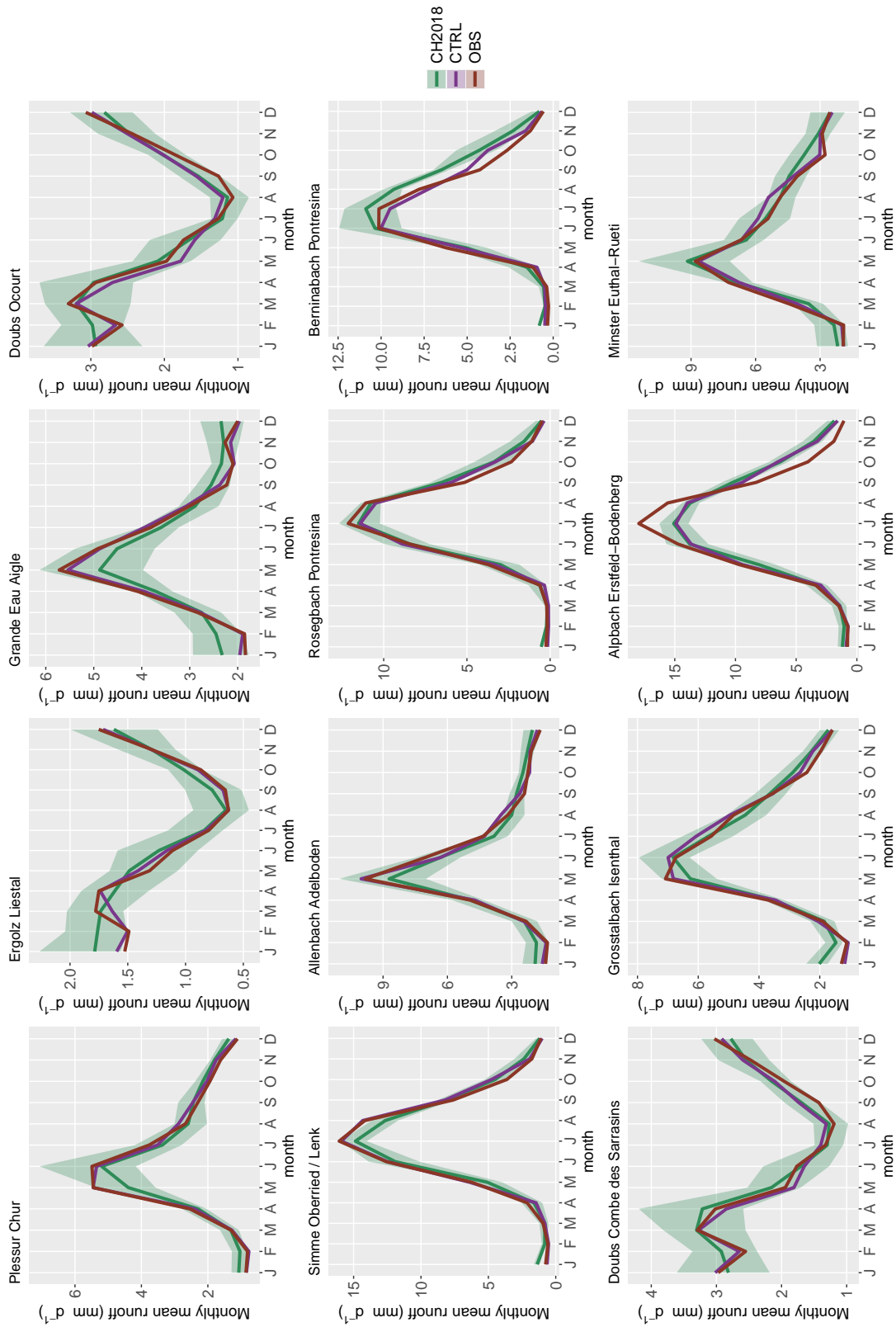


Figure A.3: Runoff regimes for observations (OBS, red) for 1985-2014, control simulations with calibrated parameters (CTRL, purple) for 1985-2014, and simulations driven by the CH2018 scenarios (CH2018, green) for the reference period 1981-2010.

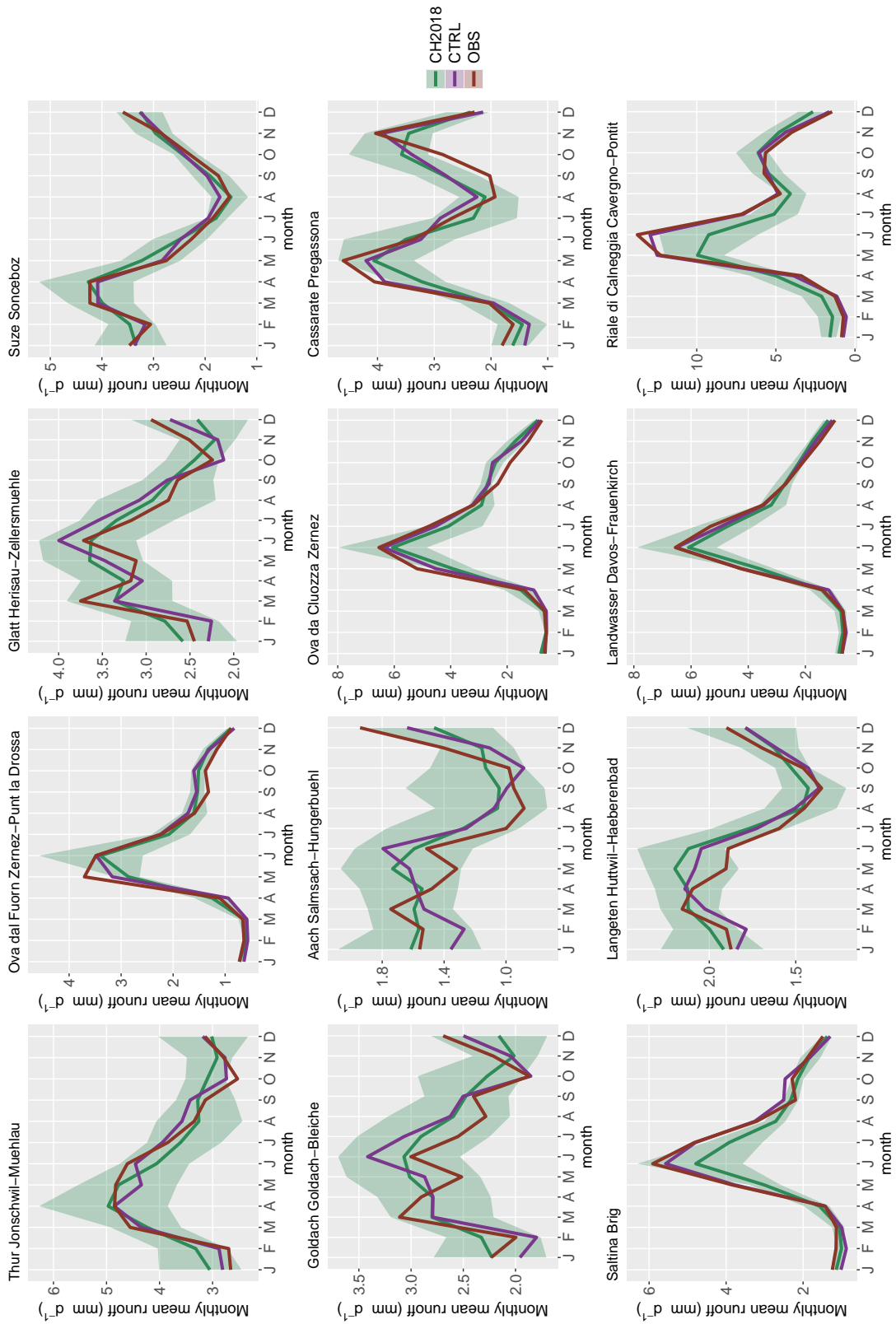


Figure A.4: Runoff regimes for observations (OBS, red) for 1985-2014, control simulations with calibrated parameters (CTRL, purple) for 1985-2014, and simulations driven by the CH2018 scenarios (CH2018, green) for the reference period 1981-2010.

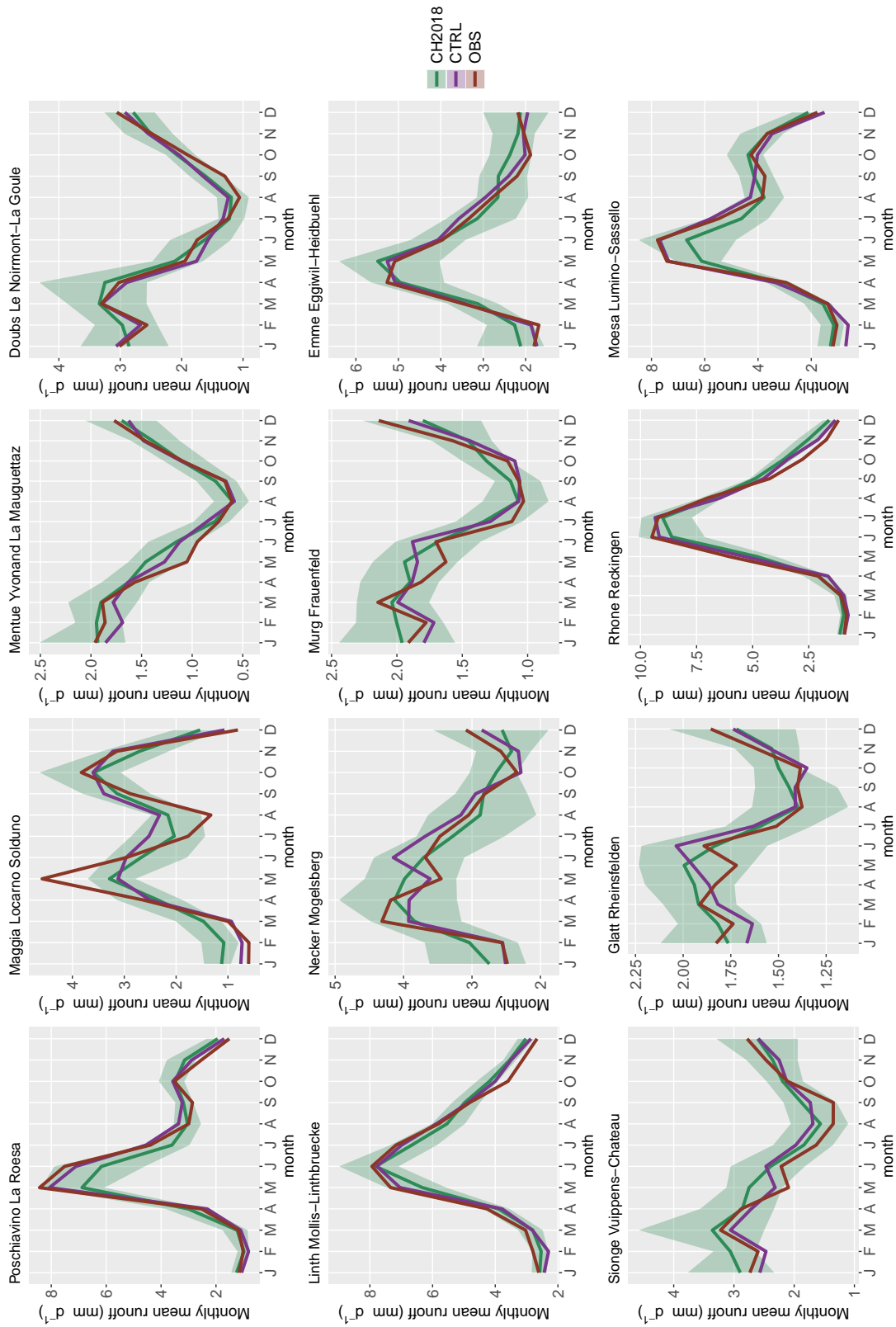


Figure A.5: Runoff regimes for observations (OBS, red) for 1985-2014, control simulations with calibrated parameters (CTRL, purple) for 1985-2014, and simulations driven by the CH2018 scenarios (CH2018, green) for the reference period 1981-2010.

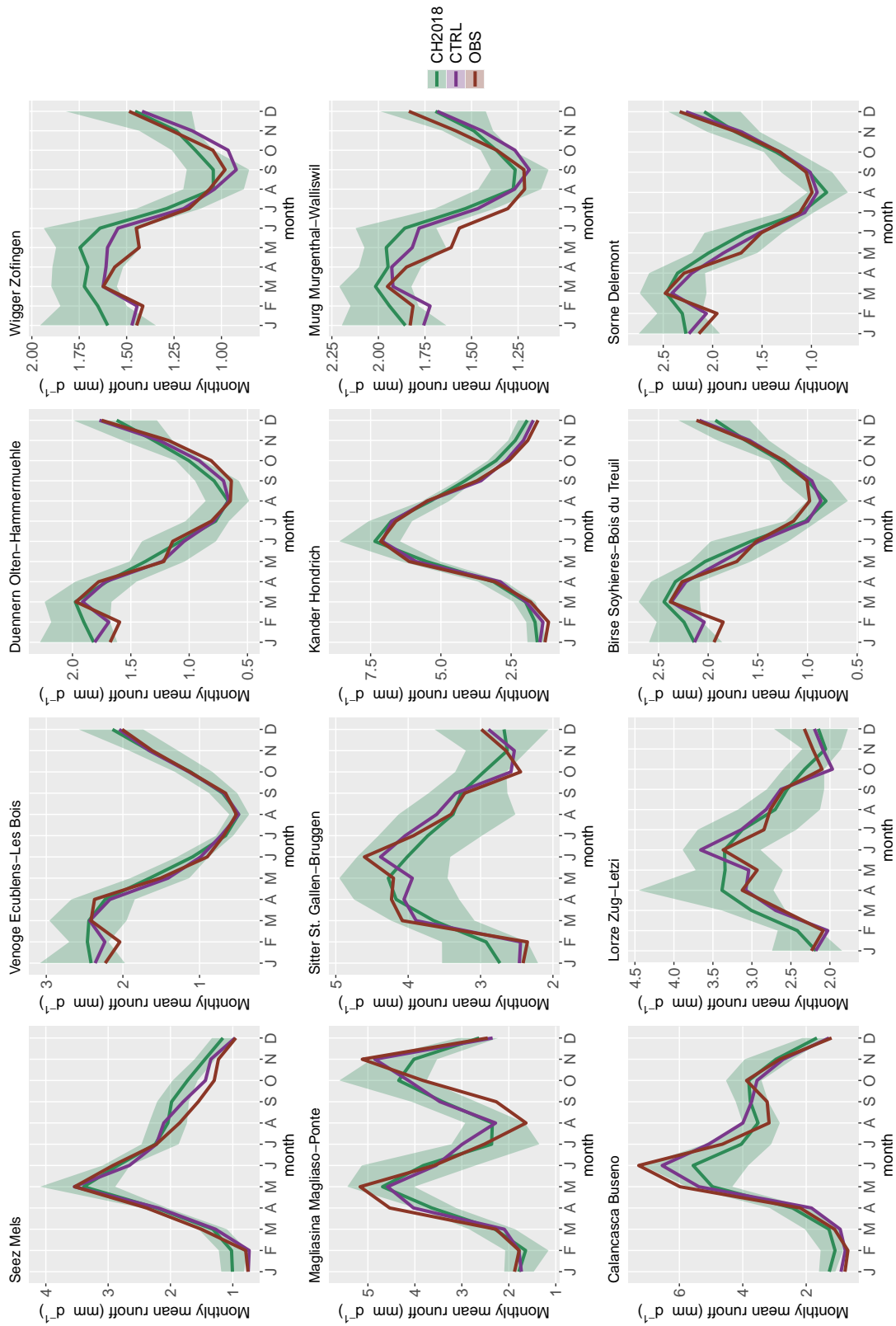


Figure A.6: Runoff regimes for observations (OBS, red) for 1985-2014, control simulations with calibrated parameters (CTRL, purple) for 1985-2014, and simulations driven by the CH2018 scenarios (CH2018, green) for the reference period 1981-2010.

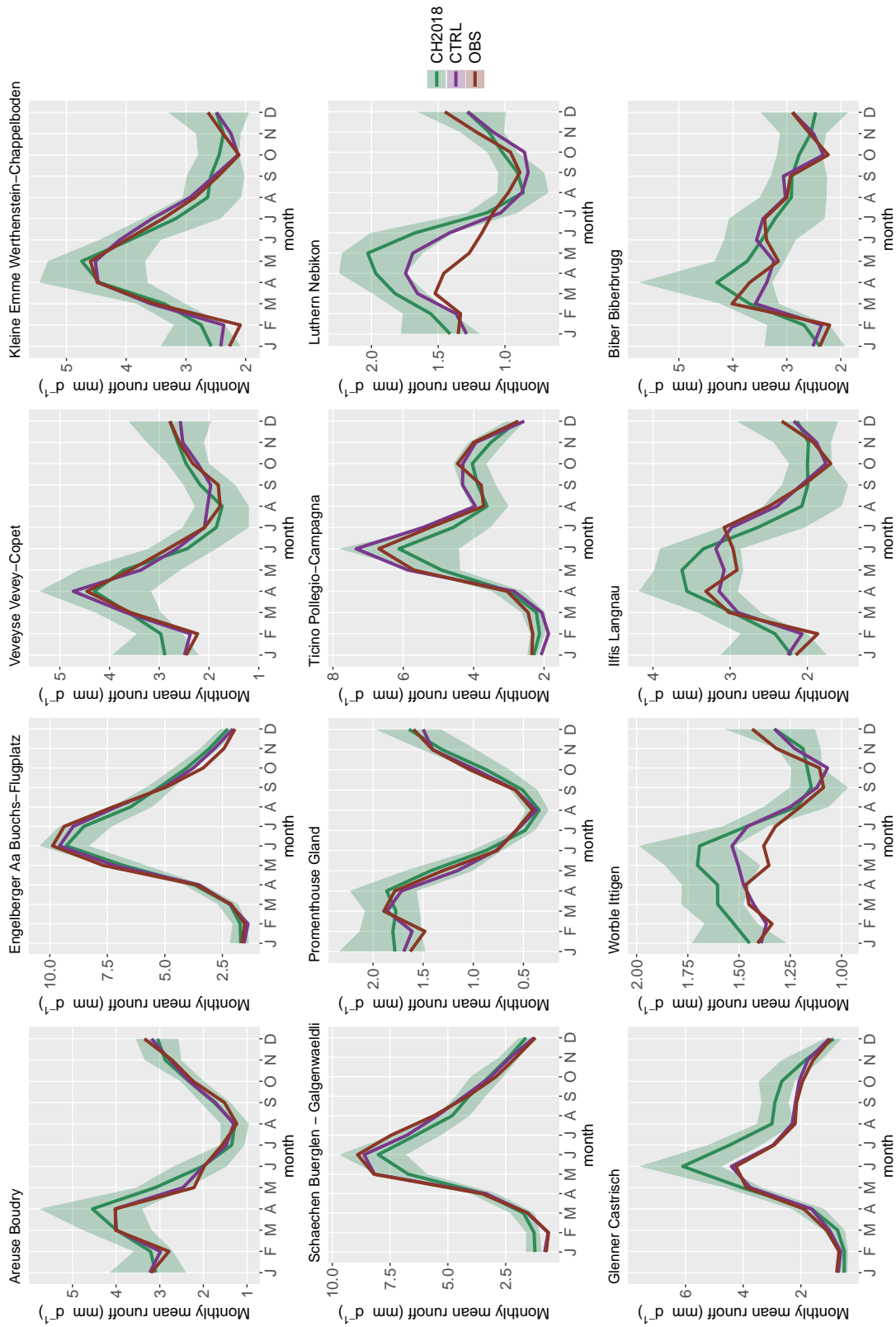


Figure A.7: Runoff regimes for observations (OBS, red) for 1985-2014, control simulations with calibrated parameters (CTRL, purple) for 1985-2014, and simulations driven by the CH2018 scenarios (CH2018, green) for the reference period 1981-2010.

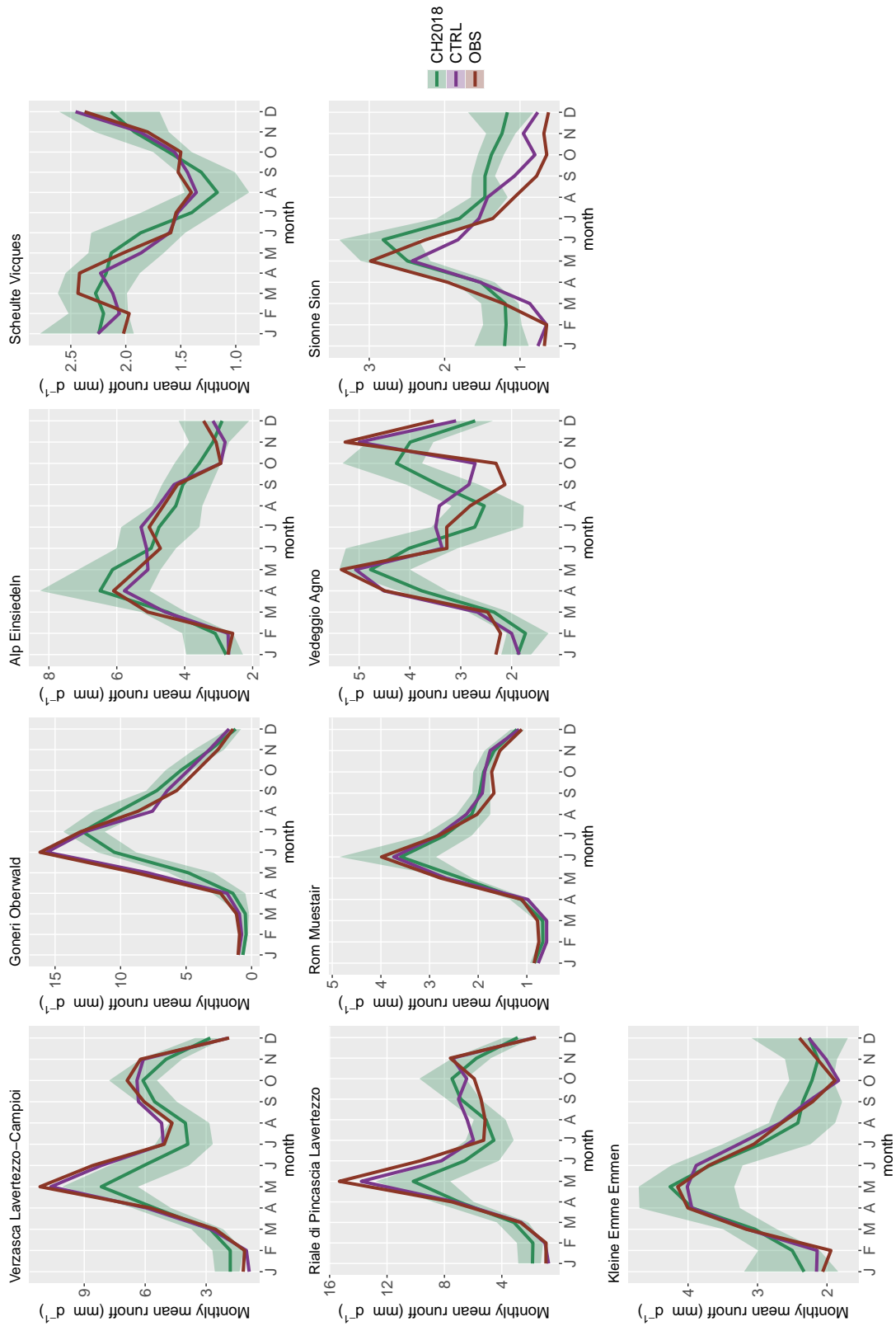


Figure A.8: Runoff regimes for observations (OBS, red) for 1985-2014, control simulations with calibrated parameters (CTRL, purple) for 1985-2014, and simulations driven by the CH2018 scenarios (CH2018, green) for the reference period 1981-2010.

Appendix B

Supporting information to chapter 3

Table B.1: Overview of the main characteristics of the 93 catchments.

ID	station	river	area (km ²)	mean altitude (masl)	min altitude (masl)	max altitude (masl)	glaciation (%)
2020	Bellinzona	Ticino	1517.5	1679	220	3345	0
2033	Ilanz	Vorderrhein	774	2026	685	3557	1.8
2034	Payerne	Broye	415.9	724	368	1574	0
2044	Andelfingen	Thur	1701.6	773	354	2431	0
2056	Seedorf	Reuss	833.2	2005	432	3598	6.4
2070	Emmenmatt	Emme	443	1072	562	2161	0
2078	Le Prese	Poschiavino	167.7	2161	962	3875	3.9
2084	Ingenbohl	Muota	316.6	1364	425	2731	0
2087	Andermatt	Reuss	190.2	2276	1125	3598	2.9
2104	Weesen	Linth	1061.5	1580	416	3557	1.6
2106	Muenchenstein	Birs	887.3	733	256	1424	0
2112	Appenzell	Sitter	74.4	1254	445	2431	0
2122	Moutier	Birse	185.8	927	493	1424	0
2126	Waengi	Murg	80.1	654	456	1113	0
2132	Neftenbach	Toess	343.3	659	380	1298	0
2141	Tiefencastel	Albula	529	2127	837	3317	0.5
2151	Oberwil	Simme	343.7	1639	778	3208	2.4
2155	Wiler	Emme	924.1	871	430	2161	0

Continuation of Table B.1							
ID	station	river	area (km ²)	mean altitude (masl)	min altitude (masl)	max altitude (masl)	glaciation (%)
2159	Belp	Guerbe	116.1	849	508	2128	0
2160	Broc	Sarine	636.3	1501	674	3207	0
2167	Ponte Tresa	Tresa	609.1	805	198	2207	0
2176	Zuerich	Sihl	342.6	1047	402	2223	0
2179	Thoerishaus	Sense	351.2	1076	524	2182	0
2181	Halden	Thur	1085	914	445	2431	0
2185	Chur	Plessur	264.4	1865	545	2923	0
2202	Liestal	Ergolz	261.2	591	296	1181	0
2203	Aigle	Grande Eau	131.6	1566	384	3167	0.8
2210	Ocourt	Doubs	1275.4	960	407	1448	0
2219	Oberried	Simme	34.7	2335	1075	3208	22.6
2232	Adelboden	Allenbach	28.8	1855	1093	2833	0
2256	Pontresina	Rosegbach	66.5	2701	1720	3981	21.7
2262	Pontresina	Berninabach	106.9	2608	1783	3981	14.4
2270	Combe des Sarrasins	Doubs	998.5	985	553	1448	0
2276	Isenthal	Grosstalbach	43.9	1810	767	2961	6.7
2299	Erstfeld	Alpbach	20.7	2181	629	3129	19.7
2300	Euthal	Minster	59.1	1352	642	2223	0
2303	Jonschwil	Thur	492.9	1027	535	2431	0
2304	Zernez	Ova dal Fuorn	55.3	2333	1666	3114	0
2305	Herisau	Glatt	16.7	836	624	1145	0
2307	Sonceboz	Suze	127.2	1044	634	1595	0
2308	Goldach	Goldach	50.4	840	391	1245	0
2312	Salmsach	Aach	47.4	476	391	609	0
2319	Zernez	Ova da Cluozza	26.9	2361	1468	3115	0
2321	Pregassona	Cassarate	75.8	991	272	2198	0
2342	Brig	Saltina	76.5	2017	661	3407	2.5
2343	Huttwil	Langeten	59.9	765	566	1123	0
2355	Davos	Landwasser	183.7	2223	1453	3180	0
2356	Cavergno	Riale di Calneggia	23.9	1982	645	2866	0

Continuation of Table B.1							
ID	station	river	area (km ²)	mean altitude (masl)	min altitude (masl)	max altitude (masl)	glaciation (%)
2366	La Roesa	Poschiavino	14.1	2286	1707	3012	0
2368	Locarno	Maggia	926.9	1534	191	3208	0
2369	Yvonand	Mentue	105.3	683	436	946	0
2370	Le Noirmont	Doubs	1046.7	985	503	1448	0
2372	Mollis	Linth	600.2	1737	427	3557	2.9
2374	Mogelsberg	Necker	88.1	962	604	1513	0
2386	Frauenfeld	Murg	213.3	596	381	1113	0
2409	Eggiwil	Emme	124.4	1283	562	2161	0
2412	Vuippens	Sionge	43.4	872	674	1457	0
2415	Rheinsfelden	Glatt	417.4	506	340	1105	0
2419	Reckingen	Rhone	214.3	2301	1307	3598	11.8
2420	Lumino	Moesa	471.9	1668	229	3169	0
2426	Mels	Seez	106.1	1796	469	3073	0
2432	Ecublens	Venoge	227.6	694	372	1662	0
2434	Olten	Duennern	233.8	714	390	1383	0
2450	Zofingen	Wigger	366.2	662	419	1393	0
2461	Magliaso	Magliasina	34.4	927	269	1904	0
2468	St. Gallen	Sitter	261.1	1045	445	2431	0
2469	Hondrich	Kander	490.7	1846	558	3675	5.1
2471	Murgenthal	Murg	183.4	659	410	1123	0
2474	Buseno	Calancasca	120.5	1930	503	3169	0.2
2477	Zug	Lorze	100.2	822	411	1556	0
2478	Soyhieres	Birse	569.5	811	380	1424	0
2479	Delemont	Sorne	213.9	785	408	1326	0
2480	Boudry	Areuse	377.7	1084	427	1573	0
2481	Buochs	Engelberger Aa	228	1605	432	3137	2.5
2486	Vevey	Veveyse	64.5	1108	372	1959	0
2487	Werthenstein	Kleine Emme	311.5	1171	525	2290	0
2491	Buerglen	Schaechen	107.9	1722	436	3221	1.5
2493	Gland	Promenthouse	119.8	1035	372	1667	0
2494	Pollegio	Ticino	443.8	1794	277	3120	0

Continuation of Table B.1							
ID	station	river	area (km ²)	mean altitude (masl)	min altitude (masl)	max altitude (masl)	glaciation (%)
2497	Nebikon	Luthern	104.7	754	474	1393	0
2498	Castrisch	Glenner	380.9	2014	685	3345	1.1
2500	Ittigen	Worble	67.1	678	494	954	0
2603	Langnau	Ilfis	187.4	1047	681	2045	0
2604	Biberbrugg	Biber	31.9	1008	602	1515	0
2605	Lavertezzo	Verzasca	185.1	1663	463	2837	0
2607	Oberwald	Goneri	38.4	2378	1353	3120	4
2609	Einsiedeln	Alp	46.7	1161	660	1783	0
2610	Vicques	Scheulte	72.7	797	419	1292	0
2612	Lavertezzo	Riale di Pincascia	44.5	1713	463	2520	0
2617	Muestair	Rom	128.5	2188	1167	3196	0
2629	Agno	Vedeggio	99.9	921	198	2198	0
2630	Sion	Sionne	27.6	1575	485	3084	0
2634	Emmen	Kleine Emme	478.3	1058	425	2290	0

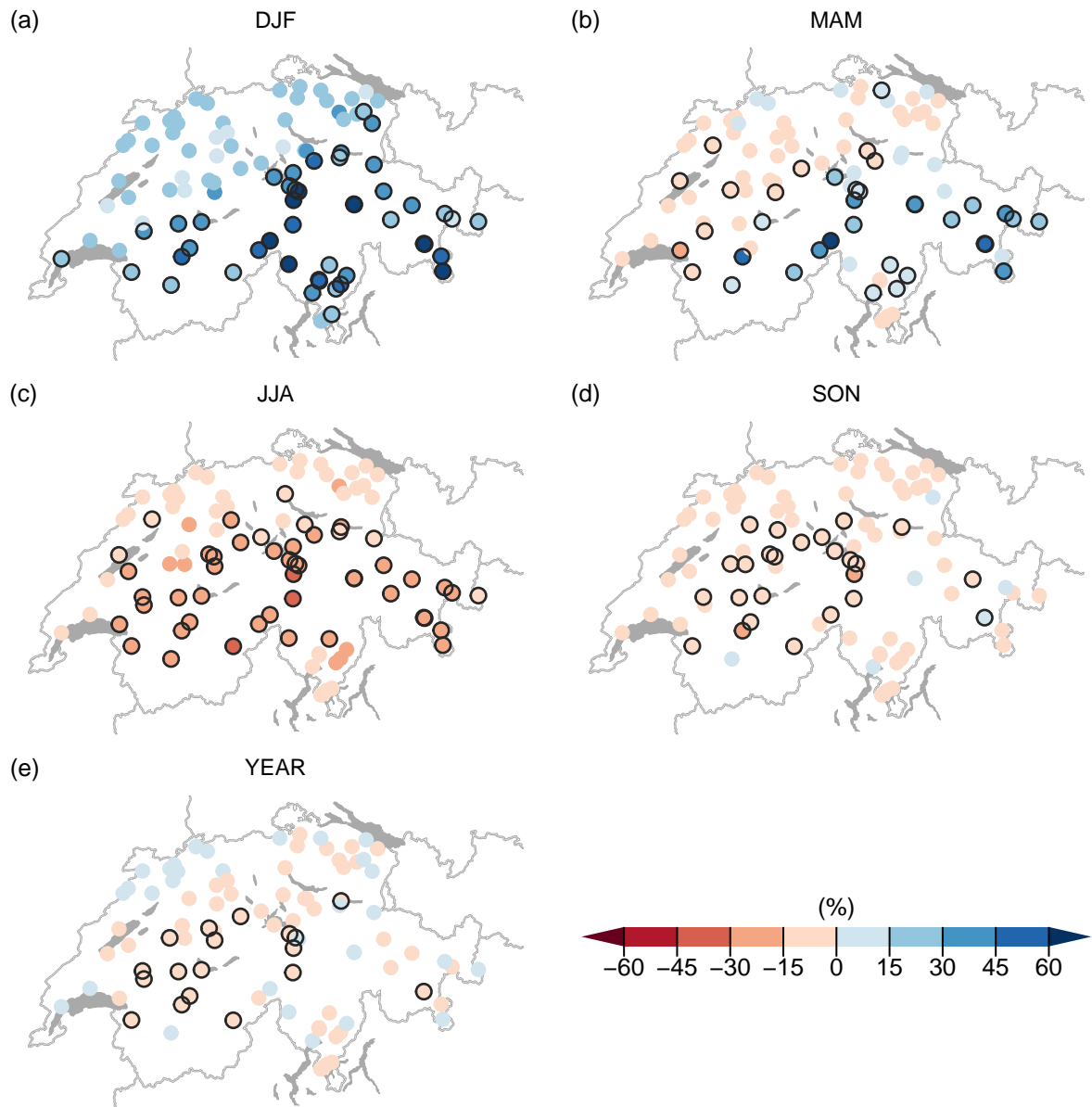


Figure B.1: Multimodel median of seasonal and yearly mean changes under RCP4.5 by 2085 for winter (a), spring (b), summer (c), autumn (d), and yearly means (e). Black circles indicate changes with at least 90% of the models agreeing on the direction of change.

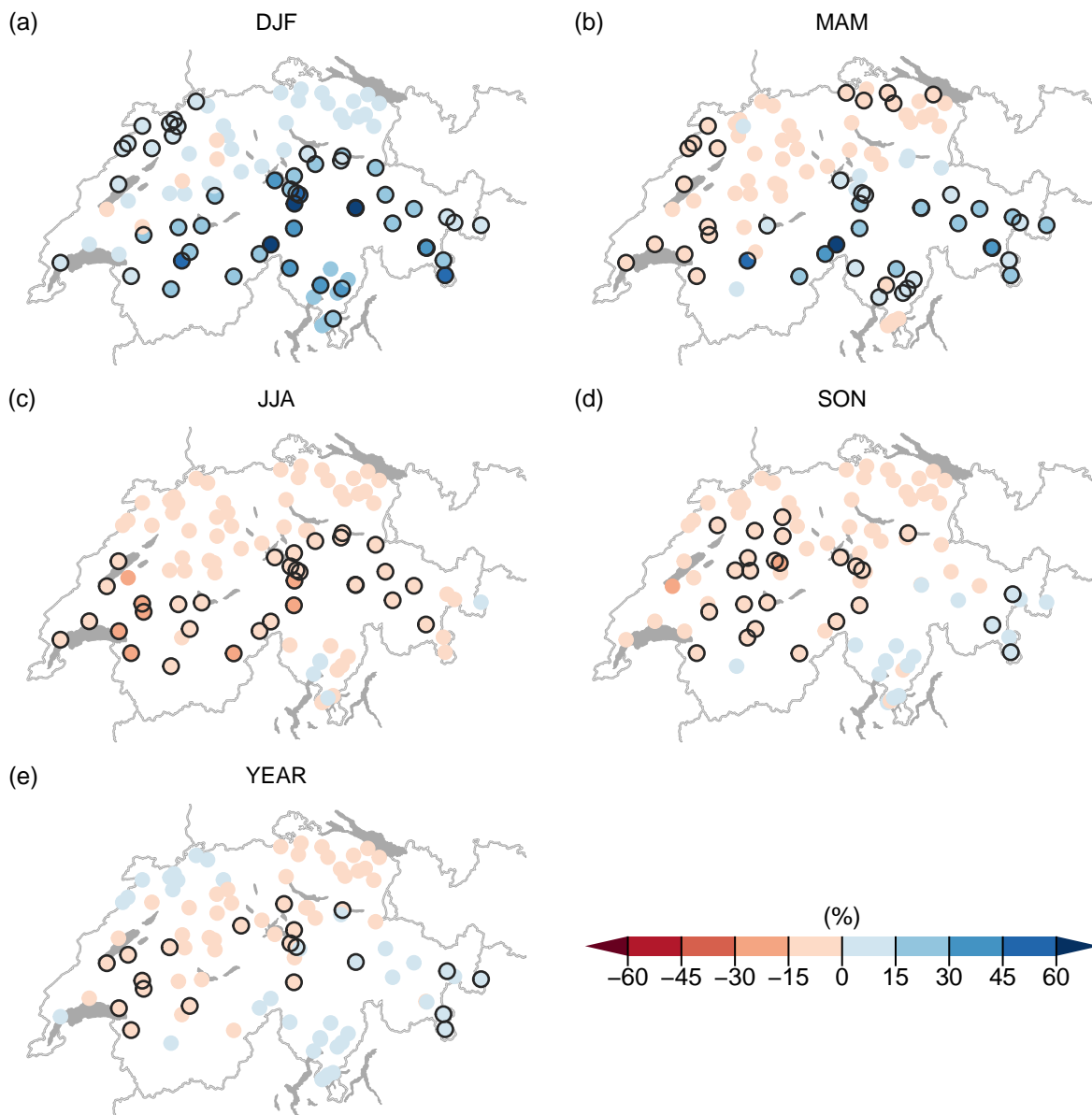


Figure B.2: Multimodel median of seasonal and yearly mean changes under RCP2.6 by 2060 for winter (a), spring (b), summer (c), autumn (d), and yearly means (e). Black circles indicate changes with at least 90% of the models agreeing on the direction of change.

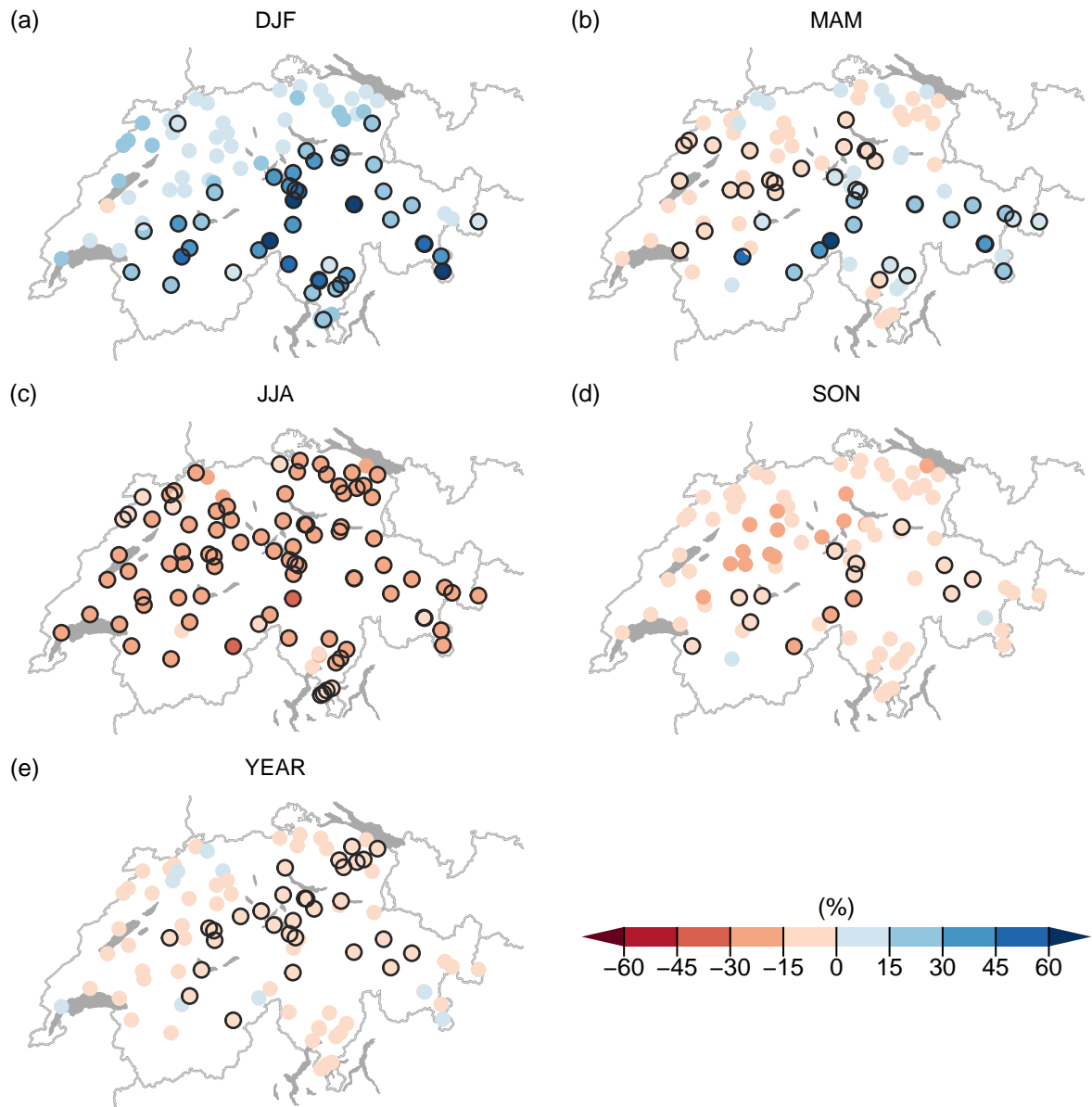


Figure B.3: Multimodel median of seasonal and yearly mean changes under RCP4.5 by 2060 for winter (a), spring (b), summer (c), autumn (d), and yearly means (e). Black circles indicate changes with at least 90% of the models agreeing on the direction of change.

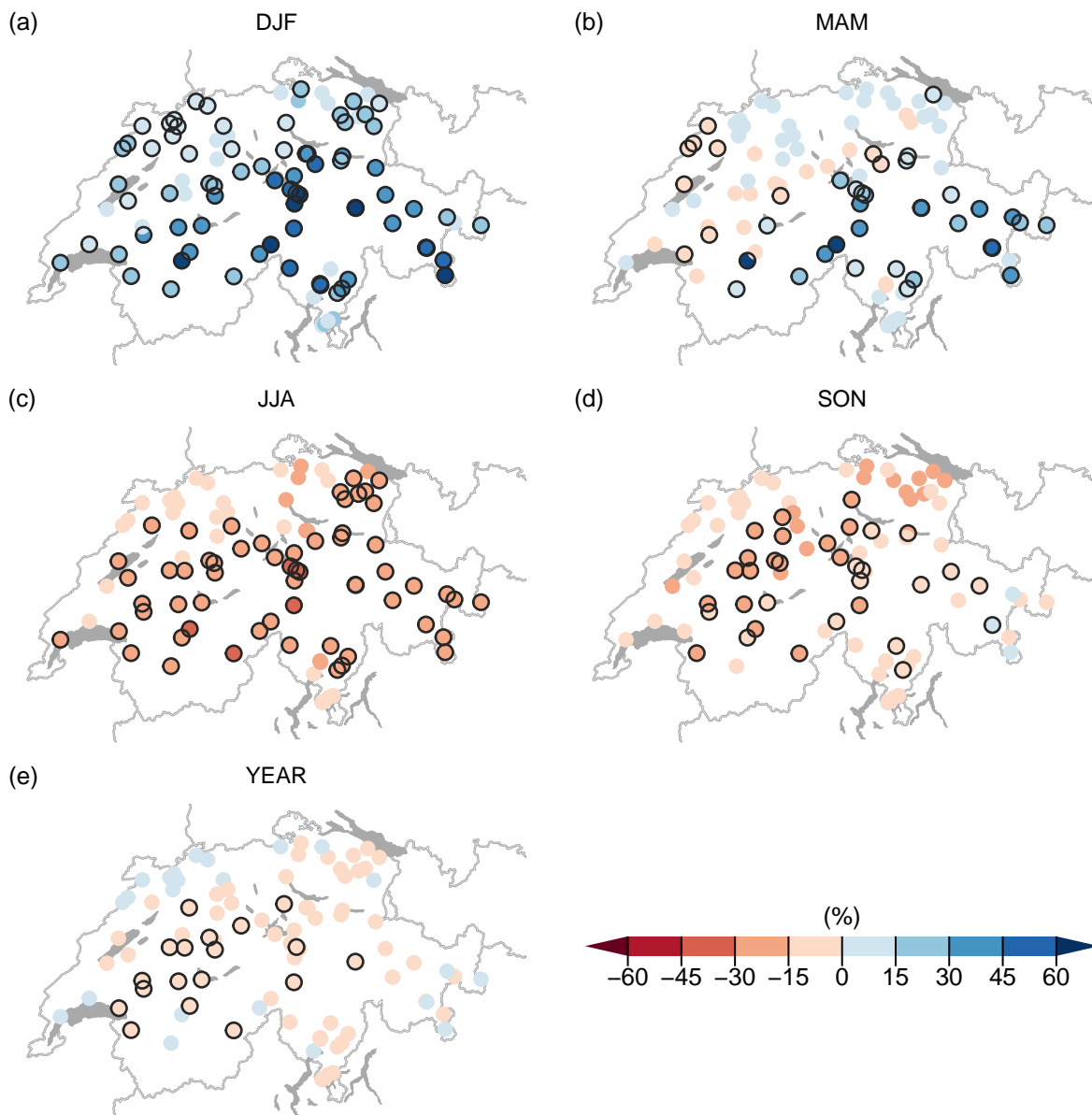


Figure B.4: Multimodel median of seasonal and yearly mean changes under RCP8.5 by 2060 for winter (a), spring (b), summer (c), autumn (d), and yearly means (e). Black circles indicate changes with at least 90% of the models agreeing on the direction of change.

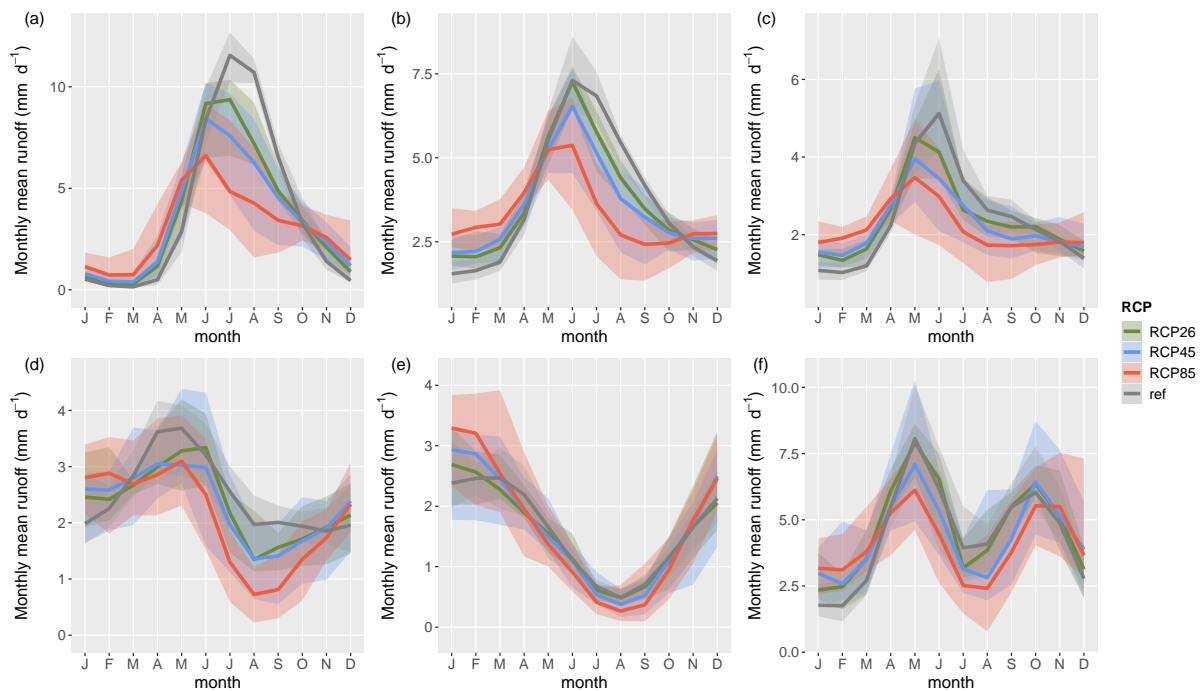


Figure B.5: Runoff regimes for the six representative catchments Rosebach (a), Kander (b), Plessur (c), Emme (d), Venoge (e), and Verzasca (f). Thick lines represent the multi-model median for the reference period (grey), for 2085 under RCP2.6 (green), for 2085 under RCP4.5 (blue), and for 2085 under RCP8.5 (red). Shadings show the full model range for each RCP.

Appendix C

Supporting information to chapter 6

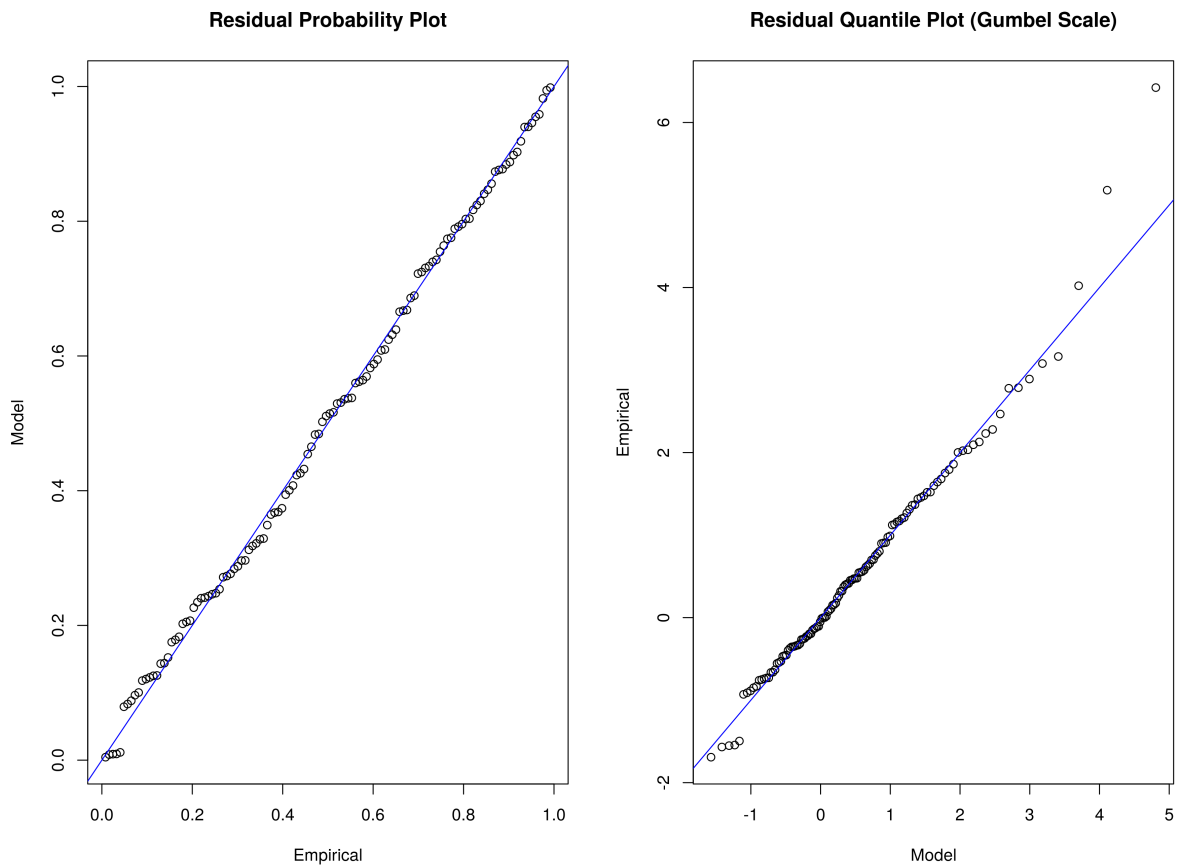


Figure C.1: Example of a Goodness-of-fit plot for a non-stationary GEV model.

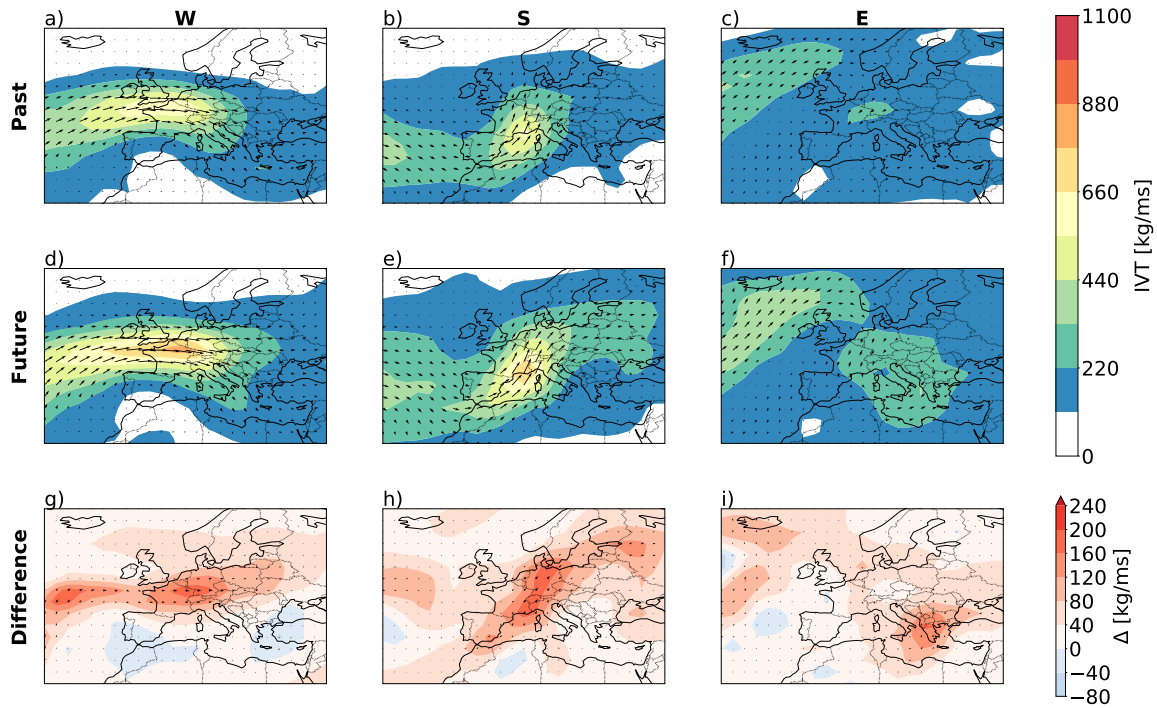


Figure C.2: Time composites of IVT intensity and direction during IVT block maxima in the *bcc-csm1-1* model for the period 1979-2008 (a-c) and 2071-2100 (d-f) for the western region (left), the southern region (middle), and the eastern region (right). Absolute differences between the two periods for the different regions are shown in the lower panels (g-i).

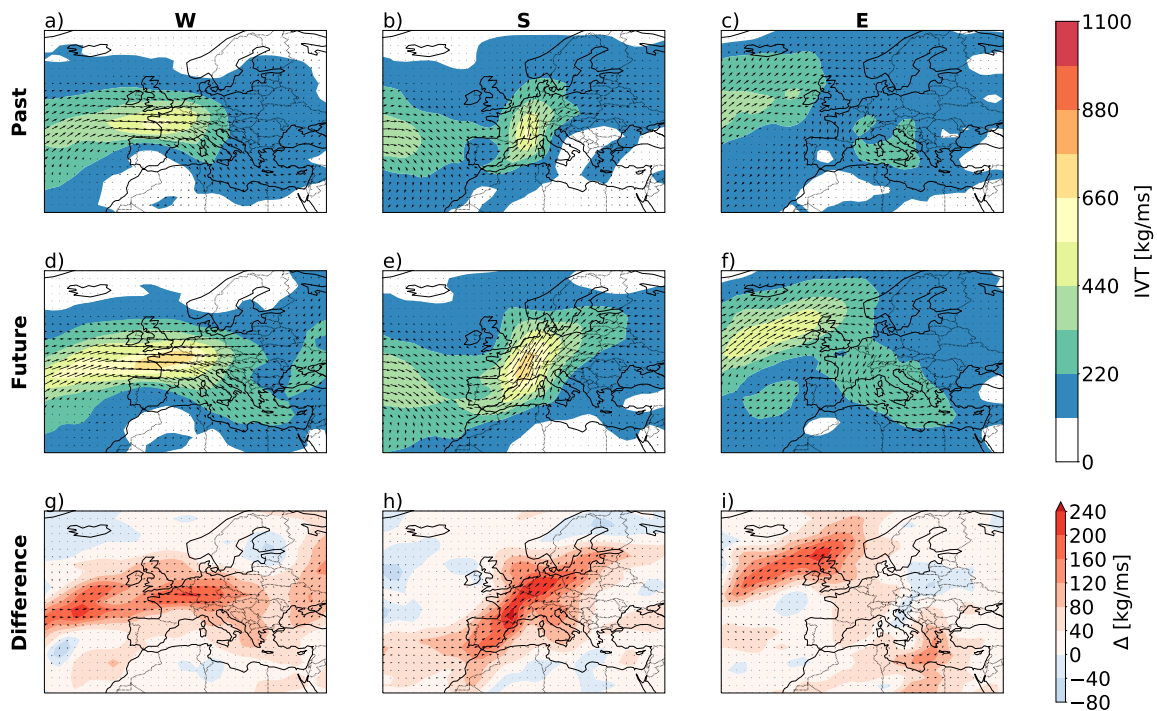


Figure C.3: Same as Figure C.2 but for model *CSIRO-Mk3-6-0*.

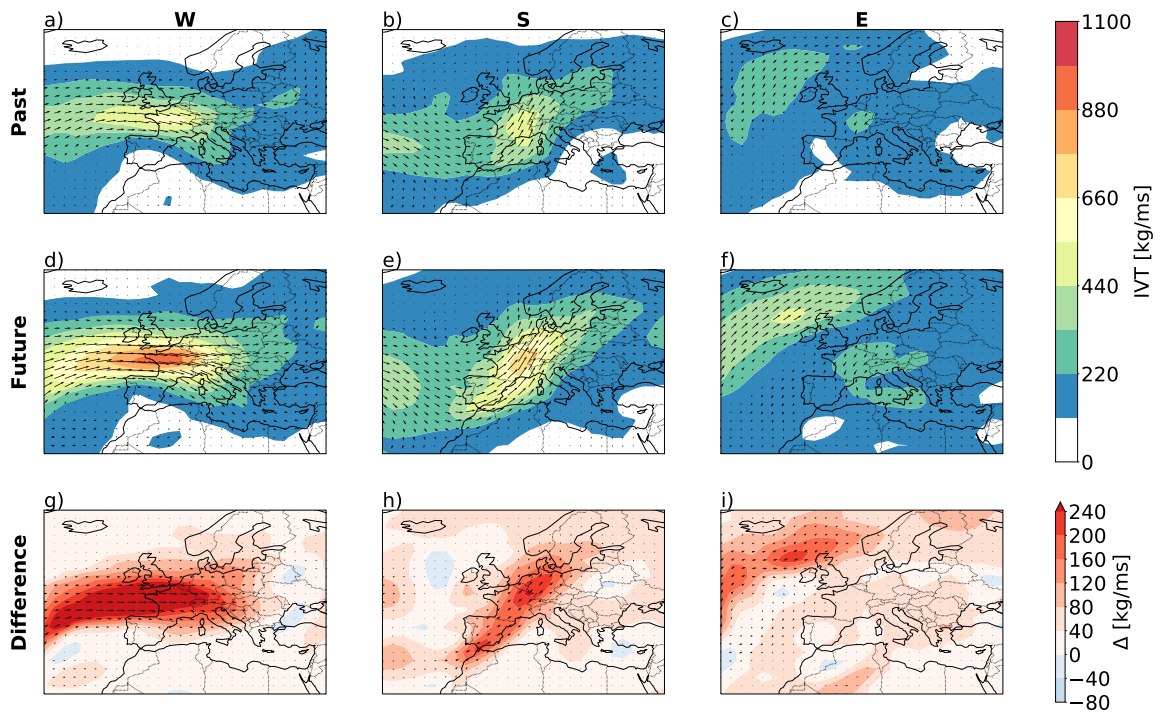


Figure C.4: Same as Figure C.2 but for model GFDL-CM3.

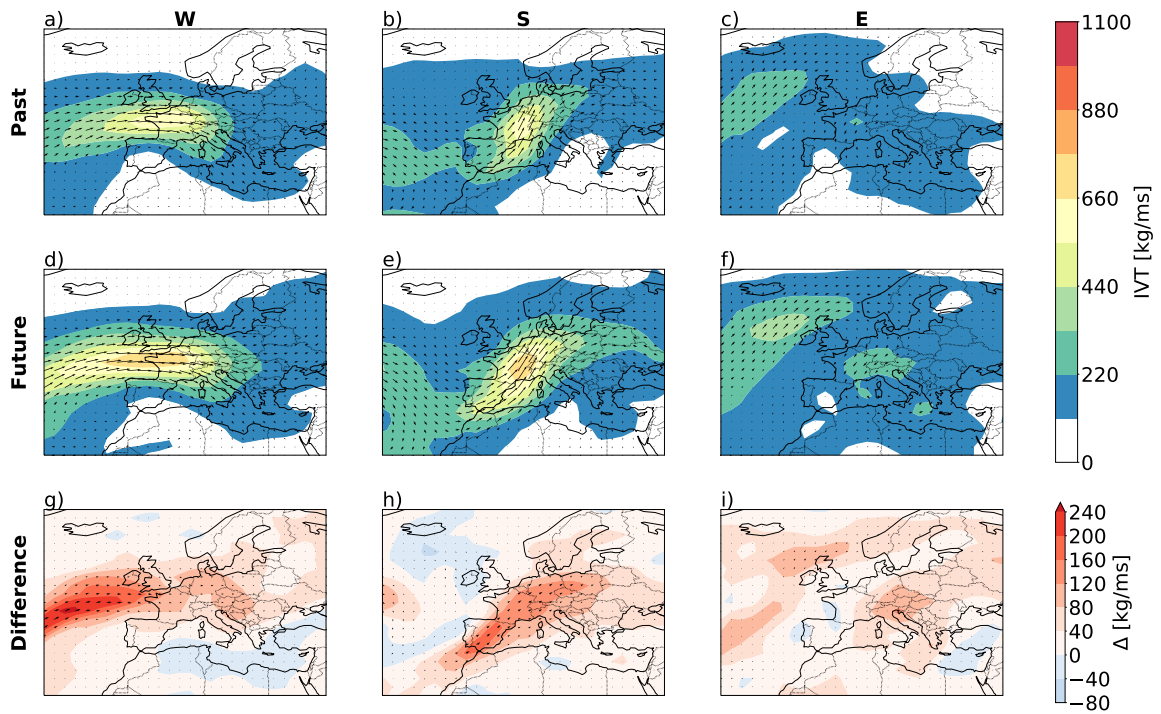


Figure C.5: Same as Figure C.2 but for model GFDL-ESM2G.

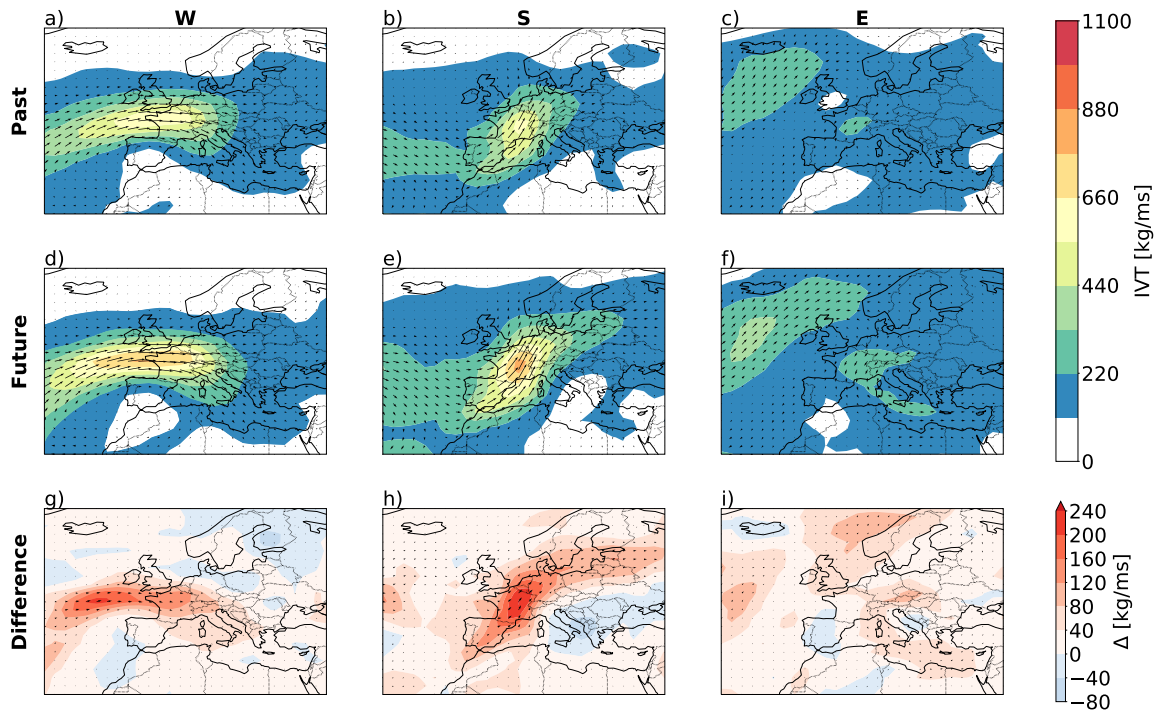


Figure C.6: Same as Figure C.2 but for model GFDL-ESM2M.

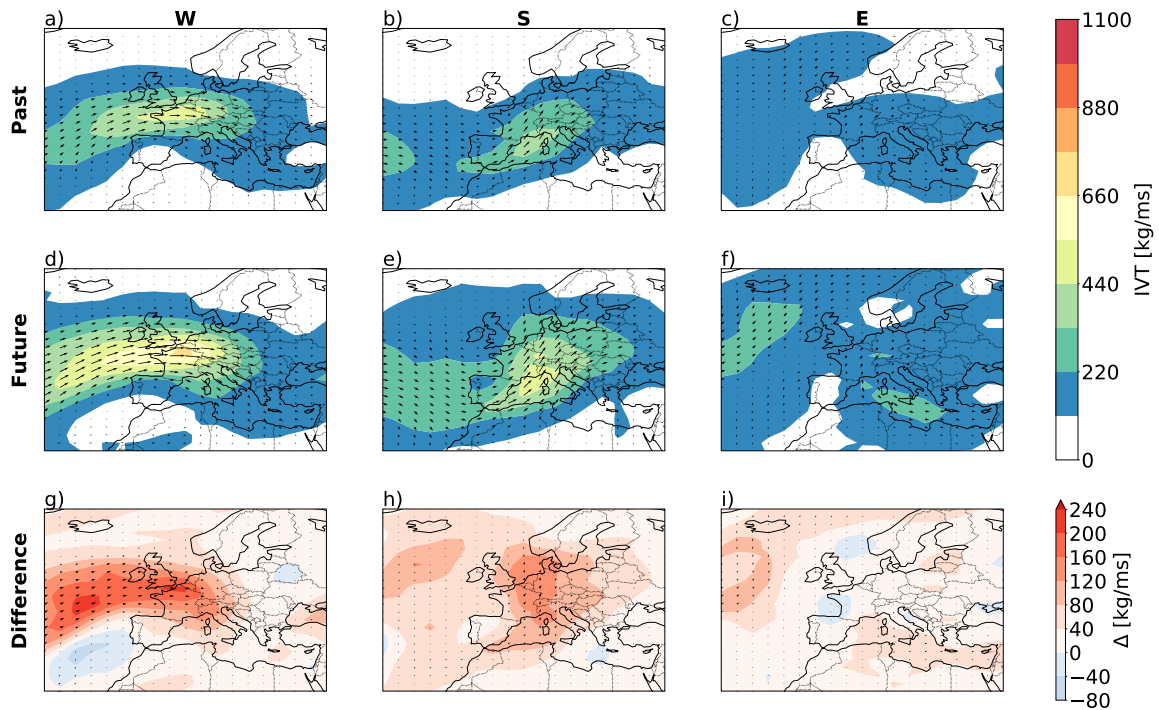


Figure C.7: Same as Figure C.2 but for model IPSL-CM5A-LR.

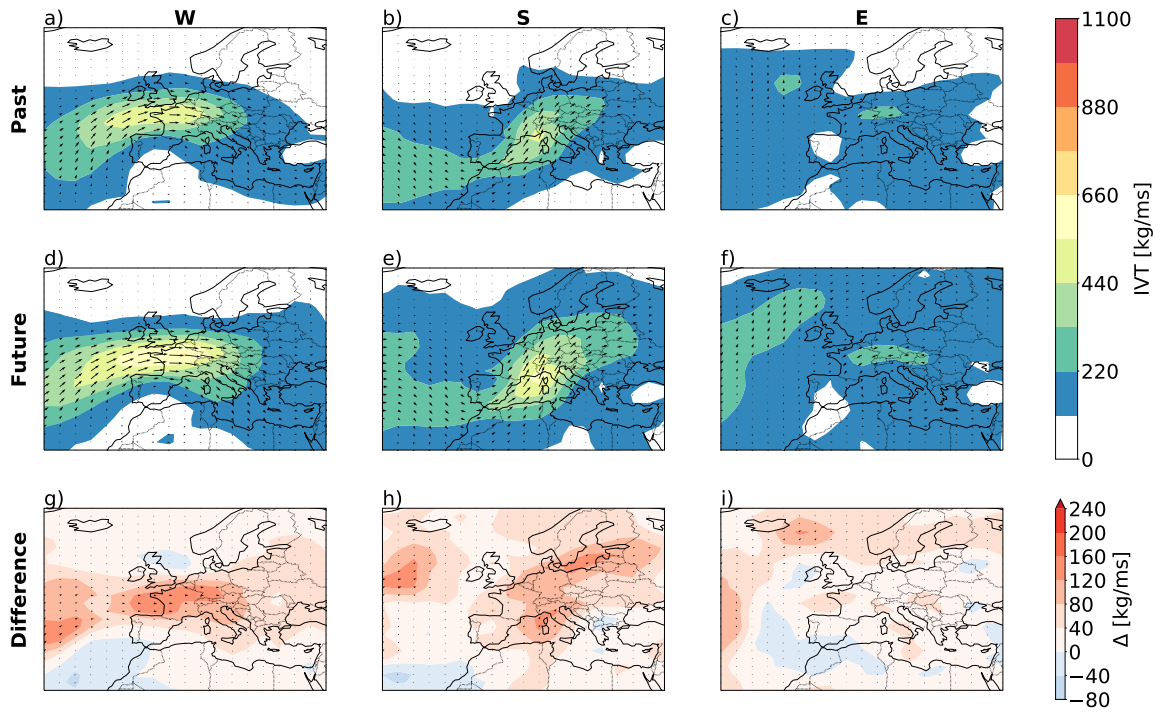


Figure C.8: Same as Figure C.2 but for model IPSL-CM5B-LR.

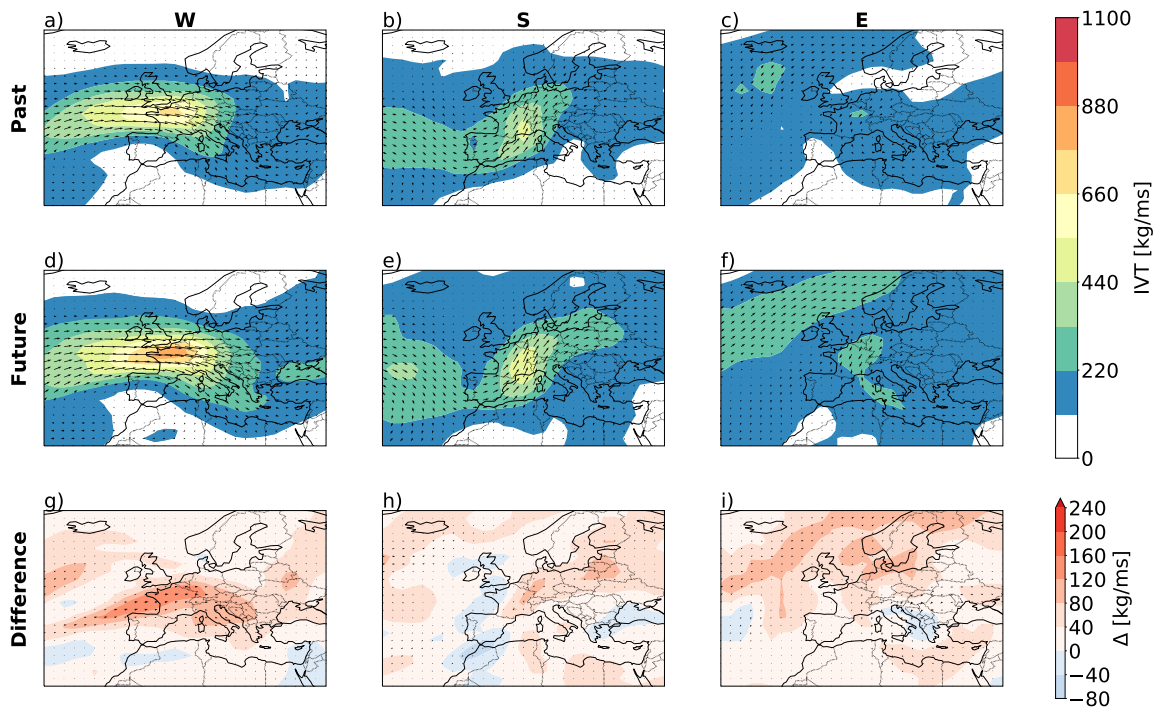


Figure C.9: Same as Figure C.2 but for model NorESM1-M.

Appendix D

Anthropogenic influence on runoff regime and runoff extremes for five catchments in Switzerland

D.1 Abstract

Attribution studies investigate the influence of anthropogenic greenhouse gas emissions on the climate and on climate impacts. This study assesses the anthropogenic influence on the runoff regimes and extremes in five catchments in Switzerland, using two forcing scenarios: an industrial scenario with year 2000/01 greenhouse gas concentrations and a non-industrial scenario with year 1900 concentrations. Global climate model data was used as input for a hydrological model to simulate the river runoff in each of the five catchments under the two scenarios. Due to systematic errors in the driving climate model, a bias correction was applied for different reference periods and the influence of the bias correction on the outcomes is discussed.

Attribution results show a shift in the runoff regimes towards higher winter and lower summer mean runoff due to anthropogenic greenhouse gas emissions. Higher winter temperatures and higher winter mean precipitation, combined with increased snowmelt, leads to enhanced winter mean runoff in the industrial scenario compared to the non-industrial scenario. In summer, less precipitation and enhanced evapotranspiration due to higher temperatures result in lower summer mean runoff in the industrial scenario compared to the non-industrial scenario. Further, an increase in the frequency of extreme runoff events, particularly in winter, is attributable to anthropogenic greenhouse gas emissions.

The hydrological simulations with bias corrected and raw climate model data agree on the direction of the change, but not on the magnitude. The magnitude is influenced by the choice of reference period for the bias correction. Raw simulations yield an overestimation of the change

signals. Hence, bias correcting climate model data prior to attribution is recommended to avoid overestimation of hydrological change signals.

D.2 Introduction

In recent years, it has become possible to quantify the influence of anthropogenic greenhouse gas (aGHG) emissions and other climate drivers on single atmospheric variables (e.g., Gillet et al., 2005; Min et al., 2008; Willet et al., 2007; Zhang et al., 2007) and climate extremes (Fischer & Knutti, 2015). In addition, the contribution of aGHG emissions to specific extreme events has been analyzed: e.g., for summer heat waves over Europe in 2003 (Stott et al., 2004) and Russia in 2010 (Otto et al., 2012), flood risk in southern Africa (Wolski et al., 2014), and severe floods over the British Isles in autumn 2000 (Kay et al., 2011; Pall et al., 2011) and winter 2013/2014 (Schaller et al., 2016). In Pall et al. (2011), a Global Climate Model (GCM) was run under two different one-year forcing scenarios for the year 2000/01, using climatic conditions with and without anthropogenic influence: an industrial scenario with year 2000 greenhouse gas concentrations, and a non-industrial scenario with year 1900 greenhouse gas concentrations. Thousands of year-long simulations, whose precipitation was subsequently fed into a precipitation-runoff model, indicated an increased risk of flood occurrence for England & Wales due to aGHG emissions. Such climate impact studies are called multi-step attribution experiments. They attribute the change of an environmental variable (flood) to a change in a climate variable (precipitation) that is in turn attributed to an external driver (aGHG emissions) (Hegerl et al., 2010).

Despite a growing number of attribution studies focusing on single variables or extreme events in different regions of the world, the human influence on the general hydrological characteristics in Switzerland is not yet known. Here we use the GCM data of Pall et al. (2011) and feed it into a hydrological model to assess the influence of aGHG emissions on the runoff characteristics of five Swiss rivers (Emme, Thur, Venoge, Verzasca, and Vorderrhein; Figure D.1). Our first goal is to investigate the influence of aGHGs on the runoff regimes of these rivers and on the frequency of runoff extremes.

Due to coarse spatial resolution and the parametrization of important processes, raw climate model output typically exhibits systematic errors (e.g., Sharma et al., 2007; Christensen et al., 2008; Maraun et al., 2010; Hewitson et al., 2014). A bias correction of the climate model output is hence necessary prior to climate impact studies to give reliable results (Hagemann et al., 2011; Teutschbein & Seibert, 2012; Teng et al., 2015). For probabilistic event attribution experiments, it is crucial to correct climate model biases in the higher statistical moments beyond the mean (Bellprat & Doblas-Reyes, 2016; Jeon et al., 2016; Sippel et al., 2016). However, most hydrological attribution studies to date have not considered applying bias correction, nor investigating the influence of the bias correction itself on results, nor examining the influence of the choice of reference period against which bias correction is performed. Therefore, the second goal of

our multi-step probabilistic attribution study is to contribute towards filling this knowledge gap.

In section 2 we describe the data used for the study, as well as the bias correction method, the hydrological model, the catchments, and the analysis methods. Results are presented and discussed in section 3 and 4 respectively, followed by overall conclusions in section 5.

D.3 Data and Methods

D.3.1 Data

The GCM simulations of Pall et al. (2011) are used to investigate the anthropogenic influence on the runoff of five rivers in Switzerland. The one-year (April 2000 – March 2001) simulations of the atmosphere-only GCM, HadAM3-N144 ($0.83^\circ \times 1.25^\circ$ horizontal resolution, 30 vertical pressure levels) (Pope & Stratton, 2002), use atmospheric composition, sea surface temperatures (SSTs) and sea ice coverage (SIC) as boundary conditions. To produce a large range of plausible realizations thousands of simulations were generated, with each simulation initially perturbed by unique adjustments of the atmospheric potential temperature.

The simulations are driven by an industrial scenario and a non-industrial scenario. The industrial scenario was constructed using observed greenhouse gas concentrations and other pollutants as well as observed SSTs and SIC for the year 2000/01. The hypothetical non-industrial scenario was constructed by reducing greenhouse gas concentrations to year 1900 levels, by adjusting SSTs via subtracting the estimated 20th century anthropogenic greenhouse gas warming, and by increasing SIC according to an observed SST-SIC relationship. The 20th century anthropogenic SST warming was estimated from the change in SST patterns attributable to greenhouse gas emissions using four coupled atmosphere-ocean models. Hence, there were four different sets of non-industrial SSTs (and associated SIC). This study considers 2'039 industrial simulations, and 14'609 non-industrial simulations pooled across the four SST sets. The GCM data was spatially averaged over the five catchments.

Observed spatially interpolated daily mean temperatures (MeteoSwiss, 2013a) and daily precipitation sums (Frei & Schär 1998; MeteoSwiss, 2013b) with a grid resolution of 2.2 km, provided by MeteoSwiss, were spatially averaged over the geographical shapes of the five catchments (Figure D.1). This data was used to calibrate the transfer functions of the statistical bias correction. The hydrological model (section 2.4) was calibrated and validated using observed spatially averaged meteorological data as well as daily mean runoff measurements from the outlet of the five rivers (provided by the Swiss Federal Office for the Environment (FOEN)). Table D.1 gives an overview of the observational periods considered in this study.

Table D.1: *Observational periods considered in this study.*

	Temperature Precipitation	Runoff
Bias correction	1961-2010 1981-2010 1995-2005 1998-2003 April 2000-March 2001	
Calibration of hydrological model	1991-1999 1990 as spin-up year	1991-1999 1990 as spin-up year
Validation of hydrological model	2000-2005	2000-2005
Spin-up of hydrological model prior to application of GCM data	April 1995-March 2000	

D.3.2 Catchment characteristics

The five catchments Emme, Thur, Venoge, Verzasca, and Vorderrhein are distributed over Switzerland (Figure D.1) representing different regions and hydrological regime types in Switzerland. Table D.2 summarizes the main characteristics of each catchment. The catchment sizes range from small scale catchments (185 km²) to medium-size catchments (1702 km²). The mean elevation of the five catchments varies from 686 masl to 2030 masl. According to the classification of Aschwanden and Weingartner (1985), the Emme, Thur and Venoge are pluvial catchments that are fed mainly by precipitation input, with low flows towards the end of summer and autumn and higher flows in winter and early spring. The catchments Vorderrhein and Verzasca are more snow and glacier (Vorderrhein) driven, with low flows in winter (due to snow accumulation) and peak flows in early summer.

D.3.3 Bias correction

Comparisons of different bias correction techniques show that quantile mapping outperforms other techniques for temperature and precipitation data (Themessl et al., 2011; Teutschbein & Seibert, 2012) and especially in alpine terrain (Ivanov & Kotlarski, 2017). Thus, quantile mapping was chosen to correct biases in the GCM simulations in this study. Among different quantile mapping approaches (parametric and non-parametric methods) the non-parametric empirical quantile mapping approach was chosen due to its good performance for temperature and precipitation (Gudmundsson et al., 2012). This method transforms the modeled values using the empirical cumulative density function for regularly spaced quantiles. Quantile mapping is known to underestimate spatial climate variability (Maraun, 2013). Therefore, the transfer function was calibrated with spatially aggregated observations to avoid this issue. Since the

Table D.2: Main characteristics of the five catchments.

	Emme	Thur	Venoge	Verzasca	Vorderrhein
Gauging station	Wiler	Andelfingen	Ecublens	Lavertezzo	Ilanz
Catchment area	924 km ²	1702 km ²	228 km ²	185 km ²	774 km ²
Station elevation	458 masl	356 masl	383 masl	490 masl	693 masl
Mean elevation	863 masl	770 masl	686 masl	1651 masl	2030 masl
Glaciation	0%	0%	0%	0%	1.80%
Regime type	pluvial supérieur	pluvial supérieur	pluvial jurassien	Nivo-pluvial méridional	Nivo-glaciaire

simulations under the two scenarios are independent of each other, the transfer function cannot be calculated for each industrial simulation separately and then applied to the respective non-industrial simulation. Therefore, a general transformation function had to be calculated for the industrial scenario to be applicable to all simulations. For this, all industrial simulations were combined into a vector. In order to avoid overfitting (particularly for the extremes) and to make the transfer function more robust, we calculated a total of 12 transfer functions. For this, the vector including all industrial simulations was split into 12 subsets, each covering the data of one particular month. The transfer function was trained 12 times. In each step, 11 subsets were used for the calibration. This procedure was repeated until each subset was left out once. The resulting transfer functions were subsequently aggregated to a general transfer function by averaging the correction factors per quantile. This general transfer function was then applied to all industrial and non-industrial simulations assuming a stationary bias between the two scenarios. This assumption is the subject of debate within the scientific community (e.g., Ehret et al., 2012), but so far no established solution for this problem exists. Extremes outside the calibration interval were linearly extrapolated as proposed by Boé et al. (2007).

To investigate the influence of the reference period on the bias correction, we applied quantile mapping to different time periods in the observational data (the GCM data always covers the year April 2000 to March 2001): a 50-year period 1961-2010, a 30-year period 1981-2010, a 10-year period 1995-2005, a 5-year period 1998-2003, and a 1-year period from April 2000 to March 2001. The last is the period for which the two climate scenarios are run.

D.3.4 Hydrological model GR4J-Cemaneige

The lumped hydrological model “Modèle du Génie Rural à 4 paramètres Journalier” (GR4J) (Perrin et al., 2003) was used to simulate the runoff of the five rivers. GR4J simulates runoff,

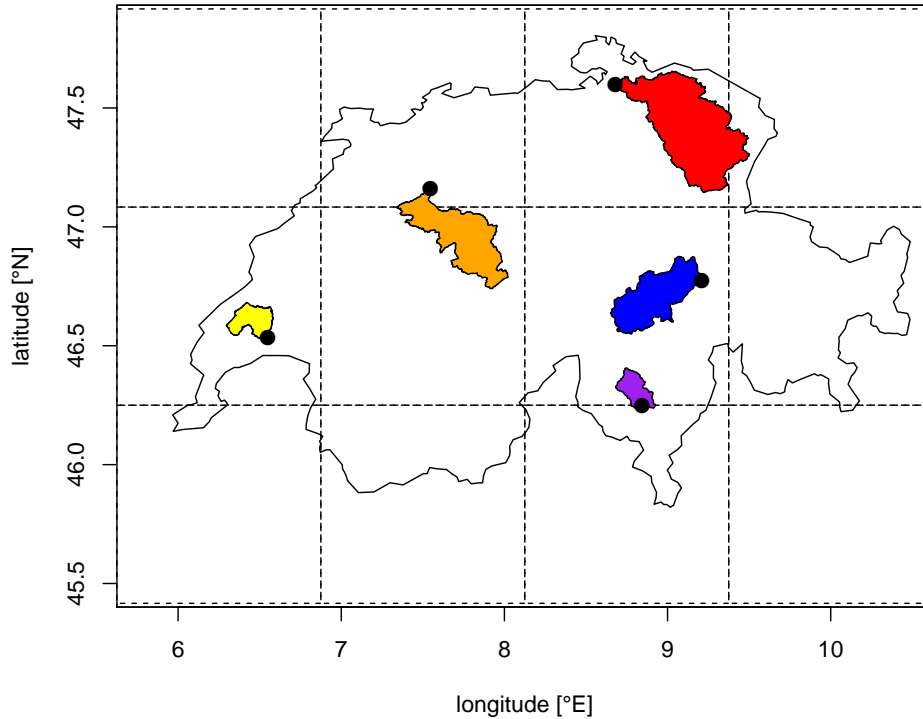


Figure D.1: Five catchments distributed over Switzerland: Emme (orange), Thur (red), Venoge (yellow), Verzasca (purple), and Vorderrhein (blue). Black dots represent the location of the runoff measurement station. Dotted black lines show the GCM grid used by Pall et al. (2011).

evapotranspiration, and soil moisture at daily resolution with four free parameters requiring calibration. It contains a routing scheme to consider runoff concentration times. The lumped GR4J model considers the catchment as a single entity and only requires spatially averaged daily precipitation and potential evapotranspiration as input. The potential evapotranspiration was calculated following Hamon (1961) as recommended for GR4J (Oudin et al., 2005). To consider snow accumulation and snow melt processes, we coupled the two-free-parameter snow module Cemaneige (Valéry, 2010; Valéry et al., 2014) to the GR4J. The snow module extrapolates the spatially averaged temperature and precipitation input to ten elevation bands, each covering 10% of the catchment area.

The model was calibrated with spatially aggregated observations for each catchment for the period 1990-1999, using 1990 as spin-up year, and subsequently validated for the period 2000-2005. A spin-up phase is required in hydrological models to fill the single-linear reservoirs. According to Moriasi et al. (2007), our calibrated models exhibit satisfactory performances in both the calibration and validation period (Table D.3). In the validation period, the Nash-

Table D.3: Performance results of the different catchments for the calibration period (Cal) and the validation period (Val): Nash-Sutcliffe-Efficiency (NSE), Kling-Gupta-Efficiency (KGE), percent bias (PBIAS), and root-mean-square error to the standard deviation of measured data (RSR).

	Emme		Thur		Venoge		Vorderrhein		Verzasca	
	Cal	Val	Cal	Val	Cal	Val	Cal	Val	Cal	Val
NSE	0.79	0.83	0.91	0.89	0.86	0.89	0.79	0.76	0.89	0.89
KGE	0.86	0.82	0.94	0.88	0.9	0.85	0.88	0.85	0.94	0.94
PBIAS	-1	-7.5	-0.2	-3.2	2.1	1.1	-2.4	-0.9	-0.2	3.4
RSR	0.46	0.41	0.3	0.33	0.37	0.33	0.46	0.49	0.34	0.33

Sutcliffe efficiency ranges between 0.76 and 0.89 (calibration: 0.79-0.91), percent bias between -7.5-3.4 (calibration: -2.4-2.1), and the ratio of the root-mean-square error to the standard deviation of measured data between 0.33-0.49 (calibration: 0.3-0.46). In addition, the Kling-Gupta-Efficiency also reveals satisfactory performance between 0.82-0.94 in the validation period (calibration: 0.86-0.94). To ensure that the same initial hydrological conditions are present in the model prior to the input of data from each GCM simulation, five years of observations from April 1995 to March 2000 are first used to spin up the model before running each simulation.

D.3.5 Analysis of temperature, precipitation, and runoff

The following climatological and hydrological indices are used to describe the differences between the industrial and the non-industrial scenario results: the climatological mean precipitation including all days (mm/d); the number of wet days (count; >1mm/d); the empirical 90th quantile (mm/d) of the precipitation distribution for wet days (>1mm/d), representing heavy precipitation on wet days; the number of snow days (count) considering days with temperatures below 0°C and precipitation above 1mm/d; the mean temperature (°C); and the number of frost days (count; <0°C). To characterize the change in the hydrology, mean runoff (m³/s) and the empirical 99th quantile (m³/s) of the daily runoff distribution are used. All indices were calculated for the bias corrected and the raw GCM simulations. The GCM simulations cover the period from April 2000 to March 2001, and we calculate indices for this year as well as for the meteorological winter (DJF 2000-01) and summer (JJA 2000). The comparison of the two scenarios is based on notched boxplots indicating roughly the 95% confidence interval for the median estimate, calculated as $m \pm 1.58 \times \frac{\text{interquartilerange}}{\sqrt{\text{sample}}}$ (Krzywinski & Altman, 2014; McGill et al., 1978). The use of notches is accurate for a large sample size. If the notches of two samples do not overlap, their medians differ significantly. In addition, we applied the non-parametric Wilcoxon-Mann-Whitney test to test the difference in the median of the two scenarios with a significance level of 95% (Wilks, 2005).

D.3.6 Analysis of extremes

For runoff extremes, the seasonal and yearly maxima of daily runoff of each GR4J-Cemaneige simulation were extracted for winter, summer, and the entire year (April 2000 – March 2001). This results in a vector of maxima per season/year comprised of one maximum per simulation. The maxima were then ranked to compute empirical return periods. This was done for each of the climate scenarios. The change in occurrence probability of maxima, expressed as a probability ratio (PR), was calculated to assess the influence of aGHG emissions on the runoff extremes. The PR is defined as

$$PR = \left(\frac{P_{\text{industrial}}}{P_{\text{non-industrial}}} \right) \quad (\text{D.1})$$

where $P_{\text{industrial}}/P_{\text{non-industrial}}$ represents the probability fraction of industrial to non-industrial maxima exceeding a given return-period threshold. A $PR > 1 (< 1)$ indicates an increase (decrease) in occurrence probability for the given threshold due to the emission of aGHGs. A non-parametric bootstrapping procedure was used to account for sampling uncertainty. For this, industrial simulations and non-industrial simulations were resampled 10'000 times (with replacement) for each return period considered, and the respective 5th-95th percentile confidence intervals were calculated.

D.4 Results

D.4.1 Comparison of climatological indices

The results for the six climatological indices (mean precipitation, wet day frequency, 90th percentile of the wet day distribution, snow day frequency, mean temperature, and number of frost days) are summarized in Figure D.2 for the Thur catchment, for raw and bias corrected simulations. The same figures for the other catchments and the different bias correction reference periods can be found in the Appendix (Figures D.6-D.9). Each panel shows a particular index for the entire year, as well as for the winter and summer, for the raw and the bias corrected (all five reference periods) ensembles of the industrial and the non-industrial scenario. Table D.4 summarizes differences in the ensemble median of the industrial and non-industrial scenario for the different indices and the five catchments. The annual cycle of the bias corrected and the raw ensemble median for different indices is exemplarily shown for the river Thur in the Appendix (Figure D.10).

The yearly mean precipitation under the industrial scenario differs from that under the non-industrial scenario. In most catchments and reference periods for the bias correction, the industrial scenario exhibits significantly higher yearly mean precipitation than the non-industrial scenario with median differences ranging between -0.2% and 8% (raw: -0.6% and +2.9%). Differences between the scenarios are larger and significant for seasonal mean precipitation: the industrial scenario shows significantly higher mean precipitation in winter between +6.8-17.5%

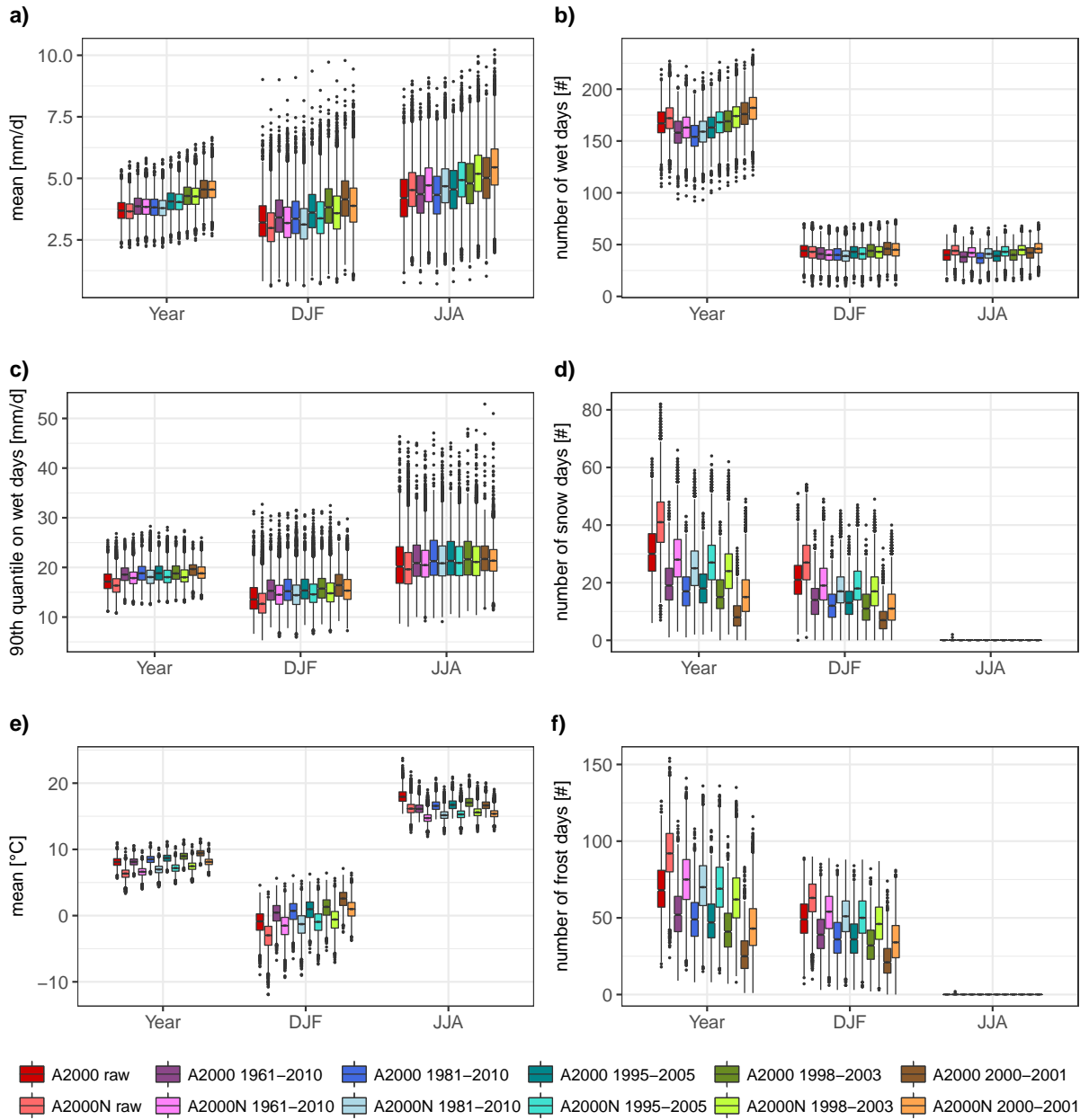


Figure D.2: Climate indices of the industrial scenario (darker hues) and the non-industrial scenario (lighter hues) for the river Thur, using bias corrected data and raw data for the entire year, winter (DJF), and summer (JJA). Shown are notched boxplots (95% confidence interval of the median) for mean precipitation (a), number of wet days (b), empirical 90th quantile of the daily precipitation distribution of wet days (c), number of snow days (d), mean temperature (e), and number of frost days (f).

(raw: +7.4-9.4%) and significantly lower mean precipitation in summer between -1.2-11.7% (raw: -2.7-11.5%). This seasonal pattern is also found in the annual cycle of the ensemble median, for mean precipitation of each day (Figure D.10). Although the differences between the industrial and the non-industrial scenario are larger for individual seasons, the spread between the ensem-

bles also increases for individual seasons.

The absolute number of wet days in the entire year and in summer is, in most catchments, significantly lower in the industrial scenario compared to the non-industrial scenario. In winter, the industrial ensemble median is significantly higher than in the non-industrial scenario. The bias correction decreases the absolute number of wet days in both scenarios in most catchments and reference periods.

Considering heavy precipitation on wet days (90th quantile of all wet days), precipitation totals under the industrial scenario are significantly higher than under the non-industrial scenario for the entire year. For all catchments and reference periods the differences range between +3.9-9.3% (raw: +4.5-5.3%). The heavy precipitation totals on wet days are also significantly higher in winter (bias corrected: +5-14.6%; raw: +6.4-8.3%). However, there is no agreement on the signal direction in summer heavy precipitation among the catchments.

Among the five catchments and the different reference periods for the bias correction, the industrial scenario ensemble contains significantly fewer snow days in the entire year and winter than the non-industrial scenario. The bias correction reduces the absolute number of snow days compared to the raw data for both scenarios in all catchments and reference periods.

The mean temperatures reflect the yearly pattern in Switzerland with lowest temperatures in winter and highest temperatures in summer. The industrial scenario exhibits significantly higher mean temperatures than the non-industrial scenario for the entire year as well as the other seasons. The differences in median range between 1.2-2.1°C depending on the catchment and the reference period (raw data: 1.6-2.3°C). The differences in temperatures also affect the potential evapotranspiration with higher evaporation rates in the industrial scenario than in the non-industrial scenario, particularly in the summer season (Figure D.10).

The absolute number of frost days is significantly lower in the industrial scenario compared to the non-industrial scenario. Furthermore, the bias correction reduces the number of frost days dramatically compared to the raw data in both scenarios and among all catchments and reference periods.

D.4.2 Comparison of the runoff regime

The comparison of runoff response of the river Thur between the industrial and the non-industrial scenario is depicted in Figure D.3, with mean runoff and extreme runoff (99th percentile of the distribution) as indices. Again, the runoff indices for the other catchments and the different reference periods for the bias correction can be found in the Appendix (Figures D.6-D.9), and median differences are shown in Table D.4.

Table D.4: Differences between the ensemble median of the industrial scenario and the ensemble median of the non-industrial scenario for different climatological and hydrological indices.

	Emme		Thur		Venoge		Verzasca		Vorderrhein		
	corr	raw	corr	raw	corr	raw	corr	raw	corr	raw	
Mean precipitation [%]	year	0.3-0.8	0.6	0.9	(-0.2)-1	(-0.6)	4.7-8	2.7	4.9-6.2	2.9	
	DJF	8-8.9	7.7	6.8-7.4	7.4	7.9-9.8	7.5	13.4-17.5	9.4	12.9-13.4	
	JJA	(-10.8)-(-11.2)	(-10)	(-7.4)-(-7.9)	(-7.1)	(-11.3)-(-11.7)	(-11.5)	(-2)-(-2.7)	(-3)	(-1.2)-(-2.6)	(-2.7)
Number of wet days [number of days]	year	(-5)-(-6)	(-6)	(-5)-(-6)	(-5)	(-6)-(-8)	(-9)	(-1)-1	(-4)	0-(-2)	(-4)
	DJF	1-2	2	1-2	1	0-1	1	2	1	1	1
	JJA	(-4)-(-5)	(-4)	(-4)-(-5)	4	(-4)-(-5)	(-5)	(-1)-(-2)	(-3)	(-1)-(-2)	(-2)
90 th quantile of precipitation at wetdays [%]	year	4.4-6	4.8	3.9-4.6	4.9	6.1-8.1	5.3	5.5-9	4.5	5.9-9.3	4.8
	DJF	5-6	6.4	5.4-7.2	7	7.1-10.4	6.5	8.8-12.8	8.3	5.6-14.6	8.3
	JJA	(-0.2)-(-0.9)	(-0.9)	1.6-2.6	2.9	3.1-3.8	1.3	(-0.5)-(-0.8)	(-0.2)	(-0.1)-(-1)	(-0.1)
Number of snow days [days]	year	(-7)-(-8)	(-10)	(-7)-(-9)	(-11)	(-3)-(-6)	(-13)	(-5)-(-9)	(-14)	(-9)-(-11)	(-13)
	DJF	(-5)	(-2)	(-4)-(-6)	(-6)	(-2)-(-4)	(-8)	(-3)-(-5)	0	(-3)-(-4)	(-1)
	JJA	0	0	0	0	0	0	0	(-2)	0	(-2)
Mean temperature [°C]	year	1.2-1.4	1.7	1.3-1.5	1.8	1.4-1.6	1.8	1.2-1.3	1.7	1.3-1.4	1.7
	DJF	1.5-1.8	2	1.6-2	2.1	1.7-2.1	2.2	1.4-1.5	1.6	1.4-1.6	1.6
	JJA	1.2-1.4	1.8	1.3-1.5	1.8	1.3-1.5	1.9	1.3-1.5	2.3	1.5-1.7	2.3
Number of frost days [days]	year	(-18)-(-22)	(-12)	(-18)-(-23)	(-24)	(-14)-(-22)	(-26)	(-21)-(-23)	(-22)	-23	(-21)
	DJF	(-13)-(-14)	(-8)	(-13)-(-15)	(-14)	(-12)-(-16)	(-16)	(-10)-(-11)	(-2)	(-7)-(-8)	(-2)
	JJA	0	0	0	0	0	0	0	0	0	0
Mean runoff [%]	year	(-1.4)-(-2.3)	2.2	(-1.4)-(-2.6)	0.9	(-1.3)-(-3.2)	3.3	8.5-11.9	4.8	5.1-5.9	3.1
	DJF	7.6-10.3	26.1	8.7-16.6	37.6	8-11.5	42.2	36-42	38.4	17.4-20.6	7.6
	JJA	(-16.3)-(-17.2)	(-17.2)	(-13.9)-(-14.4)	(-15.5)	(-16.7)-(-17.4)	(-19.3)	(-6.6)-(-7.3)	(-5)	(-0.9)-(-3.3)	1.7
99 th quantile of runoff [%]	year	1.9-3.4	6.3	1.2-2.1	2.2	4.6-9.7	11.9	7.5-14.8	2.1	4.3-6.2	4.7
	DJF	2.8-4.2	16	5.9-12.3	36.1	9.7-17.9	43.4	34.4-63.4	57	31.4-37.4	10.7
	JJA	(-12.7)-(-14.1)	(-13.6)	(-8.6)-(-9.2)	(-9.8)	(-9.6)-(-10.2)	(-10.4)	(-1.7)-(-2.5)	0.9	1.4-4.1	5.1

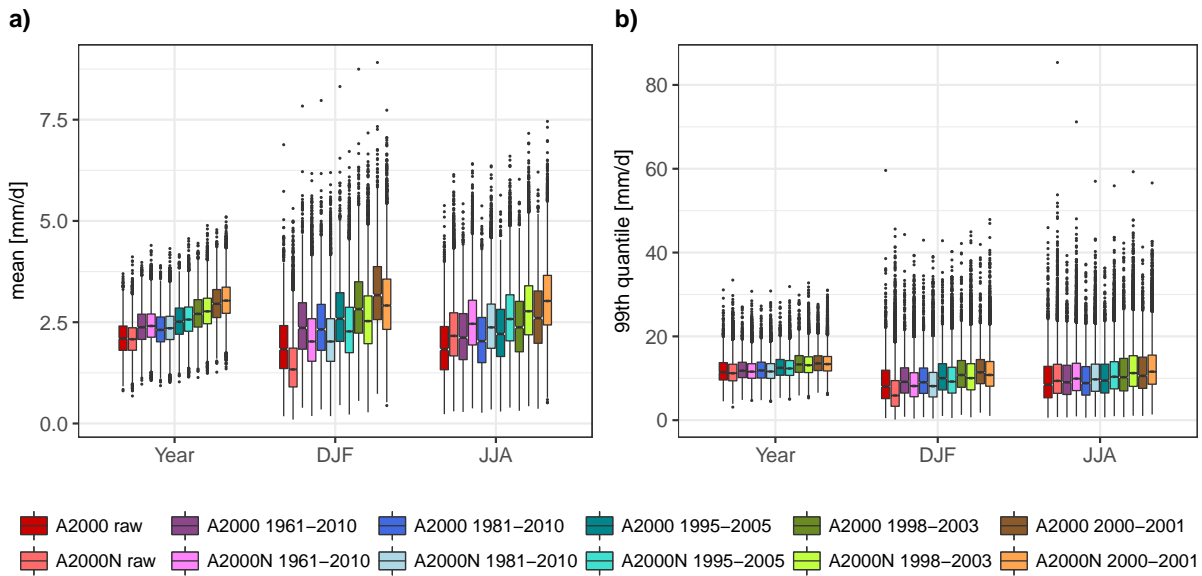


Figure D.3: Hydrological indices of the industrial (darker hues) and the non-industrial scenario (lighter hues) for the river Thur, using bias corrected data and raw data for the entire year, winter (DJF) and summer (JJA). Shown are notched boxplots (95% confidence interval of the median) for mean runoff (a) and the empirical 99th quantile of the daily runoff distribution (b).

The mean runoff of the rivers Emme, Thur, and Venoge for the entire year is lower by a small, but still significant, amount in the industrial scenario compared to non-industrial scenario for the bias corrected data (range -1.3% and -3.2%). Contrary to this, the raw simulations show significantly higher yearly mean runoff (+0.9-3.3%) in the industrial scenario compared to the non-industrial scenario. The Verzasca and the Vorderrhein show higher yearly mean runoff in the industrial scenario in both the bias corrected and the raw simulations (bias corrected: +5.1-11.9%; raw: 3.1-4.8%). The difference between the scenarios is more pronounced in the individual seasons with significantly higher winter mean runoff and significantly lower summer mean runoff in the industrial scenario. The increase in winter runoff in all catchments and for all reference periods of the bias correction ranges between +7.6% and +42% (raw: +7.6-42.2%), where the stronger increases are found in high altitude catchments (Verzasca and Vorderrhein). For summer, the decrease in mean runoff is between -0.9 and -17.4% (raw between -19.3% and +1.7%), with low altitude catchments showing the most pronounced decrease.

The 99th quantile of runoff serves as an indicator for high runoff events and follows a similar pattern as the mean runoff with higher winter and lower summer high runoff events in the industrial scenario compared to the non-industrial scenario. The median estimate for winter is +2.8-63.4% higher in the industrial scenario than in the non-industrial scenario for the bias corrected data (raw: +10.7-57%). Again, the high altitude catchments indicate a more pronounced increase than low altitude catchments. The median estimates for summer in the rivers

Emme, Thur, Venoge, and Verzasca decrease for bias corrected simulations by between -1.7% and -14.1% (raw: -13.6% and +0.9%). However, this pattern is not present in the Vorderrhein, where the summer extreme runoff increases by +1.4-4.1% (raw: 5.1%).

D.4.3 Sensitivity of the indices to the catchment and the bias correction reference period

A comparison of climatological and hydrological indices for the five different catchments show a strong agreement among the catchments (Figure D.4). Darker hues indicate significant differences as determined by the Wilcoxon-Mann test. Also, the sensitivity of the signal direction to the reference period used for the bias correction is small. The few exceptions are summarized in the following paragraph.

The yearly mean precipitation is, in most catchments, higher in the industrial simulations than in the non-industrial simulations, with the exception of the Venoge, which exhibits an insignificant lower yearly mean precipitation in the raw and the 2000-2001 bias corrected industrial simulations. The intense summer precipitation (90th percentile of wet days) is significantly higher in the industrial simulations for the Thur and the Venoge. The other catchments show non-significant lower values for the industrial simulations. Except for the Verzasca, the number of wet days per year is significantly higher in the non-industrial scenario than in the industrial scenario. There are also differences among the catchments and reference periods for the yearly mean runoff: the Verzasca and the Vorderrhein show significantly higher median estimates in the industrial scenario while the other catchments also show higher industrial medians for raw simulations but not for the bias corrected simulations. For the very high summer runoff events (99th percentile), the Vorderrhein shows higher values in the industrial scenario but the other catchments show lower medians. The Verzasca shows contrasting signals for the raw and the bias corrected 99th percentile of summer runoff. There are significant higher values in the industrial scenario for raw simulations but mostly insignificant lower values in the bias corrected simulations. However, most of these differences between the catchments and the bias correction reference periods occur in cases where the differences between the industrial and non-industrial scenario are anyway very small.

D.4.4 Extreme events

The aGHG related change in occurrence probability, PR, of yearly and seasonal maximum daily runoff is illustrated for the five catchments and for different return periods in Figure D.5, and for each time window (entire year, winter, summer). In general, the PR tends to increase with higher return periods, albeit with a corresponding increase in sampling uncertainty.

The raw simulations generally indicate higher aGHG influence on runoff than the bias corrected simulations, since raw PR values exceed bias corrected PR values for most return periods

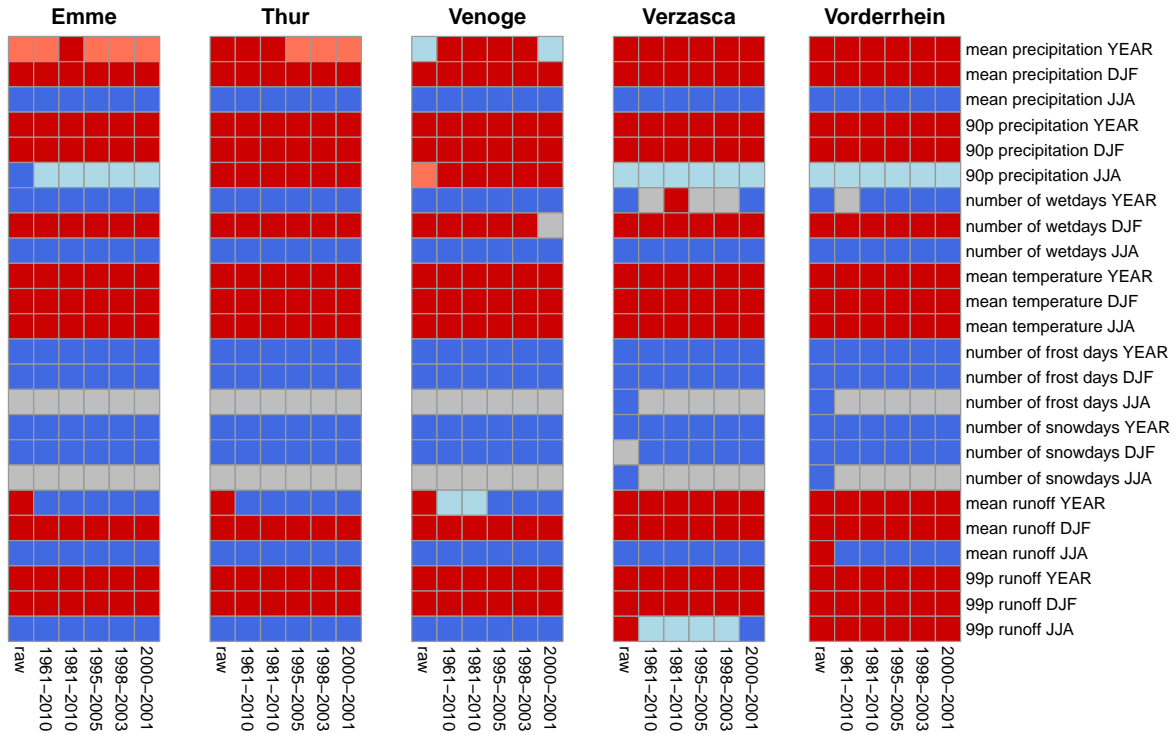


Figure D.4: Signal direction of differences in the ensemble median of the industrial and the non-industrial scenario for the five catchments. The columns of each panel show the results using different reference periods for the bias correction, or no bias correction (raw). The rows list different climatological or hydrological indices. The red hues indicate higher median values in the industrial scenario; the darker red hue indicates significant differences and the lighter red hue indicates non-significant differences. The blue hues indicate higher median values in the non-industrial scenario; the darker blue indicates significant differences and the lighter blue indicates non-significant differences. No differences in median (equal numbers) are marked in grey.

in all catchments and bias correction periods. The PR values vary strongly among the different catchments. For the entire year and winter, PR values are mostly larger than 1 for larger return periods with larger values in winter than for the entire year. An exception is the bias corrected PR of the river Emme with PR values smaller than 1 for large return periods. In summer, the PR values are again larger than 1 for large return periods for the Thur, the Verzasca, and the Vorderrhein. The Emme and the Venoge show summer PR values smaller than 1 for rare events, but the Venoge turns into PR values larger than 1 for very rare events. Overall, the PR values associated with the different reference periods for the bias correction vary in magnitude but not, in most catchments, in the sign of change (increase or decrease). However, the Emme exhibits contrasting signals in PR for the yearly and winter maximum runoffs between the bias corrected

and the raw simulations.

For events occurring on average less than once in 100 years, the uncertainties increase due to only a small number of simulations exceeding the threshold (less than 1% of all industrial simulations) and the PR often decreases or becomes unstable.

D.5 Discussion

The industrial and non-industrial scenarios were compared by analyzing six climatological indices and two runoff indices, for five catchments and five reference periods for the bias correction. The results for mean precipitation show increased precipitation in winter and decreased precipitation in summer, due to anthropogenic greenhouse gas emissions. This seasonal pattern of the response of precipitation to aGHG emissions agrees with the signal of future climate change projections for the end of the century in Switzerland (Frei et al., 2006; Fischer et al., 2012; Zubler et al., 2014) – albeit with a smaller magnitude than those future projections.

The results indicate an intensification of heavy precipitation due to aGHG emissions when looking at the wet day 90th percentiles of yearly and winter precipitation for all catchments. These findings agree with the results by Fischer and Knutti (2015) who found increasing human influence for more extreme precipitation. However, there is no clear signal in heavy precipitation on wet days in summer among the catchments. Further, the heavy precipitation on wet days show larger ranges in summer than the other periods indicating larger uncertainties in the climate simulations. One reason for these large uncertainties may be the representation of convective precipitation in summer in the GCM (Ban et al., 2014).

The temperature signal in the simulations with higher temperatures and lower number of frost days in the industrial scenario compared to the non-industrial scenario agrees with the last IPCC report, which concluded that it is very likely that more than half of the observed global warming is caused by increasing anthropogenic greenhouse gas emissions (Bindoff et al., 2013). Bias correcting the raw simulations leads to higher summer temperatures in the bias corrected data than in the raw data. Together with the generally higher temperatures this leads to a considerably lower number of frost days and snow days in the bias corrected simulations.

The comparison of runoff indices for the industrial and non-industrial scenarios indicated a shift in runoff regime towards higher winter mean runoff and lower summer mean runoff. The opposite signals of change in winter and summer seem to balance each other, and results in only little change in the yearly mean runoff. Projections of future runoff in Switzerland exhibit the same pattern with higher winter runoff and lower summer runoff due to climate change, but with more distinct signals than in our study (Köplin et al., 2012; Addor et al., 2014).

The differences in runoff response between the two scenarios can be explained by analyzing

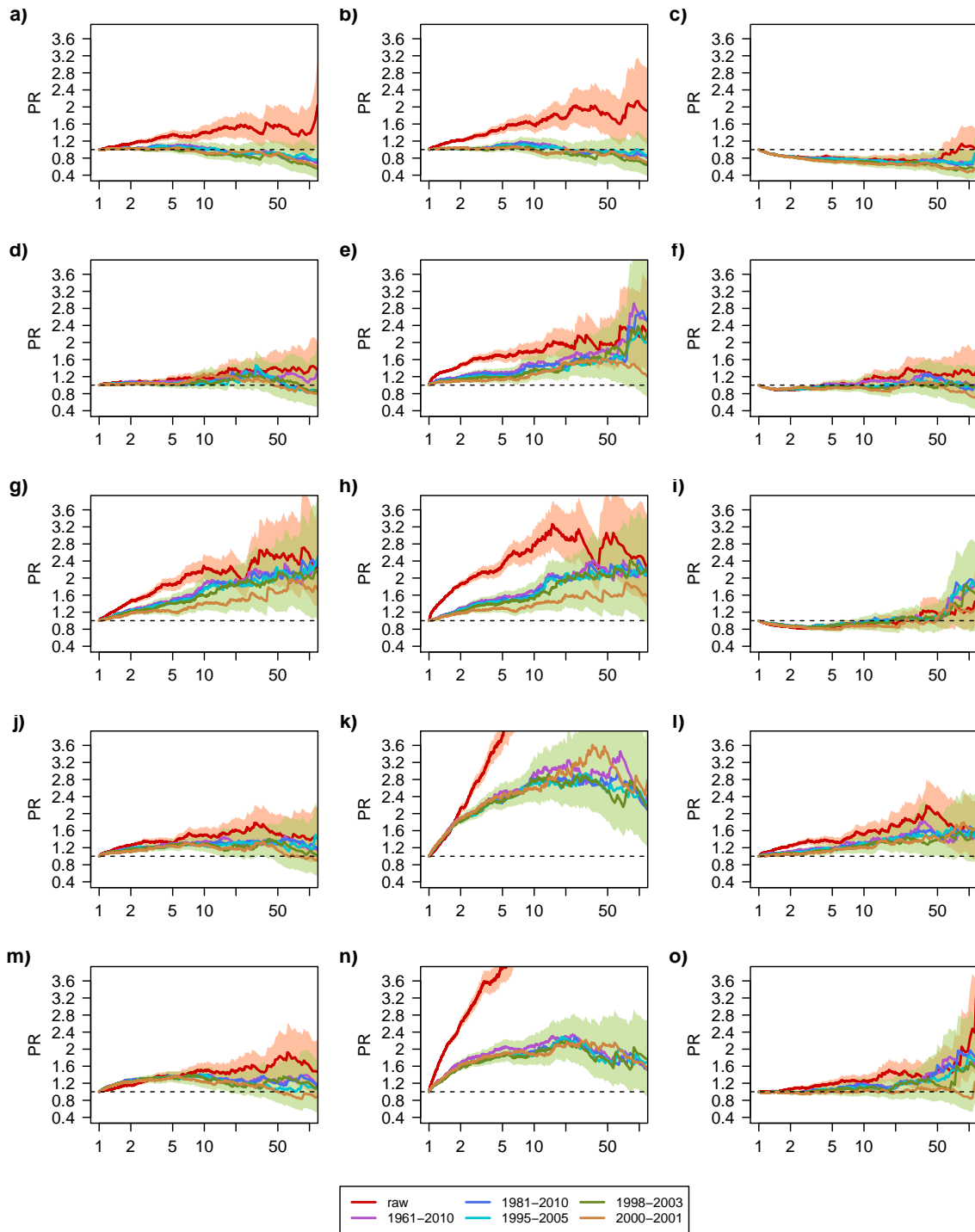


Figure D.5: Change in occurrence probability (PR) of daily runoff for the Emme (a-c), Thur (d-f), Venoge (g-i), Verzasca (j-l), and Vorderrhein (m-o) for the entire year (left panels), winter (DJF, middle panels), and summer (JJA, right panels). Shading indicates the maximum and minimum PR from resampling 10'000 times. Green shading includes the PR range over all reference periods used for the bias correction.

the climatological drivers influencing the runoff. In winter, the combination of higher mean precipitation, higher temperatures, and a lower frost and snow day frequency in the industrial scenario leads to less snow accumulation and enhanced snow melt, which results in higher winter mean runoff. In summer, the combination of lower mean precipitation and increased potential evapotranspiration due to higher temperatures leads to a deficit in the water balance causing lower mean runoff in the industrial scenario.

The shift towards higher winter runoff and lower summer runoff, but only little or insignificant change in runoff across the year, was observed in the last century in Switzerland (Birsan et al., 2005; Stahl et al., 2010; Hänggi & Weingartner, 2011). Although the observed changes cannot be fully attributed to aGHG emissions due to the additional signal of natural variability in the observations, the agreement in pattern between the observed changes and the changes found in this study point to the important role of aGHG emissions.

A strong agreement in signal of the climatological and hydrological indices was found among the five catchments. The climate change signals differ in terms of absolute values between the industrial and non-industrial scenarios, but in most cases not in the signal direction. Also, the choice of the reference period for the bias correction primarily influences the magnitude of the climate change signal but not its direction. The few exceptions with disagreement among the catchments or the bias correction reference periods occur mostly in cases where the climate change signals are small.

Regarding extreme events, the aGHG related change in occurrence probability, PR, tends to increase with higher return periods up to return periods of approximately 20 years in most catchments (except in the Emme catchment). For higher return periods the uncertainty becomes large and no general patterns emerge across all catchments. Increasing human influence with higher thresholds was also found for temperature and precipitation extremes by Fischer and Knutti (2015) and is projected to increase further and nonlinearly with global warming. Kay et al. (2011) also found increasing human influence with higher return periods for flood occurrence in autumn 2000 in England and Wales due to aGHG emissions.

The PR shows much larger values in winter than in summer due to the complex interplay of temperature, precipitation and snow processes. With the exception of the Emme, the PR in winter extreme runoff is positive and increases with higher return periods. In some catchments, the PR exceeds 2. In summer, the signal direction of PR varies among the catchments.

The PR is larger in the raw data than in the bias corrected data and this difference is most pronounced in winter due to the above mentioned snow processes. The overestimation of the PR found for the raw data is in agreement with the theoretical considerations of Bellprat and Doblas-Reyes (2016), who show that raw GCM simulations are prone to overestimate human

influence. The signal direction and the magnitude of PR differs among the catchments, which is due to different processes governing the catchments and their runoff.

The choice of reference period for the bias correction does not influence the signal direction in most cases but does influence the magnitude of the different indices and the PR. However, the differences among the reference periods are very small compared to the difference between the raw and bias corrected data, regardless of their reference period. Despite the robust climate change signals among the different catchments and bias correction reference periods, there exist different sources of uncertainty.

First, we examine the effect of aGHG emissions specifically for year 2000/01 conditions. Thus, our results may not be entirely applicable to other years that experienced exceptionally extreme situations, such as the summer heat waves of 2003 and 2018. In those two particular cases, soil moisture conditions were very extreme over Europe, and land-atmosphere feedbacks might have influenced the outcome. However, we note that the aGHG change signals we find for precipitation and temperature are both in agreement with observational studies, and with modelling experiments looking further into the future – which points to the general robustness of the findings.

Second, the use of AMIP-style global climate simulations implies that aspects of internal climate variability related to atmosphere-ocean interactions are only partially covered. Shaw and Voigt (2015) identify a circulation response both to the direct radiative forcing in the atmosphere and to SSTs during summertime. Fischer et al. (2018) found that simulations with prescribed SSTs are biased with respect to temperature extremes – albeit far more in the tropics than in central Europe. Hence by fixing the SSTs to observed values only a part of the full variability is captured. Simulations with a fully coupled model would be needed to capture the full variability. Thus, our results are valid conditional on the given observed SST conditions. However, we note that for the weather conditions dominating western/central Europe, at least for autumn-winter 2000/01, atmosphere-ocean interactions are not thought to be a major factor as instead a large-scale atmospheric ‘Scandinavia’ blocking pattern was present, as described in Pall et al. (2011). Furthermore, the use of only four non-industrial SST scenarios may underestimate the uncertainty in the true non-industrial SST conditions – but we note that these four sets of SSTs, and their uncertainties, were at least rigorously estimated using an optimal fingerprinting technique (Pall et al., 2011).

Third, the assumption of a stationary bias in both climate change scenarios is highly debated and cannot be fully assessed. To overcome this problem, this study considered the results of both bias corrected and raw data.

Fourth, the choice of the hydrological model and its calibration also introduce uncertainty.

A lumped model describes the catchment as a single entity with spatially averaged input data but does not resolve physical processes and different land use types within the catchments (Yu, 2002). Also, the calibration of the model has a substantial influence on the simulations. However, the performance in the validation period is very satisfactory.

Fifth, uncertainty arises from the fact that we only used one hydrological model and one bias correction method – as it has been proven that both steps in the modelling chain result in partly strong uncertainties (Wilby & Dessai, 2010; Addor et al., 2014; Rössler et al., 2019). An outcome of these and similar studies has been that the uncertainty introduced by the GCMs or emission scenarios are superior. However, in climate attribution studies the signal stemming from the GCMs is much smaller. Hence, the uncertainty the selection of a certain hydrological model or downscaling method introduces should be newly assessed. This is beyond the focus of this study, but a highly interesting topic.

Lastly, such a multi-step attribution study is based on many methodological choices, such as quantile mapping for the bias correction, using GR4J as a hydrological model, and using the simulations by Pall et al. (2011) that are based on one GCM. All these choices introduce uncertainties and limitations. Further studies would be needed to systematically address all these uncertainties.

D.6 Summary & Conclusions

Thousands of GCM simulations for a year 2000/01 climate, under both industrial and non-industrial scenarios (i.e., with and without aGHG emissions), were bias corrected using non-parametric empirical quantile mapping. The GCM data were subsequently fed into a hydrological model to investigate runoff changes in five Swiss catchments covering different catchment characteristics and hydrological regime types.

Changes in mean temperature, mean precipitation, and mean runoff of the rivers in all catchments are detectable between the scenarios, and hence attributable to aGHG. A shift in the runoff regime towards higher winter mean runoff and lower summer mean runoff due to aGHG emissions is apparent and significant. In winter, the increase in mean runoff can be explained by the combination of increased mean winter precipitation and higher temperatures, leading to more rainfall and less snowfall and hence less snow accumulation. In summer, higher temperatures enhance potential evapotranspiration and, combined with decreased mean summer precipitation, result in lower mean runoff. This shift in runoff regime and the changes in temperature and precipitation are in agreement with observed changes in the past, and with future climate change projections in terms of climate change signal direction.

A strong agreement among the five catchments and different reference periods used for the

bias correction was found for climatological and hydrological indices. The different catchments agree in terms of change signal direction between the bias corrected and raw simulations, but do not agree on the magnitude.

The assessment of the influence of aGHG emissions on extreme runoff events shows that yearly and winter extreme events are in most catchments more frequent in the industrial climate compared to the non-industrial climate. The difference increases with higher return-period thresholds indicating stronger influence of aGHG emissions on rare events in most catchments. The influence is strongest in the winter season and is less pronounced in the bias corrected data than in the raw data. The considerable changes in winter runoff highlight the importance of the interplay between temperature, precipitation, and resulting snow melt and accumulation. Overall, the magnitude of the attributed changes in runoff extremes depends on the return period, the season, and on whether the data is bias corrected or not.

The notable difference between the bias corrected and raw data, when examining changes in occurrence probabilities of runoff, indicates an overestimation of the influence of aGHG emissions when using raw data. Hence, our results are in agreement with the theoretical considerations of Bellprat and Doblas-Reyes (2016), Jeon et al. (2016) and Sippel et al. (2016). These findings highlight the need for bias correction approaches in future multi-step attribution studies, but related uncertainties due to the underlying assumptions as discussed by Teng et al. (2015) exist. A transparent display of the effect of the bias correction on the results is recommended, especially if sensitive dependencies between variables such as runoff, precipitation and temperature exist.

D.7 Acknowledgements

We would like to thank two anonymous reviewers who contributed to improve structure and content of the paper. The authors thank all members of the public who generated climate model simulations as part of the climateprediction.net Seasonal Attribution Experiment. The climate model data can be requested from Pardeep Pall. The observational data were provided by the Swiss Federal Office of Meteorology and Climatology, MeteoSwiss, and the Swiss Federal Office for the Environment and can be accessed for scientific purposes. We would also like to thank Nathalie Schaller for her help in dealing with PR and its uncertainty, as well as Philippe Naveau and Simon Schick for their support with statistical questions, and Daithi Stone for useful discussions.

D.8 References Appendix D

Addor N., Rössler O., Köplin N., Huss M., Weingartner R. & Seibert J. (2014). Robust changes and sources of uncertainty in the projected hydrological regimes of Swiss catchments. *Water*

Resour. Res., 50: 7541-7562. <https://doi.org/10.1002/2014WR015549>

Aschwanden H. & Weingartner R. (1992). Abflussregimes als Grundlage zur Abschätzung von Mittelwerten des Abflusses. Hydrologischer Atlas der Schweiz, Tafel 5.2.

Ban N., Schmidli J. & Schär C. (2015). Heavy precipitation in a changing climate: Does short-term summer precipitation increase faster? *Geophys. Res. Lett.*, 42: 1165-1172. <https://doi.org/10.1002/2014GL062588>

Bellprat O. & Doblas-Reyes F. (2016). Attribution of extreme weather and climate events overestimated by unreliable climate simulations. *Geophys. Res. Lett.*, 43: 2158-2164. <https://doi.org/10.1002/2015GL067189>

Bindoff N. L., Stott P. A., AchutaRao K. M., Allen M. R., Gillet N., Gutzler D.,... & Zhang X. (2013). Detection and Attribution of Climate Change: from Global to Regional. *Climate Change 2013: The Physical Science Basis. Contribution of Working Group I to the Fifth Assessment Report of the Intergovernmental Panel on Climate Change*, ed. T. F. Stocker et al. (Cambridge University Press, Cambridge, United Kingdom and New York, NY, USA)

Birsan M. V., Molnar P., Burlando P. & Pfaundler M. (2005). Streamflow trends in Switzerland. *J. Hydrol.*, 314: 312-329. <https://doi.org/10.1016/j.jhydrol.2005.06.008>

Boé J., Terray L., Habets F. & Martin E. (2007). Statistical and dynamical downscaling of the Seine basin climate for hydro-meteorological studies. *Int. J. Climatol.*, 27: 1643-1655. <https://doi.org/10.1002/joc.1602>

Christensen J. H., Boberg F., Christensen O. B. & Lucas-Picher P. (2008). On the need for bias correction of regional climate change projections of temperature and precipitation. *Geophys. Res. Lett.*, 35. <https://doi.org/10.1029/2008GL035694>

Ehret U., Zehe E., Wulfmeyer V., Warrach-Sagi K. & Liebert J. (2012). HESS Opinions “Should we apply bias correction to global and regional climate model data?” *Hydrol. Earth Syst. Sci.*, 16: 3391-3404. <https://doi.org/10.5194/hess-16-3391-2012>

Fischer A. M., Weigel A. P., Buser C. M., Knutti R., Künsch H. R., Liniger M.,... & Appenzeller C. (2012). Climate change projections for Switzerland based on a Bayesian multi-model approach. *Int. J. Climatol.*, 32: 2348-2371. <https://doi.org/10.1002/joc.3396>

Fischer E. M., Beyerle U., Schleussner C. F., King A. D. & Knutti R. (2018). Biased Estimates of Changes in Climate Extremes from Prescribed SST Simulations. *Geophys. Res. Lett.*,

45: 8500-8509. <https://doi.org/10.1029/2018GL079176>

Fischer E. M. & Knutti R. (2015). Anthropogenic contribution to global occurrence of heavy-precipitation and high-temperature extremes. *Nat. Clim. Change*, 5: 560–564. <https://doi.org/10.1038/nclimate2617>

Frei C. & Schär C. (1998). A precipitation climatology of the Alps from high-resolution rain-gauge observations. *Int. J. Climatol.*, 18: 873–900. [https://doi.org/10.1002/\(SICI\)1097-0088\(19980630\)18:8<873::AID-JOC255>3.0.CO;2-9](https://doi.org/10.1002/(SICI)1097-0088(19980630)18:8<873::AID-JOC255>3.0.CO;2-9)

Frei C., Schöll R., Fukutome S., Schmidli J. & Vidale P. L. (2006). Future change of precipitation extremes in Europe: Intercomparison of scenarios from regional climate models. *J. Geophys. Res.*, 111. <https://doi.org/10.1029/2005JD005965>

Gillett N. P., Allan R. J. & Ansell T. J. (2005). Detection of external influence on sea level pressure with a multi-model ensemble. *Geophys. Res. Lett.*, 32. <https://doi.org/10.1029/2005GL023640>

Gudmundsson L., Bremnes J. B., Haugen J. E. & Engen-Skaugen T. (2012). Technical Note: Downscaling RCM precipitation to the station scale using statistical transformations - a comparison of methods. *Hydrol. Earth Syst. Sci.*, 16: 3383–3390. <https://doi.org/10.5194/hess-16-3383-2012>

Hagemann S., Chen C., Haerter J. O., Heinke J., Gerten D. & Piani C. (2011). Impact of a statistical bias correction on the projected hydrological changes obtained from three GCMs and two hydrology models. *J. Hydrometeor.*, 12: 556–578. <https://doi.org/10.1175/2011JHM1336.1>

Hamon W. R. (1961). Estimating potential evaporation. *J. Hydr. Eng. Div-Asce*, 87: 107–120. Hänggi P. & Weingartner R. (2011). Inter-annual variability of runoff and climate within the Upper Rhine River basin, 1808-2007. *Hydrolog. Sci. J.*, 56: 34-50. <https://doi.org/10.1080/02626667.2010.536549>

Hegerl G. C., Hoegh-Guldberg O., Casassa G., Hoerling M. P., Kovats R. S., Parmesan C,... & Stott P. A. (2010). Good practice guidance paper on detection and attribution related to anthropogenic climate change. Meeting Report of the Intergovernmental Panel on Climate Change Expert Meeting on Detection and Attribution of Anthropogenic Climate Change (Geneva, Switzerland, 14-16 September 2009) (IPCC Work. Group I Tech. Support Unit, University of Bern) ed. T. F. Stocker et al. (Bern, Switzerland) pp 1–8

Hewitson B. C., Daron J., Crane R. G., Zermoglio M. F., & Jack C. (2014). Interrogat-

ing empirical-statistical downscaling. *Clim. Change*, 122: 539-443. <https://doi.org/10.1007/s10584-013-1021-z>

Ivanov M. A. & Kotlarski S. (2017). Assessing distribution-based climate model bias correction methods over an alpine domain: added value and limitations. *Int. J. Climatol.*, 37: 2633–2653. <https://doi.org/10.1002/joc.4870>

Jeon S., Paciorek C. J. & Wehner M. F. (2016). Quantile-based bias correction and uncertainty quantification of extreme event attribution statements. *Weather Climate Extremes*, 12: 24-32. <https://doi.org/10.1016/j.wace.2016.02.001>

Kay A. L., Crooks S. M., Pall P. & Stone D. A. (2011). Attribution of Autumn/Winter 2000 flood risk in England to anthropogenic climate change: A catchment-based study. *J. Hydrol.*, 406: 97–112. <https://doi.org/10.1016/j.jhydrol.2011.06.006>

Köplin N., Schädler B., Viviroli D. & Weingartner R. (2012). Relating climate change signals and physiographic catchment properties to clustered hydrological response types. *Hydrol. Earth Syst. Sci.*, 16: 2267–2283. <https://doi.org/10.5194/hess-16-2267-2012>

Krzywinski M. & Altman N. (2014). Points of significance: visualizing samples with box plots. *Nat. Methods*, 11: 119–120

Maraun D., Wetterhall F., Ireson A. M., Chandler R. E., Kendon E. J., Widmann M.,... & Thiele-Eich I. (2010). Precipitation downscaling under climate change. Recent developments to bridge the gap between dynamical models and the end user. *Rev. Geophys.*, 48. <https://doi.org/10.1029/2009RG000314>

Maraun D. (2013). Bias correction, quantile mapping, and downscaling: revisiting the inflation issue. *J. Climate*, 26: 2137-2143. <https://doi.org/10.1175/JCLI-D-12-00821.1>

McGill R., Tukey J. W. & Larsen W. A. (1978). Variations of box plots. *Am. Stat.*, 32: 12–16

MeteoSwiss (2013a). Daily mean, minimum and maximum temperature: TabsD, TminD, TmaxD. Accessed 06/15/2016, http://www.meteoschweiz.admin.ch/content/dam/meteoswiss/de/service-und-publikationen/produkt/raeumliche-daten-temperatur/doc/ProdDoc_TabsD.pdf

MeteoSwiss (2013b). Daily Precipitation (final analysis): RhiresD. Accessed 06/15/2016, http://www.meteoswiss.admin.ch/content/dam/meteoswiss/de/service-und-publikationen/produkt/raeumliche-daten-niederschlag/doc/ProdDoc_RhiresD.pdf

Min S. K., Zhang X., Zwiers F. W. & Agnew T. (2008). Human influence on Arctic sea ice detectable from early 1990s onwards. *Geophys. Res. Lett.*, 35. <https://doi.org/10.1029/2008GL035725>

Moriasi D. N., Arnold J. G., Van Liew M. W., Bingner R. L., Harmel R. D. & Veith T. (2007). Model evaluation guidelines for systematic quantification of accuracy in watershed simulations. *T. ASABE*, 50: 885–900.

Oudin L., Hervieu F., Michel C., Perrin C., Andréassian V., Anctil F. & Loumagne C. (2005). Which potential evapotranspiration input for a lumped rainfall-runoff model?: Part 2 - Towards a simple and efficient potential evapotranspiration model for rainfall-runoff modelling. *J. Hydrol.*, 303: 290–306. <https://doi.org/10.1016/j.jhydrol.2004.08.026>

Otto F. E. L., Massey N., van Oldenborgh G. J., Jones R. G. & Allen M. R. (2012). Reconciling two approaches to attribution of the 2010 Russian heat wave. *Geophys. Res. Lett.*, 39. <https://doi.org/10.1029/2011GL050422>

Pall P., Aina T., Stone D. A., Stott P. A., Nozawa T., Hilberts A. G. J., . . . & Allen M. R. (2011). Anthropogenic greenhouse gas contribution to flood risk in England and Wales in Autumn 2000. *Nature*, 470: 382–385. <https://doi.org/10.1038/nature09762>

Perrin C., Michel C. & Andréassian V. (2003). Improvement of a parsimonious model for streamflow simulation. *J. Hydrol.*, 279: 275–289. [https://doi.org/10.1016/S0022-1694\(03\)00225-7](https://doi.org/10.1016/S0022-1694(03)00225-7)

Pope V. & Stratton R. (2002). The processes governing horizontal resolution sensitivity in a climate model. *Clim. Dynam.*, 19: 211–236. <https://doi.org/10.1007/s00382-001-0222-8>

Rössler O., Kotlarski S., Fischer A. M., Keller D., Liniger M. & Weingartner R. (2019). Evaluating the added value of the new Swiss climate scenarios for hydrology: An example from the Thur catchment. *Climate Services*, 13. <https://doi.org/10.1016/j.cliser.2019.01.001>

Schaller N., Kay A. L., Lamb R., Massey N. R., van Oldenborgh G. J., Otto F. E. L., . . . & Allen M. R. (2016). Human influence on climate in the 2014 southern England winter floods and their impacts. *Nat. Clim. Change*, 6: 627–634. <https://doi.org/10.1038/nclimate2927>

Sharma D., Gupta A. D. & Babel M. S. (2007). Spatial disaggregation of bias-corrected GCM precipitation for improved hydrologic simulation: Ping River Basin, Thailand. *Hydrol. Earth Syst. Sci. Discussions*, 11: 1373–1390. <https://doi.org/10.5194/hess-11-1373-2007>

Shaw T. A. & Voigt A. (2015). Tug of war on summertime circulation between radiative forcing and sea surface warming. *Nature Geoscience*, 8:560-566. <http://dx.doi.org/10.1038/ngeo2449>

Sippel S., Otto F. E. L., Forkel M., Allen M. R., Guillod B. P., Heimann M.,... & Mahecha M. D. (2016). A novel bias correction methodology for climate impact simulations. *Earth Syst. Dyn.*, 7: 71–88. <https://doi.org/10.5194/esd-7-71-2016>

Stahl K., Hisdal H., Hannaford J., Tallaksen L. M., van Lanen H. A. J., Sauquet E.,... & Jodar J. (2010). Streamflow trends in Europe: evidence from a dataset of near-natural catchments. *Hydrol. Earth Syst. Sci.*, 14: 2367-2382. <https://doi.org/10.5194/hess-14-2367-2010>

Stott P. A., Stone D. A. & Allen M. R. (2004). Human contribution to the European heat-wave of 2003. *Nature*, 432: 610–614. <https://doi.org/10.1038/nature03089>

Teng J., Potter N. J., Chiew F. H. S., Zhang L., Wang B., Vaze J. & Evans J. P. (2015). How does bias correction of regional climate model precipitation affect modelled runoff? *Hydrol. Earth Syst. Sci.*, 19: 711–728. <https://doi.org/10.5194/hess-19-711-2015>

Teutschbein C. & Seibert J. (2012). Bias correction of regional climate model simulations for hydrological climate-change impact studies: Review and evaluation of different methods. *J. Hydrol.*, 456: 12–29. <https://doi.org/10.1016/j.jhydrol.2012.05.052>

Themeßl J. M., Gobiet A. & Leuprecht A. (2011). Empirical-statistical downscaling and error correction of daily precipitation from regional climate models. *Int. J. Climatol.*, 31: 1530–1544. <https://doi.org/10.1002/joc.2168>

Valéry A. (2010). Modélisation précipitations-débit sous influence nivale. Elaboration d'un module neige et évaluation sur 380 bassins versants. PhD thesis, Cemagref-AgroParisTech, Antony & Paris, France.

Valéry A., Andréassian V. & Perrin C. (2014). “As simple as possible but not simpler”: What is useful in a temperature-based snow-accounting routine? Part 2 - Sensitivity analysis of the Cemaneige snow accounting routine on 380 catchments. *J. Hydrol.*, 517: 1176–1187. <https://doi.org/10.1016/j.jhydrol.2014.04.058>

Wilby, R. L. & Dessai S. (2010). Robust adaptation to climate change. *Weather* 65: 180-185. Wilks, D. S. (1995). *Statistical methods in the atmospheric sciences: An introduction*. San Diego: Academic Press.

Willett K. M., Gillett N. P., Jones P. D. & Thorne P. W. (2007). Attribution of observed surface humidity changes to human influence. *Nature*, 449: 710–712. <https://doi.org/10.1038/nature06207>

Wolski P., Stone D. A., Tadross M., Wehner M. & Hewitson B. (2014). Attribution of floods in the Okavango basin, Southern Africa. *J. Hydrol.*, 511: 350-358. <https://doi.org/10.1016/j.jhydrol.2014.01.055>

Yu, Z. (2002). Hydrology: modeling and prediction. In North, G., Pyle, J., and Zhang, F., editors, *Encyclopedia of Atmospheric Science*, 3,172.

Zhang X., Zwiers F. W., Hegerl G. C., Lambert F. H., Gillett N. P., Solomon S., Stott P. A. & Nozawa T. 2007. Detection of human influence on twentieth-century precipitation trends. *Nature*, 448: 461–465. <https://doi.org/10.1038/nature06025>

Zubler E. M., Fischer A. M., Liniger M. A., Croci-Maspoli M., Scherrer S. C. & Appenzeller C. (2014). Localized climate change scenarios of mean temperature and precipitation over Switzerland. *Climatic Change*, 125: 237-252. <https://doi.org/10.1007/s10584-014-1144-x>

D.9 Appendix to Appendix D

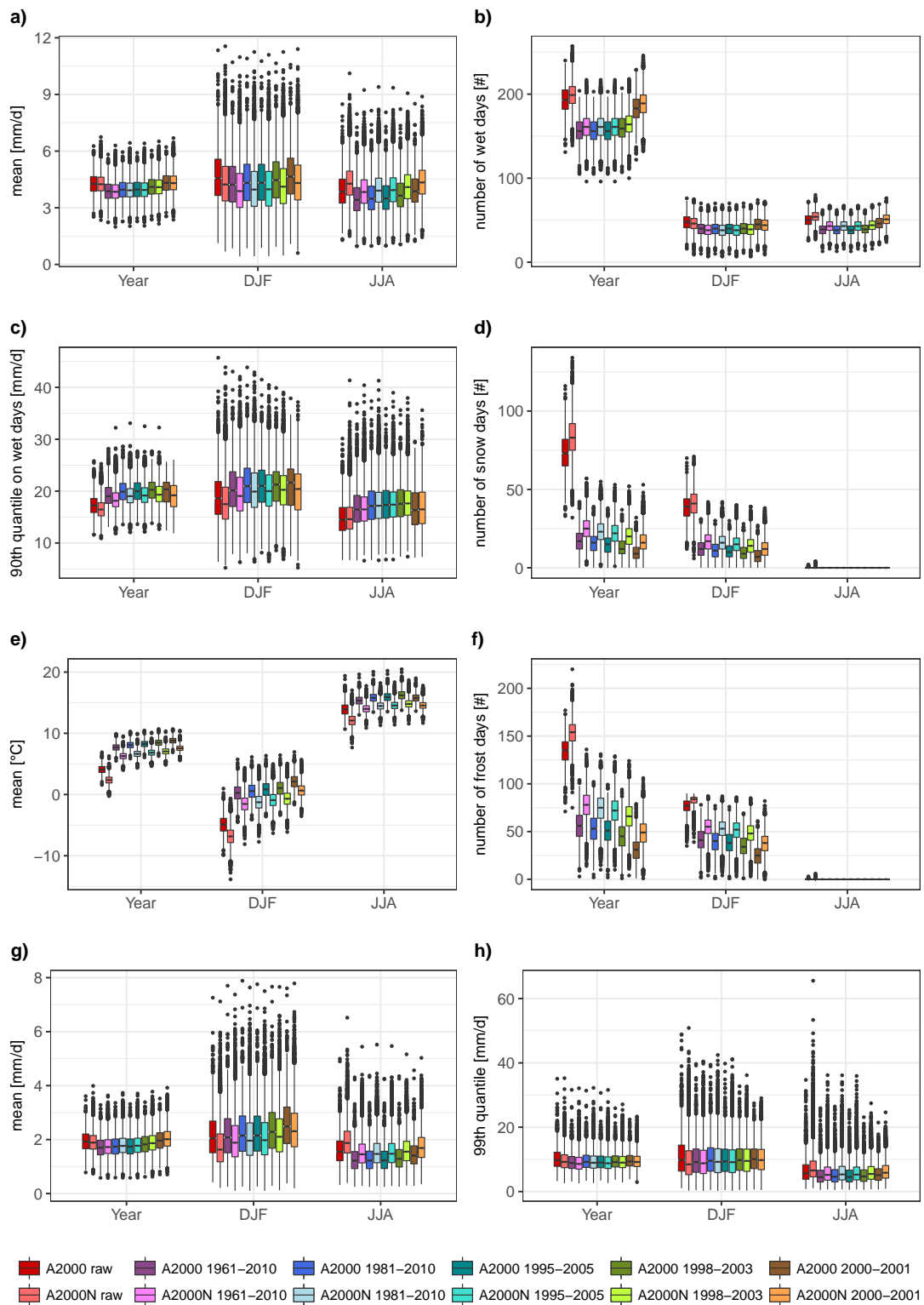


Figure D.6: Climatological and hydrological indices for the river Emme using raw data (red) and bias corrected data (other hues) with darker hues for the industrial scenario and lighter hues for the non-industrial scenario.

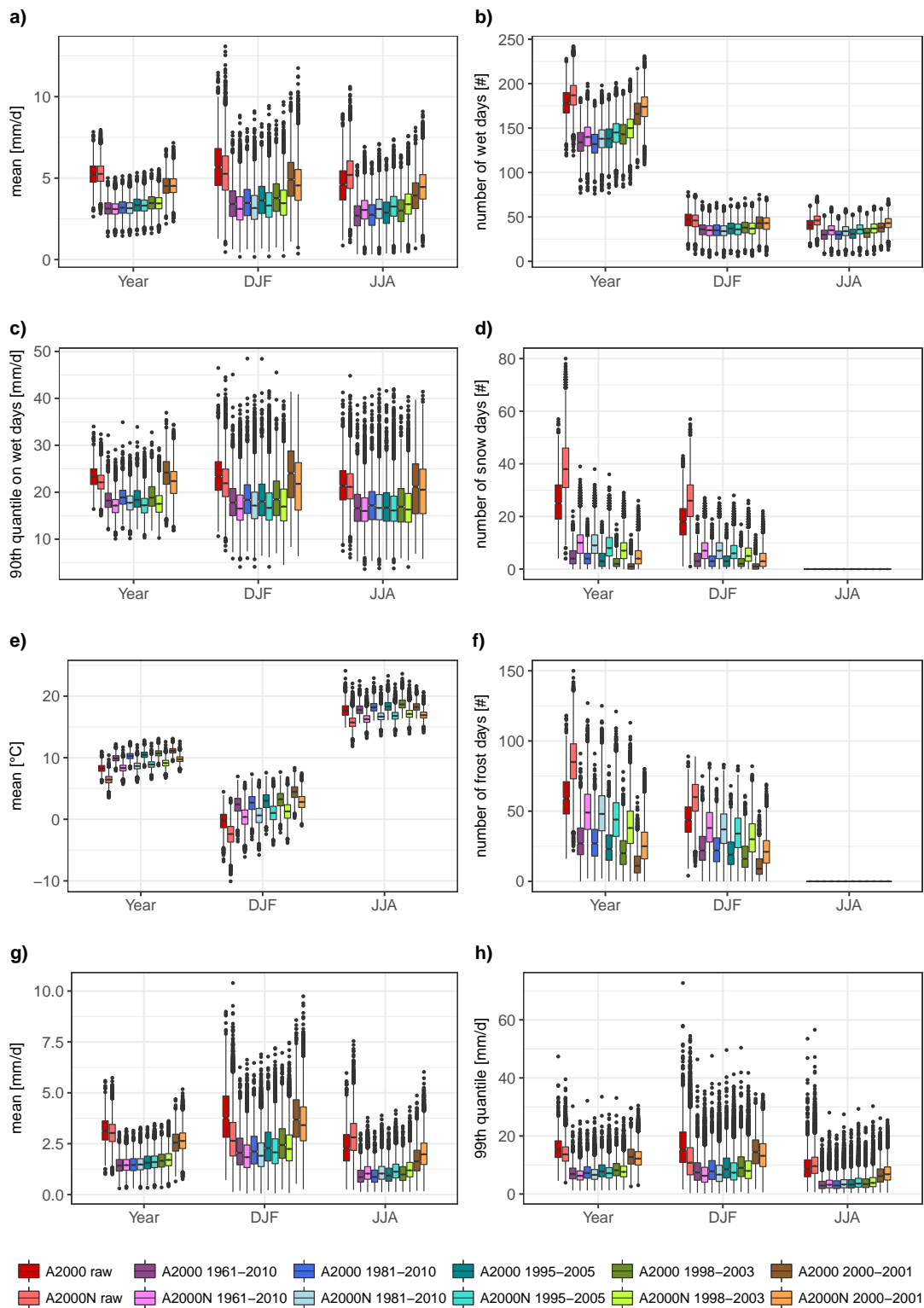


Figure D.7: Climatological and hydrological indices for the river Venoge using raw data (red) and bias corrected data (other hues) with darker hues for the industrial scenario and lighter hues for the non-industrial scenario.

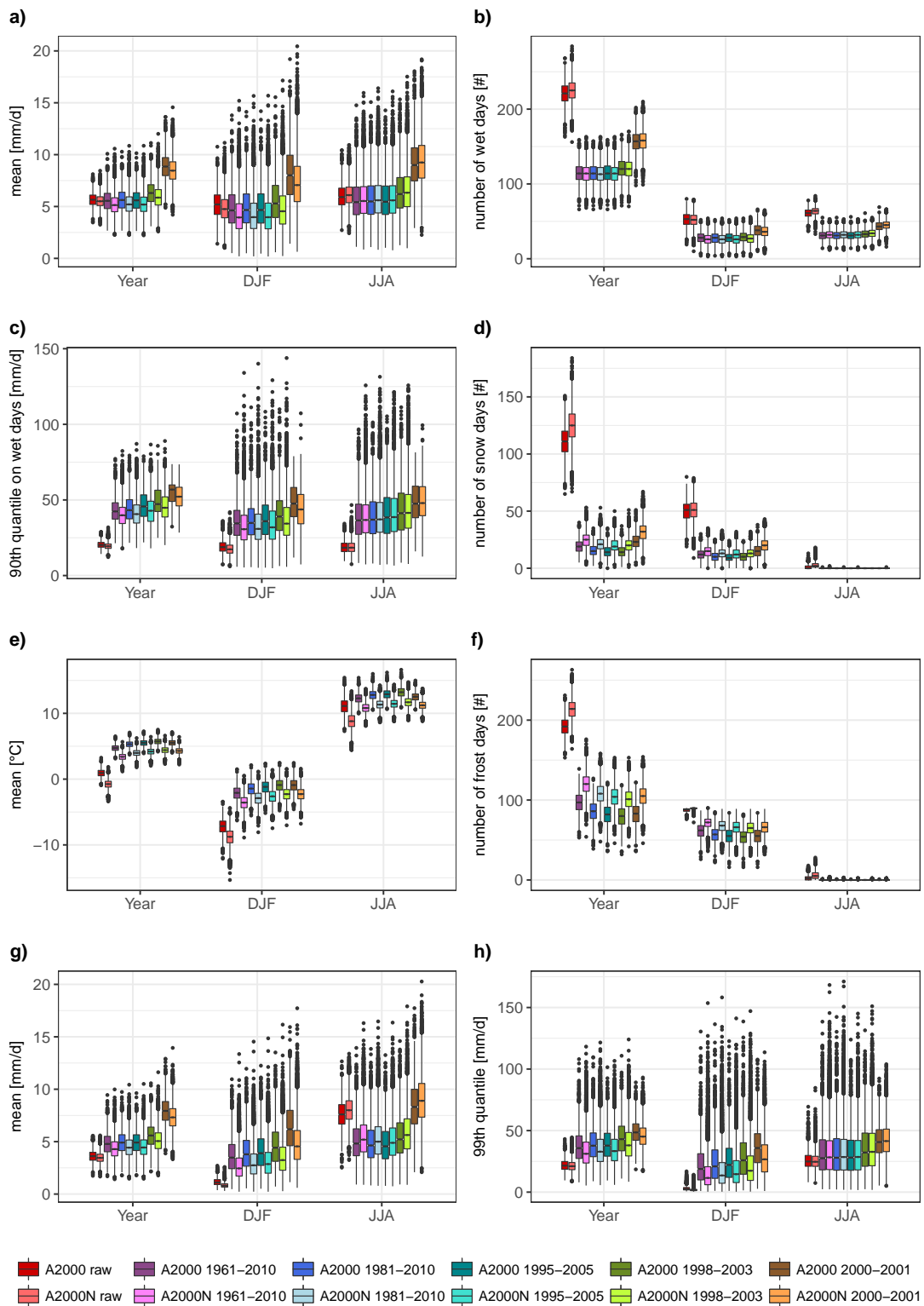


Figure D.8: Climatological and hydrological indices for the river Verzasca using raw data (red) and bias corrected data (other hues) with darker hues for the industrial scenario and lighter hues for the non-industrial scenario.

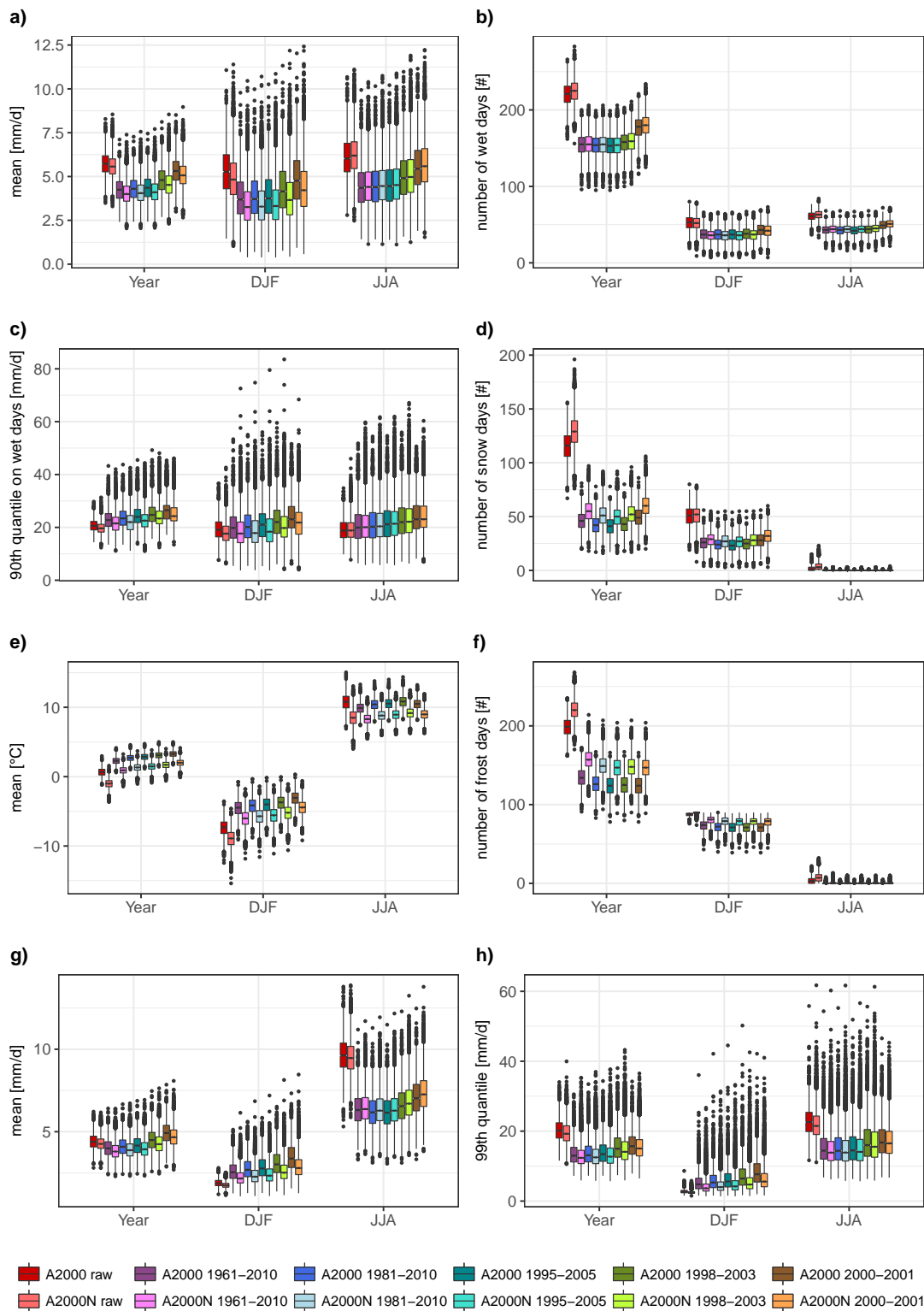


Figure D.9: Climatological and hydrological indices for the river Vorderrhein using raw data (red) and bias corrected data (other hues) with darker hues for the industrial scenario and lighter hues for the non-industrial scenario.

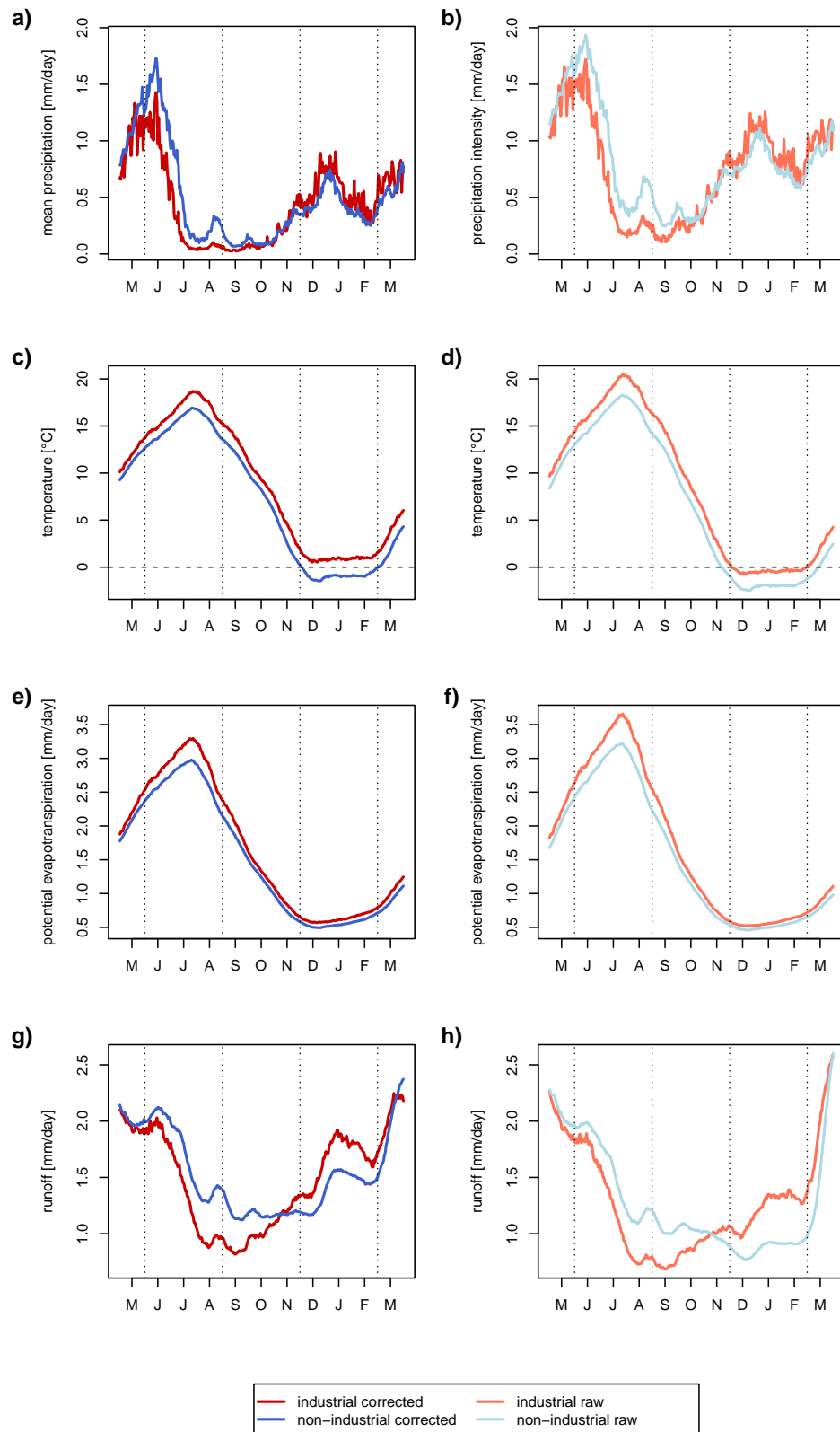


Figure D.10: Ensemble median for each day (from May to March) and for the river Thur of the variables mean precipitation (a, b), mean temperature (c, d), potential evapotranspiration (e, f), and mean runoff (g, h). The ensemble medians were calculated from the bias corrected simulations (1981-2010) (left panels) and raw simulations (right panels). Dotted lines indicate the meteorological season boundaries.

Acknowledgements

Along the exciting, enriching, rewarding and sometimes challenging journey of this PhD thesis, a long list of people have been supporting me to whom I would like to express my sincere gratitude. Additionally, I would like to mention a few individually. Special thank goes to ...

- ... **Olivia** for giving me the opportunity to write my dissertation in your group in a fascinating field of research which kept me engaged throughout the entire course of the thesis. Our much appreciated discussions and your guidance during crucial moments were invaluable to me. Thank you for your support, your encouragement, the numerous valuable inputs, all the opportunities you created for me and the time and patience you dedicated to my PhD project.
- ... **Ole** for giving me the opportunity to be part of and work for the Hydro-CH2018 project. It was a challenging but also highly fascinating and informative time. Thank you for your valuable support and the discussions during your time at the University of Bern and afterwards.
- ... **Rolf** for the many stimulating and inspiring discussions about hydrology in Switzerland and for sharing your knowledge and fascination with others.
- ... **Jana Sillmann** for taking the time to read and grade my PhD thesis.
- ... **Jan** for the support with PREVAH and screening thousands of interconnected lines of code.
- ... **Pascal** for introducing me to the UBELIX high performance cluster and all the interesting discussions on and off topic.
- ... **Samuel** for your assistance in retrieving and processing data from the CMIP5 models.
- ... **Andrey, Basilio, and Manuel** for the support in IT related issues.
- ... **my working colleagues at GIUB** (in particular the people from the 5th and the 4th floor) for all the interesting discussions and scientific input. Above all I enjoyed joking and laughing with you during lunch or coffee breaks.
- ... **my family and friends** for your encouragement and love not only throughout this thesis, but also in the years before.
- ... **Thomas** for your love, your continuous encouragement and your unshakable faith in me. Thank you for the last 15 years.

Declaration of consent

on the basis of Article 18 of the PromR Phil.-nat. 19

Last, first name: Mülchi, Regula Isabelle

Matriculation number: 07-112-741

Programme: PhD in Climate Sciences

Bachelor Master Dissertation

Thesis title: Future changes of Swiss river runoff and extreme vertically integrated moisture transport

Thesis supervisors: Prof. Dr. Olivia Romppainen-Martius,
Prof. em. Dr. Rolf Weingartner,
Dr. Ole Rössler

I declare herewith that this thesis is my own work and that I have not used any sources other than those stated. I have indicated the adoption of quotations as well as thoughts taken from other authors as such in the thesis. I am aware that the Senate pursuant to Article 36 paragraph 1 litera r of the University Act of September 5th, 1996 and Article 69 of the University Statute of June 7th, 2011 is authorized to revoke the doctoral degree awarded on the basis of this thesis. For the purposes of evaluation and verification of compliance with the declaration of originality and the regulations governing plagiarism, I hereby grant the University of Bern the right to process my personal data and to perform the acts of use this requires, in particular, to reproduce the written thesis and to store it permanently in a database, and to use said database, or to make said database available, to enable comparison with theses submitted by others

Liebefeld, February 17, 2021



Signature